

**AN ARCHITECTING METHODOLOGY FOR THERMAL MANAGEMENT  
SYSTEMS OF COMMERCIAL AIRCRAFT AT THE CONCEPTUAL DESIGN  
PHASE**

A Dissertation  
Presented to  
The Academic Faculty

By

Mingxuan Shi

In Partial Fulfillment  
of the Requirements for the Degree  
Doctor of Philosophy in the  
Daniel Guggenheim School of Aerospace Engineering  
Department of Aerospace Engineering

Georgia Institute of Technology

May 2021

© Mingxuan Shi 2021

**AN ARCHITECTING METHODOLOGY FOR THERMAL MANAGEMENT  
SYSTEMS OF COMMERCIAL AIRCRAFT AT THE CONCEPTUAL DESIGN  
PHASE**

Thesis committee:

Dr.Dimitri N. Mavris  
Aerospace Engineering  
*Georgia Institute of Technology*

Dr. Daniel P Schrage  
Aerospace Engineering  
*Georgia Institute of Technology*

Dr. Jachiel Jagoda  
Aerospace Engineering  
*Georgia Institute of Technology*

Dr. Soumya Patnaik  
Propulsion Directorate  
*Air Force Research Laboratory*

Dr. Jonathan C. Gladin  
Aerospace Engineering  
*Georgia Institute of Technology*

Date approved: April 16, 2021

To my family

## ACKNOWLEDGMENTS

Looking back on my 7-year PhD journey, it is an extremely rewarding adventure, although challenging and time consuming. Without help from my advisor, my committee members, my colleagues, my friends, and my family, it is impossible for me to be close to finishing this dissertation. So I would like to gratefully acknowledge those who guided and encouraged me along this journey.

First of all, I would like to express profound appreciation for my advisor and mentor, Professor Dimitri Mavris. There are no words that can describe my gratitude to him, for bringing me into the ASDL family, and taking care of me under his wings. He provided an amazing research environment where I could freely explore a number of research areas. His knowledge and passion for the research, his patience and understanding for the people around him, and his encouragement always inspire me to fulfill my goals.

I would also like to thank Dr. Jonathan Gladin, who has been helping me through my graduate journey from the beginning. He provided many insights not only in this dissertation but also many in other subjects such as propulsion systems and systems integration. He has been a wonderful mentor who spent hours and hours reviewing and discussing research with me.

I also want to express my appreciation to rest of my committee: Professor Jagoda, Professor Schrage, and Dr. Patnaik, for their support in this research, and for taking time to review this document. I have been benefited greatly from their expertise and feedback.

My special thanks go to Professor Imon Chakraborty, who lighted my interest in thermal management and subsystems. The subsystem integration framework that he created also inspired the integration process of the thermal management systems with the mission analysis. Besides, he has been always hard-working and rigorous in doing research, which keeps motivating me to fulfill my unrealized potential.

I also want to thank the wonderful people I met through the journey. I really appreciate



the help from Dr. Jimmy Tai, Mr. Christopher Perullo, Mr. Russel Denny, and Dr. Gokein Cinar. They have provided insights and expertise in my research. I also want to acknowledge Dr. Manish Pokhrel and Yu Cai for helping to co-author several papers. Many thanks also go to my friends Wenxin Zhang and Yun Tang, for many wonderful moments we spent and many hotpots we have had together.

Finally, I want to express my thanks to my family. Thanks to my parents, Jihua Liu and Xuefa Shi, who has been supporting me from the start of my life, I am both physically and spiritually strong enough to overcome the challenges along the path. And I also want to acknowledge my parents-in-law, Xiaoyun Zhang and Jianjun Yang, who have been helping to relieve the burden of taking care of my 1-year-old son, Noah Shi, especially in this pandemic. Without their help, I would not be able to get enough time to concentrate on my thesis. The deepest gratitude goes to my wife, Yang Yang, whose kindness, patience, and love has been empowering me to go through this difficult adventure. She is my brightest star in the dark nights.

## TABLE OF CONTENTS

<b>Acknowledgments</b> . . . . .	iv
<b>List of Tables</b> . . . . .	xiii
<b>List of Figures</b> . . . . .	xv
<b>Summary</b> . . . . .	xxiv
<b>Chapter 1: Introduction and Background</b> . . . . .	1
1.1 Aircraft Thermal Management Systems . . . . .	1
1.2 Consideration of Thermal Management Systems at Conceptual Design Phase . . . . .	2
1.3 Challenges for Thermal Management Systems Development . . . . .	4
1.3.1 More-Electric Aircraft and All-Electric Aircraft . . . . .	4
1.3.2 Turbo-Electric Distributed Propulsion System and Hybrid Propulsion System . . . . .	5
1.3.3 Supersonic Business Jet . . . . .	8
1.4 Thermal Management System Architectures of Interest . . . . .	9
1.5 Summary . . . . .	11
1.6 Initial Statement of the Overarching Research Objective . . . . .	12
<b>Chapter 2: Literature Review</b> . . . . .	13

2.1	Information Required for TMS Architecting . . . . .	13
2.2	Information Required from TMS Architecting . . . . .	13
2.3	Existing TMS Architecting Research . . . . .	15
2.4	General Systems Architecting Methods . . . . .	18
2.5	Existing Evaluation and Sizing Methods for Aircraft TMS . . . . .	20
2.6	Architecture Space Narrowing Down Methods - Multifidelity Methods . . .	21
2.7	Summary and Identified Gaps from Literature Review . . . . .	22
2.7.1	Summary of Observations . . . . .	22
2.7.2	Identified Gaps . . . . .	24
2.8	Refined Statement of Research Objectives . . . . .	25
<b>Chapter 3:</b>	<b>Research Formulation . . . . .</b>	<b>26</b>
3.1	Research Objectives . . . . .	26
3.2	Research Questions . . . . .	28
3.2.1	Research Question 1 . . . . .	28
3.2.2	Research Question 2 . . . . .	29
3.2.3	Research Question 3 . . . . .	29
3.3	Mappings of research questions, hypotheses, and experiments . . . . .	30
3.4	Hypothesis 1 and Design of Experiment Set 1 . . . . .	31
3.4.1	Formulation of Hypothesis 1 . . . . .	31
3.4.2	Statement of Hypothesis 1 . . . . .	33
3.4.3	Overview of Experiment Set 1 . . . . .	34
3.5	Hypothesis 2 and Design of Experiment Set 2 . . . . .	35

3.5.1	Formulation of Hypothesis 2 . . . . .	35
3.5.2	Statement of Hypothesis 2 . . . . .	37
3.5.3	Overview of Experiment Set 2 . . . . .	38
3.6	Hypothesis 3 and Design of Experiment Set 3 . . . . .	39
3.6.1	Formulation of Hypothesis 3 . . . . .	39
3.6.2	Statement of Hypothesis 3 . . . . .	40
3.6.3	Overview of Experiment Set 3 . . . . .	41
<b>Chapter 4:</b>	<b>Experiment Set 1 - Exploring the Architecture Space . . . . .</b>	<b>42</b>
4.1	Design of Experiment Set 1 . . . . .	42
4.1.1	Overview of Research Questions 1, Hypothesis 1, and Design of Experiment Set 1 . . . . .	42
4.1.2	Concepts of Interest in Experiment Set 1 . . . . .	44
4.1.3	Experimental Cases for Local TMS - Experiment 1.1 . . . . .	48
4.1.4	Experimental Cases for Global TMS - Experiment 1.2 . . . . .	49
4.2	Experimental Methodology: Behavior-Based Backtracking Architecting . .	50
4.2.1	Information Needed for TMS Architecting . . . . .	50
4.2.2	Behavior-Based Architecting Approach . . . . .	50
4.2.3	Backtracking Algorithm . . . . .	52
4.2.4	Conversion Behavioral to Structural Architecture . . . . .	55
4.2.5	Overview of the Methodology . . . . .	56
4.3	Local TMS Architecting . . . . .	56
4.3.1	Behaviors of Local TMS . . . . .	56
4.3.2	Conversion from Behavioral to Structural Architecture . . . . .	62

4.3.3	Form of TMS Stored in Actual Implementation . . . . .	63
4.3.4	Example of Local TMS Architecting . . . . .	65
4.3.5	Behavioral to Structural Architecture . . . . .	67
4.4	Global TMS Architecting . . . . .	68
4.4.1	Behaviors of Global TMS . . . . .	68
4.4.2	Example of Global TMS Architecting . . . . .	70
4.4.3	Form of Global TMS Stored in Actual Implementation . . . . .	72
4.5	Results and Validation of Methodology . . . . .	73
4.5.1	Results and Validation of Local TMS . . . . .	73
4.5.2	Results and Validation of the Global TMS . . . . .	83
4.6	Conclusion for Experiment Set 1 . . . . .	91
4.6.1	Validation of Hypothesis 1 . . . . .	91
4.6.2	Conclusions . . . . .	92

## **Chapter 5: Experiment Set 2 - Architecture Filtering and Optimal Down-Selection 94**

5.1	Design of Experiment Set 2 . . . . .	95
5.1.1	Overview of Research Questions 2, Hypothesis 2, and Design of Experiment Set 2 . . . . .	95
5.1.2	Cases of Interest in Experiment Set 2 . . . . .	96
5.1.3	Overall Design of the Experiment Set 2 . . . . .	98
5.2	Formulation of Methodology . . . . .	98
5.2.1	Identified Problems from Experiment Set 1 . . . . .	98
5.2.2	Filtering Method Based on Feasibility . . . . .	99
5.2.3	Filtering Method Based on Optimality . . . . .	102

5.2.4	Automatic Creation of TMS Simulation Models . . . . .	103
5.2.5	Sizing and Optimization . . . . .	103
5.3	Filtering and Optimal Down Selection Methodology . . . . .	104
5.3.1	Overview of the Methodology . . . . .	104
5.3.2	Feasibility-Based Filtering Methodology . . . . .	105
5.3.3	Low-Fidelity KPI Evaluation Methodology . . . . .	116
5.3.4	Clustering-Based Filtering Methodology . . . . .	118
5.3.5	Automation of TMS Simulation Models Construction . . . . .	121
5.3.6	MDP Sizing and Optimization Methodology of the TMS . . . . .	122
5.4	Component Modeling Methodologies . . . . .	130
5.4.1	Turbomachinery . . . . .	130
5.4.2	Heat Exchanger . . . . .	131
5.4.3	Phase Change Modeling . . . . .	135
5.4.4	Ducts . . . . .	138
5.4.5	Vapor Cycle . . . . .	139
5.4.6	Cabin . . . . .	139
5.4.7	Phase Change Material . . . . .	143
5.4.8	Electrical Systems . . . . .	147
5.4.9	Non-Cyrogenic Coolant Weight . . . . .	148
5.4.10	Cryogenic Cooling TMS Modeling . . . . .	149
5.4.11	Ram Drag due to Ram Air Intake . . . . .	151
5.4.12	Others . . . . .	152
5.5	Results . . . . .	152

5.5.1	Parameter Values Used in Experiment Set 2 . . . . .	152
5.5.2	Runtime Analysis of Feasibility-Based Filtering Methodology - E 2.1	154
5.5.3	Feasibility-Based Filtering Results - E 2.1 . . . . .	154
5.5.4	Runtime Analysis of Low-Fidelity KPI Evaluation - E 2.2 . . . . .	161
5.5.5	Clustering Results for Local TMS - E 2.2 and E 2.3 . . . . .	162
5.5.6	Clustering Results for Global TMS - E2.2 and E 2.3 . . . . .	174
5.5.7	Automatic Creation of Physics-Based Models - E 2.4 . . . . .	182
5.5.8	Optimization Results - E 2.5 . . . . .	185
5.6	Conclusion for Experiment Set 2 . . . . .	191
5.6.1	Validation of Hypothesis 2 . . . . .	191
5.6.2	Conclusions . . . . .	193

## **Chapter 6: Experiment Set 3 - Integration of TMS Architecting with Aircraft Design . . . . . 194**

6.1	Design of Experiment Set 3 . . . . .	195
6.1.1	Overview of Research Questions 3, Hypothesis 3, and Design of Experiment Set 3 . . . . .	195
6.1.2	Cases of Interest in Experiment Set 3 . . . . .	196
6.1.3	Design of Experiment 3 . . . . .	200
6.2	Integration Methodology . . . . .	200
6.3	Methodologies for Aircraft Modeling, Sizing, and Analysis . . . . .	202
6.3.1	Aircraft Conceptual Design Requirements . . . . .	202
6.3.2	Aircraft Design and Sizing Methodology . . . . .	203
6.3.3	Modeling, Integration, and Mission Analysis Environment . . . . .	203

6.3.4	Propulsion System Models . . . . .	206
6.4	Other Modules in Integration Process . . . . .	211
6.4.1	Obtaining Descriptions of Heating and Cooling Loads . . . . .	211
6.4.2	TMS Architecting Module in the Design Loop . . . . .	212
6.4.3	Convergence Criteria for the Design Loop . . . . .	212
6.5	TMS Information Feedback and Interface . . . . .	214
6.6	Results . . . . .	215
6.6.1	Integrated Design and Analysis on 160-PAX SSA . . . . .	216
6.6.2	Integrated Design and Analysis on 300-PAX TeDP . . . . .	225
6.6.3	Integrated Design and Analysis on 78-PAX Non-Cryo HTeDP . . . . .	248
6.7	Conclusion for Experiment Set 3 . . . . .	267
6.7.1	Validation of Hypothesis 3 . . . . .	267
6.7.2	Conclusions . . . . .	269
<b>Chapter 7: Conclusions, Contributions, and Recommendations for Future Work</b>		<b>270</b>
7.1	Overview of the Thesis . . . . .	270
7.2	Conclusions . . . . .	272
7.3	Contributions . . . . .	277
7.4	Recommendations for Future Work . . . . .	278
<b>Appendices</b> . . . . .		<b>281</b>
Appendix A: Phase Change Modeling Equations and Parameters . . . . .		282
<b>References</b> . . . . .		<b>286</b>



## LIST OF TABLES

3.1	Mapping of research questions (RQ), hypotheses (H), and experiment sets (E) . . . . .	30
4.1	Design specifications of the 160-pax conventional aircraft . . . . .	45
4.2	Design specifications of the N3-X-like TeDP concept [23, 77] . . . . .	46
4.3	Design specifications of the HTeDP concept . . . . .	47
4.4	Behaviors of direct heat reject systems . . . . .	61
4.5	Behaviors of refrigeration cycle systems for non-cryo application . . . . .	62
4.6	Behaviors of refrigeration cycle systems for cryogenic application . . . . .	63
4.7	Linkages between components and behaviors . . . . .	64
5.1	Electrical Element Computation Logic . . . . .	147
5.2	Operation conditions for E 2.1 and E 2.2 . . . . .	152
5.3	Heat Sink Properties for E 2.1 . . . . .	153
5.4	Heat Sink Properties for E 2.2 . . . . .	153
5.5	Component Performance for E 2.1, under hot-day on-ground condition . . .	153
5.6	Component Performance for E 2.2, under cruise condition . . . . .	153
6.1	Design specifications of the 160-pax conventional aircraft [46] . . . . .	196
6.2	Design specifications of the N3-X-like TeDP concept [23, 77] . . . . .	197

6.3	Design specifications of the HTeDP concept [28, 29]	198
A.1	List of coefficients for calculating RH	283

## LIST OF FIGURES

1.1	Architecture of a conventional TMS [2] . . . . .	3
1.2	NASA N3-X Concept [25] . . . . .	6
1.3	HTeDP configuration for the ULI aircraft [28, 29] . . . . .	8
1.4	Hierarchical decomposition of the TMS [32] . . . . .	10
1.5	Four-wheel condensing air cycle machine [33] . . . . .	11
2.1	Mattingly's Aircraft Design Process [37] . . . . .	14
2.2	Raymer's Aircraft Design Process [38] . . . . .	15
4.1	305-PAX TeDP concept configuration [23, 77] . . . . .	46
4.2	HTeDP configuration for the ULI aircraft [28, 29] . . . . .	47
4.3	Linkages between SysML and proposed architecting methodology . . . . .	52
4.4	Backtracking in proposed TMS architecting method . . . . .	54
4.5	Conversion from behavioral to structural architecture illustration . . . . .	56
4.6	Overview of TMS architecture space populating methodology . . . . .	57
4.7	Behaviors to manage loads requiring heating . . . . .	58
4.8	Behaviors to manage loads requiring cooling . . . . .	59
4.9	Motor TMS as illustration of list representation . . . . .	65

4.10 ECS architecting process from cooling load to the architecture construction starting point . . . . .	66
4.11 ECS architecting process . . . . .	67
4.12 ECS architecting backtracking example . . . . .	68
4.13 Example architecting process for a HX in obtained TMS architecture . . . .	69
4.14 Overall ECS behavioral architecture example . . . . .	70
4.15 Components that perform certain behaviors . . . . .	70
4.16 Behavioral to structural architecture conversion example . . . . .	71
4.17 Selection of local TMS . . . . .	72
4.18 Interaction architecting for the global TMS . . . . .	72
4.19 Generated three-wheel TMS architecture . . . . .	75
4.20 Generated four-wheel TMs architecture . . . . .	75
4.21 Novel TMS following reversed bootstrap to cool cabin . . . . .	76
4.22 Novel ECS with vapor cycle cooling re-circulation path . . . . .	76
4.23 Novel ECS with vapor cycle cooling major supply stream without ACS . . .	77
4.24 Conventional motor TMS 1 . . . . .	79
4.25 Conventional motor TMS 2 . . . . .	79
4.26 Novel motor TMS with PCM . . . . .	79
4.27 Novel motor TMS with PCM, ECS air, and vapor cycle . . . . .	80
4.28 Conventional battery TMS . . . . .	81
4.29 Novel battery TMS using air from an open-loop air cycle . . . . .	82
4.30 Another novel battery TMS using air from an open-loop air cycle . . . . .	82
4.31 Novel battery TMS using a closed-loop heat pump . . . . .	83

4.32	Generated global TMS for 160-pax conventional aircraft . . . . .	84
4.33	Generated global TMS for 160-pax conventional aircraft with electrified compressed supply air . . . . .	85
4.34	Generated global TMS for non-cryo TeDP configuration aircraft . . . . .	86
4.35	Generated global TMS for cryo TeDP configuration aircraft . . . . .	87
4.36	Generated global TMS for HTeDP configuration aircraft . . . . .	88
4.37	Another generated global TMS for HTeDP configuration aircraft . . . . .	89
5.1	Overall process of the Experiment Set 2 . . . . .	99
5.2	Overview of methodology for Experiment Set 2 . . . . .	105
5.3	Overview of feasibility-based architecture filtering methodology . . . . .	106
5.4	Example to illustrate the maximum thermal management capability . . . . .	108
5.5	Example for computation process of maximum thermal management capa- bility . . . . .	108
5.6	TMS architecture to illustrate the feasibility evaluation process . . . . .	115
5.7	Example feasibility evaluation process . . . . .	116
5.8	Influences of the TMS on vehicle and mission . . . . .	117
5.9	Overview of low-fidelity KPI evaluation and clustering-based TMS archi- tecture filtering methodology . . . . .	121
5.10	Overview of the MDP sizing methodology for the TMS . . . . .	124
5.11	Map scaling [129] . . . . .	131
5.12	On-design calculation flow for the heat exchanger . . . . .	132
5.13	Off-design calculation flow for the heat exchanger . . . . .	132
5.14	Cabin heat transfer relation [46] . . . . .	140
5.15	1-D melting process of the PCM [32] . . . . .	144

5.16	Electric element solver setup and data flow [141]	148
5.17	Passive cryogenic cooling using stored coolant	149
5.18	Passive cryogenic cooling using fuel (LH2)	149
5.19	Active cryogenic cooling following Claude process)	150
5.20	Runtime of feasibility check vs. problem size $n$	154
5.21	Number of feasible architectures vs. varying gallery load	155
5.22	Number of feasible architectures vs. varying motor efficiency	156
5.23	Number of feasible architectures vs. varying battery efficiency	157
5.24	Fraction of infeasible architectures for the cabin in terms of different reasons	159
5.25	Fraction of infeasible architectures for the motor in terms of different reasons	160
5.26	Fraction of infeasible architectures for the battery in terms of different reasons	160
5.27	Runtime of KPI evaluation vs. problem size $n$	161
5.28	Clustering results for cabin KPI	165
5.29	Cabin TMS architecture at Pareto frontier: No.1	166
5.30	Cabin TMS architecture at Pareto frontier: No.2	166
5.31	Cabin TMS architecture at Pareto frontier: No.3	166
5.32	Cabin TMS architecture at Pareto frontier: No.4	166
5.33	Clustering results for motor KPI	169
5.34	Motor TMS architecture at Pareto frontier: No.1	169
5.35	Motor TMS architecture at Pareto frontier: No.2	170
5.36	Motor TMS architecture at Pareto frontier: No.3	170
5.37	Motor TMS architecture at Pareto frontier: No.4	170
5.38	Motor TMS architecture at Pareto frontier: No.5	170

5.39	Clustering results for battery KPI . . . . .	173
5.40	Battery TMS architecture at Pareto frontier: No.1 . . . . .	174
5.41	Battery TMS architecture at Pareto frontier: No.2 . . . . .	174
5.42	Battery TMS architecture at Pareto frontier: No.3 . . . . .	174
5.43	Battery TMS architecture at Pareto frontier: No.4 . . . . .	175
5.44	Clustering results for 160-pax SSA global TMS . . . . .	177
5.45	Clustering results for 300-pax TeDP non-cryo global TMS . . . . .	179
5.46	Clustering results for 78-pax non-cryo HTeDP global TMS . . . . .	181
5.47	Selected TMS architecture descriptor and visualization for the model cre- ation example . . . . .	182
5.48	Created model files for the model creation example . . . . .	184
5.49	Selected cabin TMS for optimization . . . . .	186
5.50	Pareto frontier for selected cabin TMS . . . . .	187
5.51	Selected motor TMS for optimization . . . . .	188
5.52	Pareto frontier for selected motor TMS . . . . .	189
5.53	Selected battery TMS for optimization . . . . .	190
5.54	Pareto frontier for selected battery TMS . . . . .	190
6.1	Design mission profile for 160-pax SSA concept . . . . .	196
6.2	305-PAX TeDP concept configuration [23, 77] . . . . .	197
6.3	Design mission profile for 300-pax TeDP aircraft . . . . .	198
6.4	HTeDP configuration for the ULI aircraft [28, 29] . . . . .	199
6.5	Design mission profile for 78-pax HTeDP aircraft . . . . .	199
6.6	Overview of integrated design loop of aircraft and TMS . . . . .	201

6.7	Mattingly's Aircraft Design Process [37]	203
6.8	Raymer's Aircraft Design Process [38]	204
6.9	GT-HEAT functional architecture [151, 152, 153]	205
6.10	Gas turbine model architecture for 160-pax SSA [156]	206
6.11	300-pax TeDP propulsion system model schematic [153]	207
6.12	Parallel compressor model architecture [77]	209
6.13	Nozzle algorithm overview [160]	210
6.14	Nozzle pressure drop calculation process [160]	210
6.15	Architecture of the propulsion system [28, 29]	211
6.16	TMS architecting process in the integrated design loop	213
6.17	Interactions of TMS design and loads	215
6.18	Cabin heat that needs to be removed by TMS	217
6.19	Cabin TMS using bleed for 160-pax SSA	217
6.20	Cabin TMS using E-Charged-Air for 160-pax SSA	217
6.21	Generator TMS for 160-pax SSA	218
6.22	Fuel tank TMS for 160-pax SSA	218
6.23	Oil reservoir TMS for 160-pax SSA	218
6.24	Hydraulics TMS for 160-pax SSA	218
6.25	Avionics TMS for 160-pax SSA	218
6.26	Global TMS for 160-pax SSA using Bleed for Cabin	219
6.27	Global TMS for 160-pax SSA using E-Charged-Air for Cabin	220
6.28	Generator heat generation comparison for 160-pax SSA between initially sized aircraft and the aircraft with E-Charged-Air for cabin cooling	220



6.29	Required cabin supply air mass flow rate for 160-pax SSA . . . . .	221
6.30	Generator heat generation through the mission for 160-pax SSA with bleed for cabin cooling . . . . .	221
6.31	Weight comparison among aircraft without TMS and aircraft with two types of global TMS . . . . .	222
6.32	$\Delta$ mission block fuel burn of aircraft with bleed for cabin cooling relative to aircraft sized without TMS . . . . .	224
6.33	$\Delta$ mission block fuel burn of aircraft with E-Charged-Air for cabin cooling relative to aircraft sized without TMS . . . . .	224
6.34	$\Delta$ mission block fuel burn of aircraft with E-Charged-Air for cabin cooling relative to aircraft with bleed to cool the cabin . . . . .	225
6.35	Shaft-power of motor and generator through the mission . . . . .	226
6.36	Heat generation of non-superconducting motor and generator through the mission . . . . .	227
6.37	Heat generation of conducting motor and generator through the mission . . . . .	227
6.38	Passive cryogenic cooling TMS for motor and generator . . . . .	228
6.39	Active cryogenic cooling TMS for motor and generator . . . . .	229
6.40	Motor TMS using PCM and fan bleed . . . . .	229
6.41	Motor TMS using vapor cycle . . . . .	230
6.42	Motor TMS using closed-loop air cycle . . . . .	230
6.43	Non-cryogenic TMS for generator, using fuel and fan air to cool the oil . . . . .	231
6.44	Loads cooling using exhaust with superconducting systems cooled by pas- sive cryogenic cooling approach . . . . .	231
6.45	Global TMS for 300-pax TeDP with passive cryogenic cooling . . . . .	232
6.46	Global TMS for 300-pax TeDP with active cryogenic cooling . . . . .	233
6.47	Global TMS for 300-pax TeDP with motor cooled by PCM and fan bleed . . . . .	234

6.48	Global TMS for 300-pax TeDP with motor oil cooled by vapor cycle . . . .	235
6.49	Global TMS for 300-pax TeDP with motor oil cooled by closed-loop air cycle	236
6.50	Shaft-power requirement of the generator . . . . .	237
6.51	Shaft-power requirement of the motor . . . . .	237
6.52	Heat generation from the generator without cryogenic cooling . . . . .	238
6.53	Heat generation from the generator with cryogenic cooling . . . . .	238
6.54	Heat generation from the motor without cryogenic cooling . . . . .	239
6.55	Heat generation from the motor with cryogenic cooling . . . . .	239
6.56	Heat generation from the motor with non-cryogenic cooling . . . . .	240
6.57	Gap between cooling capability and heat generation of the generator using the initially selected TMS architecture (aircraft sized with closed-air cycle as TMS for the motor) . . . . .	242
6.58	New local TMS for generator with closed-loop air cycle . . . . .	242
6.59	Global TMS for 300-pax TeDP with motor oil cooled by closed-loop air cycle, with new generator TMS . . . . .	243
6.60	Weight comparison for aircraft with selected TMS . . . . .	244
6.61	$\Delta$ mission block fuel burn of aircraft with passive cryo-cooling relative to aircraft sized without TMS . . . . .	246
6.62	$\Delta$ mission block fuel burn of aircraft with active cryo-cooling relative to aircraft sized without TMS . . . . .	246
6.63	$\Delta$ mission block fuel burn of aircraft with PCM for motor cooling relative to aircraft sized without TMS . . . . .	247
6.64	$\Delta$ mission block fuel burn of aircraft with vapor cycle for motor cooling relative to aircraft sized without TMS . . . . .	247
6.65	$\Delta$ mission block fuel burn of aircraft with closed-loop air cycle for motor cooling relative to aircraft sized without TMS . . . . .	248

6.66 Global TMS for 78-pax HTeDP with without battery installed: battery TMS strategy 1 . . . . .	251
6.67 Generator and motor power for design mission without battery . . . . .	252
6.68 Battery TMS architecture using ACS air . . . . .	252
6.69 Integrated illustration of battery TMS and ACS . . . . .	253
6.70 Method to determine ACS shaft speed schedule . . . . .	253
6.71 Generator, motor, and battery power for selected hybrid mission . . . . .	255
6.72 Global TMS with battery TMS design strategy 1 for hybrid missions . . . .	256
6.73 Battery temperature profile for selected typical mission with battery TMS strategy 1 . . . . .	257
6.74 Updated integrated design loop of aircraft and TMS for hybrid aircraft . . .	257
6.75 Battery TMS architecture using vapor cycle . . . . .	258
6.76 Global TMS for 78-pax HTeDP with battery installed: battery TMS strategy 3 . . . . .	259
6.77 Generator power comparison for selected hybrid mission . . . . .	260
6.78 Motor power comparison for selected hybrid mission . . . . .	261
6.79 Battery power comparison for selected hybrid mission . . . . .	261
6.80 Battery temperature comparison for selected hybrid mission . . . . .	262
6.81 Battery temperature comparison for hybrid mission with shorter range . . .	262
6.82 Weight comparison for aircraft with selected TMS . . . . .	263
6.83 $\Delta$ mission block fuel burn of aircraft with strategy 1 . . . . .	265
6.84 $\Delta$ mission block fuel burn of aircraft with strategy 2 . . . . .	265
6.85 $\Delta$ mission block fuel burn of aircraft with strategy 3 . . . . .	266

## SUMMARY

A thermal management system (TMS) of the aircraft is a subsystem to handle the cooling and heating requirements of the whole aircraft to keep the temperature of each system within an acceptable range during the operation. Meeting such temperature requirements is essential to ensure the correct functionality of the aircraft. The thermal management system itself will also influence the performance at the vehicle level and the mission level besides satisfying the thermal requirements, by adding more weight or ram drag, as well as consuming more power through bleed extraction from the engine or requiring more electric power. The traditional approach to consider the thermal management systems influence at the early design phase is to predict its impacts using historical data. The architecture of a thermal management system is then gradually constructed as the emergence of the designs of other systems with thermal requirements.

However, the heating problem becomes much more serious than before because of more applications of the electrical systems and the increasing use of composite material which limits the heat transfer from the internal to the ambient. Meanwhile, novel aircraft concepts that generate much larger amount of heat are emerging. The concept More Electric Aircraft or All Electric Aircraft is coming into development or even application due to the rising trend to electrify the secondary power systems, accompanied with increasing cooling loads in such systems. Electrification of the propulsion system leads to novel concepts such as the turbo-electric distributed propulsion system or hybrid propulsion system, which may increase the heat to be removed by more than an order of magnitude. Kinetic heating for commercial aircraft also becomes severer due to the increasing interest in supersonic business jet. For such larger cooling loads and emerging novel concepts, empirical data may be very limited or even non-existent. Thus, the traditional approach to construct thermal management system architectures may not apply to such problems. Furthermore, considering thermal management system architectures at later phases can result in suboptimal thermal

management solutions, and can also cause budget and schedule overruns due to increasing complexity in modern aircraft systems. Therefore, a physics-based thermal management systems architecting and design methodology is required at the conceptual design phase. The overarching objective of this research proposal then can be formulated as: To develop a thermal management systems architecting methodology suitable for conceptual design phase of commercial aircraft, which is capable of handling increasing cooling loads and emerging aircraft concepts with limited historical data and only information available during early design stage.

The importance of the consideration of thermal management systems at the early design phase has already been realized, and there are a lot of research studying the methods for architecting and evaluation of different architectures. Existing methods relying on physics-based modeling and simulation are suitable for conceptual design because there is no need for large amount of past data. However, existing literature always evaluate only pre-selected architectures which limited intuition or experience, ignoring other innovative and non-intuitive architectures that might be potentially optimal. Besides, due to limited number of pre-selected architectures in literature, the existing evaluation methods are only suitable for comparing a small number of competing architectures, incapable of handling a large number of candidates in the magnitude of tens or hundreds of thousands. Therefore, to achieve the proposed overarching research objective, the following sub-objectives should be addressed:

The first sub-objective is to develop a capability of the proposed method that sufficiently explores the thermal management systems architecture space by systematically identifying both intuitive and non-intuitive architectures. This sub-objective is motivated by the observation that there is not any methodology that can systematically generate intuitive and non-intuitive thermal management system architectures, which are potentially feasible for given heating and cooling load requirements. Without sufficiently exploring the architecture space, suboptimal design decisions might be easily reached which will further degrade

the vehicle-level and mission-level performance of the aircraft.

The second sub-objective is to develop a capability of the proposed method that rapidly narrow down the architecture space to a suitable number of candidates to perform further optimal architecture down-selection in terms of chosen metrics, using information and methods suitable for conceptual design. This sub-objective is motivated by the observation that the number of generated architectures might be too large to be evaluated by usual comparing approaches such as comparing the weight, or power consumption of each architecture, or comparing mission-level metrics such as mission block fuel with certain architecture due to computational cost.

The third sub-objective is to investigate the impacts of thermal management systems architecting process on the final converged design solutions of the aircraft and subsystems. This sub-objective is motivated by the fact that the thermal management solution may influence the vehicle design greatly by adding additional weight or ram drag, or extracting more bleed or power. Such impacts can lead to significant changes in sizing parameters which could further influence the design decisions of other subsystems, and that of the TMS itself.

To address the first sub-objectives, a backtracking architecting approach is proposed to fully explore the architecture space. For the local thermal management systems, the backtracking architecting process is guided by behaviors of fundamental refrigeration cycles.. Following the behaviors of fundamental refrigeration cycles ensures the generated architectures are thermodynamically reasonable, that is, guided by the first and second laws of thermodynamics. By applying this method, the architectures of local thermal management systems are constructed first. Then the local thermal management systems will serve as components to construct the global thermal management system following a similar backtracking behavior. The second sub-objective is addressed by proposing a multi-fidelity architecture filtering methodology which firstly greatly narrows down the architecture space in terms of the feasibility to handle the cooling loads, then an optimal architecture down-selection is performed through physics-based modeling and simulation based on selected

performance metrics. A method integrating the architecture space population process and the architecture filtering process to the overall aircraft design loop is proposed to address the third sub-objective. This proposed approach initially chooses the optimal thermal management system architectures based on the initial design decisions at the aircraft level, then the updated information of the thermal management system is fed back to the vehicle-level design, and the thermal management system and other subsystems will be re-designed based on the updated information. Such design iteration is performed until the solutions for the design of vehicle, thermal management systems and other subsystems are converged.

The experiments are designed to show and validate the capabilities of the proposed methodology by testing the hypotheses for the research questions that are derived from the research objectives. Three sets of experiments are proposed. The first set of experiments is designed to perform local and global thermal management system architecture space exploration using the proposed backtracking method. The second set of experiments is expected to narrow down the architecture space which is generated in the first set of experiments down to a reasonable number of candidates and then perform down-selection of optimal architectures. The third set of experiments is designed to integrate the first set and the second set of experiments to the vehicle sizing loop to produce converged solutions, where the designs of both vehicle and thermal management systems can interact with each other. These experiments will be conducted on the concepts of a More-Electric Aircraft, a 300-pax N3-X-like Turbo-electric distributed propulsion system, and a 78-pax hybrid turbo-electric distributed propulsion system to demonstrate that capability to handle different types of heating and cooling loads and to show how thermal management solutions vary in terms of different concepts.

The completion of the research creates to create a framework that is capable of populating thermal management system architectures, rapidly narrowing down the architecture space, and then performing the down-selection of optimal architectures based on selected subsystem-, system-, and mission-level metrics. This framework also allows for feeding

back the influences of thermal management solution to the vehicle level to update the design decisions. One of the remarkable features is that the resulted thermal management system architectures from this framework are selected and evaluated using physics-based modeling and simulation, suitable for constructing architectures of thermal management systems where there is a lack of empirical data. The application of the framework to designing a thermal management system for a commercial aircraft at the conceptual design phase will provide insight in selecting the optimal architectures, and also in updating the aircraft design decisions with the selected thermal management system architectures.



# **CHAPTER 1**

## **INTRODUCTION AND BACKGROUND**

### **1.1 Aircraft Thermal Management Systems**

Aircraft thermal management system (TMS), which may also be called modern Environmental Control Systems in some other contexts, is a system that “must cope with widely differing temperature conditions, ..., to enable pilot and crew to work comfortably, and to provide safe and comfortable conditions for passengers”, and “also includes the provision of suitable conditions for the avionic, fuel and hydraulic systems by allowing cooling loads to be transferred from one medium to another”, which was defined by Moir [1]. In summary, TMS’s are aircraft subsystems that handle the cooling and heating load requirements of the entire aircraft to keep the temperature of each system within an acceptable range during the operation. Failing to meet such temperature requirements might lead to performance degradation or failure of systems, or extreme discomfort of passengers and crews. Therefore, the TMS’s play a crucial role in ensuring the correct functioning of the aircraft.

In this study, cooling load is defined as the amount of heat that need to be removed to maintain the target temperature, and the heating load is defined as the amount of heat that should be added to maintain the target temperature. Common cooling loads may include: heat generated by hydraulic systems operation, heat in cabin generated by human metabolism and the gallery electrical loads, heat in fuel caused by performing cooling functions, heat generated in the whole electronic systems from generators to the final power usage, and etc. Common heating requirements may maintaining cabin and cargo temperature to a comfortable level, ensuring the battery temperature to be above the lower limit, and etc.

A conventional TMS in commercial aircraft is usually comprised of a fuel thermal

management system (FTMS), an environmental control system (ECS) for the cabin, and some systems directly cooled by ram air, which is illustrated in Figure 1.1. Generally, the FTMS uses the fuel to cool the hydraulic systems and engine oil, but the heated fuel in the FTMS will also be cooled by ram air. The ECS is usually applied to supply cold air to cool the cabin and the avionics. The supply air is sourced from either the high pressure compressor (HPC) stage of the engine or electrical compressors. Before supplied to the cabin, the supply air is cooled by ram air through an air cycle machine (ACM). It should be noted that the largest amount of heat during operation is generated in the engine. However, in the conventional propulsion systems, most of the generated heat is rejected through the exhaust, thus there is no need for a specific TMS to manage the heat generated inside the engine. The turbines may require cooling; nevertheless, it is not the type of TMS to be architected in this thesis. The scope of the TMS architecting problem of interest will be discussed in section 1.4.

## **1.2 Consideration of Thermal Management Systems at Conceptual Design Phase**

The design of the TMS is important for the aircraft for two major reasons: firstly, TMS's are essential to ensure suitable operation environment for subsystems and the vehicle; secondly, TMS's can greatly influence the aircraft performance due to additional weight and ram drag, as well as shaft-power consumption and bleed air extraction. The ECS, as part of the aircraft TMS, is the largest consumer of non-propulsive power [3]. It was also shown that the ECS can account for 64.6% of the engine power at cruise condition on a military transport plane such as C-17 [4]. Therefore, the TMS has to be considered at early design phase to ensure correct functioning of the whole aircraft as well as to improve the aircraft fuel economy.

Traditionally, the TMS is viewed as a system of interactions that arise from emergent properties, that is, the TMS is constructed after the energy dissipation in the aircraft systems is determined [1, 2]. Therefore, the TMS may not be envisaged in the initial design [1, 2].

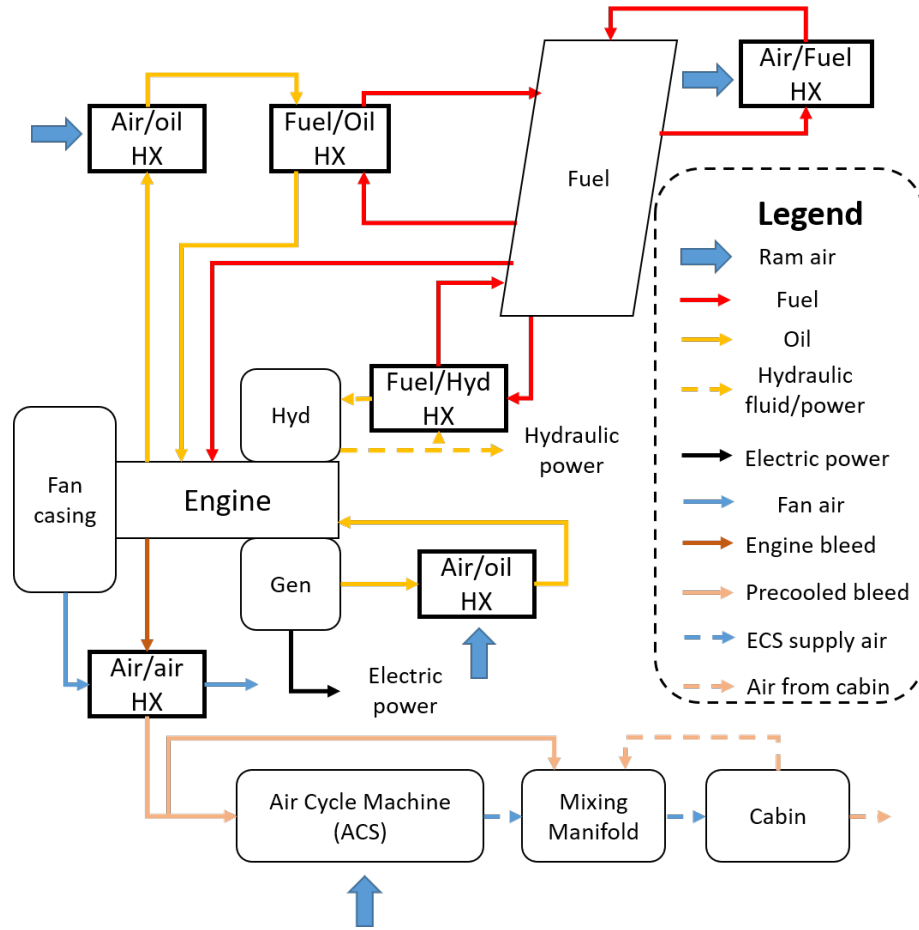


Figure 1.1: Architecture of a conventional TMS [2]

This architecting method can guarantee that the temperature requirements of each system are satisfied. However, such method may lead to suboptimal TMS architectures, because it is constrained by the other developed subsystems. Meanwhile, this traditional architecting method does not provide any information regarding the properties of TMS itself at the conceptual design phase. The properties, or the influences on vehicle design, of the TMS, are predicted using empirical equations that are derived from historical data, which can be found in aircraft design manuals [5].

Nonetheless, the statistical data and corresponded empirical equations may not apply to the development of the TMS in the future: the cooling loads in the commercial aircraft are greatly increasing due to expanded functionality and higher power demand of electronics [6, 7, 8, 9], rising trend to electrify subsystems [10, 11, 12, 13], and more application

of composite material which reduces the amount of heat that can be convected to the environment [6, 7, 8, 9]. Moreover, many novel commercial aircraft concepts that generate much larger amount of heat are emerging, and there is a lack of historical data for such novel concepts. Therefore, new challenges for the development of the TMS in commercial aircraft are rising. These challenges will be discussed in detail in the next section.

### **1.3 Challenges for Thermal Management Systems Development**

As discussed before, the cooling loads are increasing due to rising power consumption of electronics, trend of electrification of subsystems, and application of composite aircraft skins. New aircraft concepts that generate great amount of heat also bring challenges due to large cooling loads and lack of data. Three new aircraft concepts will be discussed here in detail to address the challenges, and the fore-mentioned increasing cooling loads could also be reflected in these three concepts. The three concepts to be discussed are: More-Electric Aircraft (MEA) or All-Electric Aircraft (AEA), Turbo-Electric Distributed Propulsion System (TeDP), and Supersonic Business Jet (SSBJ).

#### 1.3.1 More-Electric Aircraft and All-Electric Aircraft

The concepts of More-Electric Aircraft (MEA) [13] and All-Electric Aircraft (AEA) [11, 12, 14] are driven by the More Electric Initiative [10] which aims to improve the aircraft performance by electrifying all subsystems that consume non-propulsive power. Strictly speaking, the MEA and the AEA are different, where in the AEA all the secondary power requirements are electric while in MEA only some but not all of the conventional subsystems are electrified. Despite the differences in configuration, the reason for the increase of cooling loads for both MEA and AEA is the same, which is the electrification of subsystems, thus they are addressed here together.

The largest contributor to the increased cooling load in MEA and AEA are the added electric components and the corresponding buses and control panels. An example of an

MEA today is Boeing 787. Compared to other conventional commercial aircraft of the similar type, two liquid cooling cycles have been added to the cabin to cool the control panel [1]. A vapor cycle is also recommended to be added to the mixing manifold of the ECS for an MEA or AEA to accommodate the increased cooling loads [15, 16]. The additional devices are undesired in terms of the aircraft performance due to additional weight, drag, and power consumption. However, a compromise has to be made to meet the growing cooling requirement by adding these TMS's. It can be shown from this example that the increased cooling loads greatly influence the TMS design. Therefore, a TMS architecting method at the conceptual design phase considering the increase use of electrical power is desiring.

### 1.3.2 Turbo-Electric Distributed Propulsion System and Hybrid Propulsion System

Turbo-electric distributed propulsion (TeDP) system utilizes gas-turbine-driven generators to power motor-driven fans which are distributed along the wing [17, 18]. Almost all the thrust is produced by the electrical fans. A famous example is the NASA N3-X concept [17], in which two generators are mounted at the tip of the wing, and the ducted electrical fans are distributed on the upper surface at the trailing edge, as illustrated in Figure 1.2. The large amount of heat is generated due to electrification of the propulsion system. The major heat sources are electric propulsors that drive the electrical fans and the corresponding power transmission system. It should be noted that substantial heat is also generated in the gas-turbine-driven generators, but most of the heat is rejected through the exhaust, therefore, this cooling load in the generator will not be the major challenges for the TMS. Researchers have made assumptions for the TMS for the turboelectric concepts in their studies: some assumed a non-cryogenic cooling system application (no superconducting electric devices) [19], while others considered using a cryogenic cooling system (superconducting electric system) [17, 18, 20]. In addition to these research, some other researchers on TeDP configuration also only assumed the method to cool the propulsion

system, while not considering the TMS cooling capability or penalties on the aircraft performance. For example, Liu [21] studied the thermal cycle of a TeDP system, assuming a superconducting approach for the propulsion system. However, the weight, drag, and power consumption due to this TMS were totally ignored. Shi and Pokhrel [22, 23, 24] also conducted a series of research on the losses due to Boundary Layer Ingestion (BLI) on TeDP aircraft, but the authors failed to include impacts of the TMS, following the same assumptions made by Felder [17, 20].



Figure 1.2: NASA N3-X Concept [25]

The amount of heat generation from N3-X assuming no cryogenic cooling is roughly estimated here to show thermal management challenges. As specified in the reference [17], the flight condition of N3-X at its Aerodynamic Design Point (ADP) is: 30000 ft, 0.84 Mach, minimum thrust 26750 lbf, and at International Standard Atmosphere (ISA). From air property tables, the speed of sound can be read, which is 589 knots or 303.1 m/s. Then the air speed  $v$  can be computed to be 254.6 m/s. The required power  $P$  can be calculated by  $P = Fv$  where  $F$  is the thrust. The resulted power requirement is 30.3 MW. Overall

electrical efficiency of the motors and the transmission system can be assumed to be 0.9 without cryo-cooling (no superconducting devices). Then the heat generation is around 3 MW. Now consider the heat generation from a cabin of a conventional 350-pax commercial aircraft, which is the largest cooling load needs to be handled by the current TMS. The heat generation is 75 W/person for metabolism [26], 50 W/person for the In-Flight Entertainment System [27], and 320 W/person for galley load [27]. Then the overall heat generation in a 350-pax cabin is 0.16 MW, which is almost only 1/20 of the heat generated by TeDP without cryo-cooling. Therefore, it can be seen that there is a large gap of the amount of heat to be managed between the existing TMS for commercial aircraft and the ones that are able to handle the TeDP concept. Due to this large gap of the cooling load requirement as well as the lack of statistical data for the TeDP concept, the traditional TMS architecting method may not apply.

TeDP concepts considering cryogenic cooling utilize superconducting electrical systems, arguing the motor efficiency could be increased to 0.997 [17], which could greatly reduce the cooling loads. However, there is no existing cryogenic cooling system applied to aircraft systems yet. Moreover, considering the large temperature difference between the cryogenic temperature and the environment temperature, the large weight of cooling devices and coolant of existing cryo-cooling cycles, there must be a method to architect the cryogenic TMS at the early design phase before putting it into application. However, the traditional TMS architecting method does not provide guidance for it.

In addition to the All-Fuel (only powered by fuel) TeDP aircraft, battery is also proposed to be utilized to enhance the performance. For example, the NASA University Leadership Initiative (ULI) program [28, 29] proposed a Hybrid Turbo-electric Distributed Propulsion (HTeDP) aircraft for a regional jet, where an additional battery was added to reduce the mission fuel burn and CO<sub>2</sub> emissions. The corresponding configuration is illustrated in Figure 1.3. In such scenario, the new cooling loads are not only the electric propulsors, compared to other ALL-Fuel TeDP systems. However, the battery itself be-

comes another significant cooling load that needs to be considered. In the author's previous work [29], it is already demonstrated that the battery temperature can greatly limit the feasible missions that the ULI aircraft can operate. The cooling load of such batteries is much larger than the ones in conventional aircraft, because the power consumption of the battery in a hybrid aircraft is much larger. Therefore, the traditional battery TMS may not be able to handle the heat from the battery in hybrid aircraft, and new TMS's are in need.

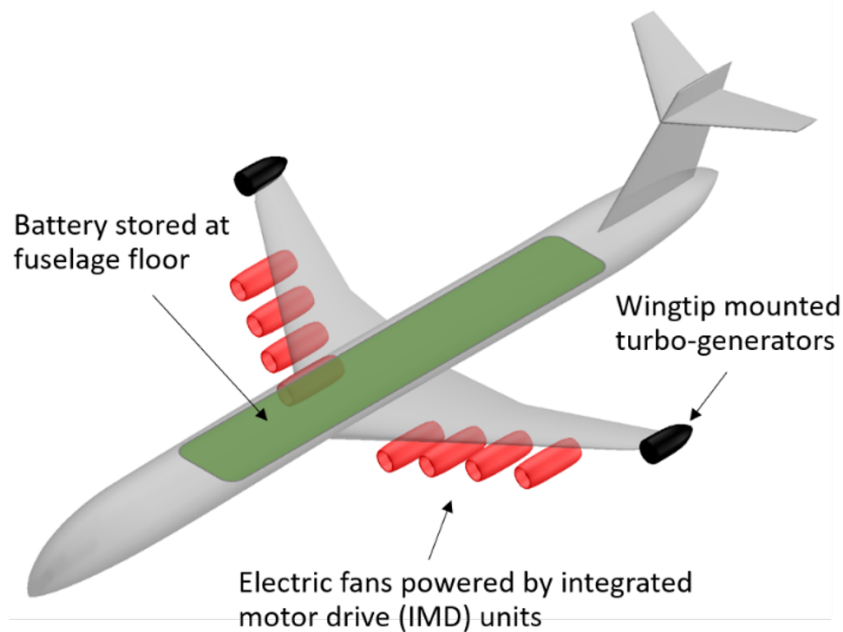


Figure 1.3: HTeDP configuration for the ULI aircraft [28, 29]

### 1.3.3 Supersonic Business Jet

Supersonic business jets (SSBJ) are a class of business jets that perform civil supersonic transportation. The interest in this concepts is intensified by identifying such types of business jets can take up about a 10% market share [30, 31]. The heating problem for a supersonic jet is mainly created by kinetic heating. Kinetic heating can cause two problems: 1. aircraft skin temperature can be as high as over  $212^{\circ}F$  [1] during flight; 2. the ram air can be very hot. The high skin temperature reverses the temperature gradient between the aircraft and the ambient, where more heat is transferred from the ambient to the aircraft



while a lot of heat in subsonic commercial aircraft is convected and conducted to the ambient during high altitude flight. The high temperature of ram air greatly reduces the cooling effectiveness of conventional TMS's which utilize the ram air as a major heat sink.

The only supersonic commercial aircraft that was in service is Concorde, resulting in limited existing data for supersonic aircraft TMS for civil application. The differences in classes of Concorde and SSBJ also lead to the necessity to further evaluation and testing the TMS architecture in Concorde before using it in SSBJ. Indeed, a lot of TMS information can be obtained from military supersonic aircraft. However, the design objectives, requirements, configurations are quite different, thus the data of the TMS in military aircraft may not apply to SSBJ as well. Therefore, a TMS architecting method for SSBJ at conceptual design phase is also needed.

#### **1.4 Thermal Management System Architectures of Interest**

Aircraft TMS can be decomposed hierarchically into three levels as shown in Figure 1.4 which has been identified in the author's previous work [32]: the global TMS, the local TMS, and the component TMS. The global TMS's are comprised of all the local TMS's, managing heat paths from each local TMS and heat rejection of the whole aircraft. An example of the global TMS architecture is the TMS for conventional aircraft as shown in Figure 1.1. The local TMS manages the thermal requirements within an aircraft subsystem, where the components in this subsystem are rejecting heat (requiring cooling) to or acquiring heat (requiring heating) from the local TMS. An example of the local TMS architecture is a four-wheel condensing air cycle machine inside an ECS, which is used to cool the cabin. The corresponding architecture is presented in Figure 1.5, which was developed by the author [33]. The component TMS's perform the function that rejects (requiring cooling) or acquires (requiring heating) heat from the local TMS. Examples of the component TMS's are air distribution systems for the cabin and the heat sink structures of a integrated circuit chip.

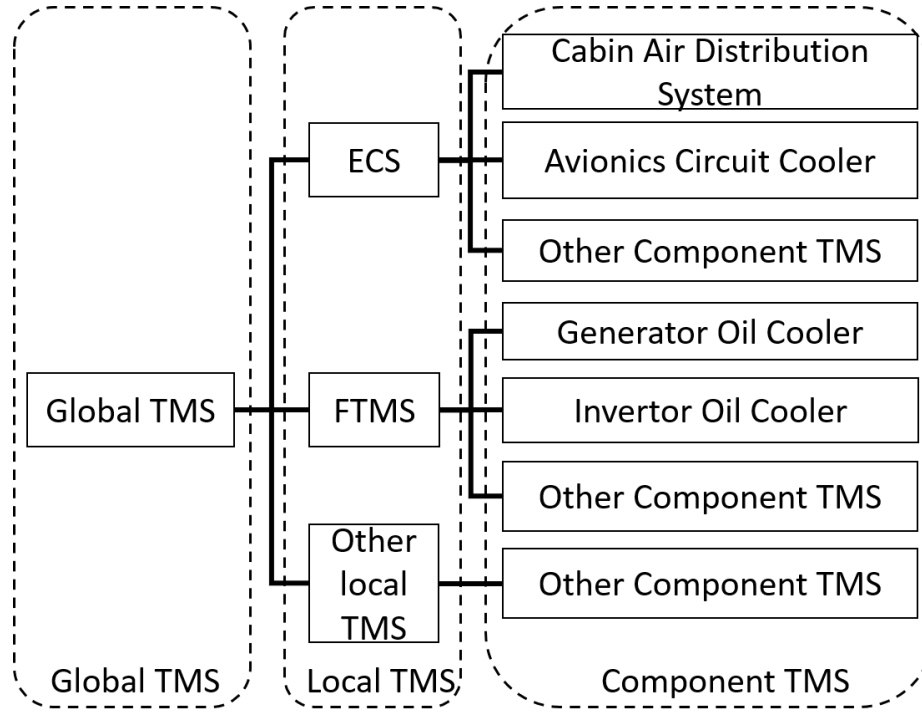


Figure 1.4: Hierarchical decomposition of the TMS [32]

This thesis focuses on architecting the heat paths from the hot or cold source to the components that require heating or cooling, that is, to construct global and local TMS architectures while treating the component TMS with the cooling load together as one component with characteristics of heat generation and transfer. Therefore, the architecting problem will be focused on the global and the local TMS architectures. It should be noted that even though the architectures of the component TMS will not be constructed, different options of the component TMS will be considered in the architecting process of the global and the local TMS.

As discussed in section 1.1, the thermal management inside the conventional propulsion systems in commercial aircraft such as turbine cooling is out of the scope for this study, because these cooling functions are rather mature and only interact with components inside the engine, which has almost no interactions with other subsystems in the aircraft.

In addition, it should be noted that the controller is also important in the architecture design. However, this study only focuses on steady-state analysis, without considering tran-

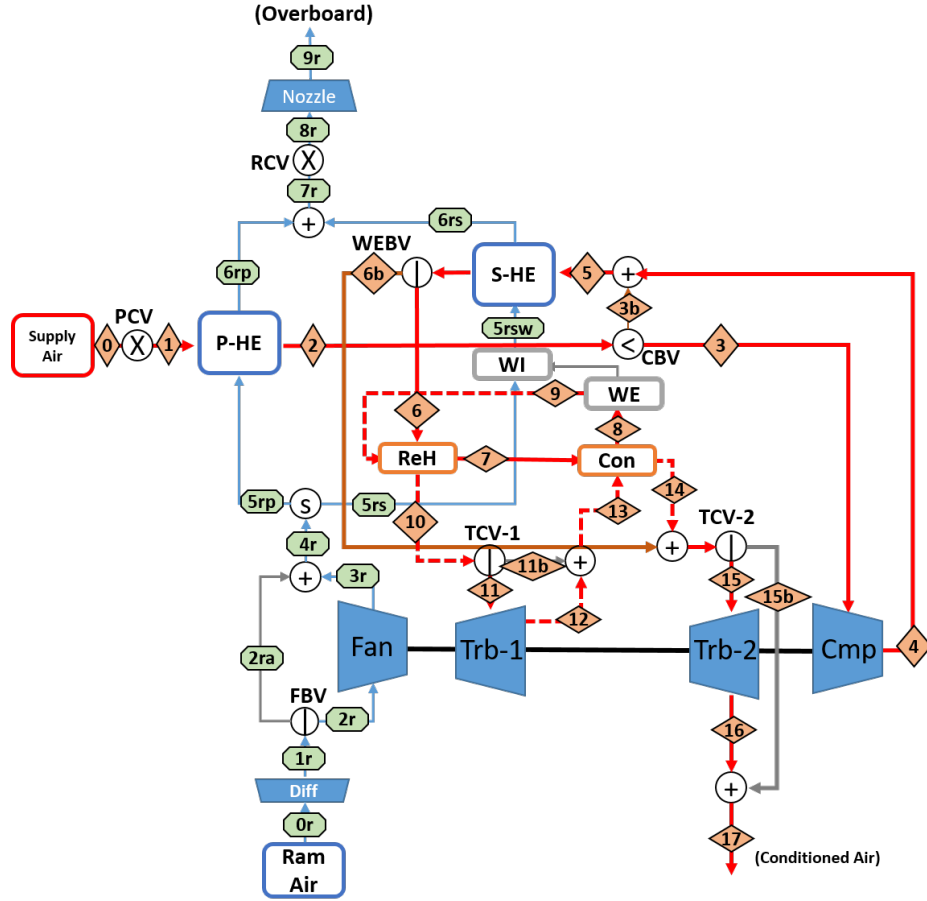


Figure 1.5: Four-wheel condensing air cycle machine [33]

sient analysis. Therefore, the detailed controller architecture will not be studied, although a control logic is implemented to ensure the discharge temperature of a certain TMS to meet the target temperature by controlling the amount of heat sinks/sources that are used by it.

## 1.5 Summary

Thermal management systems in aircraft perform critical functions to ensure suitable operation conditions for the whole aircraft. Traditionally, the architecting of the TMS is performed after the determination of the energy dissipation of other major subsystems. The impacts of the TMS on the aircraft design at early design phase is predicted by using historical data. However, the cooling loads greatly are increasing due to increased power consumption of electronic devices, electrification of subsystems, more application

of composite material. The novel aircraft concepts generating a large amount of heat are also emerging, such as More-Electric Aircraft or All-Electric Aircraft, Turbo-electric Distributed Propulsion System, and supersonic business jets. There is a lack of historical data for such increasing cooling loads and novel aircraft concepts, therefore, the traditional way to consider the TMS in the early design phase may not apply in the future. Therefore, an architecting methodology for the TMS for future commercial aircraft at early design stage without the need of historical data is desired.

## **1.6 Initial Statement of the Overarching Research Objective**

An initial statement of the research objective can be formulated from the observations and challenges presented above for the architecting of the TMS in commercial aircraft:

*To develop a thermal management systems architecting methodology suitable for conceptual design phase of commercial aircraft, which is capable of handling increasing cooling loads and emerging aircraft concepts with limited historical data and only information available during early design stage.*

## **CHAPTER 2**

### **LITERATURE REVIEW**

Before developing the actual method, the existing research and studies have to be reviewed to understand the information required to develop the TMS, capabilities of current architecting methodologies of aircraft thermal management systems, and gaps to achieve the initially proposed research objective in section 1.6. Therefore, some of the notable studies and research related to TMS architecting are reviewed in this chapter.

#### **2.1 Information Required for TMS Architecting**

From research regarding the TMS design and analysis at early design phase, it is discovered that the TMS architecting and analysis always start from the identification of the major heating and cooling loads in the aircraft. Staack [15] and Seki [16] discussed the necessity of application of a vapor cycle into a MEA ECS by firstly identifying the increased cooling load in the cabin. Petly [34] started the TMS research for a Mach 5 cruise aircraft with the understanding of the extreme kinetic heating problem. Donovan [35] began the research on a vehicle-level transient TMS modeling and simulation by defining the major heating sources in the aircraft of interest. Actually, most of all the research regarding the TMS need to identify the major heating and cooling loads, but due to space limitation only some typical studies are presented as examples here. Therefore, it can be concluded that a high-level description of the heating and cooling loads is required for the architecting of TMS.

#### **2.2 Information Required from TMS Architecting**

To identify the information required from the TMS architecting at early design stage, the common methods of aircraft conceptual design are to be reviewed. Traditional aircraft

conceptual design process can be view as three activities by Nam [36]:

1. Power matching: balancing the required power and available power. This can be interpreted as the thrust must be sufficiently produced for certain operation requirements.
2. Energy matching: balancing the required energy and available energy. This can be interpreted as enough fuel has to be carried to perform a complete mission.
3. Volume matching: balancing the required volume and available volume. This requirement is sometimes assumed satisfied implicitly when the aircraft configuration is conventional [13]. However, for novel architectures as mentioned in section 1.3, this activity still needs to be performed.

Common aircraft sizing processes also include Mattingly's method [37] and Raymer's method [38], which are illustrated in Figure 2.1 and Figure 2.2.

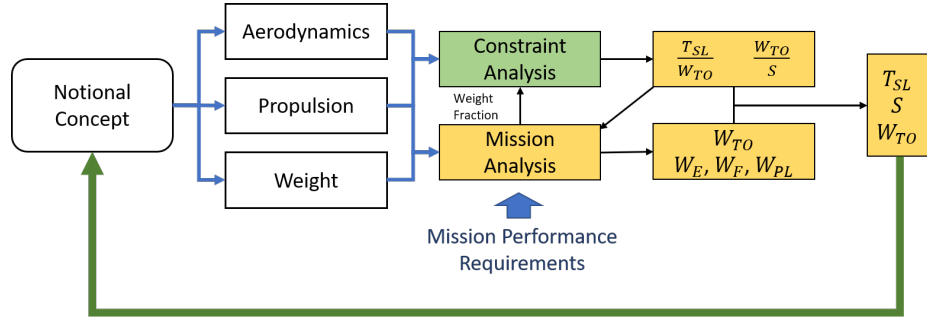


Figure 2.1: Mattingly's Aircraft Design Process [37]

It can be seen from the presented methods from Nam, Mattingly, and Raymer, the aerodynamics, weight, and propulsion are the main three disciplines that required for the conceptual design phase of the aircraft. These three disciplines can be influenced by the characteristics of the TMS, similar to any other subsystems. The subsystem-level impacts were discussed by Moir [2] and Chakraborty [13]: the aerodynamics is affected by the ram drag increased by taking in ram air to the subsystems; the weight is affected by the equipment weight associated with the subsystems; the propulsion is affected by the bleed

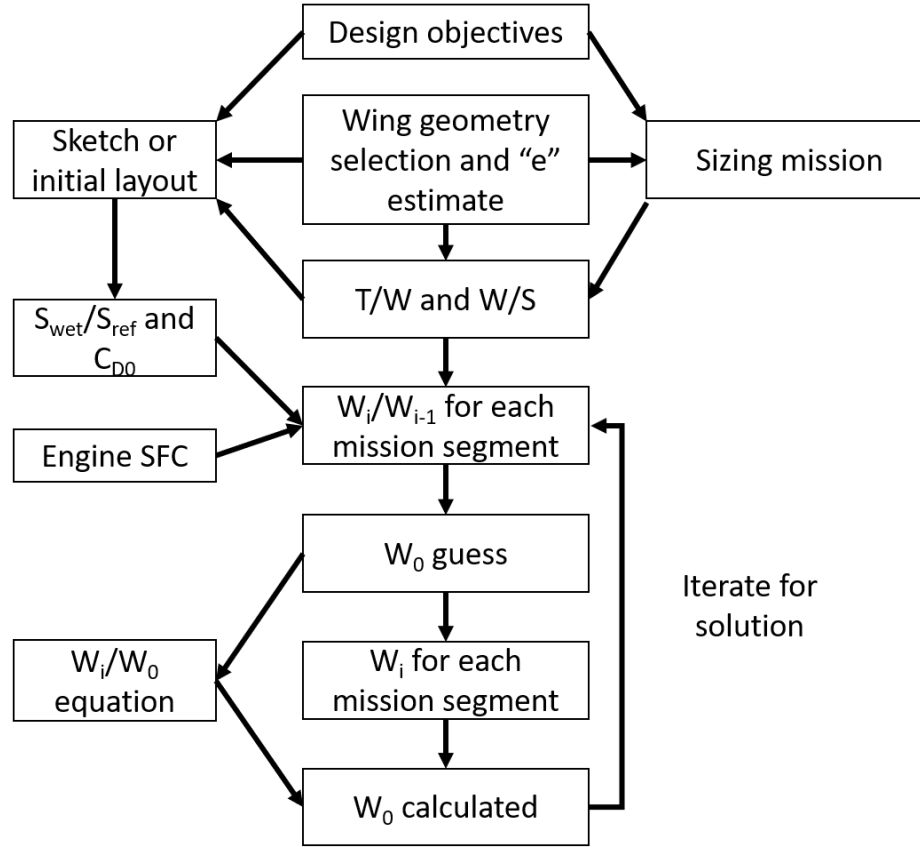


Figure 2.2: Raymer's Aircraft Design Process [38]

and power requirement of subsystems. Therefore, information of these characteristics of the TMS is required for the aircraft conceptual design. Chakraborty [13] also pointed out the design decisions on subsystems themselves would influence the final design decisions of the aircraft, and subsystems including itself and others. However, there is no such literature showing the interactions among designs decisions of the TMS, the vehicle, and other subsystems.

### 2.3 Existing TMS Architecting Research

To acquire the characteristics of an aircraft TMS, the TMS has to be architected, optimized, and sized. Before optimization and sizing of an actual TMS, the architecture should be identified first. This section will go through some notable literature that study the architecture of the TMS.

First of all, some researchers only published the final design of their proposed TMS architectures, along with the analysis of the characteristics of the TMS. However, they did not share the way to generate the alternative TMS architectures or they did not even consider alternative architectures. For example, the ULI program [39] utilized an oil-air cooling TMS, where Polyalphaolefins (PAO) was used as the coolant for motor cooling, and the fan cooling air was extracted to cool the PAO. No other alternatives were proposed initially, but later it was discovered that the this initial design was unable to fully cool the motor during takeoff. Therefore, Shi [39] proposed to include an additional PCM architecture to solve this heating problem. Similarly, Traci [40] conducted research on a TMS integrated to a hybrid electric vehicle, and also demonstrated the capability of the proposed architecture. However, no other candidate architectures were compared. Nuzum [41] also investigated the cryogenic-based TMS at the vehicle level by dynamic modeling a single TMS architecture, which was compared to the only conventional baseline, without showing possibilities of other TMS architectures. McCarthy [42] also did a dynamic modeling of an MEA. However, the focus was on the component modeling, while the overall TMS architecture was fixed to a prescribed one. Kabircitekabir2018investigation did an investigation on a TMS for a hybrid aircraft, focusing on the parameters selection while utilizing a simple architecture. Maser [43] conducted research on TMS design which was integrated to the propulsion system, where the thermodynamic irreversibility was used as the metrics. While Maser's paper gave enough details on the modeling of the components, only one TMS architecture was provided. It can be seen from these literature that there are indeed many existing researches on the TMS, but some of them do not provide any instructions on the selection of the optimal architectures.

Some researchers studied different TMS architectures by investigating different types of heat sinks. Dooley [44] discussed the challenges for heat sinks by reviewing different types of heat sinks and the technologies or fundamental cooling cycles associated with them, but such analyses were at very high level, without providing any guidance for the structural



architecture. Vredenburg [45] investigated the thermal management architectures for fuel cell systems on-board commercial aircraft. Three types of heat sinks and possible heat paths were discussed. However, such choice of heat sinks and heat paths were generated by intuition, potentially missing other viable but non-intuitive architectures in the design space. In addition, Shi [33, 46] and Chakraborty [47, 48] also varied the compressed air source of the cabin ECS to investigate the impacts of the electrification of ECS. Such research on heat sinks provide information about the capability of each type of heat sinks, but the guidance of architecting the heat paths in the TMS is not presented.

Some researchers generated local or global TMS architecture candidates by varying heat paths or types of cooling devices of a basic refrigeration cycle. Chen [49] proposed a highly stable two-phase thermal management system architecture. Several alternative architectures were generated by varying flow paths and adding additional components to an basic two-phase pump cycle. Rheume [50] did the TMS analysis on TeDP aircraft where the ECS for pilot and passengers was not included. The architecture of interest was limited to a combination of oil loop and a coolant loop. Donovan [35] investigated adaptive power thermal management systems. The candidate architectures were TMS's that utilized different pumping systems. Alyanak [51] architected the FTMS where the candidate FTMS architectures were generated by varying the re-circulation paths. Park [52] studied the global TMS architecture for hybrid electric vehicles. Three different global TMS heat paths were generated for the further analysis while leaving the local TMS's pre-selected and fixed. These authors indeed tried to explore the architecture space by constructing multiple architecture candidates, however, the candidate architectures were always pre-selected limited by intuition without a systematic architecting approach. Therefore, some of the viable but non-intuitive architectures may not be identified in the architecture space.

Some researchers focused on the studies of the component TMS capabilities. Fleming [53] researched the some heat tube TMS architectures on high acceleration environment. McCluskey [54] reviewed several thermal management methodologies for turbo-

electric and hybrid electric propulsion, where the methodologies reviewed were specific cooling method such as heat pipe, water spray or phase-change material. However, such research did not discuss the local TMS options associated with these component TMS's.

## **2.4 General Systems Architecting Methods**

From the reviewed research on architecting methodologies of the TMS, it can be discovered that the architecture space was mostly populated through intuitions. Therefore, a systematic approach that is able to generate both intuitive and non-intuitive architectures is required to explore the design space. For this purpose, some general architecting methods are reviewed in this section.

There are four general systems architecting methodologies [55, 56, 57, 58]:

1. Normative: The normative architecting method is a solution-based approach. It is based on the existing solutions to similar problems, such as standards.
2. Rational: The rational architecting method is a method-based approach. It architects the systems relies on the engineering methods such as systems analysis and engineering.
3. Participative: The participative architecting method requires the participation of stakeholders. An example of such method is concurrent engineering and brainstorming.
4. Heuristic: The heuristic architecting method is an approach based on the abstraction of experience.

The normative approach which is based on existing solutions may not apply to novel aircraft concepts and the corresponded TMS architectures. However, standards are still critical in designing the TMS such as the minimum amount of fresh air is required for cabin by regulations, which can determine the types and minimum mass flow rate of heat

sinks used for the ECS. Most of existing research utilized rational method, performing data-based or physics-based analysis on the TMS architecting. However, such method is not able to explore the architecture space, because an architecture has to be established before the actual analysis. The participative method may apply to the TMS architecting by addressing the requirements from different aspects or from different subsystems, which may require a simultaneous development of the TMS along with the vehicle and other subsystems. Even though the heuristics of details of historical TMS architectures may not be suitable for the novel aircraft concepts, the heuristics of fundamental physics will still apply, that is, the cooling and heating requirement will be still fulfilled by obeying laws of thermodynamics. For example, the heat in the aircraft to be rejected has to be removed to somewhere else by doing work, transferring to certain media, or radiation, which follows the first law of thermodynamics. The heat transfer to other media could only happen when the temperature of the heat source is higher than the media, or additional work has to be done to the cooling cycle, which follows the second law of thermodynamics.

A notable approach, Architecture Enumeration and Evaluation (AEE) [59, 60, 61], which was proposed to fully explore the architecture space for general systems, is also reviewed here. The necessity to develop this method was argued by Becz [61] that methods that automatically explore the architecture space must be included due to the limitations of humans to manually search the large number of potential architecture candidates. This method populates the architecture space by identifying the required components first, then enumerate the interactions of each component. This method may apply to the generation of the global TMS architecture once each local TMS is determined, while it may not be suitable for the generation of the local TMS, because the components of a local TMS cannot be identified before determining the type of the fundamental refrigeration cycle and its heat paths. However, AEE method still provides insights on the development of the global TMS, showing that the potential interactions among components can be enumerated.

## 2.5 Existing Evaluation and Sizing Methods for Aircraft TMS

Once the TMS architecture space is explored, an evaluation method is required to compare each candidate to perform optimal architecture down-selection. Some examples of the existing evaluation methods are reviewed. Some authors may evaluate the TMS architectures by experience or intuitions. Vredenburg [45] studied the TMS architectures for fuel cell systems by investigating three types of heat sinks and the several possible heat paths. However, the authors eliminated many possibilities by personal judgment without real analyses, leaving only one architecture was evaluated.

Some authors evaluated the candidate TMS's based on subsystem-level metrics. Homitz [62] compared two-phase pump and vapor cycle using heat sink and cooling load properties instead of vehicle or mission level metrics.

Some authors evaluated different TMS architectures based on system-level performance. Pellegrini [63] compared different ECS architectures based on exergy analysis on cruise condition. Seki [16] assessed a proposed vapor cycle application in the TMS of More-Electric Aircraft by analyzing the fuel consumption at different mission points. Alyanak [51] compared four FTMS architectures based on the additional weight added by each candidate and the fuel consumption at different points.

Some other authors chose mission-level metrics for comparison of different TMS architectures. Roberts [9, 7, 64] investigated the performance of a TMS architecture by integrating it to a Tip-to-Tail aircraft modeling and simulation environment. The TMS architecture was evaluated by analyzing the temperature of each cooling load through a mission, and the total mission fuel burn. Similarly, Bodie [65] studied the thermal analysis solutions based on the temperature of heat sinks and fuel burn through the whole mission. Parrila [66] and Chakraborty [13] assessed different ECS architectures using the block-fuel for given mission.

From these reviewed literature, it is observed that such evaluations are mostly based on

models which has to be sized in terms of certain conditions, and the sizing variables are usually determined by an optimization process. Thus, the research on the optimization and sizing approaches for the TMS are also discussed here. Common optimization objectives may be the aircraft performance metrics at either subsystem level, system level, or mission level. Roberts optimized the TMS by minimizing the mission fuel burn to size the heat exchangers [8]. Rancruel [67] modeled an ECS and integrated it with the vehicle to do the sizing and optimization in terms of weight and mission fuel burn.

The exergy-based methods are also very popular for the TMS optimization and sizing. Figliola [68] proposed an exergy-based method to optimize and size the ECS at the cruise condition. Pellegrini [63] discussed the capability of the exergy-based method by evaluating the ECS performance. Bender [69] evaluated the ECS based on exergy analysis by computing the entropy generation through each component at its cruise point. Pérez-Grande [70] optimized and sized the heat exchanger within a TMS by minimizing the exergy. Following Pérez-Grande, Leo [71] performed a thermoeconomic analysis of the ECS in terms of the exergy using the constructed exergy model.

It should be noted such exergy-based proposed optimization and sizing methods are only conducted at the cruise point, which is difficult to consider the capability of the TMS to handle the worst case during a mission. Therefore, some authors (for example, McCarthy [42], Parrila [66], and Chakraborty [13]) argued that the TMS or ECS should be sized for the worst case where the cooling loads are the highest while the cooling capacity is the lowest. However, approaches that size the TMS for the worst case can lead to suboptimal design in terms of fuel economy.

## **2.6 Architecture Space Narrowing Down Methods - Multifidelity Methods**

The most approaches shown in the previous section require modeling, optimization, and sizing. However, if the number of candidates in the architecture space of TMS is large, the modeling, optimization, and sizing process might be very computationally, especially for

the optimization. Therefore, a method required to narrow down the architecture space. As shown by the work by Garcia [72] to design More-Electric Actuation system from a large architecture space (in the order of  $10^6$ ), the multifidelity method, which tries to improve the accuracy of model estimates while reducing the computational cost by including models of different fidelities, is suitable for evaluation of a large number of architecture candidates. Several notable research on multifidelity concepts are presented.

The management strategies of multifidelity models are distinguished into three categories by Peherstorfer [73]: 1. adaption; 2. fusion; 3. filtering. The adaption strategy uses the information from high-fidelity model to enhance the low-fidelity model. The fusion strategy combine the information from outputs from both low-fidelity and high-fidelity models. The filtering process eliminates inaccurate or inappropriate low-fidelity models and then perform high-fidelity analysis. The filtering strategy applies the most to the research narrowing down the design space and here presents some examples of filtering. Bryson [74] constructed a multifideility framework for aeroelastic vehicle design optimization. A coarse mesh was generated for low-fidelity method first for an initial optimization then followed by a high-fidelity optimization with finer mesh. Böhnke [75] presented a multifidelity design environment which performed the low-fidelity analysis to the aircraft using handbook methods, and then enhance the fidelity with replacement of the parameters in the analysis or even replacement of the methods. Garcia [72], Zeidner [60], Becz [61], and Strauss [59] have performed multifidelity approach to narrow down the architecture space. Most of the architectures were filtered out in terms of feasibility, then a higher fidelity analysis was performed to evaluate the feasible candidates. However, there is no application to the TMS architecture filtering yet.

## **2.7 Summary and Identified Gaps from Literature Review**

### **2.7.1 Summary of Observations**

From the preceding reviewed literature, it can be summarized that:

1. The architecting of the TMS requires a high-level description of heating and cooling loads, and the design of the TMS should provide its influence on the aircraft in three aspects: aerodynamics, weight, and propulsion.
2. Architecting of the TMS will influence the final design decisions on the aircraft, the TMS itself.
3. Most TMS architecture candidates in existing research are generated by adding components or varying heat paths to a fundamental refrigeration cycle.
4. Heating functions are much easier to be realized by using bleed air, electrical heating panel, or existing cooling system to supply hot stream.
5. The candidate architectures are always pre-selected by intuition or experience, without a systematic architecting approach that is able to explore the architecture space by generating both viable intuitive and non-intuitive TMS architectures.
6. From the review of general architecting methods, a desired TMS architecting approach should include normative, rational, participative, and heuristic aspects.
7. Heuristics of fundamental physics may be able to guide the construction of architecture candidates.
8. Existing systems architecting methodologies can enumerate the interactions with identified components, but cannot provide reasonable selections of components.
9. TMS architectures are mostly evaluated based on their influences on subsystem-level, system-level, and mission-level performance, such as subsystem weight, thrust specific fuel consumption at certain operation points, and mission fuel burn.
10. Evaluation approaches that are suitable for conceptual design of novel concepts should not require empirical data, and such methods are always physics-based instead of

statistics-based. However, such physics-based methods are computationally expensive so that they may not be appropriate to apply to a large number of candidate architectures.

11. Evaluation of the TMS requires sizing and optimization, where subsystem-level, system-level, or mission-level metrics could all be chosen as optimization objectives.
12. The sizing, optimization, and analysis of a large number of architectures require the architecture space to be narrowed down. Multifidelity methods may be suitable to narrow down the architecture space, but there is no existing method applied to the TMS yet.

### 2.7.2 Identified Gaps

By looking at the observations from existing studies on the TMS architecting along with the initially proposed research objective, the gaps in methodologies to meet achieve such objective can be identified:

1. Existing TMS architecting methodologies are mostly limited by the intuition and the experience of the authors, and there is not an existing methodology to systematically explore the TMS architecture space by identifying both intuitive and non-intuitive architectures.
2. Optimal TMS architecture down-selection has to be performed with reasonable number of candidate architectures due to expensive computational cost of the sizing, optimization, and analysis process. However, there is not any method suitable for conceptual design phase, which can filter out large number of infeasible TMS architectures, keeping competent candidates for further down-selection of optimal architectures.
3. The influences of the TMS architecting process on the final design decisions of the aircraft and subsystems which include the TMS itself as well as other subsystems are



still unknown from existing literature. Therefore, it is desirable to study the interactions among the designs of the aircraft, the TMS, and other subsystems, which may provide insights on finding optimal designs of novel aircraft concepts that generate a large amount of heat.

## **2.8 Refined Statement of Research Objectives**

To fill the identified gaps between the current methodologies and the proposed research objective with knowledge from the literature, three sub-objectives that support the overarching objective are proposed to refine the original statement. The refined research objectives are stated below:

**Overarching Research Objective:** To develop a thermal management systems architecting methodology suitable for conceptual design phase of commercial aircraft, which is capable of handling increasing cooling loads and emerging aircraft concepts with limited historical data and only information available during early design stage.

**Sub-Objective 1:** To develop a capability of the proposed method that sufficiently explores the thermal management systems architecture space by systematically identifying both intuitive and non-intuitive architectures.

**Sub-Objective 2:** To develop a capability of the proposed method that rapidly narrows down the architecture space to a suitable number of candidates to perform further optimal architecture down-selection in terms of chosen metrics, using information and methods suitable for conceptual design.

**Sub-Objective 3:** To investigate the interactions between the TMS architecting process and the aircraft sizing process.

## CHAPTER 3

### RESEARCH FORMULATION

From chapter 1, the challenges for the TMS architecting are addressed and the overarching research objective is formulated which is to develop a TMS architecting methodology capable of addressing such challenges at early design phase. Existing literature are viewed in chapter 2 to obtain the necessary knowledge and identify the gaps in current methodologies to realize this objective, and three sub-objectives are formulated to support the overarching objective. In this chapter, the research objectives are restated in section 3.1, and research questions that must be addressed to achieve the objectives are presented in section 3.2. The hypotheses to answer the research questions are stated in section 3.2 along with an overview of the design of experiments proposed to demonstrate such hypotheses. The formulation of the hypotheses are also discussed with an overview of the design of experiments is presented in this chapter. Greater details of the design of experiments and the experimental methodologies to conduct these experiments will be shown in subsequent chapters.

#### 3.1 Research Objectives

The research objectives for this thesis have been presented in section 2.8, and they are restated here as a guideline for this chapter followed by the discussions that lead to these objectives:

**Overarching Research Objective:** To develop a thermal management systems architecting methodology suitable for conceptual design phase of commercial aircraft, which is capable of handling increasing cooling loads and emerging aircraft concepts with limited historical data and only information available during early design stage.

**Sub-Objective 1:** To develop a capability of the proposed method that sufficiently explores the thermal management systems architecture space by systematically identifying

both intuitive and non-intuitive architectures.

**Sub-Objective 2:** To develop a capability of the proposed method that rapidly narrows down the architecture space to a reasonable number of candidates to perform further optimal architecture down-selection in terms of chosen metrics, using information and methods suitable for conceptual design.

**Sub-Objective 3:** To investigate the interactions between the TMS architecting process and the aircraft sizing process.

The overarching objective is motivated by the appearing challenges for the TMS architecting. These challenges include greatly increased cooling loads as well as the emerging of new aircraft concepts accompanied with a large amount of heat generation. Traditional approach for architecting the TMS may be no longer applicable in the future due to lack of historical data for such design conditions.

The sub-objective 1 is motivated by the observation that there is not any methodology that can systematically generate intuitive and non-intuitive thermal management system architectures, which are potentially feasible for given heating and cooling load requirements. Without sufficiently exploring the architecture space, suboptimal design decisions might be easily reached which will further degrade the vehicle-level and mission-level performance of the aircraft.

The sub-objective 2 is motivated by the observation that the number of generated architectures might be too large to be evaluated by usual comparing approaches such as comparing the weight, or power consumption of each architecture, or comparing mission-level metrics such as mission block fuel with certain architecture due to computational cost. Meanwhile, the evaluation process should be capable of handling new thermal management requirements with limited empirical data. However, there is not any existing evaluation approach appropriate to narrow down the TMS architecture space for further study.

The sub-objective 3 is motivated by the fact that the thermal management solution may influence the vehicle design greatly by adding additional weight or ram drag, or extracting

more bleed or power. Such impacts can lead to a large change in the sizing parameters which could further influence the design decisions on the TMS in return. However, no literature has shown the interactions among the design of the aircraft, the TMS, and other subsystems.

## 3.2 Research Questions

Each of the sub-objective is addressed by one research question. The research questions and the formulation of the research questions are presented in this section.

### 3.2.1 Research Question 1

The research question 1 is asked to address the sub-objective 1:

**Sub-Objective 1:** To develop a capability of the proposed method that sufficiently explores the thermal management systems architecture space by systematically identifying both intuitive and non-intuitive architectures.

The research question 1 is stated as:

**Research Question 1:** *With given potential heating and cooling load descriptions and aircraft concepts, how can the thermal management systems architecture space be populated, without over-conservatism that eliminates unconventionally but potentially optimal architectures?*

The first research question is formulated by asking how to populate the architecture space to reach the goal of sub-objective 1. To realize the capability of systematically identifying both intuitive and non-intuitive architectures while exploring design space, the elimination of over-conservatism is posed as a constraint to the question. As shown from the literature review, heating and cooling loads and aircraft concepts are required to architect the TMS, such information is provided as premises for this question. It should be noted that such premises can be identified by integration of the TMS architecting process with aircraft design loop, which will be discussed research question 3.

### 3.2.2 Research Question 2

The research question 2 is asked to address the sub-objective 2:

**Sub-Objective 2:** To develop a capability of the proposed method that rapidly narrow down the architecture space to a suitable number of candidates to perform further optimal architecture down-selection in terms of chosen metrics, using information and methods suitable for conceptual design.

The research question 2 is stated as:

**Research Question 2:** *With a number of thermal management systems architecture candidates, how can the architecture evaluation process rapidly filter out inviable architectures, and perform further down-selection of optimal architectures on the left competent architectures based on chosen metrics, where the information required are suitable for conceptual design phase with limited historical data.*

A physics-based evaluation method is desired due to lack of historical data. However, it is impractical to evaluate a large number of architecture candidates due to excessive computational expense. Therefore, it is important to filter out a great number of inviable architectures before application of physics-based method. Then a proper method should be selected to perform further down-selection in higher fidelity. Based on these discovered requirements to meet the sub-objective 2, the research question is formulated.

### 3.2.3 Research Question 3

The research question 3 is asked to address the sub-objective 3:

**Sub-Objective 3:** To investigate the interactions between the TMS architecting process and the aircraft sizing process.

The research question 3 is stated as:

**Research Question 3:** *How can the interactions of thermal management systems architecting process and aircraft sizing process be identified, what are the differences between the initial solutions before resizing and the final converged solutions of both the aircraft*

*and the TMS, and how to explain such differences?*

The aircraft heating and cooling loads requirements are generated from the initial design of the aircraft, which determines the architecture of the TMS, while the characteristics of the TMS will also have impacts on the design of the aircraft and other subsystems. Then the new design of aircraft will update the heating and cooling loads requirements which may change the design of the TMS. Thus the design process of the aircraft, the TMS, and other subsystems is iterative in such a manner until the solutions are converged. However, there is no existing literature to show or to study the interactions of the design of the TMS and the aircraft. Therefore, the research question 3 is formulated to address these gaps.

### **3.3 Mappings of research questions, hypotheses, and experiments**

An overall mapping of the research questions, hypotheses, and the corresponded experiment sets are illustrated in Table 3.1, where each hypothesis is mapped to address one of the research questions and each set of experiments is planned to demonstrate each of the hypotheses. The details of the hypotheses with the corresponded formulation process and an overview of the experimental plan will be discussed in following sections. The details of experiments and the experimental methods will be discussed in chapter 4, chapter 5, and chapter 6.

Table 3.1: Mapping of research questions (RQ), hypotheses (H), and experiment sets (E)

Research Question	Hypothesis	Experiment Set
RQ 1	H 1	E 1.1
		E 1.2
RQ 2	H 2	E 2.1
		E 2.2
		E 2.3
		E 2.4
		E 2.5
RQ 3	H 3	E 3

### 3.4 Hypothesis 1 and Design of Experiment Set 1

The Research Question 1 is re-stated here, which is to be addressed by Hypothesis 1:

**Research Question 1:** *With given potential heating and cooling load descriptions and aircraft concepts, how can the thermal management systems architecture space be populated, without over-conservatism that eliminates unconventionally but potentially optimal architectures?*

#### 3.4.1 Formulation of Hypothesis 1

Some of the content in this section has already been discussed in the author’s previous publication [32]. The content is used here to address how the hypothesis 1 is reached.

##### *Architecture Generation Guidance*

From the literature review, the TMS architectures are initially generated by guidance of heuristics or experience in existing solutions. However, too detailed heuristics or experience, such as “supersonic aircraft has to use vapor cycle”, or “hydraulic fluid should be cooled by fuel”, can greatly limit the types of architecture candidates, leading to architectures only generated by intuition or experience.

However, it is also observed that all the local TMS architectures either directly reject heat to the other media based on temperature gradient or follow the fundamental refrigeration cycle, which is stated by the second law of thermodynamics. The fundamental refrigeration cycle mentioned here refers to the cycle that requires energy to reject heat from a low temperature source to higher temperature medias. The alternative architectures are generated by varying components or heat paths. The varied components or heat paths are still served to the same cooling behavior for the fundamental cycle. For example, the compression behavior is required to lift the thermal state of the hot stream in the cooling cycle, and an expansion behavior is required to expand the hot stream for further cooling,

and the compression behavior can be realized by turbine-driven compressors or electrical compressors, and the expansion process can be realized by turbine or expansion valve. From this example, it can be seen that even the types of component utilized in the cooling cycle are different, the same behavior is performed. Therefore, a hypothesis can be made for the guidance of generating local TMS architectures: **all local TMS architectures reject heat following the behaviors of fundamental refrigeration cycles or behaviors of direct heat rejection based on temperature gradient.**

The global TMS is defined as the system that arranges the interactions between each local TMS and heat sinks as in chapter 1. The arrangement are determined by the behaviors of the local TMS in terms of the requirement for heat sinks and the type of cooling cycles. For example, if one of the local TMS requires ram air as heat sink and produces exhaust and another local TMS requires exhaust for cooling, these two TMS's can be linked by routing the exhaust from the first local TMS to the latter one. Another example is that if two local TMS's require vapor cycle cooling, then these two TMS's may be cooled by the same vapor cycle. Therefore, a hypothesis can be made for the guidance of the global TMS architecting: **all global TMS's link their local TMS by following behaviors of each local TMS in terms of required heat sinks and applied thermal cycles..**

### *Architecture Enumeration*

Assuming the architecture can be generated by following the behavior, an enumeration method is still required. The enumeration method presented in previous studies [59, 60, 61] enumerates the interactions, which requiring the a determined set of components. However, the behaviors are used instead in this study to construct the TMS architectures, and the behavior options at one point are always constrained by the preceding behaviors in a cooling cycle. Therefore, a hypothesis for the architecture enumeration can be formulated: **the architecture can be enumerated by trying each options of behaviors as well as satisfying the compatibility among each of the behaviors.**



### *Validation of Hypothesis 1*

If the behavior-based process as stated in subsection 3.4.1 for the construction of architectures is valid, it is expected that some of the generated architecture should match the existing TMS solutions, while the others are quite different but also perform reasonable thermal management functions. It is also expected that the number of architectures from the architecture populating process should be much more than the TMS architectures shown in past studies. The stated hypothesis can be validated if the following capabilities can be achieved:

1. With the same heating and cooling load requirements and aircraft concepts, some of the local TMS architectures will match the existing local ones.
2. With the same heating and cooling load requirements and aircraft concepts, some of the global TMS architectures constructed by integration of generated local TMS architectures will match the existing global ones.
3. With the same heating and cooling load requirements and aircraft configurations, local and global TMS architectures that are different from existing ones can be generated, and they must follow the fundamental thermal cycle behavior (fundamental thermal cycle).
4. The number of architectures generated through the proposed methodology is much larger than the one from previous studies.

#### 3.4.2 Statement of Hypothesis 1

Combining all the hypotheses made and validation requirements in preceding discussions, the hypothesis 1 can be formulated as:

**Hypothesis 1:** The architecture space of thermal management system architectures can be populated without over-conservatism by using a behavior-based backtracking thermal

management system architecting methodology.

### 3.4.3 Overview of Experiment Set 1

An overview of Experiment Set 1 is discussed here, and the details of the corresponding design of experiment and the experimental methodology will be discussed in chapter 4.

**Experiment 1.1 - Local TMS Architecting:** Generate the local TMS's for given local cooling/heating requirements using the proposed TMS architecting method. The aircraft concepts selected to perform this experiment are: a More-Electric Aircraft, a 300-pax N3-X-like TeDP aircraft, and 78-pax Hybrid TeDP aircraft. Then compare the generated local TMS architectures with existing ones.

- **Overview of E 1.1:** The local thermal management requirements may include the maintain suitable temperature for the following subsystems:

1. Cabin
2. Avionics
3. Electronics
4. Battery
5. Electric propulsion systems
6. Hydraulic systems
7. Fuel and fuel tank
8. Other subsystems with specified cooling/heating requirements

**Experiment 1.2 - Global TMS Architecting:** Generate the global TMS's for given set of candidate TMS's using the proposed TMS architecting method. The aircraft concepts selected to perform this experiment are: a 160-pax conventional aircraft, a 300-pax TeDP concept, and a 78-pax HTeDP concept. Then compare the generated global TMS architectures with existing ones.

- **Overview of E 1.2:** The generated architectures from E 1.1 are used as candidates for each local TMS. Then global TMS architectures are constructed using such candidates. Generated global TMS architectures are compared to existing ones for similar thermal management requirements and aircraft concepts. Some of the generated architectures are expected to be similar to the existing ones while others are expected to be much different.

### 3.5 Hypothesis 2 and Design of Experiment Set 2

The Research Question 2 is stated here, which is to be addressed by Hypothesis 2:

**Research Question 2:** *With a number of thermal management systems architecture candidates, how can the architecture evaluation process rapidly filter out inviable architectures, and perform further down-selection of optimal architectures on the left competent architectures based on chosen metrics, where the information required are suitable for conceptual design phase with limited historical data.*

#### 3.5.1 Formulation of Hypothesis 2

##### *Infeasible Architecture Filtering*

The TMS architecture evaluation and down-selection approaches existing in past studies are mostly based on subsystem-level, system-level, or mission-level metrics. To obtain such metrics with limited historical data, physics-based methods are popular among researchers. However, the computational cost for physics-based optimization, sizing, and analysis is too high to be practical. Inspired by multi-fidelity methods, the filtering strategy seems viable to solve the problem. The low-fidelity filtering process can be applied to greatly reduce the number of inviable number of architecture candidates. The metrics selected for the filtering process may be the feasibility, argued by other researchers [72, 59, 60, 61]. However, their proposed feasibility tests were based on the compatibility of the generated architectures, which is already guaranteed by the approaches done in Experiment set 1 in this study. Re-

alizing that the TMS should be capable of handling the extreme flight conditions during the mission, the feasibility criterion for this study is chosen as the capability to provide sufficient cooling/heating at the worst flight conditions. Therefore, the hypothesis for the filtering process can be made: **the filtering process in terms of the feasibility to handle extreme flight conditions can greatly reduce the number of candidate TMS architectures.**

#### *Down-Selection of Optimal TMS Architectures*

After the feasibility filtering, the remaining number of candidates might be still large, therefore, a low-fidelity evaluation process without construction of models is still required to further narrow down the design space. The subsystem key performance indicators (KPI) can be used to conduct such analysis. KPI may include the component weight, bleed and power requirement. Such metrics can be estimated using heating and cooling loads requirements and empirical performance data for components such as turbomachines, heat exchangers, heat sinks, and etc., which are commonly accessible, although the data for the overall novel TMS architectures is almost non-existent. The KPI-based filtering process is achieved by clustering, where only clusters at the Pareto front are considered optimal. Then the architectures with rather optimal KPI will be selected for physics-based optimization, sizing, and analysis in terms of chosen metrics for higher-fidelity evaluation.

Thus the hypothesis for down-selection of optimal TMS architectures process can be formulated: **clustering-based low-fidelity analysis on subsystem level will further reduce the number of architecture candidates. Further physics-based optimization, sizing, and analysis can be conducted to evaluate the candidates in terms of chosen metrics at subsystem, system, or mission level.**

### *Creation of Physics-based Models*

Physics-based optimization, sizing, and analysis requires physics-based models, however, the architectures generated from Experiment Set 1 might be only a description of the heat paths, heat sinks, and applied components, instead of a model. An automated model construction process which enables the model to be created from the architecture description will fill such a gap. Therefore, the hypothesis of physics-based model creation can be stated: **An automated model construction process will enable the creation of physics-based models from the architecture descriptions.**

### *Validation of Hypothesis 2*

If large number of inviable architecture candidates can be eliminated from the feasibility-based low-fidelity KPI-based filtering process, then the capability of the proposed approach in Hypothesis 2 to narrow down the architecture space is validated. If the model can be automatically constructed from the architecture descriptors generated from Experiment Set 1, which the optimization and sizing process can be directly performed on, then the optimal down selection approach in Hypothesis 2 is validated.

#### 3.5.2 Statement of Hypothesis 2

Combining preceding hypotheses and validation requirement, the hypothesis 2 can be formulated as:

**Hypothesis 2:** Large number of inviable architectures can be eliminated by filtering process in terms of feasibility and low-fidelity subsystem-level analysis on key performance indicators, and further down-selection of optimal architectures can be done by evaluations using physics-based optimization, sizing, and analysis, where the physics-based models are created automatically from the architecture descriptions.

### 3.5.3 Overview of Experiment Set 2

An overview of Experiment Set 2 is presented here, and greater details of the design of experiment and experimental methodologies are discussed in chapter 5.

**Experiment 2.1:** Filter out inviable TMS architectures based on feasibility of each TMS architecture to handle the thermal management requirements at the extreme flight conditions where the cooling loads are the largest.

- **Overview of E 2.1:** The feasibility of each TMS is tested to show if the TMS can fulfill the thermal management requirements. Temperature, volume, and component performance limitations are used as the criteria for testing the feasibility. Infeasible TMS architectures will be eliminated from the architecture space. Most critical operation conditions are chosen to check the TMS feasibility.

**Experiment 2.2:** Verify if subsystem-level KPI of each TMS architectures can be rapidly analyzed using low-fidelity method.

- **Overview of E 2.2:** The weight, ram drag, amount of bleed extracted, and power consumption are estimated using low-fidelity analysis, without creating detailed physics-based models. Historical data on parameters such as power-to-weight ratio, effectiveness, heat capacity of heat sinks are used for the analysis because such kinds of data for the components are easily accessible even though there is a lack of data on the overall architecture of the TMS for novel aircraft concepts.

**Experiment 2.3:** A clustering-based filtering process is performed based on the KPI on the TMS architecture candidates.

- **Overview of E 2.3:** The architectures are grouped into different sets in terms of the similarity of the KPI. The sets of architectures that are non-competent are eliminated.

**Experiment 2.4:** Automatically create physics-based TMS models from the architecture descriptions generated from the Experiment Set 1.

- **Overview of E 2.4:** Automated process is utilized to create physics-based TMS models from the architecture descriptions. In this context, a description of a TMS is in the form of list, which is able to give enough information to construct a TMS model. The detailed rules to translate the list to the actual architecture models will be discussed in chapter 4, where the Research Question 1 is answered.

**Experiment 2.5:** Perform optimization, sizing, and analysis using physics-based modeling and simulation. The optimal architectures are selected based on chosen metrics.

- **Overview of E 2.5:** The constructed physics-based models from the Experiment 2.4 are used to perform optimization, sizing, and analysis. The metrics for selection of the optimal architectures can be subsystem-level such as architecture weight, system-level such as thrust specific fuel consumption at certain mission points, or mission-level such as mission fuel burn.

### 3.6 Hypothesis 3 and Design of Experiment Set 3

The Research Question 3 is stated here, which is to be addressed by Hypothesis 3:

**Research Question 3:** *How can the interactions of thermal management systems architecting process and aircraft sizing process be identified, what are the differences between the initial solutions before resizing and the final converged solutions of both the aircraft and the TMS, and how to explain such differences?*

#### 3.6.1 Formulation of Hypothesis 3

##### *Interactions of Designs of the TMS, the Aircraft, and Other Subsystems*

The research questions, hypotheses, and experiments in preceding discussion are all to architect the TMS architecture based on fixed thermal management requirements and aircraft concepts, which can be viewed as a retrofit process without feedback to the initial heating and cooling load descriptions and aircraft design. However, the design of the TMS is

similar to any other subsystems that it can influence the aircraft design in return, and may update the thermal requirements. As argued by Chakraborty [13], the interactions among the aircraft and subsystems can be identified through integration of the subsystems design to the aircraft design process. The design solutions through the integrated process are expected to vary until the convergence is reached. Therefore, the hypothesis can be stated: **the interactions of the design of the TMS can be identified by integrating the TMS architecting process into the aircraft design loop, and the differences can be explained by comparing different design solutions through the design loop.**

#### *Validation of Hypothesis 3*

The capability to feedback the influence of TMS architecting to vehicle level can be validated if the proposed integration methodology can update the design requirements for the aircraft, the TMS, and other subsystems, in terms of the initially designed TMS, thus leading to a design loop. The capability to compare the converged design solutions from the design loop with the ones generated using initial design requirements can be validated if the differences and corresponding explanations for such differences can be identified through the integrated analysis.

#### 3.6.2 Statement of Hypothesis 3

From the preceding discussions, the hypothesis 3 can be formulated as:

**Hypothesis 3:** The interactions of thermal management systems architecting process and design of aircraft can be identified by integration of the thermal management systems architecting process into the aircraft design loop, and differences between the converged design solutions and the initial solutions from the design loop can be discovered and explained through the proposed integrated process.



### 3.6.3 Overview of Experiment Set 3

The overview of Experiment Set 3 is shown in this section, and the detailed experiment design and experimental method for this set of experiments will be discussed in detail in chapter 6.

**Experiment 3:** Integrate the TMS architecting process into the design loop of the aircraft, and observe the differences of design solutions through the design loop. The concepts of interest are as presented before, a 160-pax conventional aircraft with possibility to electrify the subsystems (such as MEA), a 300-pax N3-X-like TeDP, and a 78-pax HTeDP. The integration environment and the vehicle models are constructed first without the TMS, then the TMS architecting process are integrated into them.

- **Overview of E 3:** With the initial requirements and heating and cooling load descriptions, the TMS is architected and sized, and then the characteristics of the TMS are fed into the vehicle level to perform resizing of the aircraft. After the design loop is converged, the design solutions then can be identified and compared to the initially architected solutions. This integrated process will be conducted in a 160-pax conventional aircraft, a 300-pax TeDP concept, and a 78-pax HTeDP concept.

## CHAPTER 4

### EXPERIMENT SET 1 - EXPLORING THE ARCHITECTURE SPACE

In this section, a detailed design of Experiment Set 1, the experimental methodology, and the results obtained from the Experiment Set 1, are discussed. The design of Experiment Set 1 is presented first. Then the behavior-based TMS architecting method is shown, where behavior-based idea is discussed, and the heuristics to guide the behaviors are described, following which the concept of backtracking is introduced to enumerate the architectures. Next, examples of local and global TMS's are shown to illustrate the application of the methodology. Finally, the results obtained using the proposed behavior-based TMS architecting method are used to validate the Hypothesis 1, which answers the Research Question 1. Most of the content in this chapter has already been published by the author [32].

This chapter is organized as follows: the detailed design of Experiment Set 1 is firstly discussed in section 4.1, along with the cases of interest to run through the experiments; then the behavior-based backtracking architecting methodology is presented in section 4.2; the behaviors of the local TMS and the global TMS in this document are described next in section 4.3 and section 4.4, with examples to illustrate how the proposed methodology is used to architect based on given behaviors; then the results obtained from Experiment Set 1 are shown in section 4.5, which validates Hypothesis 1; finally, the conclusions are drawn in the last section, section 4.6, in this chapter.

#### 4.1 Design of Experiment Set 1

##### 4.1.1 Overview of Research Questions 1, Hypothesis 1, and Design of Experiment Set 1

The Experiment Set 1 along with the Research Question 1 and Hypothesis 1 are restated here as a guidance for the development of the proposed architecting methodology:

**Research Question 1:** *With given potential heating and cooling load descriptions and aircraft concepts, how can the thermal management systems architecture space be populated, without over-conservatism that eliminates unconventionally but potentially optimal architectures?*

**Hypothesis 1:** The architecture space of thermal management system architectures can be populated without over-conservatism by using a behavior-based backtracking thermal management system architecting methodology.

The initial formulation of Experiment Set 1 are stated as:

**Experiment 1.1:** Generate the local TMS's for given local cooling/heating requirements using the proposed TMS architecting method. The aircraft concepts selected to perform this experiment are: a More-Electric Aircraft, an aircraft with turbo-electric distributed propulsion system, and a supersonic business jet. Then compare the generated local TMS architectures with existing ones.

**Experiment 1.2:** Generate the global TMS's for a given set of candidate TMS's using the proposed TMS architecting method. The aircraft concepts selected to perform this experiment are: a More-Electric Aircraft, an aircraft with turbo-electric distributed propulsion system, and a supersonic business jet. Then compare the generated global TMS architectures with existing ones.

#### *How Experiment Set 1 Is Used for Validation of Hypothesis 1*

If the results obtained from the Experiment Set 1 can demonstrate the following capabilities of the proposed methodology, then the Hypothesis 1 is valid:

1. With the same heating and cooling load requirements and aircraft concepts, some of the local TMS architectures will match the existing local ones.
2. With the same heating and cooling load requirements and aircraft concepts, some of the global TMS architectures constructed by integration of generated local TMS architectures will match the existing global ones.

3. With the same heating and cooling load requirements and aircraft configurations, local and global TMS architectures that are different from existing ones can be generated, and they must follow the fundamental cooling cycle behavior (fundamental refrigeration cycle).
4. The number of architectures generated through the proposed methodology must be much larger than the one from previous studies.

#### 4.1.2 Concepts of Interest in Experiment Set 1

As mentioned before, the concepts of interest to perform the behavior-based architecting method are chosen to be: a 160-pax conventional aircraft with potential to electrify subsystems, a 300-pax N3-X-like TeDP, and a 78-pax HTeDP as shown in ULI program. The corresponding heating and cooling loads with the design characteristics for these concepts are discussed in the following subsections.

##### *160-PAX Conventional Aircraft*

The aircraft design specifications are presented in Table 4.1, which has been used to conduct ECS studies by the author in previous work [46]. This aircraft is a Small Single-aisle Aircraft (SSA) [76]. The concept is allowed to be made as a conventional aircraft or an MEA aircraft. Thus, the available heating sources are the high pressure compressor (HPC) extracted bleed, electrical heating, and electrically compressed ram air. The available heat sinks are the cooled HPC extracted bleed, electrically compressed ram air, ram air, fan bleed, fuel, oil, refrigerants, cooling fluid, and phase change material (PCM). The major components need to be cooled are: cabin, avionics, hydraulics, fuel, engine oil, and generators (either mounted on the engine or the auxiliary power unit (APU)). The major components need heating are: cabin and wing ice protection system. This concept is selected to show potential different TMS's for an conventional aircraft, with the possibility to electrify subsystems. If the subsystems are allowed to be electrified, then a significant

difference compared to a conventional commercial aircraft in TMS is that the ECS can take electrically compressed air instead of extracted bleed from the engine.

Table 4.1: Design specifications of the 160-pax conventional aircraft

<b>Parameters</b>	<b>Value</b>
Passenger capacity	160
Design payload weight, lbm	33 600
Design range, nmi	3020
Cruise Mach number	0.78
Maximum cruise altitude, ft	41 000
Maximum payload weight, lbm	47 000

### *300-PAX TeDP*

The design specifications of the N3-X-like 300-PAX TeDP are listed in Table 4.2. The configuration is shown in Figure 4.1. This concept utilizes a hybrid wing body (HWB) configuration, where 14 electric ducted fan (driven by 14 electric motors) are distributed along the rear part of the fuselage. Two turbo-shaft generators are placed at the two wingtips. The major heating sources are the same as the conventional aircraft: HPC extracted bleed, electrical heating, and electrically compressed ram air (assuming subsystems can also be electrified in the TeDP configuration). The available heat sinks are cooled HPC extracted bleed, electrically compressed ram air, ram air, fan bleed, fuel, oil, refrigerants, cooling fluid, PCM, and cryogenic refrigerant. Strictly speaking refrigerant used for cryogenic cooling is a type of refrigerant. However, its properties are quite different from the usual refrigerant, so it is listed separately. The largest differences in the types of load that need cooling compared to the conventional or MEA aircraft is the electrified propulsion system: the motors to drive the distributed ducted fans and the turboshaft generators.

### *78-PAX HTeDP*

The design specifications of the HTeDP concepts are shown in Table 4.3, of which the model was constructed by the authors in previous work [39] for the ULI program. This

Table 4.2: Design specifications of the N3-X-like TeDP concept [23, 77]

Parameters	Value
Passenger capacity	305
Design payload weight, lbm	64 000
Design range, nmi	7530
Cruise Mach number	0.84
Maximum cruise altitude, ft	43 000

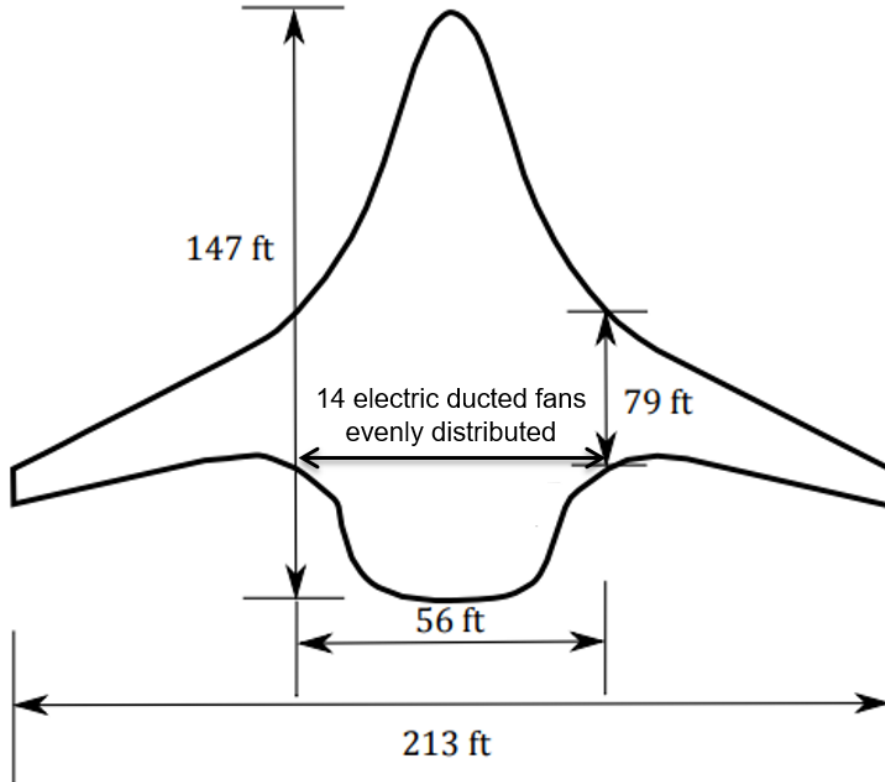


Figure 4.1: 305-PAX TeDP concept configuration [23, 77]

configuration has eight electric fans to produce the thrust. A turboshaft engine is mounted on each wingtip to produce the required electric power. The available heating sources are the HPC extracted bleed, electrical heating, and electrically compressed ram air. The available heat sinks are the cooled HPC extracted bleed, electrically compressed ram air, ram air, fan bleed, fuel, oil, refrigerants, cooling fluid, and PCM. Since the ULI program requires non-cryogenic cooling options, the cryogenic refrigerant are removed from the available heat sinks. The major components need to be cooled are: cabin, avionics, hydraulics, fuel,

oil, battery, buses and control panels, generators (mounted on the turboshaft engines), and motors to drive the electric fans. The major components need heating are: cabin and wing ice protection system. A notional visualization is illustrated in Figure 4.2. The feature that distinguishes this concept from the previous All-Fuel TeDP is the added large battery, which should be able to supply enough energy due to specified hybridization schedule. Thus, this battery becomes a new outstanding cooling load in terms of the TMS compared to the All-Fuel TeDP.

Table 4.3: Design specifications of the HTeDP concept

Parameters	Value
Passenger capacity	78
Design payload weight, lbm	18 060
Design range, nmi	1980
Cruise Mach number	0.80
Maximum cruise altitude, ft	41 000
Maximum payload weight, lbm	23 350

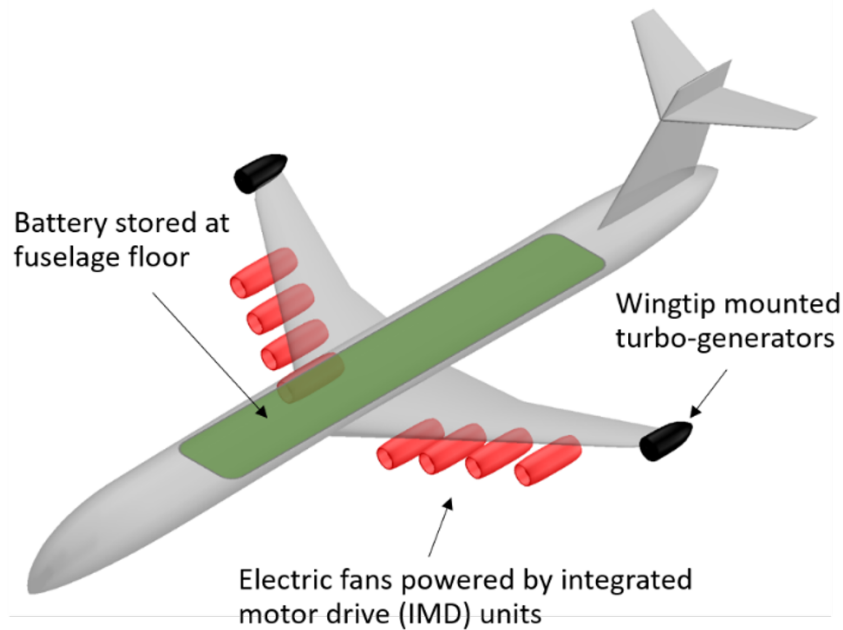


Figure 4.2: HTeDP configuration for the ULI aircraft [28, 29]

#### 4.1.3 Experimental Cases for Local TMS - Experiment 1.1

To validate Hypothesis 1 and the proposed behavior-based architecting methodology for the local TMS, representative local loads are selected to perform the architecture populating process. From the preceding discussions, the loads that stand out for the selected concepts, conventional/MEA, TeDP, and HTeDP, are the cabin, electric motor, and the battery. Therefore, these three types of loads are chosen to perform the architecture populating. In the current stage, there is no need for the detailed performances for the loads, only simple requirements on the heat sinks are used.

##### *Cabin*

The major heating sources from the cabin are the metabolic heat from passengers and the heat generated by avionics and entertainment systems. As specified in Federal Aviation Administration (FAA) regulation [78], the minimum amount of the fresh supply air is 0.55 lb/person/min. Meanwhile, the cabin supply air needs to perform sufficient pressurization. Therefore, the air must be pressurized, as well as taken from the fresh source (outside). Thus, the heat sink for the cabin must be charged fresh air, either the engine bleed or the electrically compressed ram air.

##### *Electric Motor*

Generally the electric motor will either be cooled by non-cryogenic or cryogenic approaches. In the non-cryogenic approaches, the motor is cooled usually by certain types of oil which cools and lubricate the motor at the same time. Regarding the cryogenic approaches, there is no such application in aircraft yet. Thus, the electric motor with cryogenic cooling is assumed to be submerged in the cooling liquid, as studied in the literature [79].



### *Battery*

According to the ULI program[28, 29], the battery can be viewed as a load that gradually accumulate the heat, and the temperature of it can increase until reaching its temperature limit. This means that through the mission, the heat generation can be larger than the cooling capability at certain operation conditions, if the accumulated heat does not make the temperature over its limit. For such type of load, there is no specific cooling requirement. Therefore, any types of the TMS can be considered. However, it should be noted that since the ULI program does not allow for cryogenic cooling, the battery must be cooled by non-cryogenic approaches.

#### 4.1.4 Experimental Cases for Global TMS - Experiment 1.2

For the validation of the proposed methodology for the global TMS architecting, the three concepts mentioned before are also selected, with all the potential local loads. Then the local TMS's generated in Experiment 1.1 are used to populate the global TMS architectures for Experiment 1.2. However, it should be noted that the number of architectures generated in Experiment 1.1 is too large to be fully enumerated, which will be shown in the results section of the Experiment Set 1. Therefore, only a few candidates are selected in this experiment to demonstrate the capability of the global TMS architecture populating. In application, the filtering method in Experiment Set 2, which will be discussed in chapter 5, is used to effectively reduce the number of candidates. These details will be shown as we go through the Experiment Set 2. And the integrated application of the architecting method will be shown in the Experiment Set 3, which will be presented in chapter 6.

## **4.2 Experimental Methodology: Behavior-Based Backtracking Architecting**

### 4.2.1 Information Needed for TMS Architecting

From research regarding the TMS design and analysis at early design phase, it is discovered that the TMS architecting and analysis always start from the identification of the major heating and cooling loads in the aircraft. Staack [15] and Seki [16] discussed the necessity of application of a vapor cycle into a MEA ECS by firstly identifying the increased cooling load in the cabin. Petly [34] started the TMS research for a Mach 5 cruise aircraft with the understanding of the extreme kinetic heating problem. Donovan [35] began the research on a vehicle-level transient TMS modeling and simulation by defining the major heating sources in the aircraft of interest. Dooley [44] studied the TMS in terms of different types of heat sinks and Vredenburg [45] varied the TMS architectures in his work by using three different heat sinks. Most of the research regarding the TMS need to identify the major heating and cooling loads as well as heat sources and heat sinks, but due to space limitation only some typical studies are presented as examples here. Therefore, it can be concluded that a high-level description of the heating and cooling loads as well as heat sources and heat sinks is required for the TMS architecting.

### 4.2.2 Behavior-Based Architecting Approach

From the literature review, the TMS architectures are initially generated by guidance of rules or experience in existing solutions. However, too detailed rules or experience, such as "supersonic aircraft must use vapor cycle for air conditioning", or "hydraulic fluid should be cooled by fuel", can greatly limit the types of architecture candidates, leading to architectures only generated by intuition or experience. However, it is also observed that all the local TMS architectures either directly reject heat to the other media based on temperature gradient or follow the fundamental refrigeration cycle, which is stated by the second law of thermodynamics. The fundamental refrigeration cycle mentioned here refers to the cy-

cle that requires energy to reject heat from a low temperature source to higher temperature medias. The alternative architectures are generated by varying components or heat paths. The varied components or heat paths are still served to the same cooling behavior for the fundamental cycle. For example, the compression behavior is required to lift the thermal state of the hot stream in the cooling cycle, and an expansion behavior is required to expand the hot stream for further cooling, and the compression behavior can be realized by turbine-driven compressors or electrical compressors, and the expansion process can be realized by turbine or expansion valve. From this example, it can be seen that even the types of component utilized in the thermal cycle are different, the same behavior is performed. Therefore, a hypothesis can be made for the guidance of generating local TMS architectures: all local TMS architectures manage the heat following the behaviors of fundamental physics (thermal cycles or behaviors of direct heat transfer based on temperature gradient).

The global TMS is defined as the system that arranges the interactions between each local TMS and heat sinks as in chapter 1. The arrangements are determined by the behaviors of the local TMS in terms of the requirement for heat sinks and the type of cooling cycles. For example, if one of the local TMS requires ram air as the heat sink and produces exhaust and another local TMS requires exhaust for cooling, these two TMS can be linked by routing the exhaust from the first local TMS to the latter one. It should be noted here the "exhaust" from a TMS is defined as the media after it performs the heating or cooling function on a load. Another example is that if two local TMS's require vapor cycle cooling, then these two TMS's might be cooled by the same vapor cycle. Therefore, a hypothesis can be made for the guidance of the global TMS architecting: all global TMS's link their local TMS's by following behaviors of each local TMS in terms of required heat sinks and applied thermal cycles.

After realizing that all the TMS's follow certain behaviors, the corresponding architectures then could be constructed based on these behaviors. Inspired by the System Modeling Language (SysML) [80] in Model-Based System Engineering (MBSE) [81], an architec-

ture can be viewed as comprised of three parts: 1. behavior; 2. requirements; 3. structure. The part of behavior for the TMS can be seen as the functions to be realized through the TMS, which can relate to the behaviors of fundamental physics. The requirements can refer to the heating or cooling loads that are managed by the TMS. The part of structure can be viewed as the final TMS architecture that gives the heat paths, heat sinks, and applied components. Thus, a behavior-based TMS architecting approach is proposed that a TMS behavioral architecture is firstly constructed by following the the behaviors of fundamental physics to satisfy the heating or cooling requirements, then the structural architecture can be created from the behavioral architecture. The linkages between the architecture description in SysML and the proposed architecting method are illustrated in Figure 4.3.

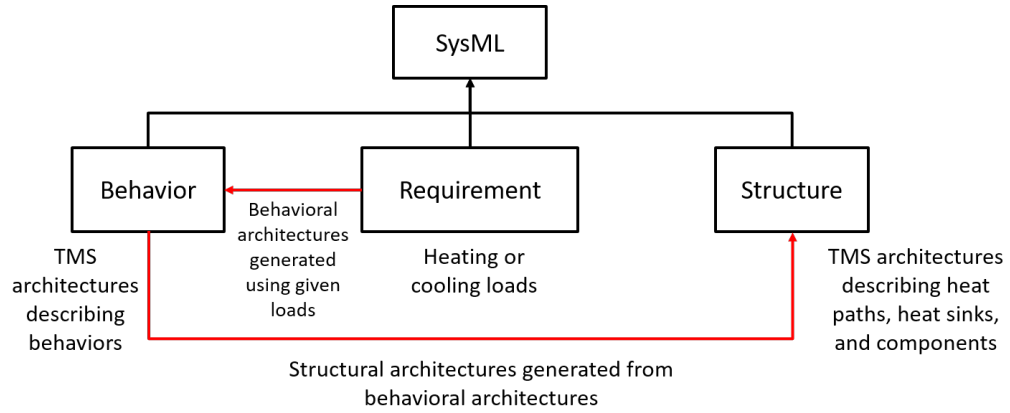


Figure 4.3: Linkages between SysML and proposed architecting methodology

#### 4.2.3 Backtracking Algorithm

To sufficiently populate the architecture space, an enumeration approach that is capable of trying every combination of behavioral options in terms of the compatibility is required. The backtracking method can fulfill such requirement. Backtracking is a general algorithm to find all solutions to problems, notably constraint satisfaction problems [82]. A generic backtracking algorithm can be described in the following procedure, in Algorithm 1 as shown in the book by S. Dasgupta, C.H. Papadimitriou, and U.V. Vazirani [83]:

In the application of the TMS behavioral architecting, a subproblem is a set of behavior

---

**Algorithm 1** Generic backtracking procedure

---

Start with some problem  $P_0$   
Let  $S = \{P_0\}$ , the set of active subproblems  
Repeat while  $S$  is nonempty:  
    Choose a subproblem  $P \in S$  and remove it from  $S$   
    Expand it into smaller subproblems  $P_1, P_2, \dots, P_k$   
    For each  $P_i$ :  
        If test( $P_i$ ) succeeds, halt and announce this problem  
        If test( $P_i$ ) fails:, discard  $P_i$   
        Otherwise: add  $P_i$  to  $S$   
Announce that there is no solution

---

with sequence, the "expand" process is to append other behaviors to the current selected subproblem. The test process is to check if the subproblem encounters the termination condition (test succeeds) or violates the constraint (test fails). If the appended behavior is compatible to the current subproblem while not triggering the termination condition, then the procedure continues by adding the current subproblem to the subproblems that have not been discovered. In the TMS behavioral architecting step, the compatibility of behaviors can be viewed as the constraints to be satisfied. In addition, a rule is needed to guide the selection of subproblems in the backtracking process. Three options are usually applied: depth-first, breadth-first, or best, which correspond to three types of data structure [84] in respect: stack (First in, Last out), queue (First in, First out), and priority queue. For our application, the depth-first rule is chosen, which is to expand one solution until it succeeds or fails.

However, this generic backtracking algorithm is only able to find the first feasible solution, instead of all feasible solutions. The procedure to find all feasible solutions is illustrated in Figure 4.4. From the top level, it picks an option which is the node of the next level, and then picks a node that is compatible with previous nodes, and then move the next level in the same manner until a solution is complete. Then it backtracks to the parental node of the last node (assuming the last node is at level  $n$ , and the parental node is at level  $n-1$ ), and picks another sub-node and proceed until another solution is complete. When

the sub-nodes of the parental node at level  $n-1$  are all explored, the process backtracks one level up of the parental node, which is at level  $n-2$ , and proceed with picking another node at level  $n-1$ . This process will continue until all the nodes are explored, indicating all the compatible architectures are solved. To realize this process, the generic backtracking procedure is re-written in a recursive manner [85], which can also handle the First in, Last out requirements without using an actual stack data structure. Moreover, in the actual implementation, a compatibility function is used to identify the sub-nodes that are compatible to the current partial solution. A generic pseudocode for the backtracking algorithm using the compatibility function for this behavior-based architecting method is shown Algorithm 2. The compatibility for local behaviors will be discussed later in section 4.3, and that for global behaviors will be discussed in section 4.4.

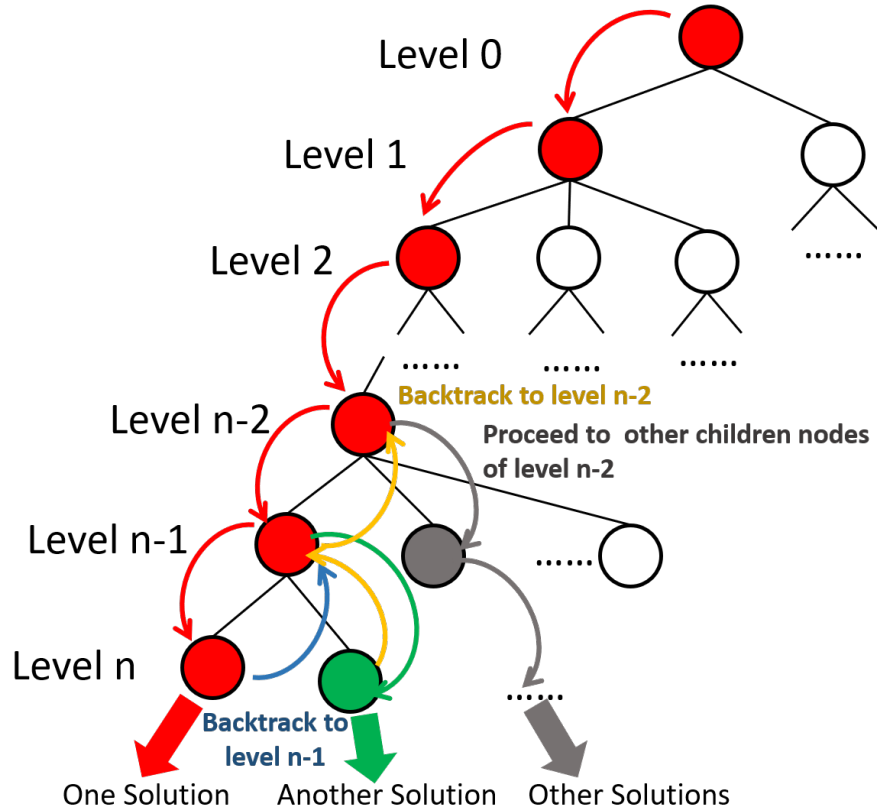


Figure 4.4: Backtracking in proposed TMS architecting method

---

**Algorithm 2** Behavior-based backtracking TMS architecting

---

```
function FIND_SOLUTION(Load)
    Initialize a list Sol to store solutions
    find_sol_backtracking(Load, Sol)
    return Sol

function FIND_SOL_BACKTRACKING(Load, Sol)
    Select behaviors based on Load: beh
    if len(Sol)  $\neq$  0 then
        if Sol[-1][-1] determines termination for current solution then
            Sol.append(Sol[-1].copy())
            return
        else
            for i in beh do
                if i is compatible with Sol[-1] then
                    Sol[-1].append(i)
                    find_sol_backtracking(Load, Sol)
                    Sol[-1].pop()
            else
                Sol.append([])
                for i in beh do
                    if i is compatible with Sol[-1] then
                        Sol[-1].append(i)
                        find_sol_backtracking(Load, Sol)
                        Sol[-1].pop()
    Sol.pop()
```

---

#### 4.2.4 Conversion Behavioral to Structural Architecture

With the constructed TMS behavioral architectures, the behaviors of each architecture can be determined. However, a structural architecture is also needed for the design and analysis during conceptual design phase. In the behavioral diagrams, each behavior can be realized by a set of candidate components. Therefore, the structure architecture space can be fully explored if all possible compatible combinations of the components for each behavior are enumerated. An illustration of the conversion from behavioral to structural architecture is shown in Figure 4.5, where all components in this figure are assumed to be compatible. For the implementation, it should be noted that the architectures are represented in the form of

a list of components, which will be discussed later in the subsection 4.3.3.

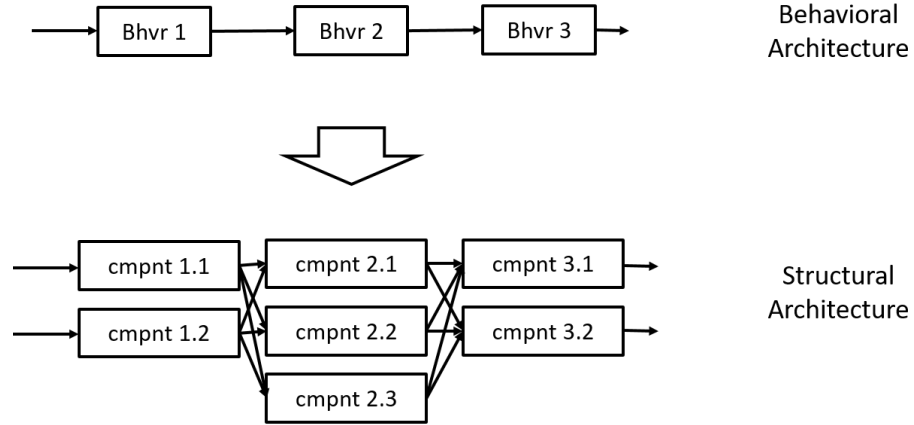


Figure 4.5: Conversion from behavioral to structural architecture illustration

#### 4.2.5 Overview of the Methodology

In summary, the proposed behavior-based backtracking methodology can be described as: the local TMS architecture space is populated firstly by backtracking based on behaviors of fundamental physics, then the global TMS architecture space is explored by enumeration of local TMS's for each heating and cooling load and the interactions among these local TMS's, following the behavior of the interactions of local TMS's. There is also a need for conversion from a behavioral architecture to a structural architecture, which is done by enumeration of components for each behavior. The overview of the architecting process is presented in Figure 4.6.

### 4.3 Local TMS Architecting

#### 4.3.1 Behaviors of Local TMS

Compatibility is needed for the backtracking algorithm. The compatibility included in this section are mostly based on fundamental physics, although the compatibility of some behaviors are subject to user preferences such as the maximum number of compression or expansion processes. It should be noted that these compatibilities shown in this paper are



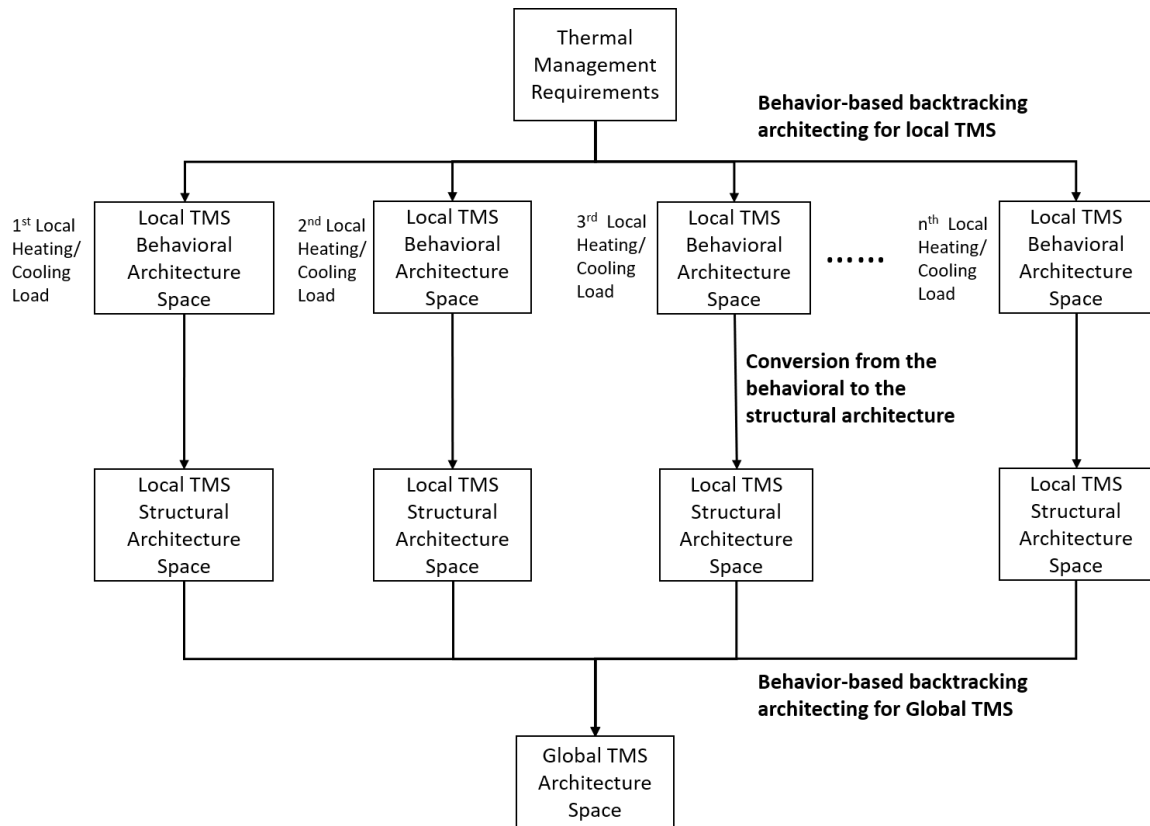


Figure 4.6: Overview of TMS architecture space populating methodology

only to demonstrate the capability of the method. Other specific constraints in terms of the actual application can also be added. A hierarchical diagram showing the behavioral compatibility for a load needing heating is illustrated in Figure 4.7, and a hierarchical diagram showing the behavioral compatibility for a load needing cooling is illustrated in Figure 4.8. In these two diagrams, the sub-nodes mean the only behaviors that are compatible with their parent node. Both heating and cooling load management will consider corresponded regulations to check if there are specific requirements to be obeyed. Such requirements might eliminate certain optional behaviors. For example, the regulation requires that the ECS should supply enough fresh air to the cabin while pressurizing it, which means that the ECS has to use the charged air (either from bleed or electrically compressed) as the heat sink. It should be also noted that the cooling nodes with "\*" in Figure 4.8 mean they are the same cooling behavior with the same sub-options. For example, if the "Cooling"

node is reached under "Storage", then the next step will be to select "Direct heat reject" or "Refrigeration cycle".

It should be also noted that the cryogenic cooling solution is included in the closed loop option under refrigeration cycle. When the coolant is selected to be the cryogenic coolant, the cryogenic architecting procedure is triggered. However, since cryogenic cooling is quite different from other refrigeration cycles, the behaviors for the cryogenic options are only passive cryogenic cooling (PCryo) and active cryogenic cooling (ACryo). The passive cooling here simply refers to the approach that uses stored coolant or special fuel such liquid hydrogen (LH2) to directly cool the load without using heat pump. And the active approach refers to the method that uses cooling cycles on the cryogenic refrigerant to perform cooling. Since there is not much information regarding the cryogenic cooling application in aircraft, there is only one architecture assumed for PCryo and one for ACryo for modeling simplicity. The PCryo architecture is simply coolant comes from a reservoir to a load and then recirculates to another storage tank. The ACryo architecture is assumed to be of a model using Claude process [86], which combines a Joule-Thomson [87] and a Brayton process [88]. More details will be shown in chapter 5 when discussing the modeling approaches.

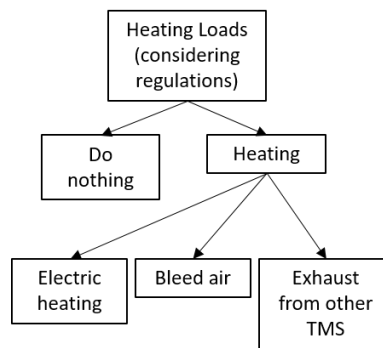


Figure 4.7: Behaviors to manage loads requiring heating

In Figure 4.7, the node "Do nothing" means it does not take any other approach to treat this load. The sub-nodes under "Heating" are the selected options for heating a load: "Electric heating": apply electric heating panels; "Bleed air": use engine bleed air as heating

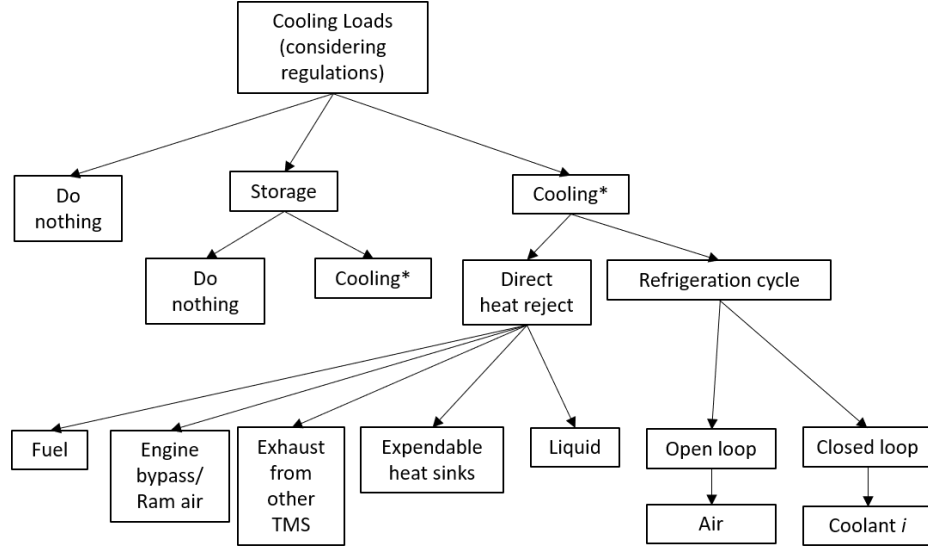


Figure 4.8: Behaviors to manage loads requiring cooling

source; "Exhaust from other TMS": use exhaust from other TMS's as the heating source. In Figure 4.8, "Do nothing" has the same meaning as in Figure 4.7 that no specific actions will be taken to treat this load. "Storage" means to store the heat in certain energy storage materials such as phase change materials (PCM). As stated before, the "Cooling" option with "\*" refers to the same node that has the same sub-nodes: "Direct heat reject" and "Refrigeration cycle", where "Direct heat reject" indicates cooling methods without using heat pump (without using external power) while "Refrigeration cycle" refers to cooling methods requiring heat pump. The sub-nodes of "Direct heat reject" are the potential heat sinks, and it should be also noted that oil is a sub-option included in "Liquid". For all "Direct heat reject" sub-options, the actual behaviors related to heat reject are: "Start", "Heat exchange (HX)", "Cooling the load (Load)", "End". Only for Fuel, there could be an additional "Re-circulation (Rec)" behavior. The detailed explanations and compatibility of the "Direct heat reject" behaviors are discussed in Table 4.4. For "Refrigeration cycle", there can be an open-loop option and a closed-loop option. Following these two sub-nodes, the corresponding heat sinks will be selected. For an open-loop option, only air is considered in this paper. For the closed-loop option, there can be a number of coolants, and it will pick coolant  $i$  at the  $i$ th backtracking recursion for further expansion to an actual solution. The

corresponding behaviors for "Refrigeration cycle" for non-cryo applications are: "Start", "Heat exchange (HX)", "Cooling the load (Load)", "Compression (CMP)", "Expansion (EXP)", "Water Extraction (WE)" "Re-circulation (Rec)", "End". The corresponding explanations and compatibility are discussed in Table 4.5. The ones for cryogenic application are listed in Table 4.6. It should be also noted that for each load, there could be multiple cooling approaches working simultaneously to remove the heat, that is, multiple TMS's can work parallelly for a single load. For example, an electric motor can both reject heat to oil and energy storage material at the same time. For this paper, it is allowed at most two TMS's working on the same load to limit the number of generated architectures. It should be also noted here that these listed compatibility mostly follow fundamental physics, and are only to demonstrate the capability of the method. They are subject to changes in terms of the actual applications.

When the backtracking step reaches the bottom level in Figure 4.8, the behaviors stated in Table 4.4 and Table 4.5 are then used to construct the actual TMS behavioral architectures. When the behavior HX is encountered, it is treated as another load to be cooled, which starts from the top level of the backtracking tree as illustrated by Figure 4.8. Therefore, a cooling architecture might be cooled by another, and this new one could also be cooled by another new one. If there is no limitations, then there could be an infinite number of populated TMS architectures. So to limit the number of generated architectures, it is allowed at most four cooling architectures linked together in this paper, and the final one must be an open-loop architecture, discarding the heat sink used in the final cooling architecture from the current local TMS.

The compatibility of some behaviors listed in the two tables will be described below, while the other obvious ones are not discussed due to space limit of the paper. For the direct heat reject architectures: HX is only compatible to the closed-loop system, because the heat sink needs to be cooled before going back to the reservoir, while assuming heat sinks in open-loop architecture do not need further cooling; Re-circulation to the Start

Table 4.4: Behaviors of direct heat reject systems

Behavior	Explanation	Compatible if all conditions are satisfied
Start	Starting point in the architecture	No Start exists in the partial solution;
Load	Load is cooled	Start exists in the partial solution; Load does not exist in the partial solution;
HX	Heat exchanging with another heat sink, treating the current architecture as a load to be cooled	Start exists in the partial solution; Total number of HX in partial solution $< k$ ( $k$ is a user specified number, 1 for this study); Current architecture is closed-loop; Load in partial solution;
Rec	Re-circulates back to the reservoir for closed-loop architecture	Start exists in the partial solution; Load exists in the partial solution; Current architecture is closed-loop;
End	End of the partial solution, termination condition for a solution in backtracking	Start exists in the partial solution Load exists in the partial solution Rec exists in the partial solution if closed-loop

only happens after the load is cooled in a closed-loop system; the current partial solution is complete (End is compatible) when the load is cooled and the re-circulation has been performed. For the refrigeration cycle architectures: HX is used to remove heat from the heat sink, thus it happens when the thermal state is high, that is, it only happens before EXP; If CMP happens before EXP, it is used to lift the thermal state of the heat sink to improve the performance of heat removal, so an HX must follow it to perform the heat removal; the water extraction always corresponds to an expansion process, so WE is compatible when the last behavior is EXP; the load is cooled when heat sinks are at low thermal state, which must happen after EXP; the termination condition (End) is compatible only when the load is cooled, and when EXP and CMP have been performed.

Table 4.5: Behaviors of refrigeration cycle systems for non-cryo application

Behavior	Explanation	Compatible if all conditions are satisfied
Start	Starting point in the architecture	No Start exists in the partial solution;
HX	Heat exchanging with another heat sink, treating the current architecture as a load to be cooled	Start exists in the partial solution; The last behavior in partial solution is not HX; Load not in partial solution; EXP not in partial solution;
CMP	Compress the heat sink to lift its thermal state (if CMP happens before EXP, then a HX must follow CMP)	Start exists in the partial solution; Total number of CMP in partial solution $< c$ ( $c$ is a user specified number, 1 for this study);
EXP	Expand the heat sink for cooling	Start exists in the partial solution; Total number of EXP $< e$ ( $e$ is a user specified number, 2 for this study); Load not in partial solution;
WE	Water extraction from air	Selected heat sink is air; The last behavior is EXP;
Load	Load is cooled	Start exists in the partial solution; Load not in the partial solution; The last behavior in partial solution is EXP;
Rec	Re-circulates back to certain points (to start for closed loop, to perform secondary cooling or partially mixing with stream coming into the load for open loop)	Start exists in the partial solution; Load is last behavior in the partial solution is; No same type of Rec exists in partial solution;
End	End of the partial solution, termination condition for a solution in backtracking	Start exists in the partial solution At least one CMP in partial solution; At least one EXP in partial solution; Load in partial solution;

#### 4.3.2 Conversion from Behavioral to Structural Architecture

As mentioned before, the behavioral architecture is the architecture that describes the TMS behaviors, and the structural architecture is the architecture that describes the types of com-

Table 4.6: Behaviors of refrigeration cycle systems for cryogenic application

Behavior	Explanation	Compatible if all conditions are satisfied
Start	Starting point in the architecture	No Start exists in the partial solution;
PCryo	Passive cooling using cryogenic coolant	Coolant is of cryogenic type; PCryo or ACryo does not exist in the partial solution;
ACryo	Active cooling using cryogenic coolant, following Claude cycle	Coolant is of cryogenic type; PCryo or ACryo does not exist in the partial solution;
End	End of the partial solution, termination condition for a solution in backtracking	PCryo or ACryo exists in the partial solution;

ponents that are used and the linkages among components. The enumeration of the components is also realized in a similar recursive backtracking approach as in the behavioral architecting procedure, where the compatibility is determined by the type of the heat sink and previously selected components. The linkages between components and the behaviors are listed in Table 4.7.

#### 4.3.3 Form of TMS Stored in Actual Implementation

In the current implementation, the TMS architecture is stored as a list of lists. The top-level list contains  $n$  sub-lists, where the  $i$ th sub-list is the  $i$ th level of the sub-architecture TMS. The sub-architectures at level  $i$  are the ones to manage the heat or coldness from the sub-architectures at the level  $i - 1$ . For a sub-list in each level, it may contain multiple sub-architectures, where each sub-architecture corresponds to a heat exchange process from the sub-architecture at previous level, following the sequence of the heat exchange processes. In addition, each sub-architecture is also in the form of a list, which is composed of the behaviors (behavioral architecture) or components (structural architecture), along with

Table 4.7: Linkages between components and behaviors

Behavior	Component	Notes
Start	Flow start	Determined by the selected heat sinks or heat sources
CMP	Compressor	Compressors can be driven by turbine or electric motor;
EXP	Turbine or Expansion Valve	Turbines are used when phase change is not included in selected sinks; Expansion valve is used when phase change is included in selected sinks;
HX	Heat Exchanger or Condenser or Evaporator	Determined by the chosen sinks and whether phase change is included;
Load	Cooling/Heating Load or Components from HX	It can be a basic heating/cooling load as set in the aircraft; Heat rejection from one TMS is considered as a load of another TMS;
WE	Water Extraction Loop	A pre-defined water extraction loop, which will be shown in the section in chapter 5 on Modeling approach later;
Rec	No specific component	Weight and driving power is calculated, but the actual components are not included;
End	Flow End	

selected sinks and types as specified in Figure 4.8. Here presents a simple example to explain this representation using a motor cooling architecture, where the architecture can be visualized in Figure 4.9. The corresponding list-of-lists form is:

```
[[['Start', 'Load', 'HX_1', 'HX_2', 'End', 'Oil', 'ClosedLoop_Direct']], [['Start', 'Load', 'End', 'FanAir', 'OpenLoop_Direct']], ['Start', 'Load', 'End', 'Fuel', 'OpenLoop_Direct']]].
```

It should be admitted that the list form is difficult to be visualized, but it is quite easy to be managed and used to construct the actual models on the computer. For the visualization purpose in this thesis document, the architectures shown in the following chapters and sections will all be in figure form instead of the list form.



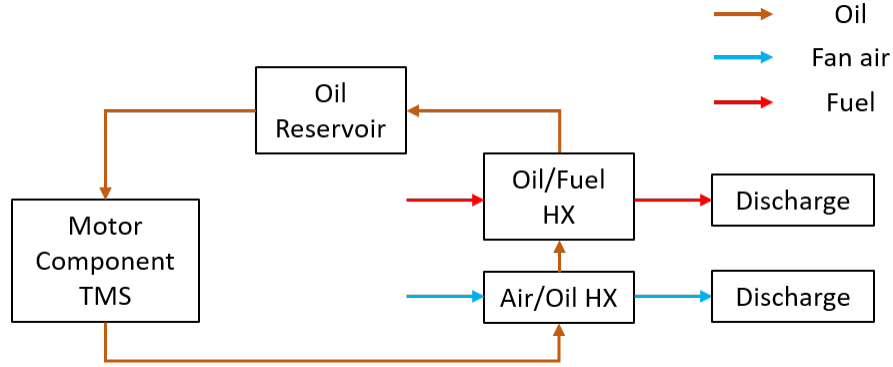


Figure 4.9: Motor TMS as illustration of list representation

#### 4.3.4 Example of Local TMS Architecting

The architecture of a cabin ECS, which is a local TMS, is constructed using the proposed method to illustrate the architecting process. The behavioral architecture is constructed first. The process of establishing the behavioral ECS architecture is shown following the backtracking steps. From the starting point, the top level in Figure 4.8, the cooling load of the cabin is considered with the regulations. As the regulations [78, 89, 90] dictate that the supply air of the ECS should be able to pressurize the cabin as well as to provide enough fresh air as much as 0.55 lb/person/min, the heat sink in the ECS to supply the cabin has to be compressed air, which leads to the only behavior through refrigeration cycle to provide cooling compressed air. Compressed air has to correspond to an open-loop system with refrigeration cycle. Therefore, the behavioral architecture construction can directly start from the node "Air" which is a child of "Open loop" following the "Refrigeration cycle" node. The preceding behaviors identification can be illustrated in Figure 4.10.

From the last reached node, the behavioral architecture starts to be constructed. Following the backtracking algorithm, Algorithm 2 with the compatibility table, Table 4.5, the compatible behaviors are enumerated one by one, until the termination condition is triggered. Figure 4.11 illustrates an example to construct one solution of the ECS. When one solution is obtained, the backing tracking process starts, and an example is shown in Figure 4.12. The last step in the previous solution was done by selecting "End". After

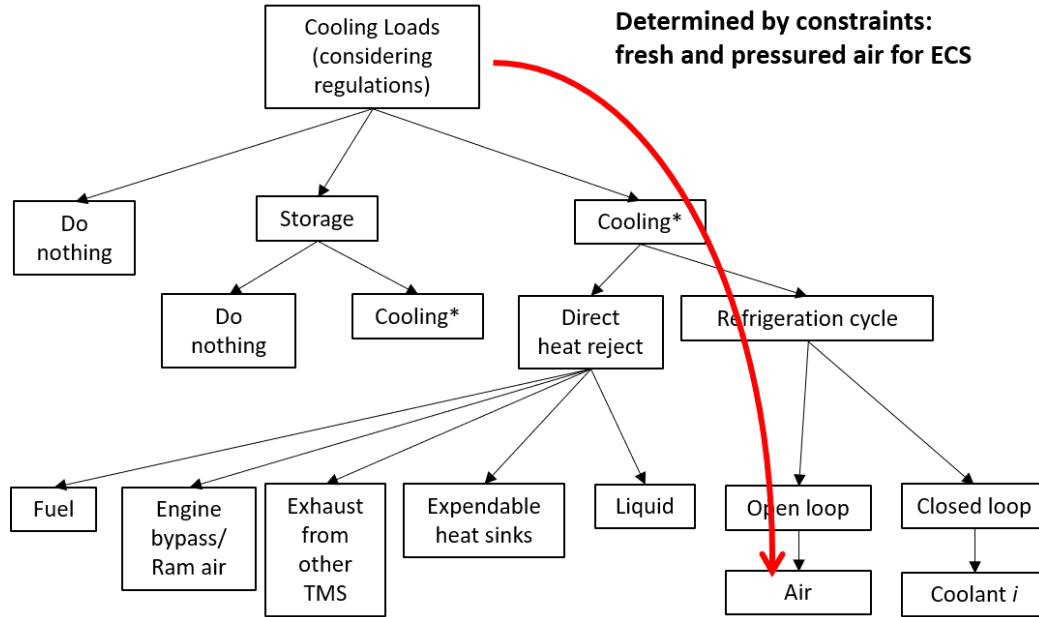


Figure 4.10: ECS architecting process from cooling load to the architecture construction starting point

backtracking, the "End" is removed, and the other option "Rec" is appended to the partial solution, and then the algorithm continues to append compatible behaviors to the partial solution, until another termination condition is triggered.

As discussed before, each HX acts as a new load to be cooled. For the previously obtained ECS architecture, there are two HX, thus there will be two new loads to be cooled, starting from the top level shown in Figure 4.8. And the same backtracking method will be implemented. For the illustration purpose and to avoid the repetition, we could just assume these two loads are cooled by the same type of the TMS, and assume the TMS's are direct heat reject systems using ram air without loss of generality. The architecting process is illustrated in Figure 4.13. Thus the obtained overall TMS architecture solution can be shown in Figure 4.14.

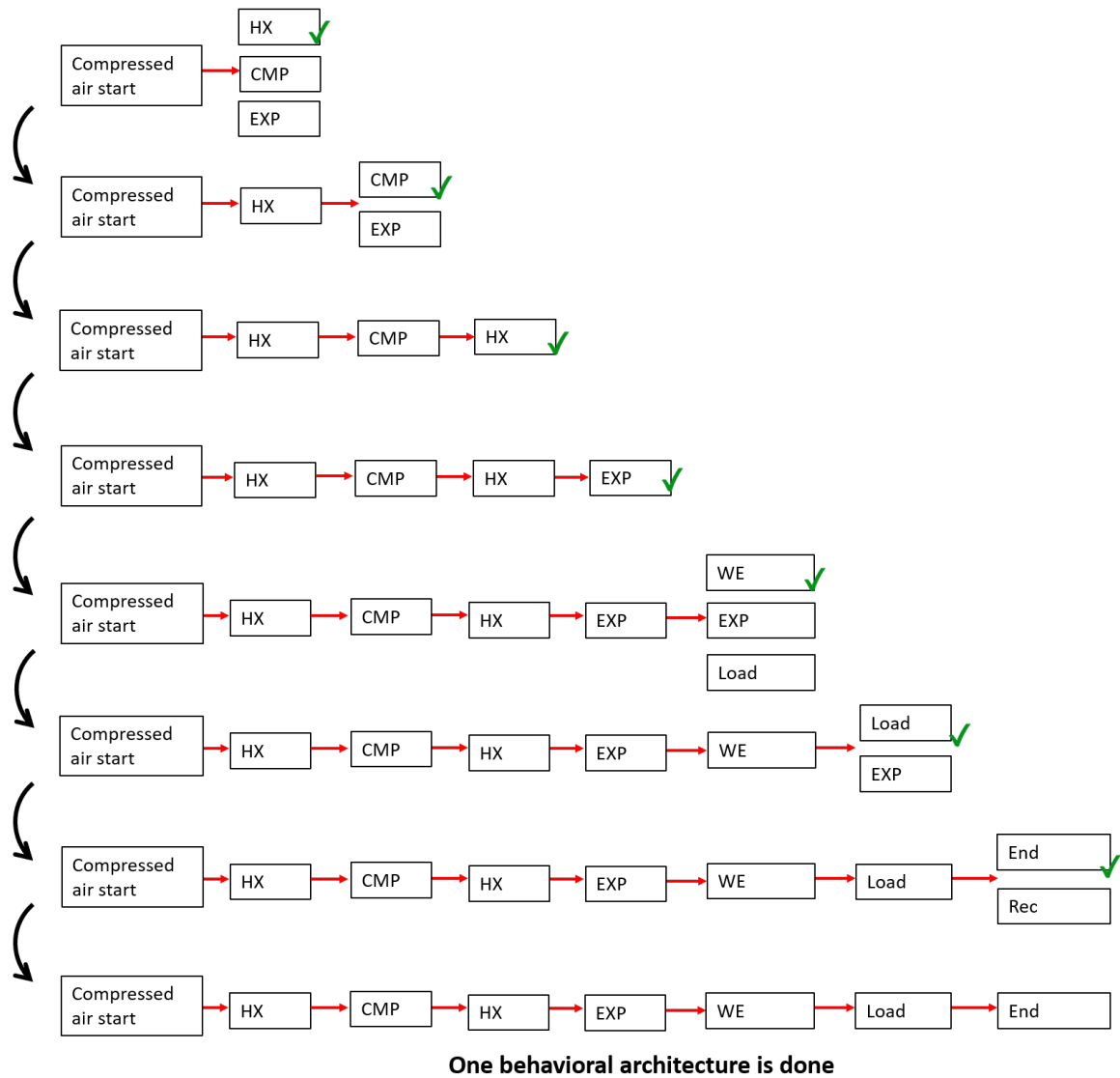


Figure 4.11: ECS architecting process

#### 4.3.5 Behavioral to Structural Architecture

From the constructed behavioral architecture, the structural architecture can be created by replacing the behaviors by the components that are capable of performing such functions. The components that can perform the behaviors in the constructed architecture is listed in Figure 4.15. Using these components, the behavioral architecture can be converted to a structural architecture, shown in Figure 4.16. It should be noted that the same behavior can be performed by different components, thus the same behavioral architecture can generate

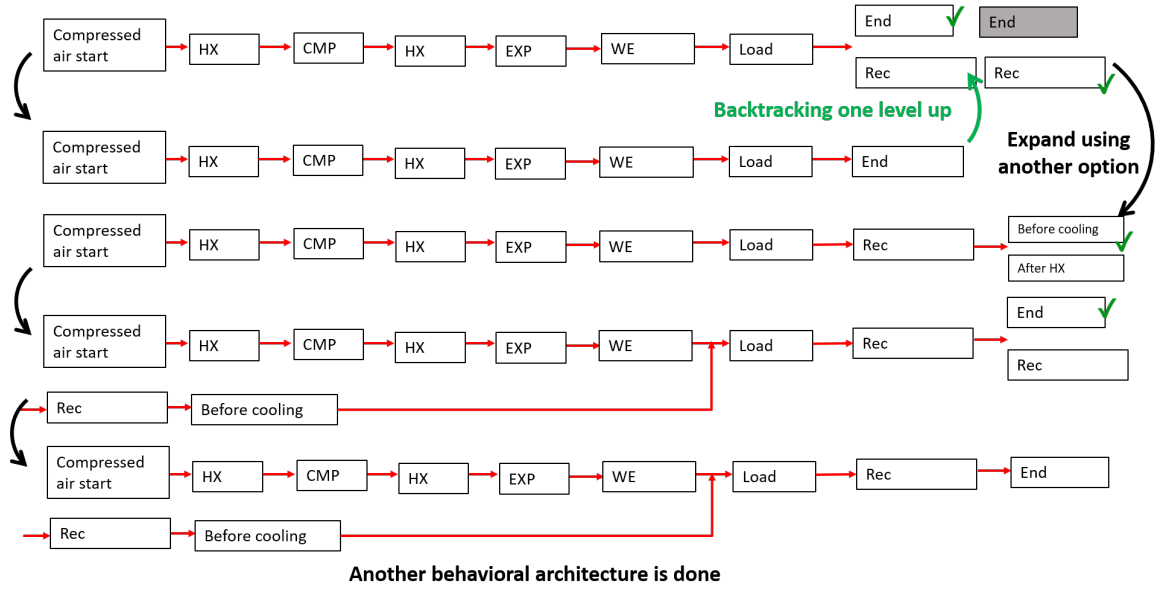


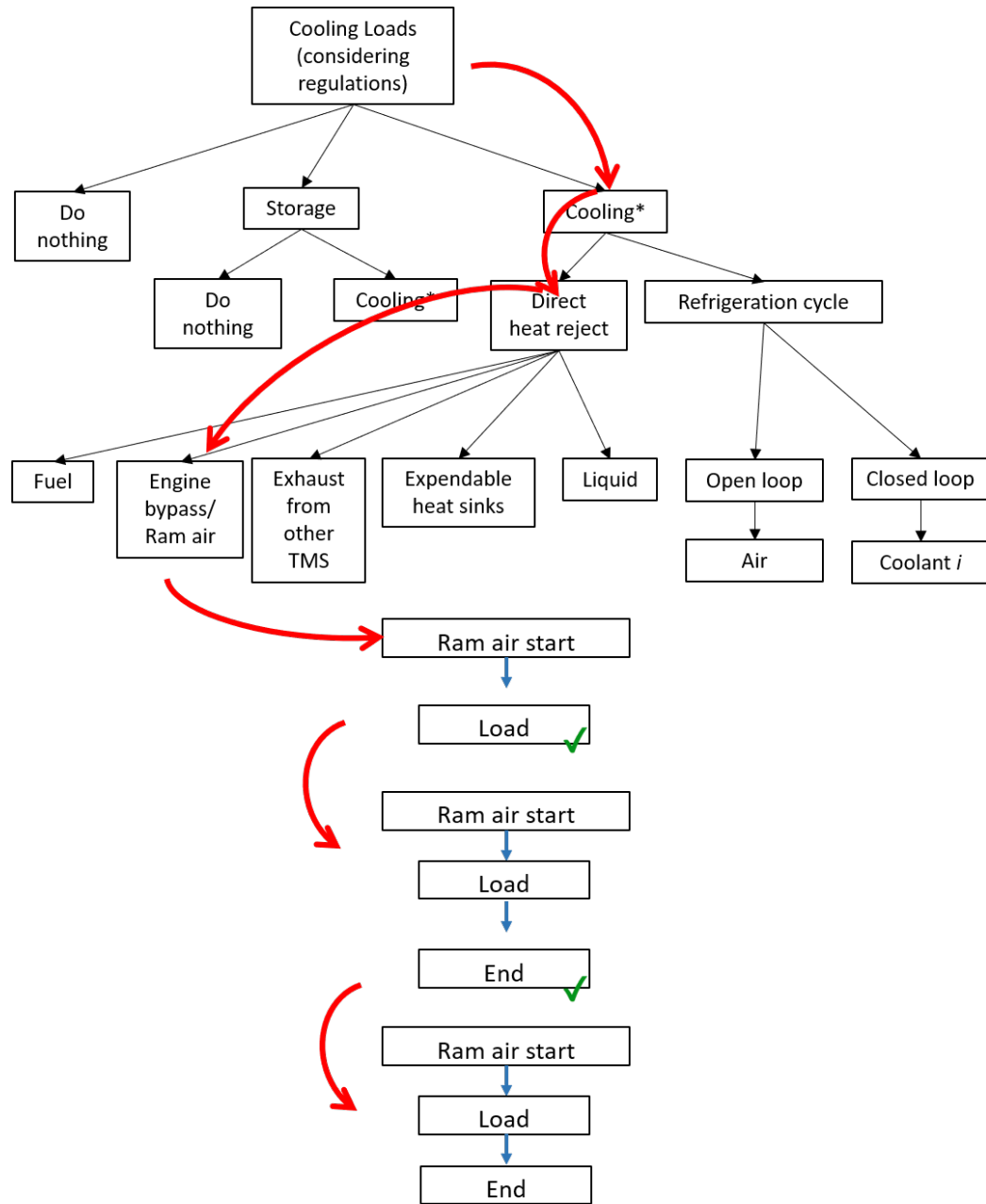
Figure 4.12: ECS architecting backtracking example

different structural architectures. However, for simplicity, only one example of the structural architecture is presented here. It should be also noted that the components for each behaviors in this paper are just to demonstrate the capability of the approach. In the actual implementation, users can change these candidate components in terms of preferences or specific requirements.

## 4.4 Global TMS Architecting

### 4.4.1 Behaviors of Global TMS

The global TMS can be interpreted as interactions among each local TMS. Therefore, the variations of the global TMS are created by varying local TMS's for each heating or cooling load or interactions among local TMS's. Firstly, the local TMS's for each load are enumerated by the backtracking method. There are not many constraints on the compatibility when constructing the global TMS. The only constraint is that heat sinks for the local TMS cannot be all "exhaust". After enumerating the local TMS's, then the linkages among local TMS's that do not use exhaust and local TMS's use exhaust are enumerated, using the



**One behavioral architecture obtained**

Figure 4.13: Example architecting process for a HX in obtained TMS architecture

same backtracking approach. It should be noted that although there is no specific compatibility constraint except for the exhaust one in this paper for the purpose of demonstrating only the proposed methodology, other compatibility constraints can be added in terms of the actual applications. For example, if a certain local TMS uses cryogenic TMS, then

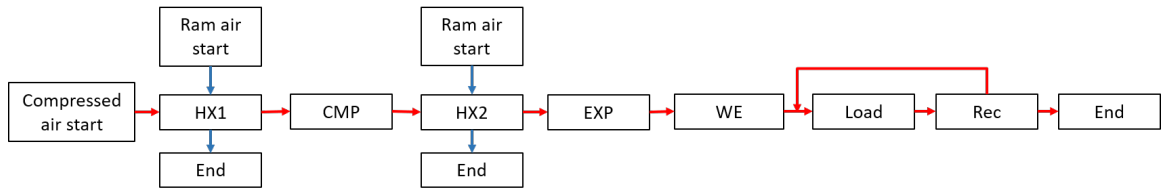


Figure 4.14: Overall ECS behavioral architecture example

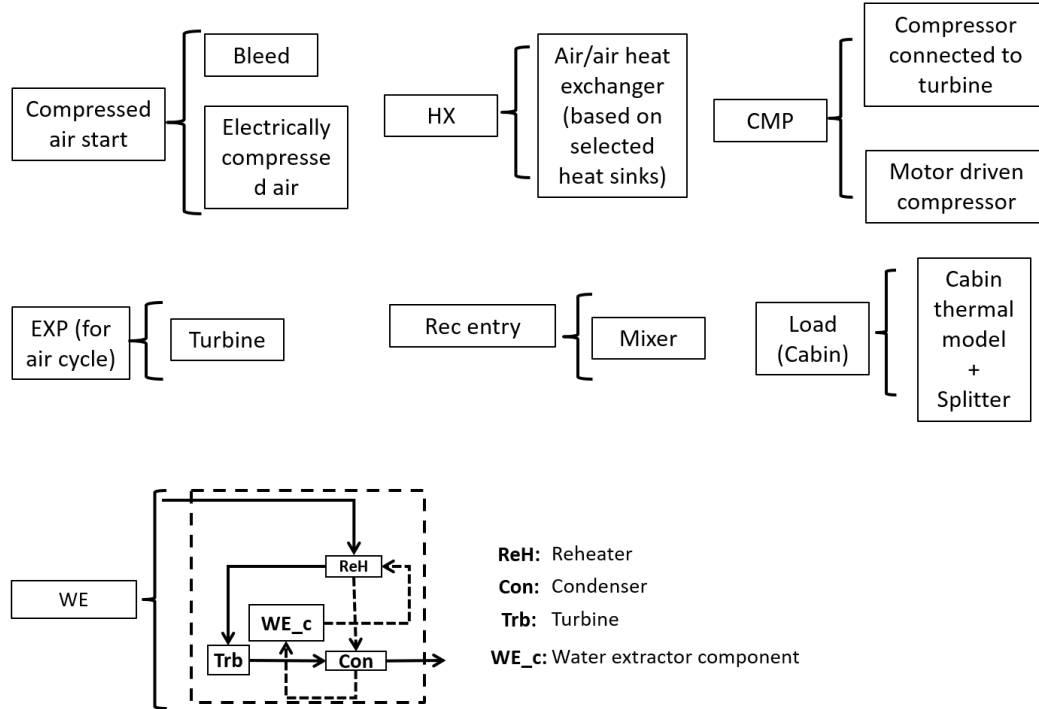


Figure 4.15: Components that perform certain behaviors

TMS's that are suitable for other loads might not be compatible to the cryogenic one. Another example is that some loads may not be allowed to be cooled by certain types of exhaust, so some types of exhaust may not be compatible to some TMS solutions.

#### 4.4.2 Example of Global TMS Architecting

An example showing construction of the global TMS is presented in this section. In this example, each local TMS is represented by a label such as A 1 standing for TMS architecture for load 1. It is assumed that there are 7 loads (Load 1 to 7) in total. First 7 backtracking steps are corresponded to the selection of the local TMS from Load 1 to Load 7. This process is illustrated in Figure 4.17, and for simplicity, results of all 7 steps are shown at

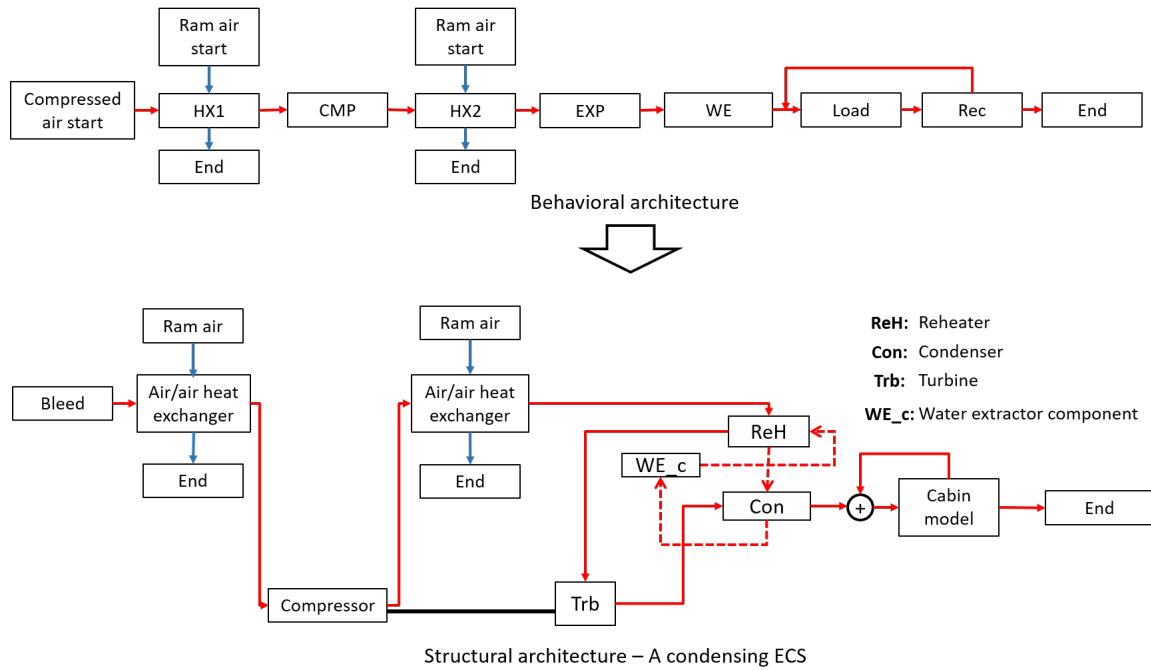


Figure 4.16: Behavioral to structural architecture conversion example

the same time.

Assuming A 1.1 and A 6.3 require ram air, A 3.2 and A 5.1 require fuel, A 2.3 requires both ram air and fuel, A 7.1 requires exhaust, and A 4.1 requires nothing. The next backtracking step is to route the ram air, the fuel, and then the exhaust until all options of the local TMS and exhaust routes are enumerated. Such interactions architecting is shown in Figure 4.18. It should be noted that for this example fuel is not considered as a load to be cooled, but in reality it can serve as a cooling/heating load.

The backtracking process in the global TMS is simple so that there is no need for an example to illustrate it. The backtracking process starts from the level of routing exhaust since it is the last level. When the options of exhaust route has been fully explored, the process backtracks back to the level of selecting the component for the last load. Then another component is selected for the last load, and interactions are built around the new layout. Such process will continue until all options of the local TMS and interactions among them are tried out.

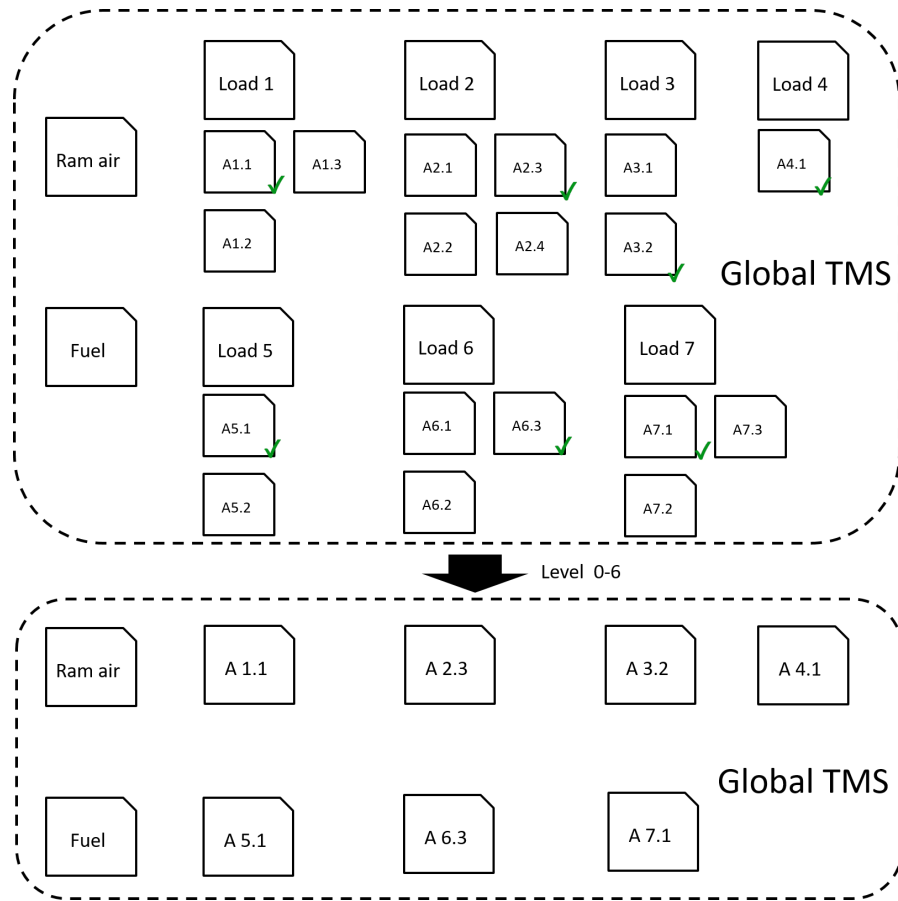


Figure 4.17: Selection of local TMS

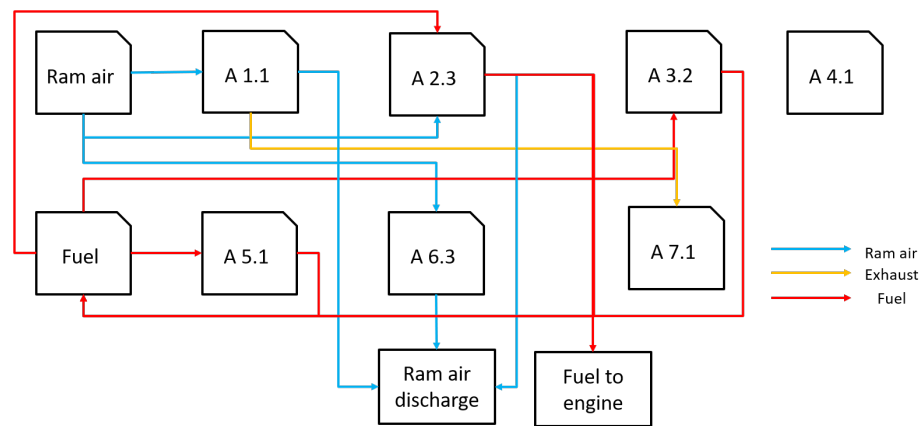


Figure 4.18: Interaction architecting for the global TMS

#### 4.4.3 Form of Global TMS Stored in Actual Implementation

The stored global TMS is of a simpler form than that of the local TMS, which is still a list of lists. Each sub-list stands for a local TMS for a load of the aircraft.  $n$  loads in the aircraft



are firstly assigned indices, from 0 to  $n - 1$ . The generated local TMS for each load is also assigned an index. The first bit of the  $i$ th sub-list, for example, say it is  $k$ , indicates the  $k$ th local TMS for load  $i$  is selected in the global TMS. Then the other bits in the sub-list  $i$  indicates what other local TMS's are linked to the local TMS for load  $i$ . For example, if the list for a global TMS is  $[[3,1,2],[187,0],[43,0]]$ , assuming there are only three loads. Then it means the local TMS indexed 3 for Load 0 is selected, the local TMS indexed 187 for Load 1 is selected, the local TMS indexed 43 for load 2 is selected, and the TMS for Load 0 is linked to the TMS for Load 1 and Load 2. For visualization purposes, the generated global TMS in this thesis document will all be represented in figure form.

## 4.5 Results and Validation of Methodology

The generated local TMS's and global TMS's are shown and validated in this section. Due to the space limit of the documentation, three local loads are selected to validate the capability to generate both intuitive and non-intuitive architectures of the local TMS: cabin for the 160-pax traditional aircraft, motor for the 300-pax TeDP, and battery for the HTeDP. Traditionally, TeDP, and HTeDP aircraft are all selected to validate the capability to generate the global TMS.

### 4.5.1 Results and Validation of Local TMS

There are some user specified requirements to the local loads: cabin must be cooled by pressurizing air according to regulations [78, 89, 90]; motor must be directly cooled by oil; battery can be cooled by any type of methods; if an open-loop refrigeration cycle with air is used to cool a certain load, the ECS for the cabin will be used, so there cannot be another independent air cycle machine to produce cold air. It should be noted that these constraints are only used for testing purposes. Users can remove any of them or add more in actual applications.

As discussed in subsection 4.3.3, the local TMS architectures take the form of list of

lists. Therefore, a certain sequence and combination of behaviors or components can be directly used to search in the generated architectures to see if certain TMS architectures have been generated. For this validation purpose, a sequence of components from expected TMS architectures is used to search in the generated TMS group to see if such architectures are correctly populated.

### *Cabin*

There are in total 1362240 generated TMS architectures for the cabin load. All of them use bleed extracted from the engine as the supply air. Because of this large number of generated architectures, only a few are selected to compare with the existing architectures to demonstrate the proposed methodology is capable of generating conventional TMS architectures. And a few are selected to demonstrate the proposed method is also able to generate non-intuitive but reasonable TMS architectures.

The generated architectures are stored as a set of lists, thus to select generated conventional architectures. Conventional architectures from literature were firstly converted into lists and then were directly searched in the solution set to check if they exist. Three-wheel and four-wheel ECS from Parrilla's study [66] are used for this validation. The generated architectures are shown in Figure 4.19 and Figure 4.20, which match the exact architectures shown in the reference [66].

Some novel and non-intuitive TMS architectures for the cabin are also generated. For example, as shown in Figure 4.21, which has not been seen but also follows the basic reversed bootstrap refrigeration cycle [1, 91]. In convention, an air cycle machine is always used for the cabin cooling, and it also always follows the reversed Brayton cycle where the heat exchange process must exist after the compression. In contrast, the novelties illustrated by Figure 4.21 are: the expansion process happens before the compression process, which is different from the conventional air cycle machine; there is no heat exchange after the compression process, which is not the same as the reversed Brayton cycle. In this ar-

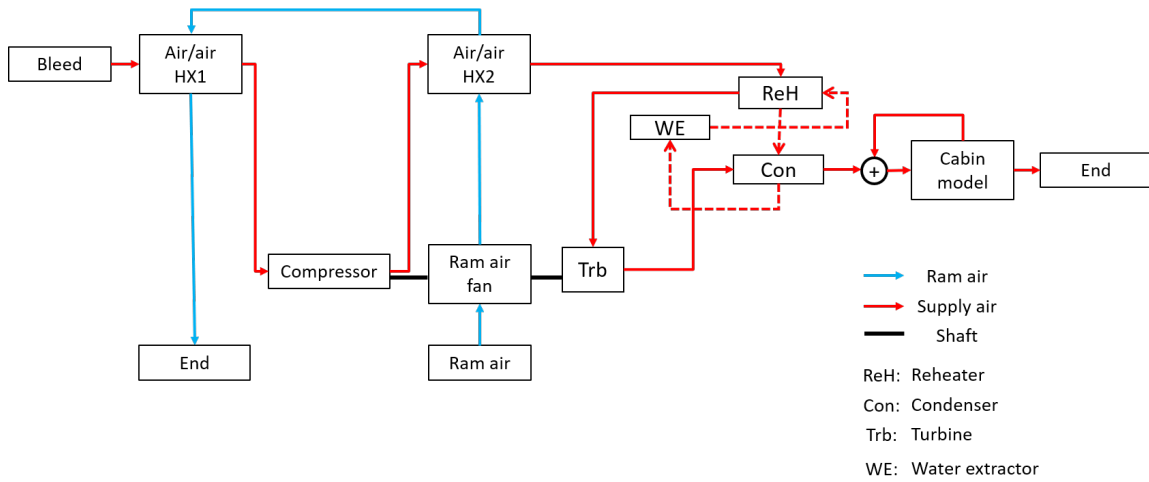


Figure 4.19: Generated three-wheel TMS architecture

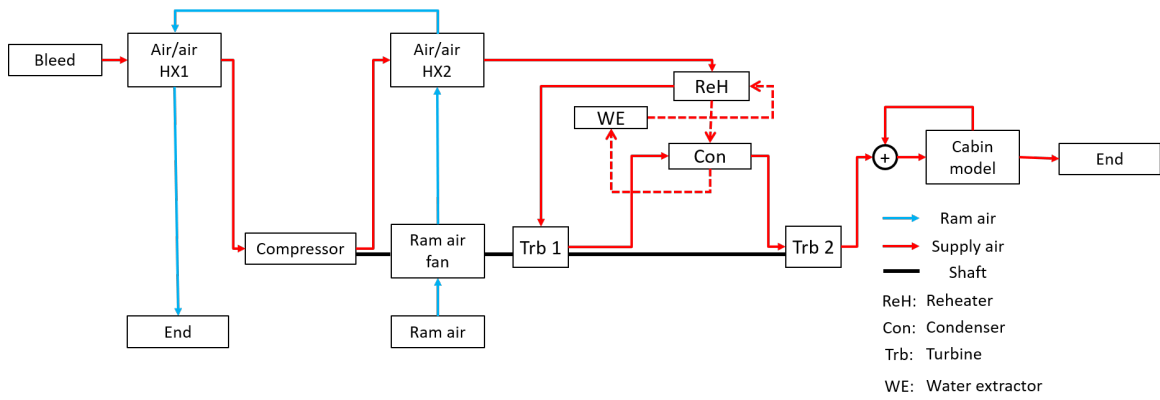


Figure 4.20: Generated four-wheel TMs architecture

chitecture, the heat exchange only happens before the expansion process, and the exhaust from the cabin is also used to further cool the heat sink.

The other two examples of novel architectures using closed-loop heat pumps are also presented here. One example is illustrated by Figure 4.22: an TMS with vapor cycle to cool the re-circulation path. Another TMS using vapor cycle while neglecting the whole air cycle machine can be also found, which is plotted in Figure 4.23. In general, the application of the vapor cycle is used to cool the supply air in the air cycle machine. In the example shown by Figure 4.22, the supply air is still cooled by ram air, but the vapor cycle is only added to the re-circulation process. In the example shown by Figure 4.23, the air cycle machine is fully removed, and the vapor cycle is used to directly cool the supply air.

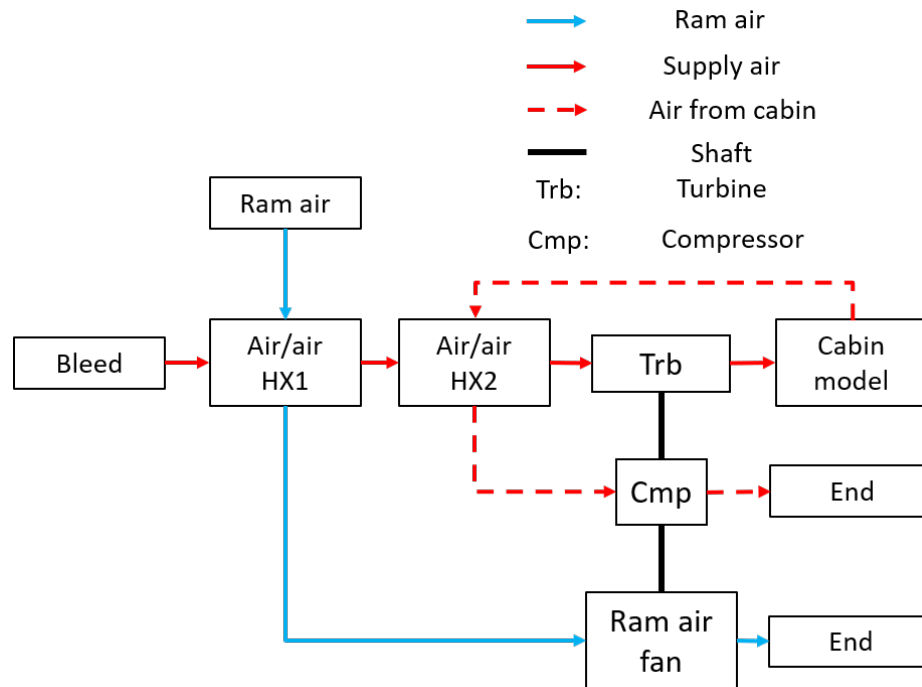


Figure 4.21: Novel TMS following reversed bootstrap to cool cabin

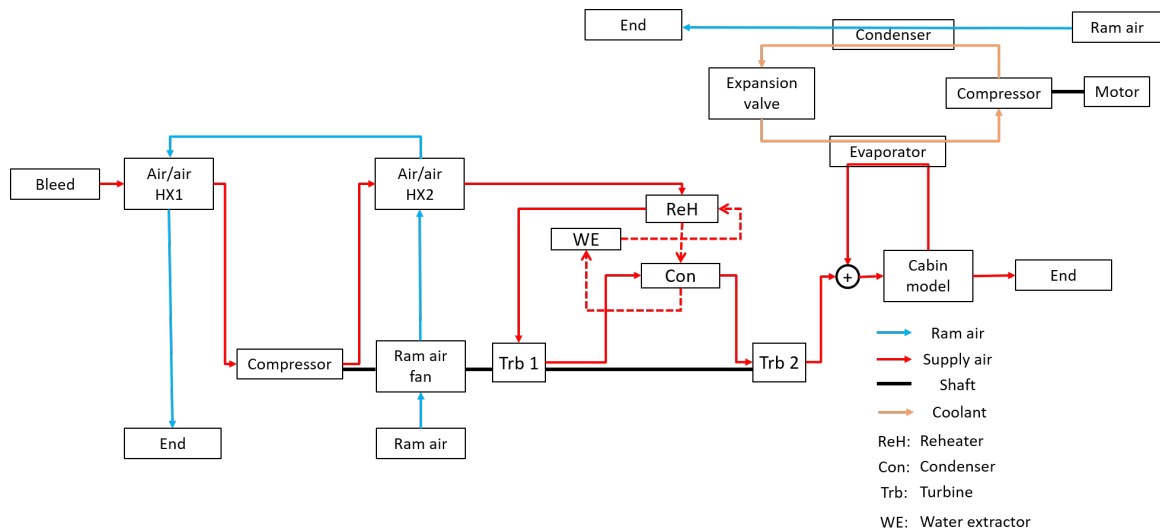


Figure 4.22: Novel ECS with vapor cycle cooling re-circulation path

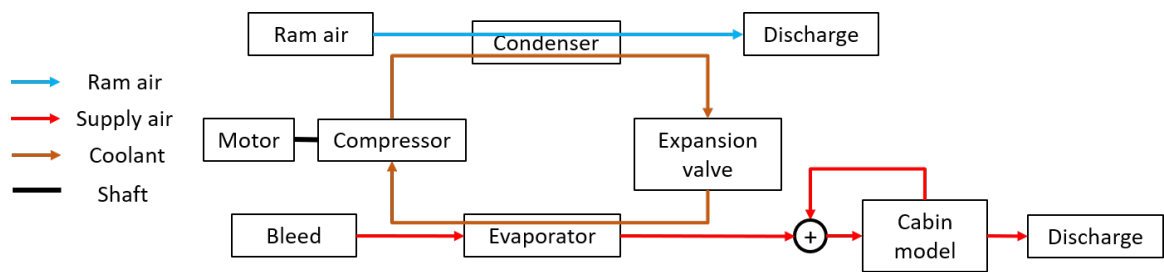


Figure 4.23: Novel ECS with vapor cycle cooling major supply stream without ACS

### *Motor*

For motor as a cooling load, this example only constrains it to use cooling oil as coolant, and there are 160624 architectures generated. Among these generated architectures, conventional architectures have also been found. One generated TMS cools the motor by oil, and then the oil is cooled by fan case air, as shown in Figure 4.24, which corresponds to the architecture shown in Perullo's work [29]. The other generated TMS cools the motor by oil, and then the oil is cooled firstly by fan case air and fuel, as presented in Figure 4.25, which is similar to the oil loop in Moir's book [2]. Thus, these two generated TMS architectures are found similar to conventional ones.

Some novel TMS architectures for the motor are also found. An example is shown in Figure 4.26, which incorporates a PCM to store partial generated heat. It should be acknowledged that the idea to incorporate energy storage material is not uncommon in design the TMS. However, in the existing research on the aircraft motor TMS, similar applications are hardly found. Another example of the generated novel motor TMS is be also found in Figure 4.27. The motor is appended to a PCM, while the oil is firstly cooled by the ECS air, from the air cycle machine, and then cooled by a closed-loop heat pump. The novelty of this architecture is represented by the combination of different sub-architectures, instead of the cooling cycles themselves. In this application, the cooling oil is still used as the heat sink, but the sub-architectures to cool it are different from the applications that have been shown in existing studies. This architecture uses the heat sinks from other TMS (ECS supply air) and a closed-loop heat pump. Similar designs of the TMS is rarely shown for the motor cooling, because ram air or fan bleed air is usually sufficient to cool the cooling oil for existing motor TMS's. This architecture is valid in terms of the thermodynamic perspective, but it may bring significant penalties such as excessive weight and power consumption. However, in the current stage, all these architectures are allowed, and in chapter 5, a method is proposed to filter out these non-optimal architectures. It should be also noted that the inverter is assumed to be integrated with the motor for all

architectures in this study, and heat generation from the inverter is also considered into the motor.

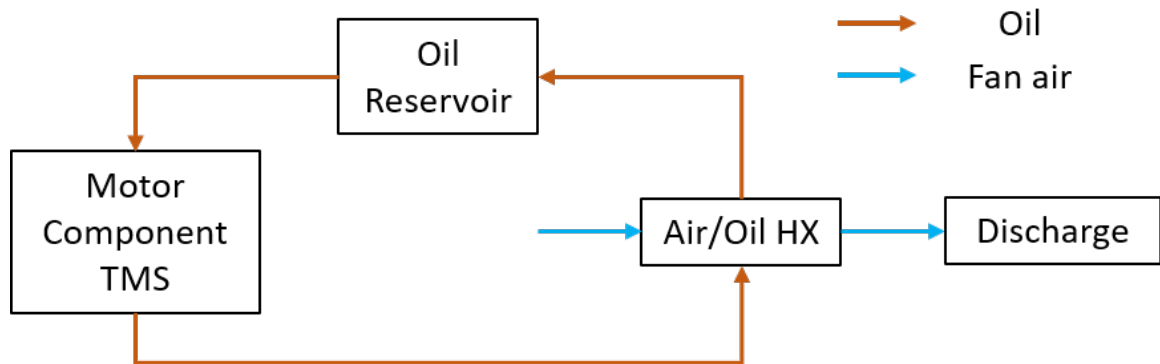


Figure 4.24: Conventional motor TMS 1

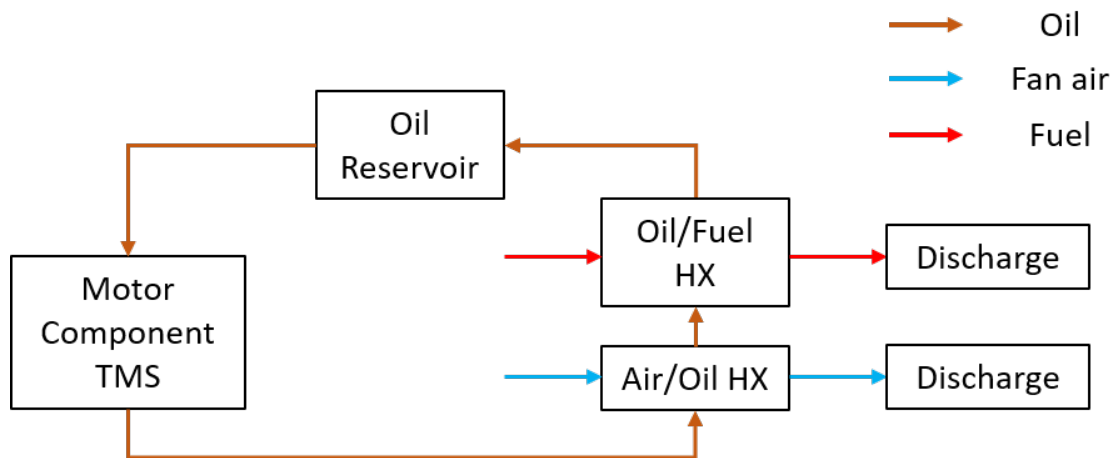


Figure 4.25: Conventional motor TMS 2

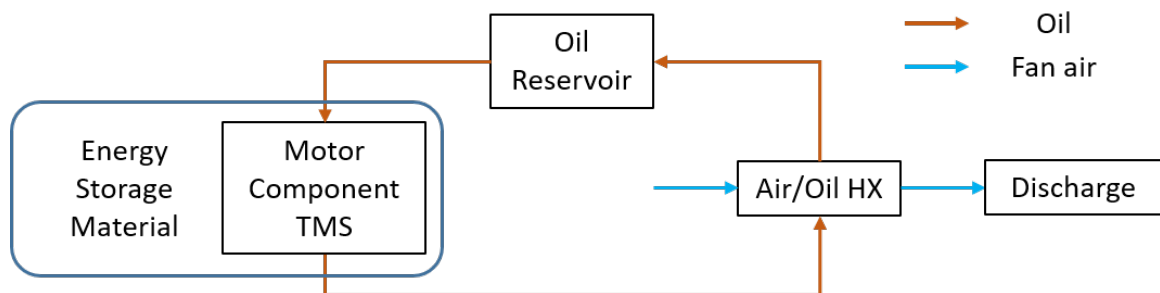


Figure 4.26: Novel motor TMS with PCM

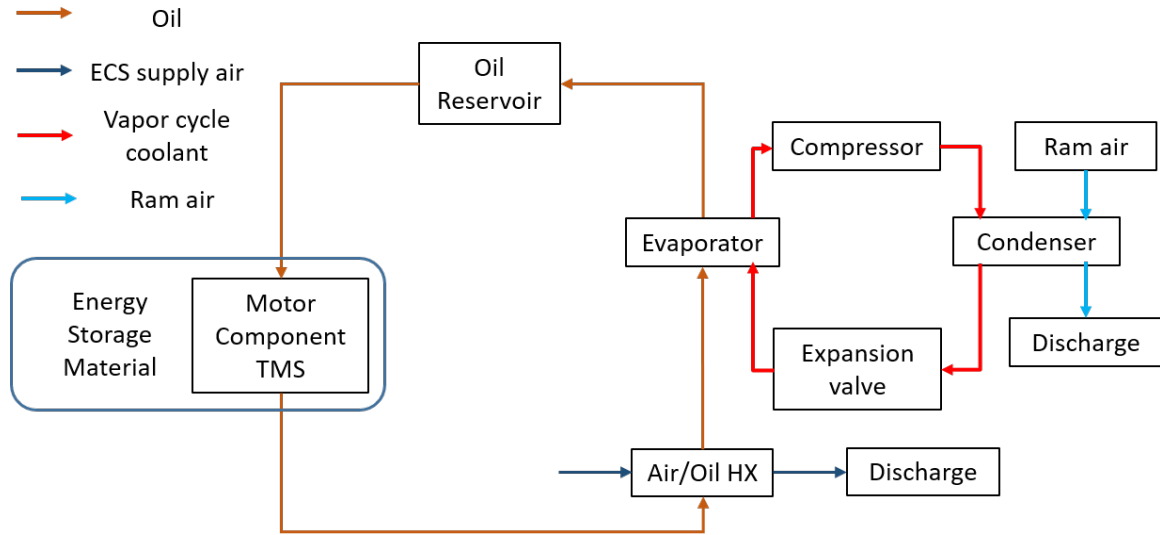


Figure 4.27: Novel motor TMS with PCM, ECS air, and vapor cycle

### Battery

For battery as a load, which incorporates all possible solutions, there are in total 863902 architectures generated. An example for the conventional one is shown in Figure 4.28, which uses a closed-loop cooling oil as the heat sink, and the oil is cooled by ram air.

Several examples for the novel TMS architectures are also presented here. The first two are very similar, both of which use the air from an open-loop air cycle as shown in Figure 4.29 and Figure 4.30. The novelty within these two architectures is that the constructed heat pumps do not use other heat sinks to cool the heat sink in this pump, but re-use the air after cooling the battery. The differences between these two generated architectures are also in the created re-circulation paths. The two heat exchangers in the one associated with Figure 4.29 both use the air directly from load. For the one associated with Figure 4.30, the heat exchanger 1 uses the air from the load but the heat exchanger 2 uses the after from the heat exchanger 1. In general, air cycle machines use ram air or other heat sinks to cool the supply air, due to high cooling effectiveness. It should be noted that these two novel architectures might not be as effective as the conventional TMS's, but they can still provide certain cooling capability by following the behaviors of heat pumps.



Another example for the novel battery TMS architecture is shown in Figure 4.31, which can be classified as a closed-loop heat pump. The coolant in this architecture is firstly compressed, and then rejects the heat to ram air through HX 1. A secondary cooling of the coolant is performed in HX 2. And the coolant is then expanded through a turbine. After the expansion, the coolant is compressed again, and rejects heat through HX 3 and HX 4. It is expanded again through a expansion valve, and then cools the target load, the battery. The re-circulated coolant after cooling the battery is used to perform secondary cooling through HX 4, and HX 2, before being re-circulated to the compressor. This architecture combines two consecutive compression-expansion processes, which is quite different from conventional closed-loop heat pumps which generally only perform one set of compression-expansion process. This architecture also automatically sets a requirement on the coolant by using a expansion valve after a turbine: the coolant before HX 3 must be of a gas form, and it must be of a liquid form after HX 4. This fact also means that HX 1 and HX 2 are gas/gas heat exchangers, and HX 3 and HX 4 are condensers.

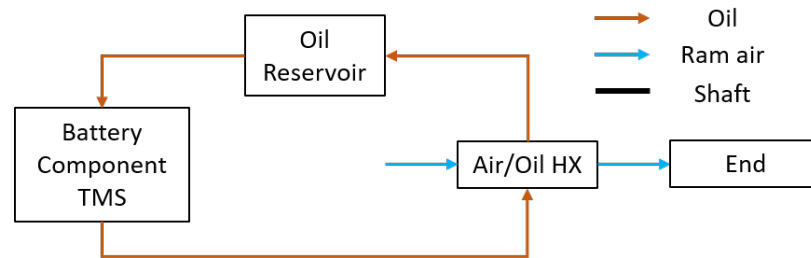


Figure 4.28: Conventional battery TMS

### *Some Other Discussions On the Local TMS Architecting*

First of all, from the architectures generated for selected local loads above, it can be concluded that the proposed architecting methodology is able to populate both intuitive and non-intuitive local TMS architectures. This is obvious because the examples shown in previous subsections have illustrated several TMS architectures that have not been seen in existing literature.

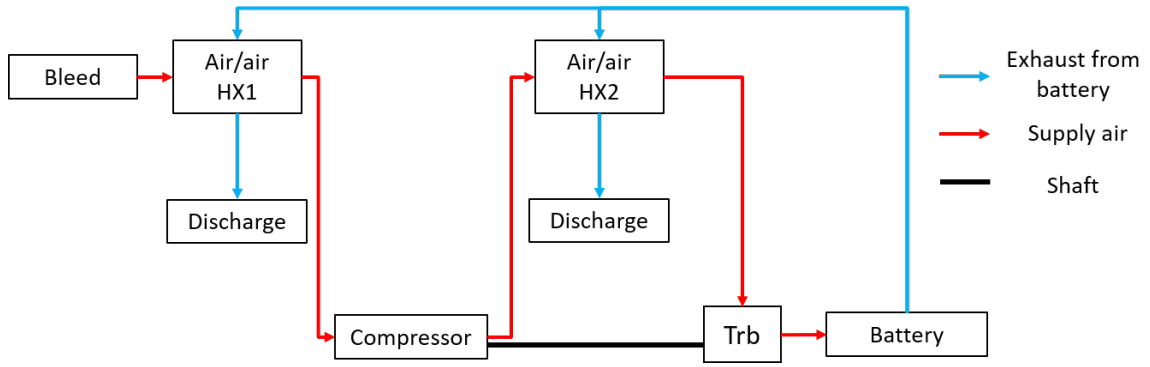


Figure 4.29: Novel battery TMS using air from an open-loop air cycle

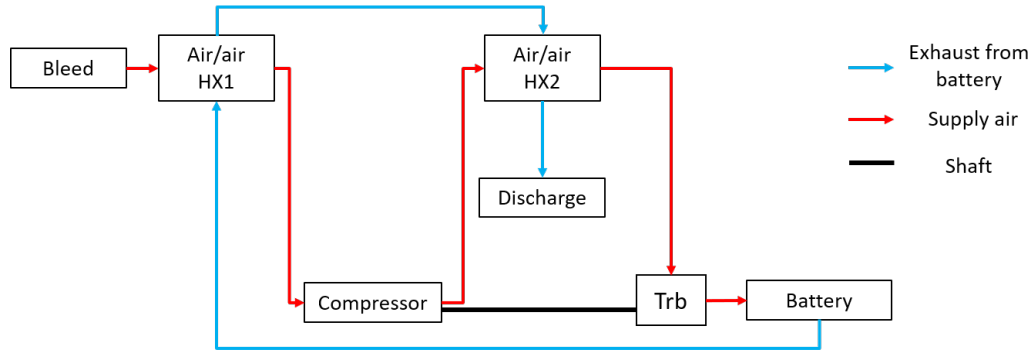


Figure 4.30: Another novel battery TMS using air from an open-loop air cycle

Secondly, the question why there are so many architectures (e.g., more than 1 million architectures for the cabin) that can be generated for a single local load by using the behavior-based backtracking method must be discussed. Let us consider an example using the behaviors but not considering the compatibility among those behaviors. Assume the top level architecture has 8 positions to place behaviors, in which 2 of them are "HX" which will lead to 2 sub-architecture at the next level. For the 6 positions that are not "HX", each has 8 candidate behaviors because compatibility is not considered. The same number of behavior positions and candidate behaviors are assumed for the sub-architectures, but no "HX" is considered for the sub-architectures. It is also assumed there are 3 types of heat sinks for each sub-architecture. Then the total number of architectures will be  $8^6 \times 8^8 \times 8^8 \times 3^3 = 2 \times 10^{21}$  which is a extremely large number compared to the 1 million architectures that are generated by considering the compatibility. Therefore, it can be seen that the proposed behavior-based backtracking methodology instead greatly limits the total

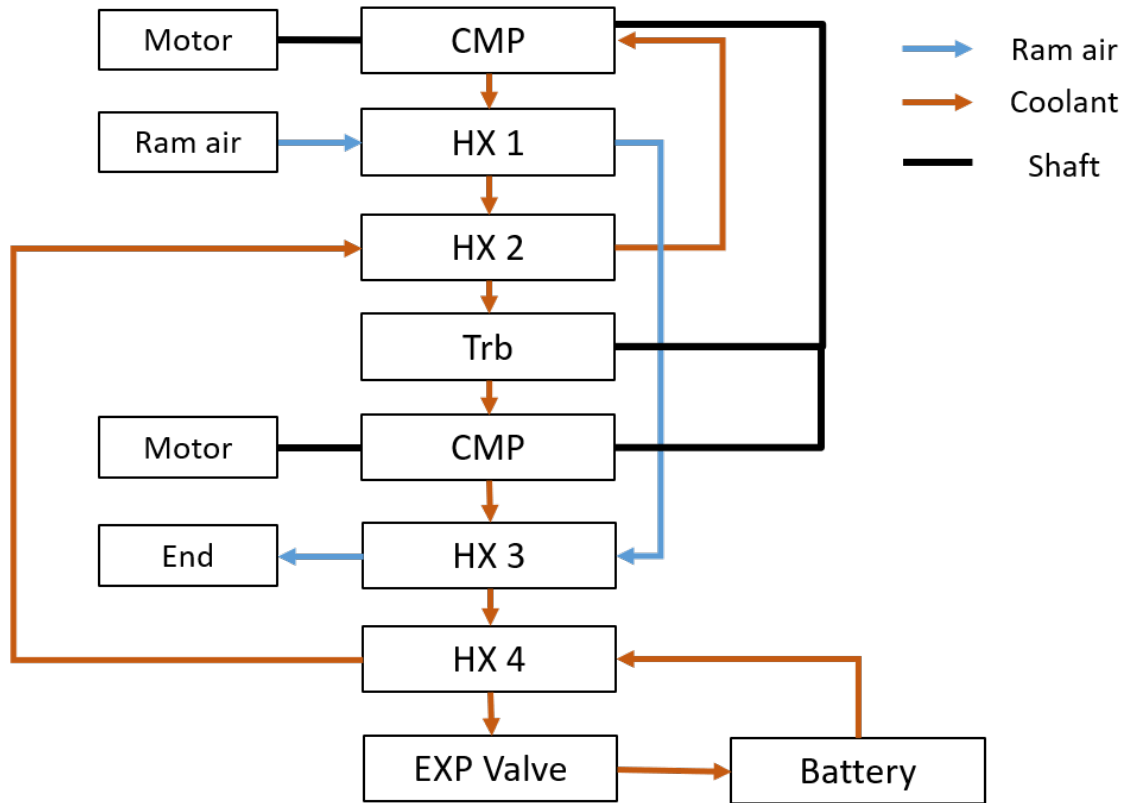


Figure 4.31: Novel battery TMS using a closed-loop heat pump

number of generated architectures by considering the compatibility. Thus, the reason that the generated number of architectures is so large (e.g., more than 1 million) by the proposed method is because the number that is generated by enumeration without compatibility is too large.

#### 4.5.2 Results and Validation of the Global TMS

In this section, local TMS's generated from Experiment Set 1.1 are used to populate the global TMS architecture space. However, if all the generated local TMS architectures are used, the total number of candidate global TMS architectures will be extremely large. To solve this problem, the filtering method will be shown in chapter 5. For the validation purpose, only a few local TMS's are selected to test if the proposed methods can generate global TMS architectures as expected. For each local load, 5 local TMS candidates are

selected to reduce the total number, including certain load requiring exhaust from other TMS's to cool it. It should be also noted that the implementation of the behavior-based backtracking TMS architecting methodology is in Python 3.8 environment [92, 93].

### *Conventional SSA Concept*

The cooling loads for the traditional, TeDP and HTeDP configuration aircraft are used to generate the global architectures. For the traditional configuration, as discussed in the previous section, the cooling loads are cabin, avionics, hydraulics, fuel tank, engine oil reservoir, and generator. In this configuration, the load of avionics is allowed to be cooled by exhaust from other local TMS's. The total number of generated global TMS are 18750. An example of the obtained global TMS is shown in Figure 4.32, where the avionics are cooled by exhaust from the cabin. This generated architecture is consistent with the one in Moir's work [2].

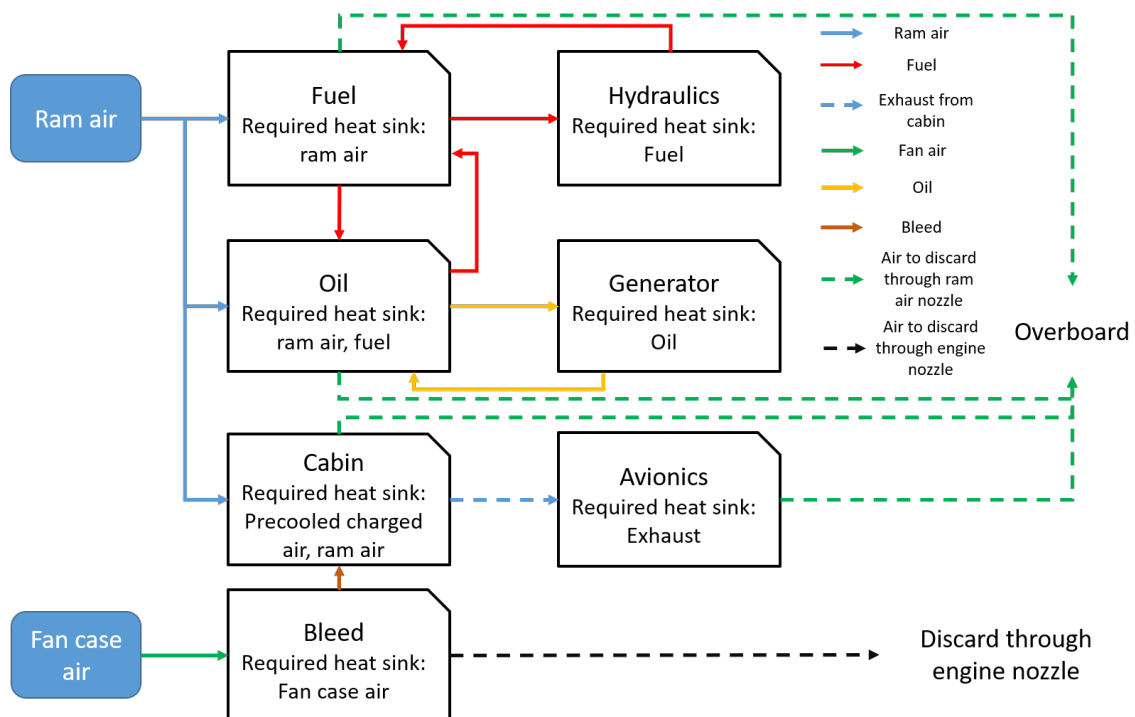


Figure 4.32: Generated global TMS for 160-pax conventional aircraft

Another global TMS that uses electrified ECS is also found, which is shown in Fig-

ure 4.33. The only difference between this architecture with the previously generated architecture as in Figure 4.32 is the different heat sinks for the ECS. Due to this variation, the heat sinks from engine bleed is fully removed.

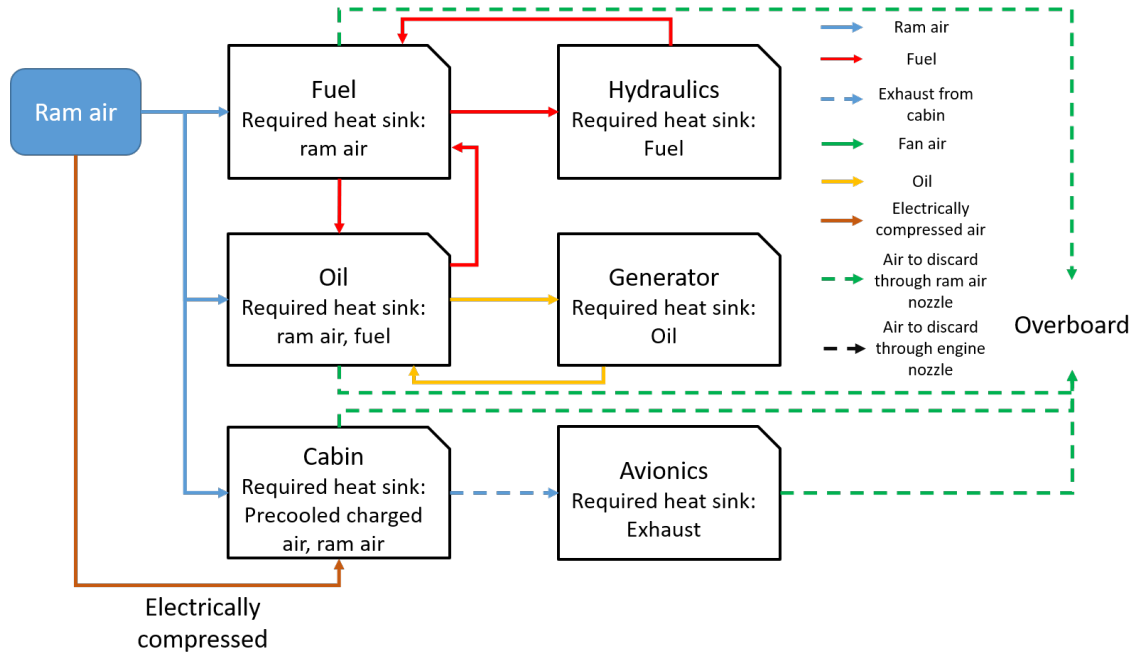


Figure 4.33: Generated global TMS for 160-pax conventional aircraft with electrified compressed supply air

### *TeDP Aircraft*

For TeDP configuration, the selected local cooling loads are cabin, avionics, hydraulics, fuel tank, oil reservoir, and generator and motor. To create variations from the previous case, cooling using exhaust from other local TMS's is allowed for both oil reservoir and avionics. If the propulsion system is required to be non-cryogenic cooling, the total number of generated global TMS architectures is 109375. One example generated global TMS can be shown in Figure 4.34. As shown in this figure, even the propulsion system is electrified, the cabin can still take bleed air as the supply air, since the turbo-shaft generators can still provide enough engine bleed. The electric motor is cooled by the fan air, and it is further cooled by fuel. The generator is cooled directly by engine oil, and the oil is further cooled

by a vapor cycle which is cooled by ram air. As discussed before, the inverter is not listed individually, by assuming it is integrated with the motor.

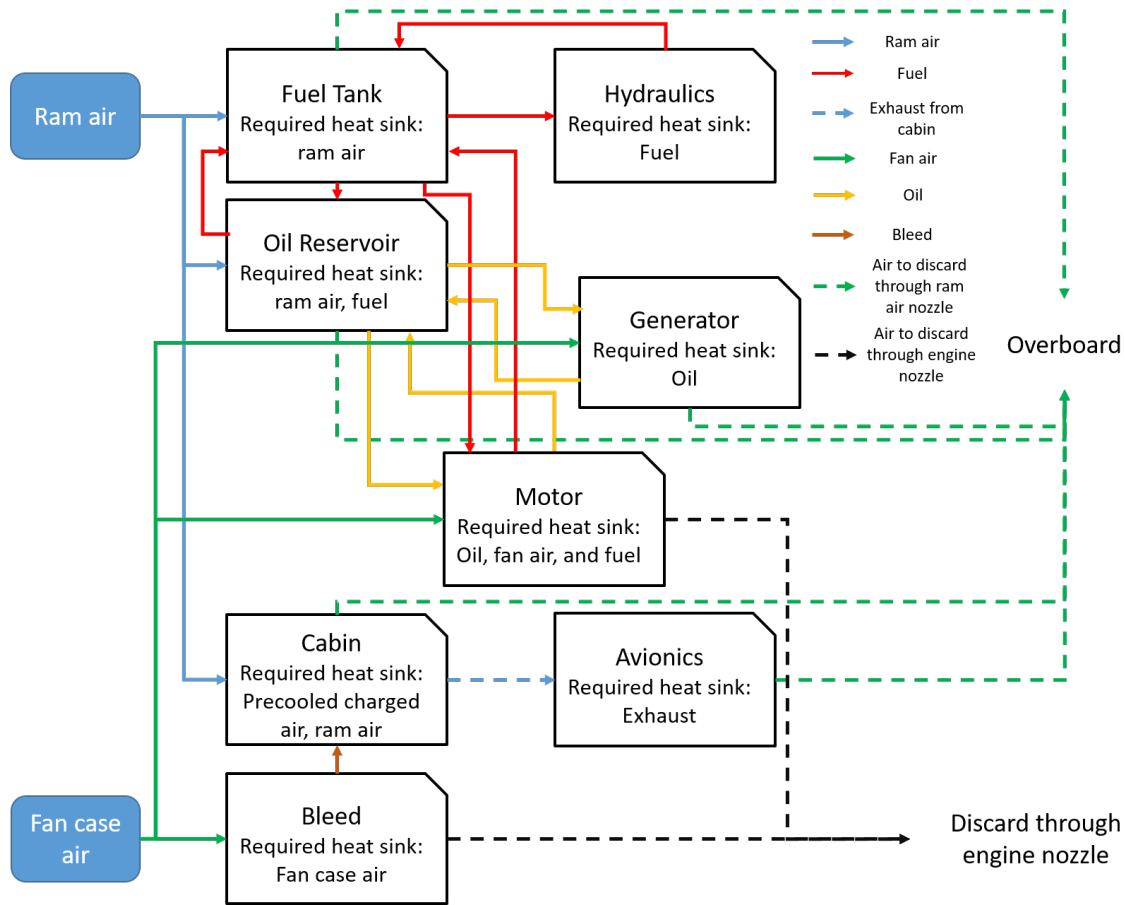


Figure 4.34: Generated global TMS for non-cryo TeDP configuration aircraft

If the propulsion system is required to be cryo-cooled, for both generators and motors, then there are only two options to cool the motor or the generator. The total number of generated global TMS architectures is 12660. Then a generated example global TMS is found to be as in Figure 4.35, where the passive cryo-cooling method is applied, using LH2 as both fuel and coolant. It can be seen that in this generated architecture, the bleed can also be cooled by LH2 to supply to the cabin.

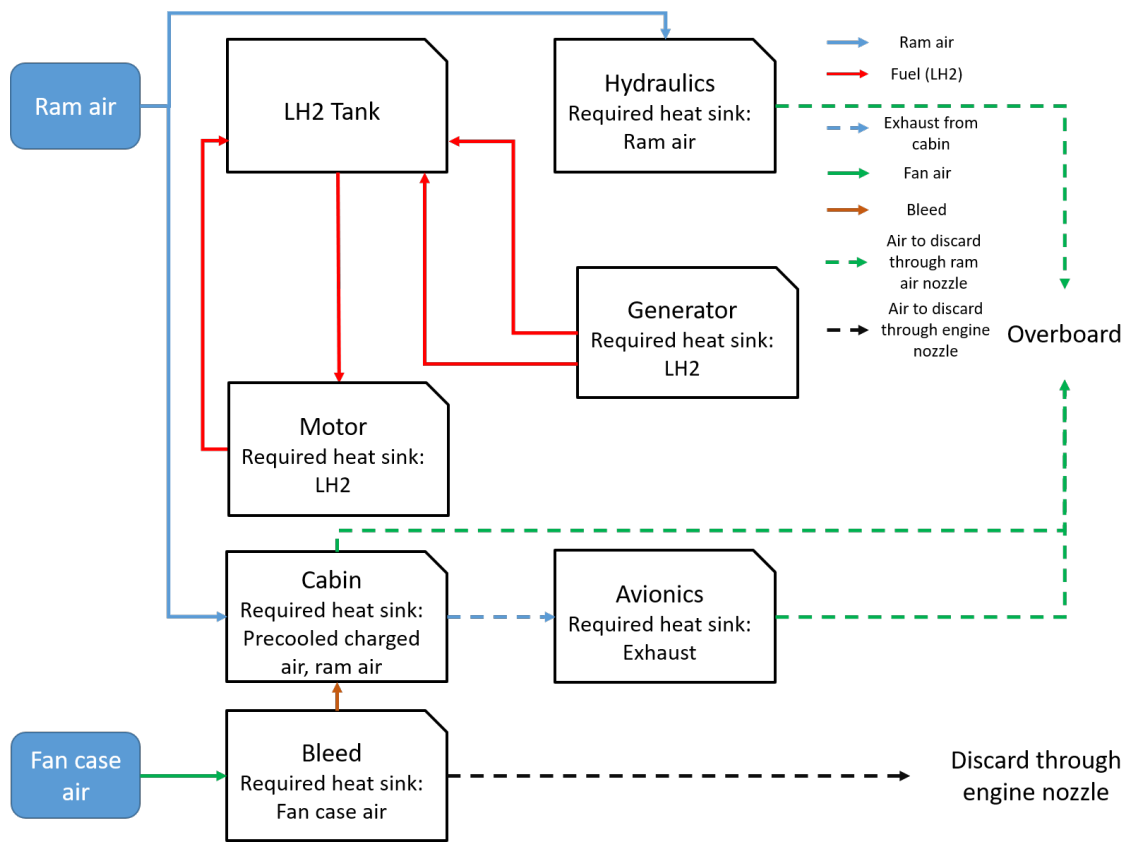


Figure 4.35: Generated global TMS for cryo TeDP configuration aircraft

For HTeDP configuration, the selected local cooling loads are cabin, avionics, hydraulics, fuel, oil, battery, and generator and motor, which are almost the same as TeDP configuration, only with an additional battery. For this configuration, only non-cryo cooling method is considered. The total number of generated architectures is 421875. One generated global TMS architecture is found to be similar to the one in an existing study [32], where motor is cooled by oil loop, and battery is cooled by ECS parallel to the cabin. This generated global architecture is shown in Figure 4.36.

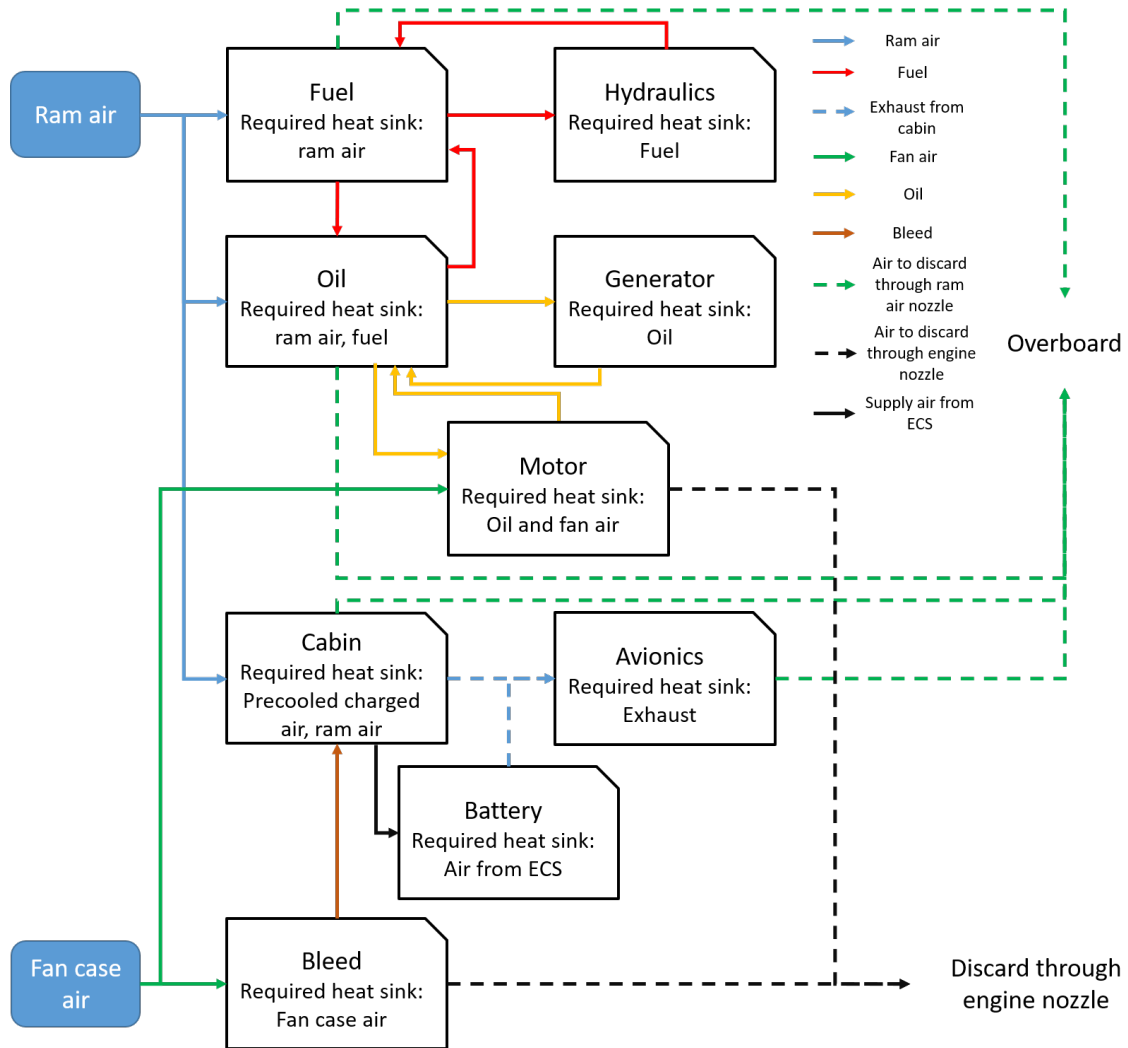


Figure 4.36: Generated global TMS for HTeDP configuration aircraft



Another example that differs from the previously generated one is that the battery is directly cooled by a vapor cycle which takes ram air as the heat sink. The avionics are firstly cooled by a closed oil loop, where the oil is further cooled by the exhaust from the battery, where the exhaust is the refrigerant after cooling the battery through the evaporator before entering the compressor. This global architecture is illustrated in Figure 4.37.

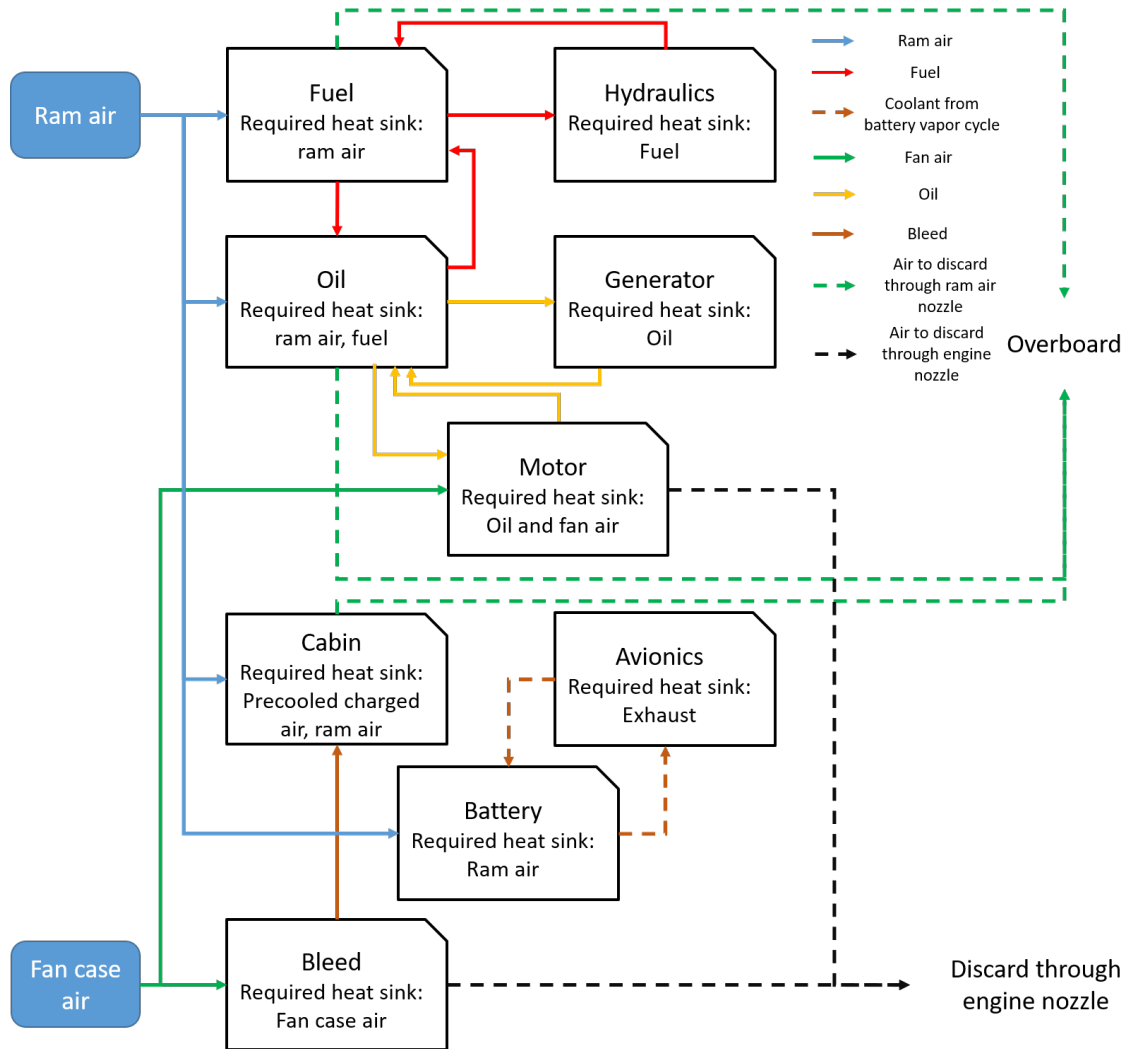


Figure 4.37: Another generated global TMS for HTeDP configuration aircraft

From the global architectures generated above for the three selected aircraft concepts, it can be seen that although the visualization of the global architecture can help the designers to get a clear idea on how the global TMS architectures look like, these visualizations are hard to be used for direct construction of the actual models. Thus, the architectures are still

stored and used in the form of lists as presented in subsection 4.4.3.

## 4.6 Conclusion for Experiment Set 1

### 4.6.1 Validation of Hypothesis 1

How the results obtained from Experiment Set 1 can validate the Hypothesis 1 are stated in this Section. The Research Question 1, Hypothesis 1, and the proposed ways to validate Hypothesis 1 are re-stated below as a reminder:

**Research Question 1:** *With given potential heating and cooling load descriptions and aircraft concepts, how can the thermal management systems architecture space be populated, without over-conservatism that eliminates unconventionally but potentially optimal architectures?*

**Hypothesis 1:** The architecture space of thermal management system architectures can be populated without over-conservatism by using a behavior-based backtracking thermal management system architecting methodology.

**Validation Criteria of Hypothesis 1:** The Hypothesis 1 is valid if the following capabilities of the methodology are shown:

1. With the same heating and cooling load requirements and aircraft concepts, some of the local TMS architectures will match the existing local ones.
2. With the same heating and cooling load requirements and aircraft concepts, some of the global TMS architectures constructed by integration of the generated local TMS architectures will match the existing global ones.
3. With the same heating and cooling load requirements and aircraft configurations, local and global TMS architectures that are different from existing ones can be generated, and they must follow the fundamental thermal cycle behavior (fundamental thermal cycle).
4. The number of architectures generated through the proposed methodology must be much larger than the one from previous studies.

As the results obtained in the Experiment 1.1 show, some of the generated local TMS architectures match the existing ones in the literature, which proves demonstrates the capability 1 here. Some of global TMS architectures from the Experiment 1.2 are similar to the existing ones, validating the capability 2. On the other hand, some of local TMS architectures are novel that they are not found in the literature, but also are reasonable in terms of physics, and novel global TMS architectures also show up, proving the capability 3. Regarding the capability 4, it can be seen that the number of either local or global TMS architectures generated is very large, at the order of one hundred thousand architectures. Thus, the capability 4 is proved. Therefore, the four capabilities are proved, and thus Hypothesis 1 is proved to be true. In summary, Research Question 1 can be answered by the statement in Hypothesis 1, which is validated by Experiment 1.1 and 1.2. Therefore, the sub-objective 1 is fulfilled, which is listed below:

**Sub-Objective 1:** To develop a capability of the proposed method that sufficiently explores the thermal management systems architecture space by systematically identifying both intuitive and non-intuitive architectures.

#### 4.6.2 Conclusions

In conclusion, a behavior-based backtracking TMS architecting methodology is proposed in this chapter to systematically populate both intuitive and non-intuitive TMS architectures at global and local levels. This proposed method is based on the behaviors that follow fundamental physics to firstly construct behavioral TMS architectures, and then convert the behavioral architectures to structural architectures by enumerating potential components that realize the function of each behavior. The backtracking algorithm is used to systematically enumerate TMS solutions while ensuring the compatibility of each behavior and components.

This proposed methodology addresses the Research Question 1 and Hypothesis 1 by conducting the Experiment Set 1. And it further fulfills the sub-objective 1 of the whole

thesis. Through the Experiment Set 1, an 160-pax conventional concept, a 300-pax TeDP concept, and a 78-pax HTeDP concept are used to validate the capability of the proposed method, which is further used to validate the Hypothesis 1. It is demonstrated that the proposed behavior-based backtracking TMS architecting methodology is able to populate the intuitive architectures that match existing ones in the literature, and that it is also able to populate the non-intuitive architectures that have not been seen.

## **CHAPTER 5**

### **EXPERIMENT SET 2 - ARCHITECTURE FILTERING AND OPTIMAL DOWN-SELECTION**

As shown in the previous chapter, the number of either local or global TMS architectures is too large to conduct detailed optimization and sizing. Therefore, Research Question 2 is driven by such problems, and Hypothesis 2 is proposed to address this research question. In this section, an optimal down-selection methodology based on feasibility and clustering of low-fidelity key performance indicators (KPI) is proposed to conduct the Experiment Set 2 as well as to validate the Hypothesis 2. The proposed methodology is expected to rapidly filter out infeasible and non-optimal local and global TMS architectures with low-fidelity models. Then higher-fidelity physics-based models are automatically constructed for the remaining TMS architectures. Finally an optimization and sizing process is performed on the constructed model, which can be further analyzed and integrated to the vehicle and mission model. It should be noted that many modeling methods and optimization approaches included in this chapter are already published by the author [33, 46, 94, 32].

This chapter is organized as follows: firstly the design of the Experiment Set 2 is shown in section 5.1; the formulation of the methodology is discussed afterwards in section 5.2; the actual filter and the optimal down selection approach is presented next in section 5.3; the component modeling methods are also introduced in section 5.4; the results are then obtained in section 5.5, which also validate the Hypothesis 2; finally, the conclusions are stated in section 5.6.

## 5.1 Design of Experiment Set 2

### 5.1.1 Overview of Research Questions 2, Hypothesis 2, and Design of Experiment Set 2

The Research Question 2, Hypothesis 2, and Experiment Set 2 are re-stated here as a guidance for development of the TMS architecture filtering and optimal down selection methodology:

**Research Question 2:** *With a number of thermal management systems architecture candidates, how can the architecture evaluation process rapidly filter out architectures which are not viable, and perform further down-selection of optimal architectures on the left competent architectures based on chosen metrics, where the information required are suitable for conceptual design phase with limited historical data.*

**Hypothesis 2:** Large number of infeasible or non-optimal architectures can be eliminated by filtering process in terms of feasibility and low-fidelity subsystem-level analysis on key performance indicators, and further down-selection of optimal architectures can be done by evaluations using physics-based optimization, sizing, and analysis, where the physics-based models are created automatically from the architecture descriptions.

The initial statement of the Experiment Set 2 is:

**Experiment 2.1:** Filter out infeasible TMS architectures based on feasibility of each TMS architecture to handle the thermal management requirements at the extreme flight conditions where the heat loads are the largest.

**Experiment 2.2:** Verify if subsystem-level KPI of each TMS architectures can be rapidly analyzed using low-fidelity methods.

**Experiment 2.3:** A further filtering is performed based on the KPI on the TMS architecture candidates using clustering.

**Experiment 2.4:** Automatically create physics-based TMS models from the architecture descriptions generated from the Experiment Set 1.

**Experiment 2.5:** Perform optimization, sizing, and analysis using physics-based mod-

eling and simulation. The optimal architectures are selected based on chosen metrics.

### *How Experiment Set 2 Is Used for Validating Hypothesis 2*

If a large number of inviable architecture candidates can be eliminated from the feasibility-based low-fidelity KPI-based filtering process, then the capability of the proposed approach in Hypothesis 2 to narrow down the architecture space is validated. If the model can be automatically constructed from the architecture descriptors generated from Experiment Set 1, on which the optimization and sizing process can be directly performed, then the optimal down selection approach in Hypothesis 2 is validated.

#### 5.1.2 Cases of Interest in Experiment Set 2

In the Experiment Set 2, the global and local TMS architectures generated from Experiment Set 1 are used. To be consistent with chapter 4, same loads are selected to show example results, as well as the validation of the Hypothesis 2. The loads are: cabin for a 160-pax conventional SSA, motor for a 300-pax TeDP, and battery for a 78-pax HTeDP.

#### *160-PAX Conventional SSA Concept*

The cabin for the 160-pax conventional SSA configuration is selected for the experiment. As for the commercial aircraft, the ECS, which is mostly to cool the cabin, is the largest consumer of non-propulsive power [3], where the major heat comes from metabolism of passengers and the electrical devices used in cabin. In this thesis, the heat generated by metabolism is assumed to be  $75W$  per person [26]. The power consumption of galley loads and In-Flight Entertainment (IFE) are assumed to be dissipated entirely as heat [13]. Thus, the heat generated by IFE is  $50W$  [27] per person and the heat load of galley load is  $320W$  per person [27]. The heat transfer between the cabin and the outside environment is also considered, where a cabin model is used to quantify such heat transfer. The detailed cabin model will be introduced in section 5.4. In this experiment, the cabin only allows



compressed air as the heat sink, because the supplied air not only needs to provide the cooling capability, but is also required to provide enough cabin pressure.

### *300-PAX TeDP Concept*

The electric motor for the 300-pax TeDP configuration is selected for the experiment. The heat generation from an electric motor is the difference between its input power and the shaft power, which is the product of the motor efficiency and the input power. The input power is determined by the required power of the whole aircraft under certain flight conditions. The aircraft model and the mission model are described in chapter 6, and the motor model is introduced in this chapter in section 5.4. In this study, two types of heat sinks are considered for the motor: oil and cryogenic coolant. The oil is selected for the case that the coolant is required to provide both cooling and lubrication functions. The cryogenic coolant works in the way that the motor is submerged in it. And the cryogenic coolant can perform either active or passive cooling.

### *78-PAX HTeDP Concept*

The battery for the 78-pax HTeDP configuration is selected for the experiment. The battery is different from the previous two configurations. The battery slowly accumulates the heat through the whole mission, and its TMS only needs to remove certain amount of heat that is generated from it to keep it under its temperature through the whole mission, while the TMS's for the cabin and the motor need to reject all the heat generated at every moment, if heat generation margin is assumed to be zero. The battery model will be introduced in section 5.4. All types of cooling methods except cryogenic cooling are allowed to cool the battery in this experiment.

### 5.1.3 Overall Design of the Experiment Set 2

The Experiment Set 2 takes the local TMS architectures generated by Experiment 1.1 as input. Then the feasibility-based filtering process is performed on these architectures (Experiment 2.1) to examine if the infeasible local architectures can be rapidly filtered by this proposed method. Then the key performance indicator (KPI) of remaining local TMS architectures are evaluated. Experiment 2.2 is to test if such low-fidelity analysis can be done in an acceptable time frame. To further reduce the number of generated local TMS architectures, clustering is applied in Experiment 2.3 to group architectures with similar KPI into same clusters. Then the representatives of each clusters that are at the Pareto frontier are used to generate all possible global TMS's as shown in Experiment 1.2. Then the clustering technique is used again to reduce the number of global TMS architectures. With remaining global TMS architectures, the physics-based TMS models are automatically created in Experiment 2.4, directly using the architecture descriptions generated in the Experiment Set 1. Finally, the Experiment 2.5 performs the sizing and optimization on the models created in Experiment 2.4, where the generated TMS architectures are eventually optimally down-selected. These experiments are summarized in Figure 5.1.

## **5.2 Formulation of Methodology**

Before introducing the actual developed methodology for the Experiment Set 2, it is necessary to discuss how it was formulated.

### 5.2.1 Identified Problems from Experiment Set 1

As shown in the Experiment Set 1, the number of the generated architectures of either local TMS or global TMS is too large to conduct optimization, sizing, or analysis on physics-based models. For example, the number of generated cabin TMS architectures is 1362240, and the number of global architectures for an HTeDP concept is 421875 where the number

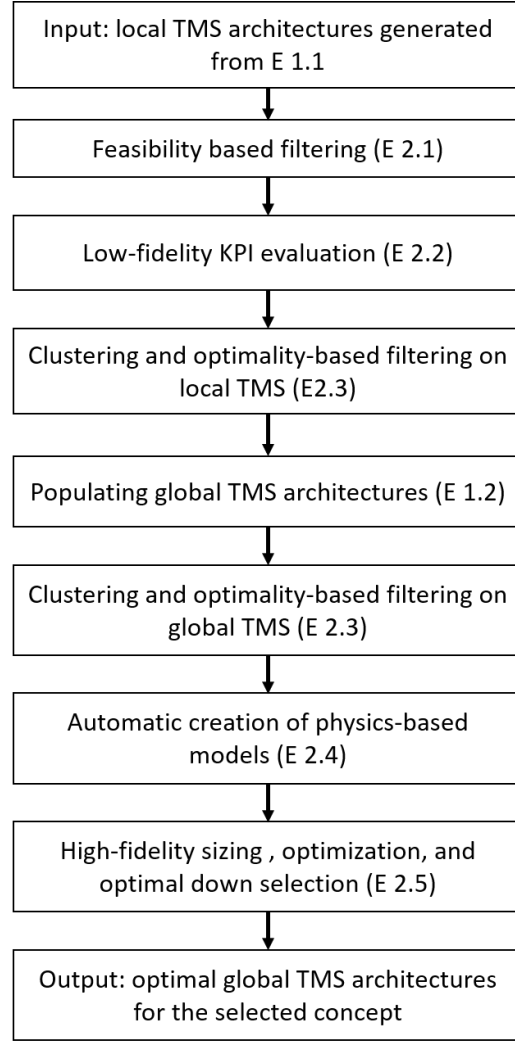


Figure 5.1: Overall process of the Experiment Set 2

of candidate local architectures is only 5 for each load. Therefore, an effective method to reduce the number of candidate architectures, at either local or global level, is needed to practically perform sizing, optimization, and analysis on physics-based models. To fill this gap, the following methodologies are proposed.

### 5.2.2 Filtering Method Based on Feasibility

Since the populating process of the local and global architectures only follows the fundamental physics, there might be some infeasible and non-optimal architectures in them. Therefore, it is natural to think that if the infeasible and non-optimal architectures can be

rapidly filtered out with low-fidelity analysis, then the number of architectures for higher-fidelity optimization and sizing can be greatly reduced. Literature [72, 59, 60, 61] as discussed in literature review in chapter 2 has suggested multi-fidelity methods to solve this problem, where feasibility is used to filter out architectures that are not viable. However, the feasibility in these literature simply refers to compatibility, which is already guaranteed by the Experiment Set 1. Thus, another definition of feasibility needs to be defined. It is noticed that certain types of TMS architectures can only be used for certain loads, because there exists a cooling capability limitation for each TMS cooling capability. For example, cryogenic devices cannot be directly cooled by ram air, or a conventional oil cooling loop cannot fully remove the heat from the electric motor [39]. Therefore, the infeasible architectures here can be defined as the ones that cannot fulfill its heating or cooling functions. While the non-optimal architectures are defined as the ones that are not competent compared to other architectures. This incompetence simply means that their KPI are worse than other architectures, or the KPI are not at the Pareto frontier. The selected KPI in this context are: shaft-power extraction, bleed air extraction, ram air, and weight, where the first three metrics are at the cruise condition. The reasons to select this four metrics will be discussed in subsection 5.3.3

To evaluate the feasibility of a certain TMS architecture, it is noticed that the thermal management capability is always mostly limited at its critical condition, where the heating or cooling load is the largest. For example, the hot-day on-ground condition for the cabin is the most critical one, because the heat reject through the cabin wall is the worst, and the ram air is of its highest temperature through the mission, while the load inside the cabin is almost the same. So the feasibility of a TMS architecture is tested at the critical condition of the corresponding load. On the other hand, to avoid creating higher-fidelity models to test the feasibility, the best performance for all the components from empirical data can be used. The best performance here refers to the maximum allowed mass flow rate for heat sinks, the best efficiency, the best heat exchanger effectiveness, and the maximum allowed

compression ratio. It can be seen that a TMS architecture will reach its highest thermal management capability with such best performance parameters. Therefore, if a TMS with the best performances still cannot provide sufficient thermal management for a certain load, then it must be infeasible in handling this load in reality.

In addition, the duty cycle of the load should also match the types of the TMS. In this context, the duty cycle of a load is defined as the time duration through the whole mission that a load generates heat. For example, most of the loads discussed before will continuously generate heat through the whole mission, but some other types of load, such as a laser system (mostly in military application), will be generating heat in a short period of time. Therefore, if a load continues generate heat, while the generated local TMS architecture uses only materials to absorb it without rejecting it out of the aircraft, such as PCM, then this architecture is defined infeasible. Theoretically if the size of such energy storage material is large enough, it should be able to absorb all the generated heat. However, it will add excessive weight to the vehicle. Such high-weight architectures can be indeed filtered out by the optimality-based filtering, which will be discussed next, but it will greatly increase the number of architecture candidates. Thus, if the duty cycle of the load does not match the type of the TMS, then the TMS will be determined infeasible.

In summary, the best performances from empirical data are assigned to components in the generated TMS architecture to test if the load can be sufficiently cooled or heated at its critical condition. If an architecture with the best performances cannot handle a certain load, then this architecture is determined infeasible for this load. It should be noted that even there are no historical data for new concepts and their TMS's, most fundamental components that the TMS's use are still conventional, of which historical data is abundant. It should be also noted that the generated heat is an estimated value, while the actual value is obtained from the aircraft or mission models, which will be discussed in the next chapter.

We must also acknowledge the fact that many of the generated TMS architectures may be eliminated by only "looking" at them without diving in to the actual quantitative analy-

sis, because these infeasible architectures might be obviously wrong in terms of the designers' own experience. Although this way to eliminate the infeasible architectures does not require quantitative analysis, which may improve the efficiency of the filtering process, it is not implemented in this research due to the following reasons: 1. accurate visualizations of the architectures are needed for designers to get a feeling of the corresponding TMS's, but the number of the generated architectures is too large to be visualized and processed (e.g., over one million); 2. the judgement made by looking at the architectures is highly dependent on the designers' experience, making it difficult for inexperienced designers; 3. such judgement is also subjective, which can lead to a small design space which is confined by individuals' own opinions, but the filtering method to be developed in this chapter incorporates physics-based analyses which eliminates the reliance on designers' experience.

### 5.2.3 Filtering Method Based on Optimality

To perform low-fidelity KPI evaluations with TMS architecture descriptions given by the Experiment Set 2, an idea that is similar to the approach examining the feasibility can be applied. However, in this low-fidelity KPI evaluation, the operation condition is cruise because the operation in this condition influences the mission performance most. In addition, the required amount of heat sink should be computed by the amount of generated heat, and the performances of the components are of average values that are used in academic research instead of best values from literature. The low-fidelity KPI is not enough to compare different architectures, and the remaining number of architectures after feasibility-based filtering process can still be large. Thus, a further filtering process based on the KPI is needed. As shown in previous studies [72], clustering can be used to reduce the number of TMS architecture candidates, Therefore, following this work, a clustering technique is implemented to narrow down the architecture space for further higher-fidelity analysis.

#### 5.2.4 Automatic Creation of TMS Simulation Models

After the two filtering processes, the number of remaining architectures are suitable to create higher-fidelity models on which sizing and optimization can be performed. To simplify the modeling process, an automatic creation process for the TMS simulation models is needed, because the manual effort can be very large if multiple architectures are compared together. It should be noted that the model creation is only for the local TMS, while the global TMS is constructed by integrate each local TMS through interfaces in the aircraft and mission models. As presented in chapter 4, the descriptor of a local TMS architecture is in the form of list of lists. An example is shown below:

```
[[['Start', 'Load', 'HX_1', 'HX_2', 'End', 'Oil', 'ClosedLoop_Direct']], ['Start', 'Load', 'End', 'FanAir', 'OpenLoop_Direct'], ['Start', 'Load', 'End', 'Fuel', 'OpenLoop_Direct']]].
```

It can be seen that the most inner list contains the components that construct the architecture, which can be viewed as an object. Therefore, if an object-oriented programming (OOP) technique, where computer programs are constructed by designing them out of objects that interact with one another [95, 96], can be used to construct the model, then as the descriptors are read by the computer, it is possible to construct the corresponding objects in parallel to create physics-based models. In summary, the automatic model creation process can be formulated as a method that reads the descriptors which are generated from Experiment Set 1, and treats each component as an object, and instantiate them in an OOP environment.

#### 5.2.5 Sizing and Optimization

The common way to size or optimize a TMS is under a single operation condition, whether the most critical condition (highest load), or the condition that lasts the longest through a mission (such as cruise). For example, the work by Chakraborty [13], Shi[33], and Parrilla [66] sized the ECS at the hottest condition, hot-day on-ground condition. And some other researchers have performed exergy-based optimization at the cruise condition [63, 69,

70, 71, 68], which has already been discussed in chapter 2. However, such single-design point sizing and optimization method might miss the constraints or degrade the performance at other points [94]. Therefore, in this thesis, a multi-design point (MDP) sizing and optimization methodology is incorporated, which was also developed by the author [94]. The development of this method was inspired by the MDP sizing method for gas turbine engines [97, 98], which is to overcome the single-design point sizing method [99, 100]. The developed MDP sizing and optimization methodology for a TMS is to ensure optimal performance of the TMS through the whole mission, as well as satisfying the constraints at all mission conditions.

### **5.3 Filtering and Optimal Down Selection Methodology**

#### **5.3.1 Overview of the Methodology**

Summarized from the previous section, the proposed methodology for the Experiment Set 2 is a multi-fidelity approach. The low-fidelity evaluations are performed in the feasibility examination and KPI assignment, where the best performance is assumed for the feasibility examination and average performance is used to quantify the KPI. With the obtained KPI, clustering is performed to further reduce the number of candidate architectures. It should be noted here that As discussed in the overall process of the Experiment Set 2, which is illustrated in Figure 5.1, the feasibility-based filtering method works on the local TMS, and the low-fidelity KPI evaluations and clustering are performed on both the local TMS and global TMS. After the filtering, the physics-based models are automatically constructed in an OOP environment, and further higher-fidelity sizing and optimization using information from multi-design points are conducted. This overall methodology, combined with the design of the overall Experiment Set 2, is shown in Figure 5.2.



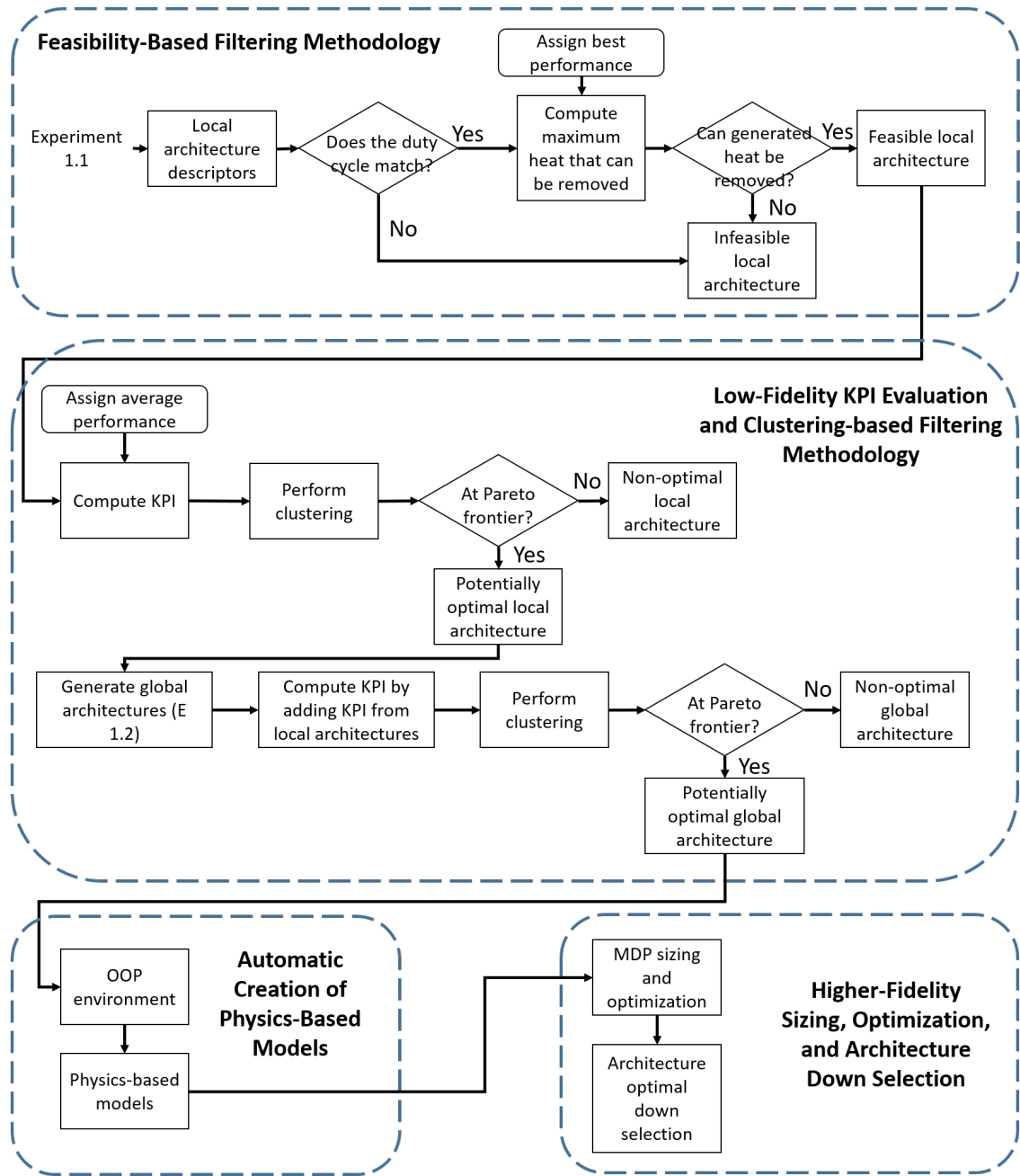


Figure 5.2: Overview of methodology for Experiment Set 2

### 5.3.2 Feasibility-Based Filtering Methodology

As presented previously, the feasibility is checked firstly in terms of the duty cycle of the target load, and the maximum thermal management capability is then examined. This process is illustrated in Figure 5.3.

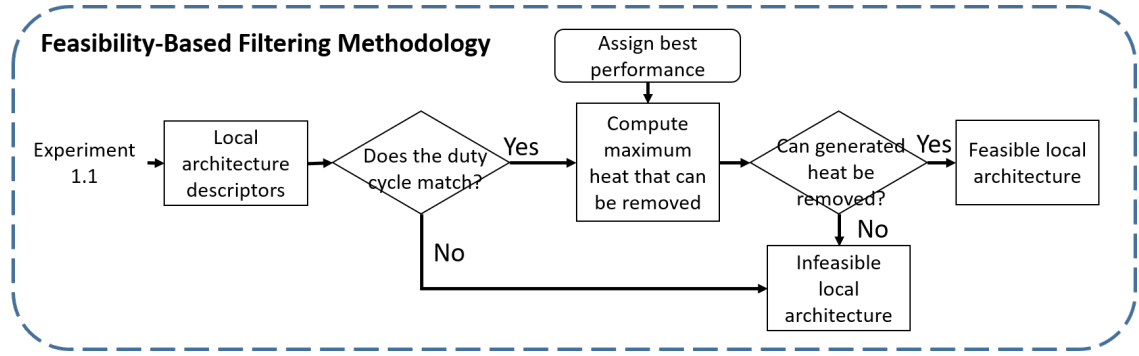


Figure 5.3: Overview of feasibility-based architecture filtering methodology

### *Duty Cycle*

In this thesis, three types of duty cycles are defined: "continuous", "accumulative", and "short period". The "continuous" load means the load continuously needs heating or cooling through the whole mission, and the required cooling or heating power must be satisfied at any moment, assuming there is no thermal management margin. The "accumulative" load means the load generates or loses heat continuously through the whole mission, but the requirement is that it cannot violate its temperature limits, allowing the heating or cooling provided by the TMS not equal to its heat loss or generation. The "short period" loads only generates heat in a very short period of time, and any type of cooling methods is allowed for it as long as the generated heat can be removed. Therefore, the TMS using only energy storage material such as PCM, are allowed for "accumulative" and "short period" loads, but are insufficient for "continuous" loads.

### *Maximum Thermal Capability Computation*

In the process that examines the maximum thermal management capability, the best performance for each component is used, where the implemented values will be shown in subsection 5.5.1. In this subsection, the process to compute the maximum thermal capability is described. The computation process for each component will be discussed in the following subsections, which are used to construct this overall process.

As introduced in chapter 4, the heat exchange process in one sub-architecture is the load for the next-level sub-architecture to cool or heat. Therefore, each heat exchange process is a linkage between the sub-architecture at the current level and the next level. So when a heat exchange process is encountered, the sub-architecture at the next level will be evaluated first. And when the next-level sub-architecture finishes evaluation, the corresponding properties will be returned to the current-level sub-architecture to analyze the thermal management capability. In summary, basic idea to compute the thermal management capability in a given TMS architecture is:

1. Initialize the properties of media that is used to cool or heat the load.
2. Start from the first component of the top level sub-architecture to update the properties of the media, following the sequence of the components instantiated in the TMS architecture descriptor.
3. When a heat exchange process (a heat exchanger, condenser, or evaporator) is encountered, the evaluation of the next-level TMS architecture begins, where the properties of the media for this level is also initialized.
4. Continue updating the properties following the sequence of the components until the "End" component is encountered
5. Next, return the required properties to the previous-level sub-architecture for further computation
6. This process ends until the "End" component is reached at the top-level sub-architecture, which returns the final properties of the media which is used to determine if the maximum thermal management capability can handle the given cooling or heating load

An example is presented below to help explain the process more clearly, where the list of lists form of architecture is:

[[['Start', 'Load', 'HX\_1', 'HX\_2', 'End', 'Oil', 'ClosedLoop\_Direct']], [['Start', 'Load', 'End', 'FanAir', 'OpenLoop\_Direct']], ['Start', 'Load', 'End', 'Fuel', 'OpenLoop\_Direct']]], and the visualization of the example architecture is shown in Figure 5.4.

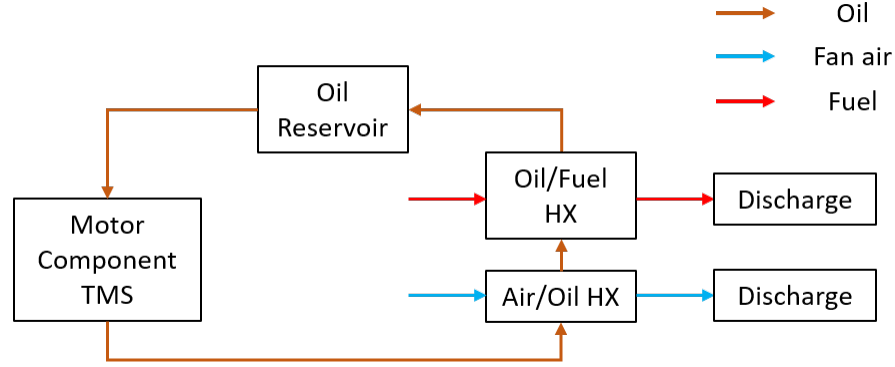


Figure 5.4: Example to illustrate the maximum thermal management capability

The process to quantify the thermal management capability using the list of lists form can be illustrated in Figure 5.5. The process starts from Oil Start component in the oil loop. After cooling the load, electric motor, the process moves to HX\_1 and starts the computation for the fan air loop, then at the "End" of the fan air loop, the properties return to the oil loop. At HX\_2, the process starts to compute properties for the fuel loop, and at the "End" of the fuel loop, the properties return to the oil loop. Finally, at the "End" of the oil loop, the properties are finalized and it can be used to check if this architecture is feasible.

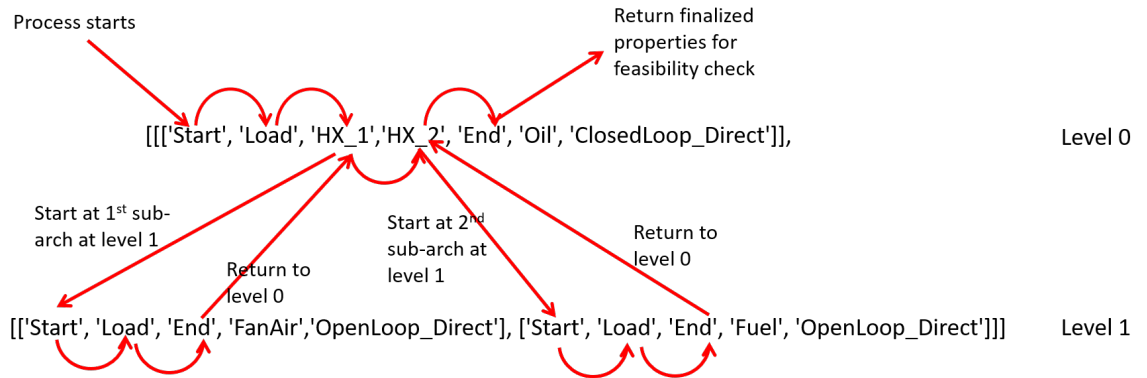


Figure 5.5: Example for computation process of maximum thermal management capability

It is discussed here how the finalized properties are used to check feasibility. Firstly,

some definitions to be used in the examination process are presented.  $T_{best}$  is defined as the best temperature that the media can be after heating or cooling the load. If the load is to be cooled,  $T_{best}$  is defined using the following equation, where  $T_{highest,media}$  is the highest temperature that the media is allowed to be, and  $T_{highest,load}$  is the highest temperature that the current media can be after cooling the load:

$$T_{best} = \min(T_{highest,media}, T_{highest,load}) \quad (5.1)$$

$T_{highest,media}$  is determined by the types of material that are selected as the heat transfer media, usually considering the safety of the material.  $T_{highest,load}$  is determined by heat transfer effectiveness of the load  $\epsilon_{load}$ , the load working temperature  $T_{load}$ , and the media temperature before cooling the load,  $T_{before,media}$ . The effectiveness of the load is still defined as the one for heat exchangers: the ratio of the actual heat transfer to the maximum possible heat transfer [101], as denoted by the following equation, where  $cp_m$  is the specific heat capacity of the media, and  $\dot{m}_m$  is the mass flow rate of the selected media:

$$\epsilon_{load} = \frac{\text{Actual Heat Transfer}}{\text{Maximum Possible Heat Transfer}} \quad (5.2)$$

$$= \frac{\dot{m}_m cp_m (T_{highest,load} - T_{before,media})}{\dot{m}_m cp_m (T_{load} - T_{before,media})} \quad (5.3)$$

$$= \frac{T_{highest,load} - T_{before,media}}{T_{load} - T_{before,media}} \quad (5.4)$$

from which  $T_{highest,load}$  can be computed, and  $T_{best}$  can be further obtained using Equation 5.1.

If the load is to be heated, similarly,  $T_{best}$  can be expressed in the following equation, where  $T_{lowest,media}$  is the lowest temperature that the media is allowed to be, and  $T_{lowest,load}$

is the lowest temperature that the current media can be after heating the load:

$$T_{best} = \max(T_{lowest,media}, T_{lowest,load}) \quad (5.5)$$

and the  $T_{lowest,load}$  can be obtained using the effectiveness of the load:

$$\epsilon_{load} = \frac{T_{before,media} - T_{lowest,load}}{T_{before,media} - T_{load}} \quad (5.6)$$

which is similar to Equation 5.4.

Then the feasibility can be examined by the obtained  $T_{best}$  and finalized temperature of the media,  $T_{final}$ : when the load is to be cooled, if  $T_{final} \leq T_{best}$ , then the TMS architecture is feasible, or it is infeasible otherwise; when the load is to be heated, if  $T_{final} \geq T_{best}$ , then the TMS architecture is feasible, and otherwise, it is infeasible. This is because the mass flow rate of the media is set to be as large as possible in this feasibility examination process, which means that the removed or added heat by this architecture should be larger or equal to the required amount if this selected architecture is feasible to handle the heating or cooling requirement.

It should also be noted here that a special type of TMS architecture for cooling load will always be determined feasible, which is the one actively cools the load while using energy storage materials to absorb excessive heat in parallel. Such decision is made by the assumption that the excessive heat that cannot be removed by the active cooling architecture can be absorbed by the PCM by increasing its size. It is also assumed that the actively cooling architecture can remove most of the heat, avoiding using too heavy PCM for such cooling tasks.

### *Pseudo-code*

The pseudo-code of the process to check both duty cycle and the maximum thermal management capability is presented in Algorithm 3 and Algorithm 4. Due to the fact that the

same process will be called each time when heat exchange is encountered, the function is written in a recursive manner to make the code short and clean.

---

### Algorithm 3 Feasibility Examination

---

```

function FEASIBILITY_CHECK(Load)
    copy generated architectures for Load to sol
    sol_feasible
    for i in range(len(sol)) do
        if dutyCheck(sol[i],load) then
            if capabilityCheck(sol[i], load) then
                sol_feasible.append(i)
            else
                pass
        else
            pass

function DUTYCHECK(solution,Load)
    if solution.type does not match Load.dutyCycle then
        return False
    else
        return True

function CAPABILITYCHECK(solution,Load)
    char, Temp_best = feasibilityEvaluation(solution[0][0], Load, [0,0,0,something],
    load.eff)
    Temp_final = char[0]
    if Load.TMS_type == 'Cooling' then
        if Temp_final>Temp_best then
            return False
        else
            return True
    else
        if Temp_final<Temp_best then
            return False
        else
            return True

```

---

---

**Algorithm 4** Feasibility Evaluation Function for The Examination Process

---

```
function FEASIBILITYEVALUATION(subsolution, Load, char_pre)
    feasibility_flag = 1
    Char_previous = char_pre.copy()
    Char = [0,0,0, 'something']
    for component in subsolution do
        if component is related to heat exchange then
            get eff using HX property
            char2, Temp_best2 = feasibilityEvaluation(subsolution corresponding to the
current HX process, Load, char, eff)
        else if component == 'Load' then
            compute Temp_best
        else if component == 'End' then
            return char, Temp_best
    update char in terms of the types of the components
```

---

*Computation Process in Flow Start*

In the flow start component, the starting temperature, pressure, mass flow rate, and type of media (heat sink or heating source) are assigned to a list named "char", where char[0] = temperature, char[1] = pressure, char[2] = mass flow rate, and char[3] = the type of the media.

*Computation Process in Compressor, Turbine, and Expansion Valve*

In the compressor component, the following equations [102] are used to compute the flow properties after the compressor and the corresponding work required, where efficiency  $\eta_c$  and pressure ratio  $PR_c$  are prescribed if turbines do not appear before the compressor:

$$P_{c,t3} = P_{c,t1} PR_c \quad (5.7)$$

$$\eta_c = \frac{PR_c^{(\gamma-1)/\gamma} - 1}{T_{c,t3}/T_{c,t1} - 1} \quad (5.8)$$



$$w_c = \frac{\dot{m}_c c p_c (T_{c,t3} - T_{c,t1})}{\eta_c} \quad (5.9)$$

where  $T_{c,t1}$  and  $P_{c,t1}$  are the total temperature and total pressure before the compressor,  $T_{c,t3}$  and  $P_{c,t3}$  are the total temperature and total pressure after the compressor,  $\dot{m}_c$  is the mass flow rate passing the compressor, and  $c p_c$  is the specific heat of the fluid passing the compressor. If the turbines appear before the compressor,  $w_c$  should equal to the shaft-power generated by the turbine  $w_t$ , then  $T_{c,t3}$  can be solved by using Equation 5.9, and then  $PR_c$  can be obtained using Equation 5.8, and finally  $P_{c,t3}$  can be calculated through Equation 5.7.

Regarding the turbine, similar to the compressor computation process, if the compressor does not appear before the turbine, then the efficiency  $\eta_t$  and pressure ratio  $PR_t$  are prescribed, and the corresponding properties can be calculated using the following equations [102]:

$$P_{t,t3} = P_{t,t1} PR_t \quad (5.10)$$

$$\eta_t = \frac{1 - T_{t,t3}/T_{t,t1}}{1 - PR_t^{(\gamma-1)/\gamma}} \quad (5.11)$$

$$w_t = \frac{\dot{m}_t c p_t (T_{t,t1} - T_{t,t3})}{\eta_t} \quad (5.12)$$

where  $T_{t,t1}$  and  $P_{t,t1}$  are the total temperature and total pressure before the turbine,  $T_{t,t3}$  and  $P_{t,t3}$  are the total temperature and total pressure after the turbine,  $\dot{m}_t$  is the mass flow rate passing the turbine, and  $c p_t$  is the specific heat of the fluid passing the turbine. If compressors appear before the turbine,  $w_t = W_c$  holds, and  $T_{t,t3}$  can be solved by using Equation 5.12, and then  $PR_t$  can be obtained using Equation 5.11, and finally the  $P_{t,t3}$  can be calculated through Equation 5.10.

For the expansion valve, an ideal expansion is assumed, that is:  $h_{exp,1} = h_{exp,4}$ , where

$h_1$  is the specific enthalpy before expansion, and  $h_4$  is the specific enthalpy after expansion. Therefore, the properties can be computed using the following equation:

$$\frac{T_{exp,t1}}{T_{exp,t4}} = \frac{P_{exp,t1}}{P_{exp,t4}} \quad (5.13)$$

where  $T_{exp,t1}$  and  $P_{exp,t1}$  are the total temperature and total pressure before expansion, and  $T_{exp,t4}$  and  $P_{exp,t4}$  are the total temperature and total pressure after expansion.

#### *Computation Process in Heat Exchanger, Condenser, and Evaporator*

The property computation in heat exchanger, condenser, and evaporator relies on the given effectiveness  $\epsilon_{hx}$ , and the temperature can be computed by the following equation [103]:

$$\epsilon_{equation} = \frac{\dot{Q}_{hx}}{\dot{Q}_{hx,max}} \quad (5.14)$$

$$= \frac{C_h(T_{h,i} - (T_{h,o}))}{C_{min}(T_{h,i} - (T_{c,i}))} = \frac{C_c(T_{c,o} - (T_{c,i}))}{C_{min}(T_{h,i} - (T_{c,i}))} \quad (5.15)$$

where  $C_c$  and  $C_h$  are heat capacity rates of the cold stream and hot stream,  $C_{min} = \min(C_c, C_h)$ ,  $T_{h,i}$  and  $T_{h,o}$  are the temperature of the inlet and outlet at the hot side of the heat exchanger,  $T_{c,i}$  and  $T_{c,o}$  are the temperature of the inlet and outlet at the cold side of the heat exchanger. The phase change in evaporator and condenser is assumed to be complete, that is, only a single phase exists before or after the component. In addition, the mass flow rate in condenser will be adjusted to the value that the transferred heat  $\dot{Q}_{hx}$  can merely realize such phase change process, further updating the mass flow rate in the sub-architecture which includes this condenser.

#### *An Example for the Feasibility-Based Filtering Process*

The example to present in this subsection uses the architecture in Figure 5.4. As a reminder of the actual architecture, it is plotted in Figure 5.6 again. The data used in this example

are the same in Table 5.2, Table 5.3, Table 5.4, and Table 5.5. The operation condition selected is the critical condition. For this example, the selected aircraft configuration is the 78-pax HTeDP, where only non-cryo cooling option is available, and the coolant is Polyalphaolefin (PAO). The lowest allowable temperature of this selected coolant is 131  $^{\circ}F$  because of the viscosity, which was discussed in the previous papers [29, 32]. The working temperature of the motor is 248  $^{\circ}F$  with a heat transfer effectiveness = 0.8. The maximum heat generation of the motor is 170 hp (120 BTU/s). The maximum fan flow is 200 lb/s. Using the computation processes discussed in preceding sections as well as the conditions as stated before, the feasibility of this architecture can be evaluation, which is illustrated in Figure 5.7, where the sequences of the computation processes are denoted by the numbers shown in each step, and the resulted temperatures are also presented. As the computation proceeds as shown in this figure, the temperature of the heat sinks in the sub-architectures at each level is updated. As the process reaches the "End" of the top-level sub-architecture, the feasibility can be determined: the resulted temperature is larger than the initial temperature, indicating this architecture cannot fully remove the heat generated from the motor, so it is infeasible. The resulted temperature needs to be lower than or equal to the initial temperature to make the architecture feasible because this architecture is closed-loop, and the temperature of the "End" must match the temperature of the "Start". If the temperature of "End" is lower than that of the "Start", then the mass flow rate of the heat sink can be reduced to match them.

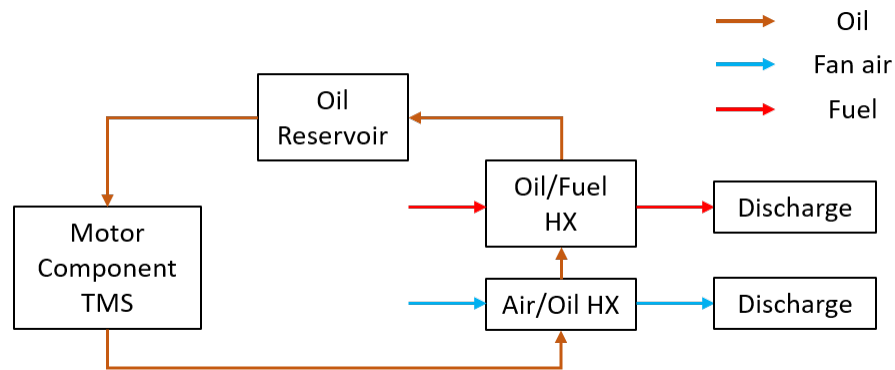


Figure 5.6: TMS architecture to illustrate the feasibility evaluation process

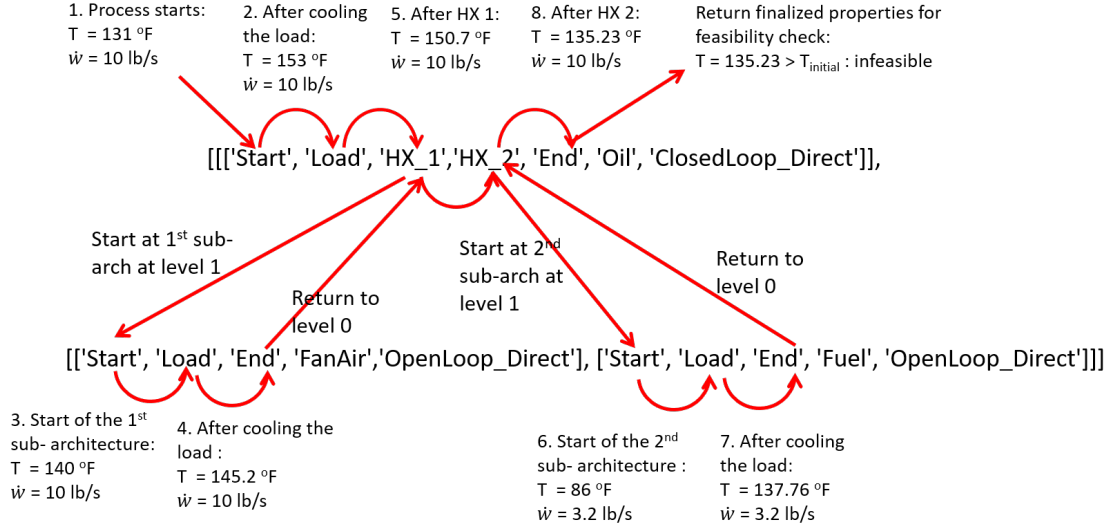


Figure 5.7: Example feasibility evaluation process

### 5.3.3 Low-Fidelity KPI Evaluation Methodology

#### *Selection of KPI*

Subsystem-level key performance indicators (KPI) are selected for the low-fidelity analysis. The major reason to select subsystem-level KPI is to reduce the computational effort of the evaluation. If system-level or mission-level metrics are used, then the integration of the subsystems (TMS) with the aircraft or the mission is unavoidable, which can be much more computationally expensive. For this study, four subsystem-level metrics are selected as the KPI: shaft-power extraction, bleed air extraction, ram air, and the TMS weight. They are selected because they can directly or indirectly influence the engine and aircraft performances, and further influencing the mission performance. Such relations are illustrated in Figure 5.8. It should be noted here that in this study, the cooling air from the fan is also considered as ram air, with a penalty factor multiplied to it.

Shaft-power and bleed extraction directly influence the engine performance. Increase in either of them requires the engine to burn more fuel to reach the same thrust, leading to an increase in the thrust-specific fuel consumption (TSFC), and the mission block fuel

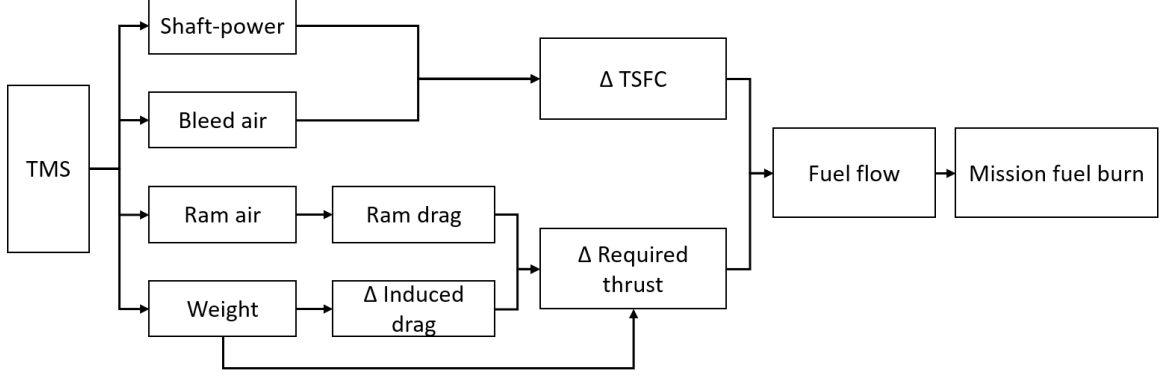


Figure 5.8: Influences of the TMS on vehicle and mission

burn will also increase. The ram air intake increases the ram drag, and the added weight increases the induced drag. Increase of both of them will increase the required thrust. And such impacts also further penalize on the mission block fuel burn.

#### *Evaluation Methodology for Local TMS*

The methodology of the low-fidelity evaluation of the local TMS KPI is almost the same as the thermal management capability evaluation approach, where at each heat exchange process, the sub-architecture at the next level starts to be recursively analyzed. The differences compared to the thermal management evaluation process are: 1. the average performances are used instead of the best performance; 2. no need to check the duty cycle; 3. the mass flow rate is not the maximum allowed value, but is updated based on the actual transferred heat. Such update in the mass flow rate can be written as

$$\dot{m}_{media} = \frac{\dot{Q}_{load}}{cp_{media}(T_{after} - T_{before})} \quad (5.16)$$

where  $\dot{m}_{media}$  is the mass flow rate through the current sub-architecture,  $\dot{Q}_{load}$  is the heat transfer rate from the load,  $cp_{media}$  is the specific heat of the selected media,  $T_{after}$  and  $T_{before}$  is the temperature of the media after and before the heat transfer at the current load (this equation assumes it is a load to cooling).  $\dot{Q}_{load}$ ,  $T_{after}$ , and  $T_{before}$  can be obtained by Equation 5.4 and the returned values from the next-level sub-architecture.

### *Pseudo-code for Local TMS Evaluation*

The pseudo-code corresponding to the methodology discussed in subsection 5.3.3 is presented in Algorithm 5. The supporting evaluation function is shown in Algorithm 6.

---

**Algorithm 5** Subsystem-level KPI Evaluation

---

```
function SCORE_EVAL(Load)
    copy indices for feasible architectures for Load to sol_feasible
    copy all generated architectures to sol
    for i in range(len(sol_feasible)) do
        index = load.sol_feasible[i]
        sol_kpi = load.solution[ind].copy()
        KPI = KPIassign(sol_kpi, load)
        load.score.append(KPI)

function KPIASSIGN(solution,Load)
    initialize KPI = [0,0,0,0] # bleed, ram, shaft-power, weigh
    KPI = KPIEvaluate(solution[0][0], load, [0,0,0,'something'], KPI, load.eff, 0)
    return KPI
```

---

### *Evaluation Methodology for Global TMS*

The KPI for global TMS are simply the summation of the KPIs for the selected local TMS for all loads, where the interactions among subsystems, systems, and missions are neglected.

#### 5.3.4 Clustering-Based Filtering Methodology

Optimal sets of architectures should be selected out in terms of their KPI to perform higher-fidelity down-selection of optimal TMS architectures. Clustering is able to fulfill such requirement. Clustering is defined as a process to group a set of data objects into multiple groups or clusters so that objects within a cluster are similar to each other while they are dissimilar to objects in other clusters [104]. The KPI can be used as the four dimensional coordinates associated with each architecture (object). Therefore, the architectures with

---

**Algorithm 6** KPI Evaluation Function for Low-Fidelity Evaluation Process

---

```
function KPIEVALUATE(subsolution,Load,char_pre, KPI_in, eff, Qact)
    KPI = KPI_in.copy()
    char = [0,0,0,0,'something']
    char_previous = char_pre.copy()
    Q_left = 0
    for component in subsolution do
        if component == 'Start' then
            assign start properties
            if at the top level then
                compute T_best
                Q = load.thermal_requirement
            else
                compute T_best
                Q = Qact
            Update mass flow rate using Q
        else if component is heat exchange related then
            get eff and Q using HX properties
            KPI = KPIEvaluate(next-level subsolution corresponding to this
HX,Load,char,KPI,eff,Q)
        else if component == 'End' then
            return KPI
    update char and KPI corresponding to the type of the component
```

---

similar KPI will be grouped together as one single architecture, leading to a reduction of candidate architectures.

### *Implementation of the Clustering Algorithm*

There are a lot of clustering methods in existence [105, 106, 107]: such as hierarchical clustering [108], squared error-based clustering of which K-means is the best-known [109, 110], mixture densities-based clustering [111], graph theory-based clustering [112, 113], combinatorial search techniques-based clustering [114, 115, 116], fuzzy clustering [117], neural networks-based clustering [118], and kernel-based clustering [119]. Based on the difficulty of implementation, robustness, space used, and computational cost, an improved version of the K-means algorithm is selected: K-means++ [120]. The improvement in K-means++ is in the initialization of the clustering to avoid sometimes poor clusters found

by standard k-means algorithm. In this implementation, the package scikit-learn [121] in Python is used to perform K-means++ algorithm on the generated KPI. The number of clusters  $K$  is unknown yet. As suggested by Garcia,  $K$  can increase starting from 2, until a preferred minimum distance is reached among the clusters. Such an approach to determine  $K$  is implemented.

#### *Pseudo-code for K-means++*

The pseudo-code for K-means++ is presented here for readers to have a better understanding of the method, which is illustrated in Algorithm 7.

---

#### **Algorithm 7** K-means++

---

##### **procedure** K-MEANS++

specify number of clusters  $K$

initialize  $K$  centroids using K-means++ Initialization procedure

**while** positions of centroids change **do**

assign each point to the closet centroid

compute the average coordinate of each cluster, and assign it as the new centroid

##### **procedure** K-MEANS++ INITIALIZATION

pick one centroid uniformly at random from all data points

**for**  $i$  in range(1, $k$ ) **do**

for point  $x_j$  that is not selected, compute distance  $D(x_j)$  to the closest centroid

randomly pick a new centroid with a probability  $\frac{D^2(x_j)}{\sum_{j=i}^{k-1} D^2(x_j)}$

---

#### *Application of Clustering Using Obtained KPI*

The clustering is performed on both the local TMS KPI and the global TMS KPI to narrow down the architecture space. The overall process is illustrated in Figure 5.9. It should be also noted that to reduce the impacts of the dimensionality of the chosen metrics, scaling and principal component analysis (PCA) [122, 123] are used before clustering.



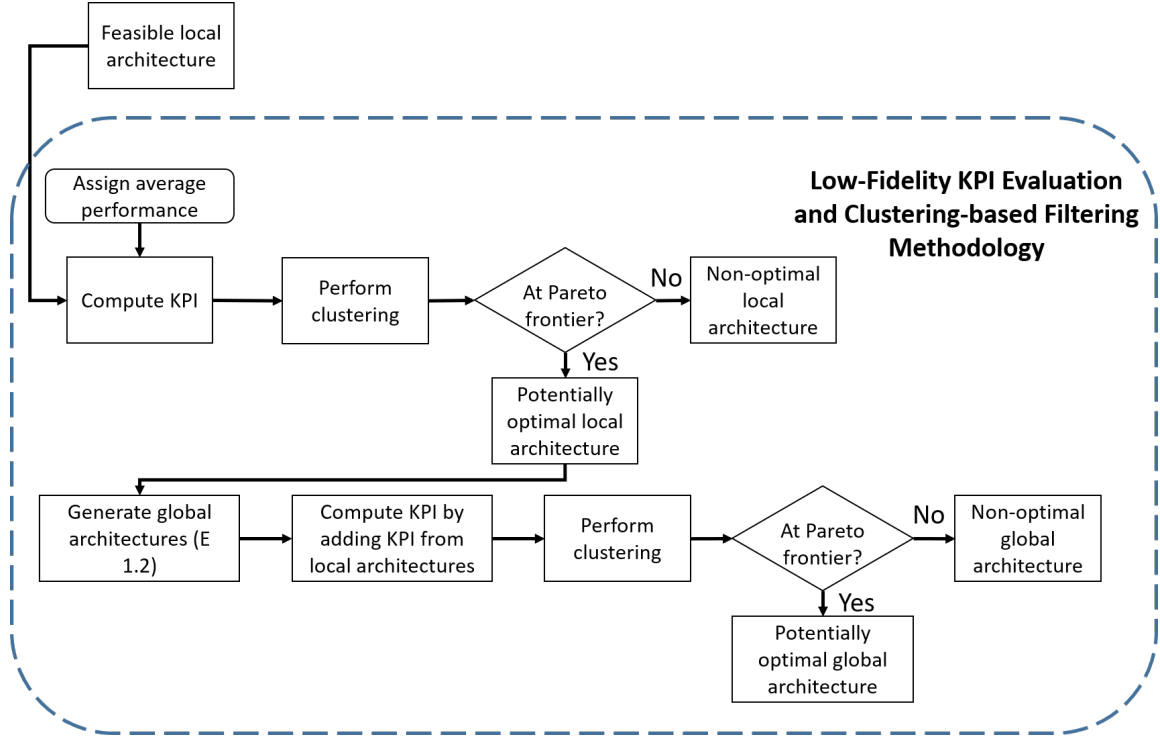


Figure 5.9: Overview of low-fidelity KPI evaluation and clustering-based TMS architecture filtering methodology

### 5.3.5 Automation of TMS Simulation Models Construction

After the previous filtering process in terms of feasibility and low-fidelity KPI analyses, the number of TMS architecture candidates is expected to be reduced to a practical number to perform higher-fidelity physics-based sizing, optimization, and analysis. However, a physics-based model needs to be constructed before such processes.

As discussed in section 5.2, the model creation process requires an OOP environment, and in this study, the Numerical Propulsion System Simulation (NPSS) [124] is selected as the OOP environment. NPSS is selected because it is able to realize such OOP capabilities as well as to provide some pre-built classes and methods that are suitable for turbomachine applications which can be used in TMS modeling.

The process to create the models from structural architecture is simple. The major idea is to read the information from the structural architecture descriptor, where the descriptor is a list of lists recording the components of both hot and cold stream in the sequence of

the components, and then an NPSS model file is written according to the read architecture descriptor. The reading and writing functions are currently performed in Python 3.8. And the overall process is described in the following bullets:

1. Read the component types in the sequence recorded in list of lists
2. Instantiate component objects in the reading sequence for the first sub-architecture
3. Instantiate component objects in the reading sequence for the next-level sub-architecture
4. Move instantiated components that are before "Load" for the the next-level sub-architecture before the corresponding HX of the current sub-architecture
5. Continue until components from all sub-architectures are instantiated
6. Link flow paths
7. Link shaft
8. Write the NPSS model file
9. Load pre-set initial values for each component
10. Modify pre-written NPSS run file

#### 5.3.6 MDP Sizing and Optimization Methodology of the TMS

The MDP sizing and optimization methodology was developed by the author, and already published [32]. And more details can be found in the corresponding reference. A lot of content in this subsection is directly used from the published paper by the author [32]. The fundamental idea of the Multi-Design Point Sizing Methodology for the TMS is to create a design space for TMS candidates where all the performance requirements and operation constraints are satisfied as well as allowing different components to be sized at different

conditions. The optimal design of the TMS is selected through optimization in the identified design space in terms of specified objectives. This fundamental idea is inspired by the MDP method for the engine design [97, 98], but the actual methodology and implementation are different. It should also be noted that the MDP sizing and optimization methodology is only for the local TMS.

The MDP TMS sizing and optimization method is capable of obtaining an optimal TMS while satisfying all the performance and operation constraints. Such capability is achieved by allowing sizing different components at different operating conditions as well as adjusting the design space topography which is defined by requirements and constraints of multiple mission points. The adjustment of the design space is realized using Newton's Method [125] to convert the dependencies among design variables, performance requirements and constraints into a set of non-linear equations. The requirements and constraints are guaranteed to be satisfied by solving this set of non-linear equations.

The MDP sizing process of the TMS is illustrated in Figure 5.10. At the Requirements and Constraints Establish Phase, the requirements and constraints are identified in terms of the selected TMS architecture, standards, and the technology constraints. The design variables are also selected in this phase. At the Setup Phase, the established requirements and constraints are used to identify the sizing point for each component, and to formulate the non-linear equations which are used to enforce the satisfaction of the performance requirements and operation constraints. Such equations are also used to enforce the consistency among sizing parameters of components that are sized at different points. At the TMS Design Space Generation Phase, the formulated non-linear equations (NPSS solvers if using NPSS as the modeling environment), by solving which along the sizing process the design variables will be ensured to be in the feasible design range. A set of design of experiments of the design variables are selected to populate the design space through such a process. At the Optimal TMS Design Selection Phase, the optimal TMS designs are selected based on the designer-specified objectives from the design space which is populated by generated

feasible designs.

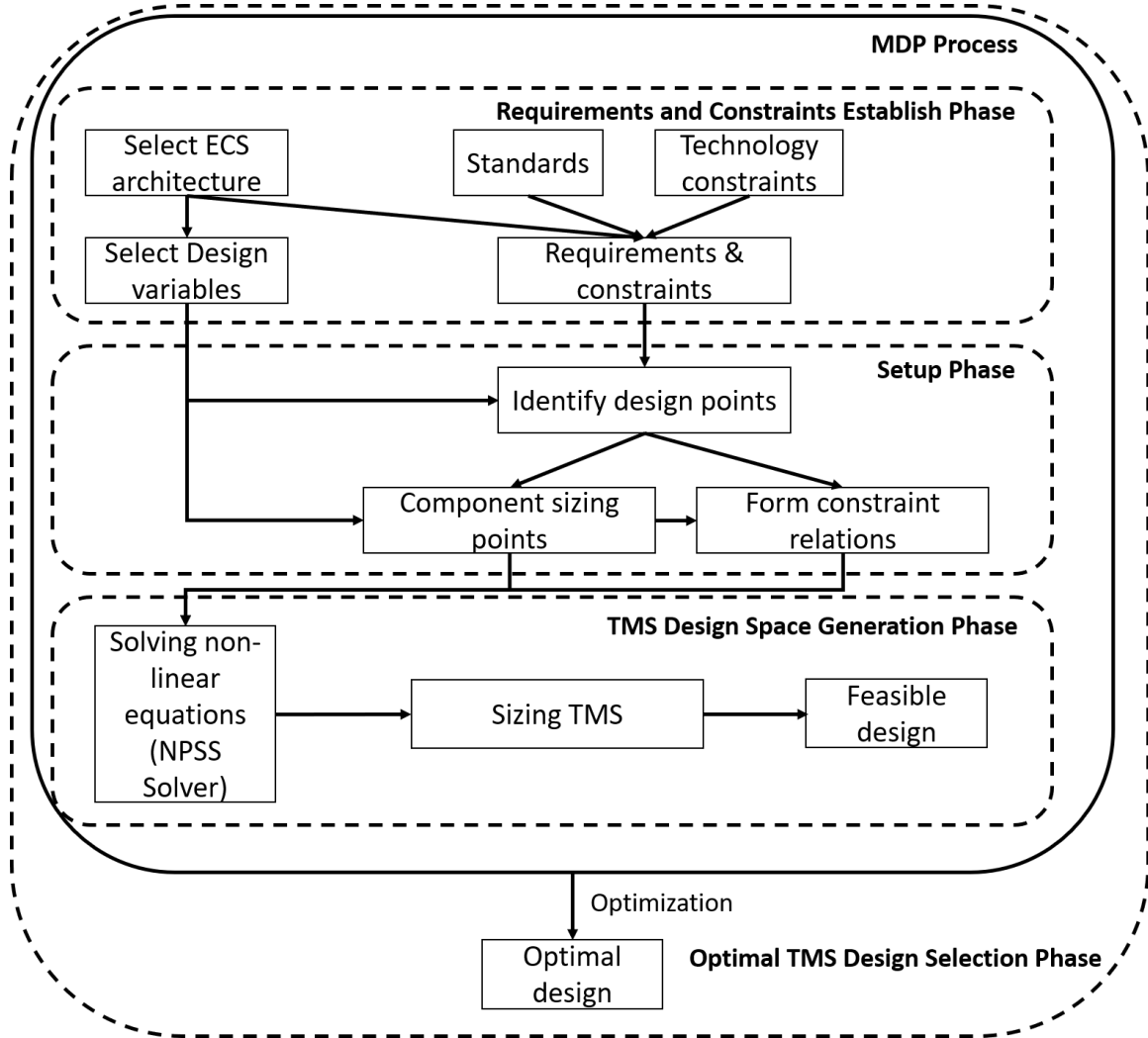


Figure 5.10: Overview of the MDP sizing methodology for the TMS

### *Requirements and Constraints Establish Phase*

At this phase, the design variables are firstly chosen based on the selected TMS architecture and modeling fidelity. For example, if the desired TMS architecture is a four-wheel condensing ECS, the design variables may be chosen from design parameters of the compressor, two turbines, and the four heat exchangers. If modeling fidelity is low, the design variables may be selected to describe high-level performance such as pressure ratio of the compressor. If the desired modeling fidelity is high, the variables can be chosen to describe

more detailed features such as the geometry parameters of the heat exchangers.

The performance requirements and operation constraints come from standards and technology limits. Standards may pose requirements that the TMS must obey, for example, to ensure safety in the ECS and comfort in the cabin, such as the temperature of the cold stream must be higher than 35 °F before entering the condenser [90], and the minimum amount of the fresh supply air is 0.55 lb/person/min as specified in Federal Aviation Administration (FAA) regulation [78]. The constraints posed by the technology may refer to the physical limitations of the components, such as the temperature of the ram air nozzle inlet and that of the compressor exit is limited by the material characteristics.

### *Setup Phase*

At this phase, the detailed requirements and constraints are set up in terms of the model parameters. The corresponding design points along with the requirements and constraints are also identified. Then certain TMS parameters need to be varied to satisfy such requirements or constraints to form a feasible design space. Such properties derived from requirements and constraints that should be matched are called dependents in this context. The TMS parameters varied to match these dependents are called independents. Such relations can be formulated as a set of non-linear equations, where the equations themselves are unknown. An example of the set of equations can be expressed in the following form:

$$\begin{aligned}
 F_1(\alpha_1, \alpha_2, \beta_1, \beta_2 \dots) &= 0 \\
 F_2(\alpha_2, \beta_2, \beta_3 \dots) &= 0 \\
 &\vdots \\
 F_n(\dots \alpha_{n-1}, \alpha_n, \beta_{n-2} \dots) &= 0
 \end{aligned}$$

where  $\alpha$ 's are the dependents and  $\beta$ 's are the independents. One equation can have multiple dependents and independents, however, the total number of dependents  $n$  should be equal to

the total number of independents. In this way, an  $n \times n$  Jacobian matrix can be constructed to solve all the non-linear equations.

The requirements and the constraints can be either equality or inequality constraints. However, they are all expressed using the four equality constraints. When the inequality constraints are not violated, the independents are set to the initial values. When the constraints are violated, the independents are varied to match limits set by the constraints. Multiple constraints can be satisfied by varying the same number or fewer independents. The most stringent constraint is handled with highest priority, and in this way all the constraints are guaranteed to be satisfied through iterations of the solving process.

#### *TMS Design Space Generation Phase*

With the set independents and dependents at the previous phase, the non-linear equations are set and solved to find the feasible design at this phase. As executed in NPSS environment, the non-linear equations are set as NPSS solvers, which will be solved to find feasible independents for a given set of design variables during the sizing process. Such independents will determine the sizing conditions for components, such as the mass flow, total pressure, total temperature, etc.

#### *Optimal TMS Design Selection Phase*

Using the process stated before, a feasible design candidate can be discovered. With multiple sets of design variables, a pool of feasible designs can be identified. Then the same optimal design selection approach as in SDP sizing method such as mathematical optimization can be performed to select the optimal sets of design variables from the feasible design space. The optimization objectives can be also selected as same as in SDP sizing method such as the TMS weight, vehicle TSFC at certain operation conditions, or mission block fuel.

### *An Example of MDP Sizing Process*

To understand the MDP process better, a simplified example is presented here to show how MDP works by using an ECS. Suppose that in the ECS of this example, the heat exchangers are sized at Point 1, all other components are sized at Point 2, and there is also a constraint that the ratio of corrected speed of compressor between point 2 and point 3 (which has the maximum compressor corrected speed) should be smaller than the speed scalar in point 2 to avoid extrapolation when using off-design performance map. Meanwhile, the ECS pack discharge temperature should equal to the desired temperature which is calculated by the cabin model, which is controlled by adjusting the intake ram air. The simplified descriptions of the formulated equations can be presented as:

1. Varying amount of ram air  $\dot{m}_{\text{ram}}$  at to meet the target discharge temperature  $T_{\text{exit}}$  for all points:

$$F_1(\dot{m}_{\text{ram,point1}}) - T_{\text{exit,point1}} = 0$$

$$F_2(\dot{m}_{\text{ram,point2}}) - T_{\text{exit,point2}} = 0$$

$$F_3(\dot{m}_{\text{ram,point3}}) - T_{\text{exit,point3}} = 0$$

2. Enforcing sizing parameters of heat exchangers  $Para_{\text{hx}}$  at point 2, and point 3 are consistent with the ones that are sized at point 1:

$$Para_{\text{hx,point2}} - Para_{\text{hx,point1}} = 0$$

$$Para_{\text{hx,point3}} - Para_{\text{hx,point1}} = 0$$

3. Enforcing sizing parameters of components other than heat exchangers  $Para_{\text{other}}$  at

point 1, and point 3 are consistent with the ones that are sized at point 2:

$$Para_{\text{other,point1}} - Para_{\text{other,point2}} = 0$$

$$Para_{\text{other,point3}} - Para_{\text{other,point2}} = 0$$

4. Ensuring the compressor corrected speed scalar  $des_{N_c}$ , which marks the position of the design scaling point on the map, at point 2 is smaller than the ratio of corrected speed of compressor between point 2 and point 3  $\frac{N_{c,\text{point2}}}{N_{c,\text{point3}}}$ . It should be noted that this relation is still expressed as the equality form, but this equation is only active when this constraint is violated.

$$des_{N_c,\text{point2}} - \frac{N_{c,\text{point2}}}{N_{c,\text{point3}}} = 0$$

Then the model executes the ECS model at point 1, 2 and 3, in an iterative manner, until the equations are solved by varying the sizing parameters. The solving process can be understood as that the sizing parameters are varied to satisfy the requirements and constraints, and the execution of the model at each certain point updates itself using the information from executions at other points until convergence.

### *Optimization Setup*

As a secondary power consuming subsystem, the TMS has an impact on vehicle-level performance through its mass contribution to vehicle empty weight, drag increment due to ram air intake, and fuel penalty due to secondary power extraction [13]. Therefore, it is natural to pose the TMS optimization problem as a multi-objective optimization problem. Therefore, the objectives considered in this work are the mass of ECS pack ( $m_{\text{pack}}$ ), required ram air mass flow rate ( $\dot{m}_{\text{ram}}$ ) at respective design condition, and bleed ( $\dot{m}_{\text{bleed}}$ ) and shaft-power ( $P_{\text{shaft}}$ ) extractions. The TMS pack mass, the required ram air, bleed and shaft-power



extractions are considered conflicting objectives when being minimized simultaneously.

The optimization problem is formally stated as follows.  $T_{\text{exit}}^*$  is the target discharge temperature of the TMS which is calculated by the load model based on the given heating or cooling load which depends on the operation conditions.

$$\begin{aligned} & \underset{\mathbf{x}}{\text{minimize}} && \begin{bmatrix} m_{\text{pack}}(\mathbf{x}) \\ \dot{m}_{\text{ram}} \\ \dot{m}_{\text{bleed}} \\ P_{\text{shaft}} \end{bmatrix} \\ & \text{subject to} && T_{\text{exit}}(\mathbf{x}) - T_{\text{exit}}^* = 0, \\ & && \mathbf{x} \in \text{Bounds of Design Variables} \end{aligned}$$

### *Optimization Methodology*

The Non-dominated Sorting Genetic Algorithm II (NSGA-II) [126, 127] is used to approach the Pareto frontier. Compared to other approaches which solve a multi-objective optimization problem by solving a set of single-objective problems using weighted aggregation function, the NSGA-II algorithm handles the original multi-objective optimization problem directly by operating on a population of design candidates and using genetic operators like cross-over, mutation, and selection to ensure that at each iteration a fraction of the population is non-dominated. When the algorithm converges, the remaining non-dominated members in the population are said to fall on the Pareto frontier.

The NSGA-II algorithm is executed in MATLAB with a population size of 500. The algorithm stops when the average change in the spread of Pareto frontier over the past 100 generations is less than  $10^{-5}$  and the final spread is less than the mean spread over the past 100 generations.

## 5.4 Component Modeling Methodologies

The physics-based local TMS architecture models with higher fidelity are created in NPSS, the current industry standard tool for the propulsion system and the TMS sizing and analysis. The component modeling methodologies implemented in the NPSS environment are introduced in this Section.

### 5.4.1 Turbomachinery

The turbomachines (compressor and turbine) are modeled using NPSS standard models with a 0-dimensional modeling approach, which can be found in most textbooks [102, 128], using the following equations, which have been shown before:

$$P_{c,t3} = P_{c,t1} PR_c \quad (5.17)$$

$$\eta_c = \frac{PR_c^{(\gamma-1)/\gamma} - 1}{T_{c,t3}/T_{c,t1} - 1} \quad (5.18)$$

$$w_c = \frac{\dot{m}_c c p_c (T_{c,t3} - T_{c,t1})}{\eta_c} \quad (5.19)$$

$$P_{t,t3} = P_{t,t1} PR_t \quad (5.20)$$

$$\eta_t = \frac{1 - T_{t,t3}/T_{t,t1}}{1 - PR_t^{(\gamma-1)/\gamma}} \quad (5.21)$$

$$w_t = \frac{\dot{m}_t c p_t (T_{t,t1} - T_{t,t3})}{\eta_t} \quad (5.22)$$

The weight of turbomachines are estimated by using given specific power.

### Map Scaling

The off-design performances of the compressors and turbines are read from parametric maps, which can be scaled by NPSS in terms of its specified design point, as illustrated in Figure Figure 5.11, which is exaggerated to show the scaling effects. Such map scaling was also discussed in the author's previous work [129].

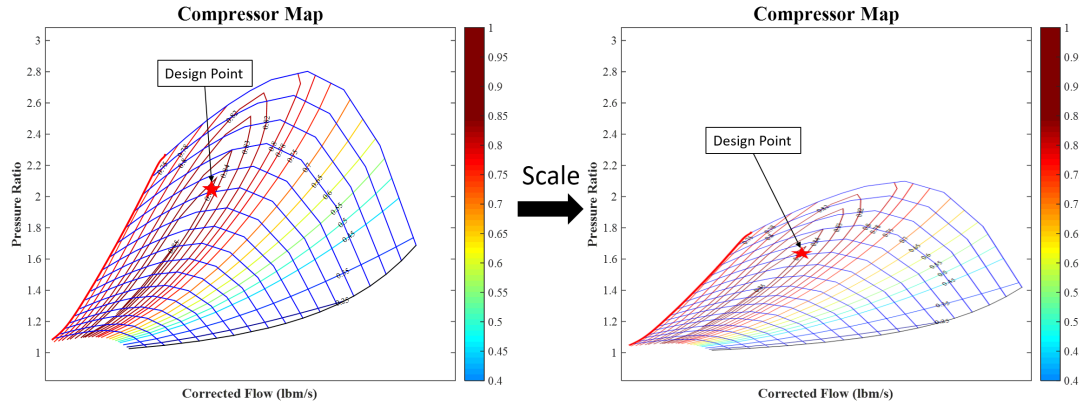


Figure 5.11: Map scaling [129]

### 5.4.2 Heat Exchanger

The heat exchanger model was developed by the author [33], following Kays and London's theory on compact heat exchangers [130]. The developed heat exchanger model can be evaluated in on-design and off-design modes. The implemented model applies to unmixed cross flow and has two configuration options: fin-tube and plate-fin. It is also modified to be able to take the presence of water vapor and occurrence of phase changes into account.

In on-design (sizing) mode, shown in Figure 5.12, the effectiveness and target relative pressure drops of the hot and cold side streams can be input by the user. These allow the heat exchanger flow areas and effective heat transfer area to be sized. In off-design mode, shown in Figure 5.13, the temperature, pressure, and flow rate of the hot and cold side flows are used to determine the off-design effectiveness, and from that the exit temperatures of the two streams. Thus, while effectiveness is specified in on-design mode, in off-design

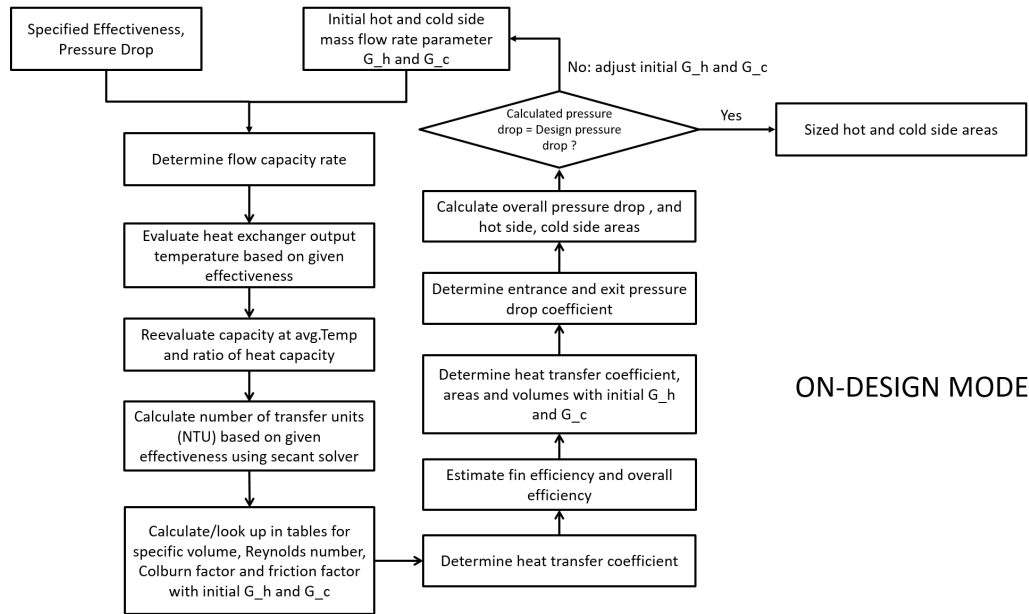


Figure 5.12: On-design calculation flow for the heat exchanger

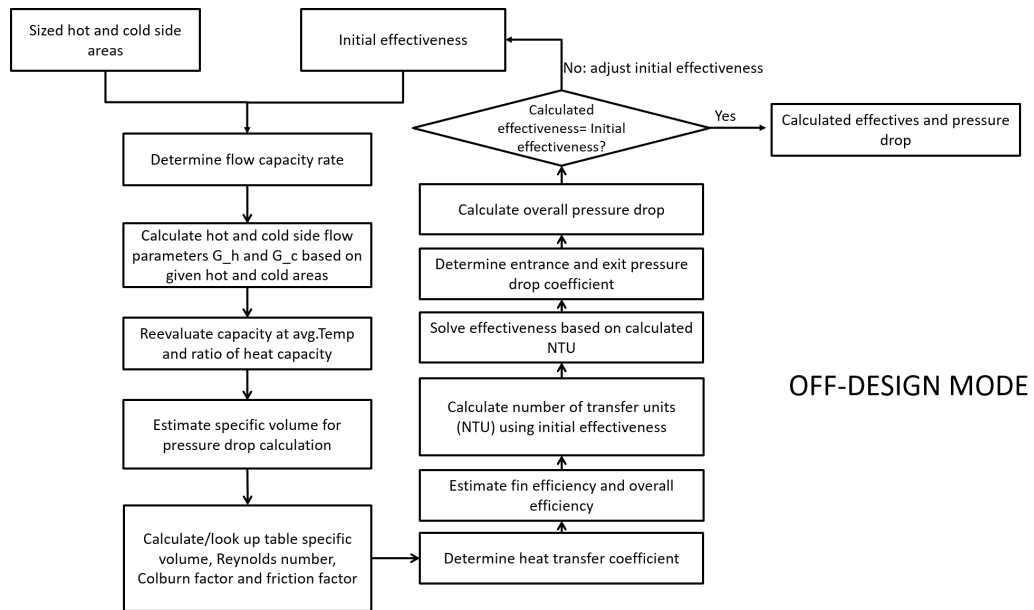


Figure 5.13: Off-design calculation flow for the heat exchanger

mode it is computed as [131]

$$\varepsilon = 1 - \exp\left[\frac{NTU^{0.22}}{C_r}[\exp(-C_r NTU^{0.78}) - 1]\right], \quad (5.23)$$

where  $C_r$  is the heat capacity ratio which is ratio of the minimum heat capacity to the maximum heat capacity (between the two flows). The number of transferred units (NTU) in the off-design scenario is computed as

$$NTU = \frac{A_c U_c}{C_{min}}, \quad (5.24)$$

where  $A_c$  is the cold side area,  $U_c$  is the cold side overall heat transfer coefficient, and  $C_{min}$  is the minimum heat capacity between the hot and the cold flows. However, the NTU in the on-design process is calculated using a secant solver to solve the following iterative relation until  $f(NTU)$  converges to 0:

$$f(NTU) = 1 - \exp\left[\frac{NTU^{0.22}}{C_r}[\exp(-C_r NTU^{0.78}) - 1]\right] - \varepsilon = 0. \quad (5.25)$$

Similarly, off-design relative pressure drops ( $\Delta p / p$ ) are computed for both streams to determine their exit pressures. It should be noted that alternatively, relationships for effectiveness and pressure drops can be provided as external inputs through *sockets*. This allows the behavior of the heat exchanger to be matched to, for instance, experimentally obtained heat exchanger performance data.

The effectiveness of the heat exchanger,  $\varepsilon$ , is defined as the ratio of the actual heat transfer  $Q_{act}$  to the maximum possible heat transfer  $Q_{max}$ . This basic definition is applicable for heat exchangers handling both dry and moist air streams. However, in case of moist air or in the presence of liquid water, the heat transfer process may involve condensation and vaporization, which makes determination of the maximum possible heat transfer  $Q_{max}$  more complicated [132]. Accordingly, the heat exchanger model was modified to compute

$Q_{max}$  for the case of moist air.

First, assuming that the hot side has infinite thermal capacity, the exit temperature of the cold side flow would equal the entry temperature of the hot side flow ( $T_{c,out} \approx T_{h,in}$ ). Thus, the maximum heat that the cold side would absorb during this heating process is given by

$$Q_{c,max} = H(W_c, T_{h,in}, P_{c,in}, WAR_c) - H(W_c, T_{c,in}, P_{c,in}, WAR_c), \quad (5.26)$$

where  $H(\cdot)$  represents the enthalpy calculation function described previously. Similarly, if the cold side had infinite thermal capacity, then the exit temperature of the hot side flow would equal the entry temperature of the cold side flow ( $T_{h,out} \approx T_{c,in}$ ). The maximum heat lost by the hot side flow during this cooling process is given by

$$Q_{c,max} = H(W_h, T_{h,in}, P_{h,in}, WAR_h) - H(W_h, T_{c,in}, P_{h,in}, WAR_h) \quad (5.27)$$

Since the heat lost by the hot stream must always equal the heat gained by the cold stream, the maximum heat transfer possible in the heat exchanger is given by the minimum of the above two quantities, i.e.,

$$Q_{max} = \min(Q_{c,max}, Q_{h,max}). \quad (5.28)$$

The actual heat transfer  $Q_{act}$  is then related to the maximum heat transfer  $Q_{max}$  computed above and the heat exchanger effectiveness  $\varepsilon$  as

$$Q_{act} = \varepsilon Q_{max}. \quad (5.29)$$

Noting that the final temperature calculation function has the functional form  $T_{fin} = f(W, T_{init}, P, WAR, \Delta Q)$ , where  $T_{init}$  and  $T_{fin}$  are the initial and final temperatures, WAR is the total water-to-air ratio, and  $\Delta Q$  is the heat exchanged (considered positive if heat is

supplied to the flow). Using this, the final temperatures of the hot and cold sides are computed as

$$\begin{aligned} T_{h,out} &= f(W_h, T_{h,in}, P_h, WAR_h, -Q_{act}), \\ T_{c,out} &= f(W_c, T_{c,in}, P_c, WAR_c, +Q_{act}). \end{aligned} \quad (5.30)$$

The above formulation accounts for the presence of moisture in the two air streams when computing the maximum possible heat transfer  $Q_{max}$  and also the effect of phase changes while computing the exit temperatures  $T_{h,out}$  and  $T_{c,out}$ .

### 5.4.3 Phase Change Modeling

The modeling of phase change of water was also discussed by the author's previous work [33], where the proposed method was also validated against a standard psychrometric chart. In order to handle phase changes such as water vaporization and condensation within the ACS pack, functions were implemented in NPSS to compute specific enthalpy of moist air based on water-to-air ratio (WAR) and relative humidity (RH). The water-to-air ratio (WAR) is a flow station property of GasTb1 (the NPSS thermodynamics package used for this paper), and is propagated across linked components. Therefore this parameter is directly used in the ACS pack for moist air calculations. The definition of WAR is as follows:

$$WAR = \frac{\text{mass of water}}{\text{mass of dry air}} \quad (5.31)$$

The deficiency of the definition above is that it does not contain any information about the state of the water (i.e., whether it is in gaseous or liquid form). Therefore the following definitions for water vapor and liquid water are defined as:

$$WAR_{vap} = \frac{\text{mass of water vapor}}{\text{mass of dry air}} \quad (5.32)$$

$$WAR_{liq} = \frac{\text{mass of liquid water}}{\text{mass of dry air}} \quad (5.33)$$

Since only gaseous and liquid water is considered (not solid), the WAR definitions are related as:

$$WAR = WAR_{vap} + WAR_{liq} \quad (5.34)$$

The relative humidity (RH) is the ratio of the mole fraction of water vapor in a given moist air sample to the mole fraction in a saturated sample at the same temperature and pressure. By definition, the range of values for RH goes from 0% (bone dry air) to 100% (fully saturated air) at any temperature and pressure. The corresponding WAR for a given RH, however, is dependent on the temperature and pressure. This dependency between RH and WAR was captured by implementing the following two functions.

In total, five functions were implemented in NPSS for calculation of water-to-air ratio (WAR), relative humidity (RH), enthalpy of a moist air mixture, the final state of a moist air mixture following heat supply or removal, and the effective  $C_p$  of a moist air mixture:

1. **RH calculation function:** The relative humidity (RH) calculation function takes the form of  $RH = f(P, T, WAR)$ , which is based on the humidity conversion formulas [133]. The detailed equations are listed in the Appendix, Section Appendix A. The corresponding coefficients are also listed in the same section in the Table Table A.1.
2. **WAR calculation function:** Using the same relationships listed in previous section for RH calculation, this function computes the WAR as a function of given temperature, pressure, and RH, taking the form of  $WAR = f(P, T, RH)$ . It is interesting to note that, for a given temperature and pressure, evaluating this function with  $RH = 100\%$  yields  $WAR_{sat}$ , the WAR corresponding to saturation conditions at that given temperature and pressure. In fact, this is used within the ACS pack components to check whether the incoming moist air stream contains only water vapor ( $WAR_{liq} = 0$ ,  $WAR_{vap} = WAR$ ) or both water vapor and liquid water



( $WAR_{liq} \neq 0$ ).

3. **Enthalpy Calculation Function** The ASHRAE relationships [134] are used to compute the specific enthalpies of dry air  $h_{da}$ , saturated water vapor  $h_{wv}$ , and saturated liquid water  $h_{lw}$  as a function of temperature  $t_c$  (in degrees Celsius). The detailed equations are listed in the Appendix, Section Table A.
4. **Final Temperature Calculation Function:** The final enthalpy  $H_{fin}$  is computed simply as the sum of the initial enthalpy  $H_{init}$  and the enthalpy change  $\Delta H$ :

$$H_{fin} = H_{init} + \Delta H \quad (5.35)$$

Then, a secant solver is used to iterate over temperature by repeatedly calling the enthalpy calculation function until a value of final temperature  $t_{fin}$  is found that satisfies

$$H_{ma}(t_{fin}) = H_{fin} \quad (5.36)$$

Note that for each call to the enthalpy calculation function, the state of saturation of the moist air and the presence of any liquid water for that iteration's temperature value are being factored into the total enthalpy calculation. This allows phase changes (either condensation or vaporization) to be accounted for, as demonstrated in subsequent examples.

5. **Effective  $C_p$  Calculation Function** This function factors in the moisture content of the air to compute the effective  $C_p$  of the moist air. Its basis is the thermodynamic relationship  $h = C_p T$ , and it uses a finite difference formula to estimate the effective  $C_p$  as follows:

$$C_{p,eff} = \frac{\Delta h}{\Delta T} = \frac{h(T + \Delta T) - h(T)}{\Delta T} \quad (5.37)$$

As described previously, the specific enthalpy is computed using the enthalpy calculation function with a unit mass flow rate and the given temperature, pressure, and

WAR.

#### 5.4.4 Ducts

The pressure drop in the ducts is a fixed value, and here presents weight estimation of the ducts, which was presented in the author's previous work [46], based on some concepts from Cai's paper [76]. The duct mass calculation uses the following parameters: the inner diameter, the material yield strength, the wall thickness, the duct length, and the material density. The inner diameter  $D_i$  is derived from Parrilla's thesis [66], where  $R$  is the specific gas constant,  $T_{norm}$  is the nominal duct temperature,  $p_{norm}$  is the nominal duct pressure,  $\mu$  is the dynamic air viscosity,  $\dot{m}$  is the maximum mass flow rate,  $\Delta p$  is the maximum pressure loss between the pneumatic systems and the actuators, and  $L$  is the longest path of duct:

$$D_i^{4.8} = 0.14211 \left( \frac{RT_{norm}}{p_{norm}} \right) \mu^{0.2} \dot{m}^{1.8} \left( \frac{\Delta p}{L} \right)^{-1} \quad (5.38)$$

The duct wall thickness  $t_{w,duct}$  is computed based on the material yield strength  $\sigma$  and the burst pressure. The wall thickness is calculated as

$$t_{w,duct} = \frac{p_b D_i}{2\sigma}, \quad (5.39)$$

where  $p_b$  is the burst pressure obtained by multiplying the nominal pressure  $p_{nom}$  by the burst pressure factor. Then, the mass of the duct  $m_{duct}$  can be obtained as

$$m_{duct} = \rho L \pi \{ (D_i + t_{w,duct})^2 - D_i^2 \} \quad (5.40)$$

where  $\rho$  is the material density.

#### 5.4.5 Vapor Cycle

The modeling of vapor cycle is based on Müller and Scholz's work [135]. Since the model was not developed by the author, only brief ideas are introduced here, while more details can be found in this reference. The vapor cycle model includes three specific maps on specific enthalpy vs. pressure, saturation pressure vs. saturation temperature, and specific enthalpy vs. temperature. The characteristics on the map can be modified in terms of selected refrigerant. The algorithm implemented in this vapor cycle model includes the processes in the evaporator, compressor, condenser, and expansion device, where the values are looked up from the three characteristic maps. This model was also validated against the data provided by Baehr's book [136].

#### 5.4.6 Cabin

The cabin compartment model was also developed by the author [33]. The cabin compartment component is to model the cabin heat load. The cabin heat load modeling approach considers the internal heat generation (avionics and passengers), solar radiation, fuselage radiation to the air, and heat transfer through conduction/convection.

The main sources of the internal heat generation are electronic equipment and metabolic heat from occupants. The metabolic heat load per passenger  $\dot{Q}_p$  is 75W [26]. The power consumption of galley loads and In-Flight Entrainment (IFE) are assumed to be dissipated entirely as heat [13], therefore heat generated by IFE  $\dot{Q}_{IFE}$  is 50W [27] per person and the heat load of galley load  $\dot{Q}_{galley}$  is 320W per person [27]. Therefore the cabin heat generation  $\dot{Q}_{gen}$  can be expressed as

$$\dot{Q}_{gen} = N_{pax}(\dot{Q}_p + \dot{Q}_{IFE} + \dot{Q}_{galley}) \quad (5.41)$$

where  $N_{pax}$  is the number of passengers in this compartment.

To calculate the cabin heat loss, the cabin internal convection and conduction, external

convection, solar radiation, and fuselage radiation to the sky are considered. The heat transfer relationship is illustrated in Figure 5.14.

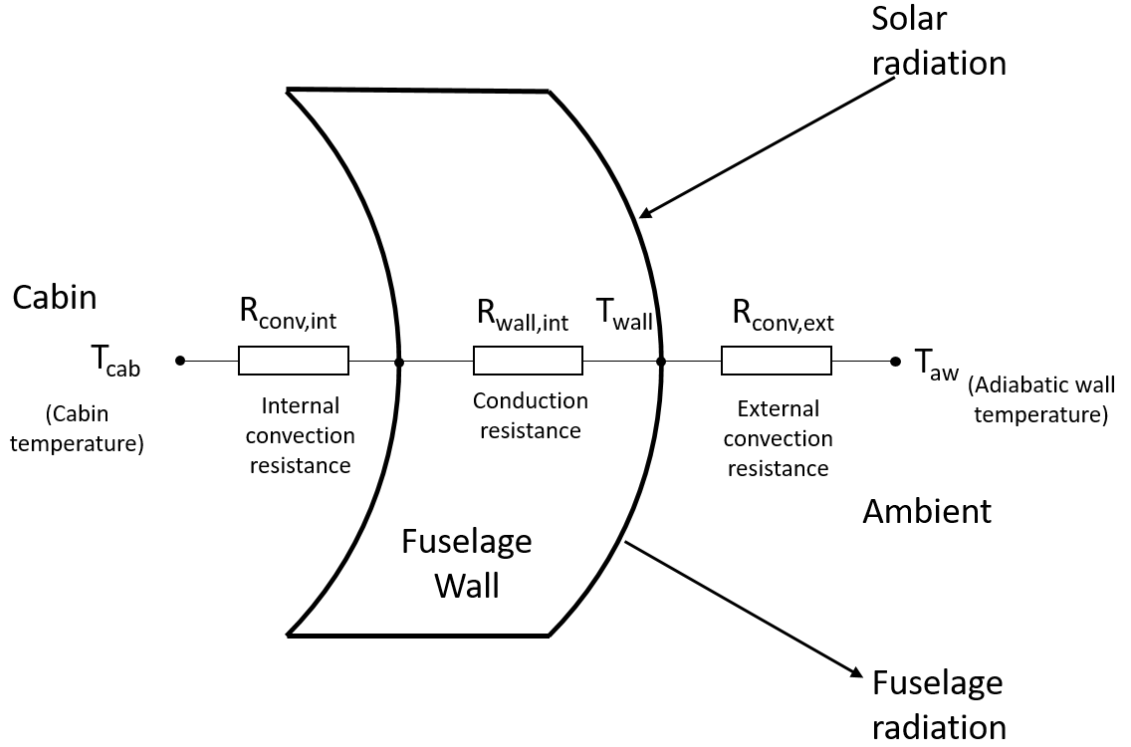


Figure 5.14: Cabin heat transfer relation [46]

If the control volume is taken as the fuselage which is bounded by the wall external surface, the  $\dot{Q}_{Inloss}$  is the heat loss from the internal cabin to the wall external surface and  $\dot{Q}_{Exloss}$  is the heat loss from the wall external surface to the ambient. The internal cabin heat loss  $\dot{Q}_{Inloss}$  are only through convection and conduction, which can be expressed as

$$\dot{Q}_{Inloss} = \frac{T_{cab} - T_{wall}}{(R_{wall} + R_{conv,int})} \quad (5.42)$$

where  $R_{wall}$  is the wall conduction heat resistance,  $R_{conv,int}$  is the internal convection heat resistance, and  $T_{wall}$  is the temperature of the wall external surface, where  $R_{wall}$  equals to  $0.2W^{-1}K^{-1}$  [13] and  $R_{conv,int}$  equals to  $0.2/A$  [13] where  $A$  is the heat transfer area for the cabin, assumed to be the external surface area of the cabin.

The  $\dot{Q}_{Exloss}$  includes the loss through external heat convection, solar radiation and fuselage radiation. For the external heat convection, the heat loss  $\dot{Q}_{conv,ext}$  is calculated in the following equation:

$$\dot{Q}_{conv,ext} = \frac{T_{wall} - T_{rec}}{R_{conv,ext}} \quad (5.43)$$

where  $T_{rec}$  is the recovery temperature, expressed as [137]:

$$T_{rec} = T_{\infty} \left( 1 + \frac{1}{2} Pr^{0.5} (\gamma - 1) M^2 \right) \quad (5.44)$$

where  $Pr$  is the Prandlt number and  $M$  is the Mach number.

The  $R_{conv,ext}$  is obtained by the following equation assuming a flat plate turbulent boundary layer approximation [66], where  $Re$  is the Reynolds number,  $L$  is the fuselage length and  $k_f$  is the material thermal conductivity of the fouling:

$$R_{conv,ext} = \frac{L}{0.036 Re^{0.8} Pr^{0.6} k_f S} \quad (5.45)$$

Expression for solar irradiance is derived from Beer's law [138]:

$$q''_{solar} = S_e e^{-a_{\alpha} H \sec(Z)} t_w^{(W \sec(Z)^q)} \quad (5.46)$$

where  $q''_{solar}$  is the solar irradiance,  $S_e$  is the solar intensity above the troposphere,  $a_{\alpha}$  is the extinction coefficient,  $H$  is the equivalent height,  $Z$  is the zenith angle,  $t_w$  is the transmission coefficient of water vapor,  $W$  is the precipitable water vapor and  $q$  is a precipitation experimental constant addressed in [138]. The heat transfer due to solar radiation then can be shown as  $\dot{Q}_{solar} = A_s q''_{solar}$ , where  $A_s$  is the irradiated area of the fuselage, which is assumed to be half of the fuselage surface area in this study.

Calculation of fuselage radiation lost is based on the gray body approximation [139],

and the corresponding heat flux  $q''_{sky}$  is expressed as

$$q''_{sky} = \epsilon\sigma[T_{wall}^4 - T_{sky}^4] \quad (5.47)$$

where  $T_{sky}$  is approximated in the following equation [139]

$$T_{sky} = T_{amb} \left[ 0.711 + 0.0056T_{dp} + 7.3 \times 10^{-5}T_{dp}^2 + 0.013\cos\left(\frac{2\pi t}{24}\right) \right]^{0.25} \quad (5.48)$$

where  $T_{amb}$  is the ambient temperature,  $T_{dp}$  is the dew point temperature and  $t$  (hour) is the time past midnight. Then heat loss due to fuselage radiation is  $\dot{Q}_{sky} = Aq''_{sky}$ , where  $A$  is the fuselage heat transfer area which is the same in the external convection calculation. Therefore the total  $\dot{Q}_{Exloss} = \dot{Q}_{conv,ext} + \dot{Q}_{sky} - \dot{Q}_{solar}$ .

The wall temperature  $T_{wall}$  is unknown yet, but assuming the fuselage wall external surface is in a steady state thermal equilibrium, the relation  $\dot{Q}_{Inloss} = \dot{Q}_{Exloss}$  can be used to solve  $T_{wall}$ , where both sides of the equation are a function of the only known  $T_{wall}$ .

To compute the required supply air temperature, let  $\dot{Q}_{supply}$  be the cabin supply air heat load, and the heat loss of the cabin has the expression  $\dot{Q}_{loss} = \dot{Q}_{Inloss}$  (the control volume is inside the fuselage wall external surface). Then steady state thermal equilibrium is shown as

$$\dot{Q}_{supply} = \dot{Q}_{loss} - \dot{Q}_{gen} \quad (5.49)$$

From this relation it can be seen that if the cabin supply air is required to remove heat from the cabin, then  $\dot{Q}_{supply} < 0$ . To compute the required cabin supply air temperature  $T_{cabsup}$  to keep the cabin at a constant temperature  $T_{cab}$ , the steady-state heat balance is extended by expressing  $\dot{Q}_{supply}$  as

$$\dot{Q}_{supply} = \dot{m}_{cabsup}C_p(T_{cabsup} - T_{cab}) \quad (5.50)$$

where  $\dot{m}_{cabsup}$  is the cabin supply air mass flow rate and  $C_p$  is the specific heat of the air.

Then, Equation 5.50 can be re-written as

$$T_{cabsup} = T_{cab} + \frac{\dot{Q}_{supply}}{\dot{m}_{cabsup} C_p} \quad (5.51)$$

which gives the cabin supply air temperature.

#### 5.4.7 Phase Change Material

The model of phase change material was included in the author's other paper [32], and here it is directly used for this study. A 1-dimensional model is applied to analyze the heat transfer from the load to the PCM as well as the phase change process. This method is based on the work done by Mansouri [140], where the phase change problem was formulated as a Stephan problem and an analytical solution of Neumann was applied to solve the problem. In the 1-D domain, the simplification of the load-PCM heat transfer geometric configuration is illustrated in Figure 5.15. At  $x = 0$ , the external surface of the stator is attached to the PCM inner surface, where the heat is transferred from the stator to the PCM. The liquid-solid interface is at  $x = X_f$ , where the melting process happens. When  $0 < x < X_f$ , the PCM is of the liquid state. When  $X_f < x$ , the PCM is of the solid state, where this formulation takes the PCM as a semi-infinite medium from  $x = 0$  to infinity. It should be also noted that such formulation is based on the melting process of a pure material. However, to simplify the computation, this paper assumes that the PCM of interest follows the behaviors of a pure material. Another assumption in this formulation is that the convection in the liquid section of the PCM is ignored. The radiation is not considered either. Thus, the heat transfer in this problem is only through conduction based on this assumption. The formulated governing equations, initial conditions, and boundary conditions are presented below, of which the detailed derivation process can be found in Mansouri's paper [140]. Some notations in the formulation are introduced here: the subscripts  $l$  and  $s$  indicate the liquid or solid state of the PCM;  $T$  refers to the temperature;  $k$  is the thermal conductivity;

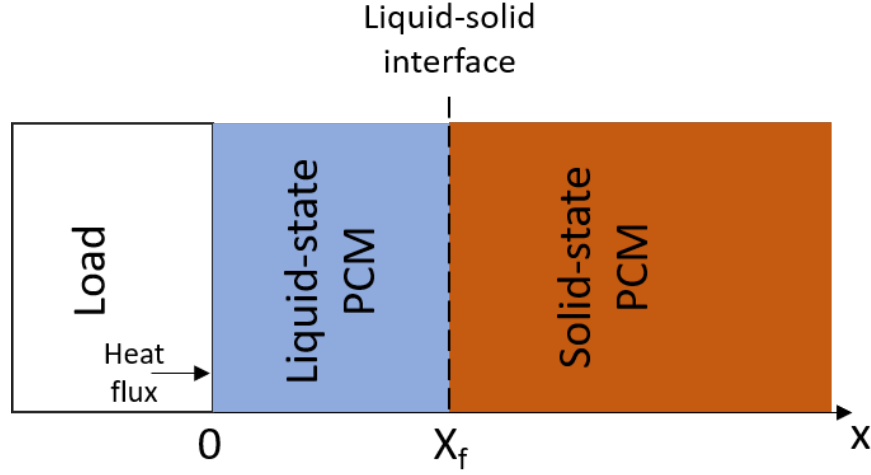


Figure 5.15: 1-D melting process of the PCM [32]

$t$  is time;  $L$  is the latent heat;  $c_p$  is the specific heat capacity;  $T_{wall}$  is the temperature of the load external surface;  $T_{melt}$  is the melting temperature; and  $T_0$  is the initial temperature of the PCM.

Governing equation:

$$\frac{\partial T_l}{\partial t} = \frac{\partial}{\partial x} \left( \alpha_l \frac{\partial T_l}{\partial x} \right), \quad 0 < x < X_f, \quad t > 0 \text{ liquid phase} \quad (5.52)$$

$$\frac{\partial T_s}{\partial t} = \frac{\partial}{\partial x} \left( \alpha_s \frac{\partial T_s}{\partial x} \right), \quad X_f < x, \quad t > 0 \text{ solid phase} \quad (5.53)$$

where  $\alpha = \frac{k}{\rho C_p}$  which is the PCM thermal diffusivity. And the heat flux from the load to the PCM can be expressed by:

$$q = \rho_l L \frac{\partial X_f}{\partial t} = k_s \frac{\partial T_s(X_f, t)}{\partial x} - k_l \frac{\partial T_l(X_f, t)}{\partial x}, \quad t > 0 \quad (5.54)$$

Initial conditions at  $t = 0$ :

$$T_s(x, 0) = T_0, \quad 0 \leq x \leq R_{PCM} \quad (5.55)$$



$$X_f(0) = 0 \quad (5.56)$$

Boundary conditions at  $t > 0$ :

$$T_l(x = 0, t) = T_{wall} \quad (5.57)$$

$$T_l(x = X_f, t) = T_s(x = X_f, t) = T_{melt} \quad (5.58)$$

$$T_s(x \rightarrow \infty, t) = T_0 \quad (5.59)$$

One assumption is made here that the load is always working in its target working temperature, that is, the working temperature of the load will not change during the operation.

The analytical solution for this problem is given by the following equations:

$$\frac{T_l(x, t) - T_{wall}}{T_{melt} - T_{wall}} = \frac{\text{erf}\left(\frac{x}{2\sqrt{\alpha_l t}}\right)}{\text{erf}(\xi)}, \quad 0 < x < X_f, t > 0, \text{liquid phase} \quad (5.60)$$

$$\frac{T_s(x, t) - T_0}{T_{melt} - T_0} = \frac{\text{erfc}\left(\frac{x}{2\sqrt{\alpha_s t}}\right)}{\text{erfc}(\nu\xi)}, \quad X_f < x, t > 0, \text{solid phase} \quad (5.61)$$

The position of the liquid-solid interface is given by:

$$X_f(t) = 2\xi\sqrt{\alpha_l t} \quad (5.62)$$

where  $\xi$  is implicitly given by:

$$\frac{St_l}{e^{\xi^2} \text{erf}(\xi)} - \frac{St_s}{\nu e^{\nu^2 \xi^2} \text{erfc}(\nu\xi)} = \xi\sqrt{\Pi} \quad (5.63)$$

The notations used in the solutions above are introduced here.  $erf$  and  $erfc$  are the error function and the complementary error function, which can be approximated by polynomials [140]:

$$erf(x) = a_0 + a_1x + a_2x^2 + a_3x^3 + a_4x^4 + a_5x^5 \quad (5.64)$$

$$erfc(x) = 1 - erf(x) \quad (5.65)$$

where  $a_0 = -0.00401$ ,  $a_1 = 1.18669$ ,  $a_2 = -0.14559$ ,  $a_3 = -0.33443$ ,  $a_4 = 0.16069$ ,  $a_5 = -0.02155$ .  $St_l$  and  $St_s$  are the Stephan number, which are expressed as:

$$St_l = C_{pl} (T_{wall} - T_{melt}) / L \text{ and } St_s = C_{ps} (T_{melt} - T_0) / L. \nu = \sqrt{\alpha_l / \alpha_s}.$$

$\xi$  is a constant parameter that can be obtained by solving the implicit equation, Equation 5.63. In the current application, a Newton solver is used to solve for  $\xi$ .

Then the Equation 5.62 is known with the calculated  $\xi$ , and the heat flux from the load to the PCM is known by substituting Eq. Equation 5.62 into Equation 5.54. Then the heat transfer rate can be calculated by multiplying the heat flux  $q$  by the heat transfer area  $S$ , which is expressed as  $S = \Pi D_{IMD} h_{IMD}$ , where  $D_{IMD}$  is the diameter of the load, and  $h_{IMD}$  is the height of the load, assuming the load is of a cylinder shape. The only value needed to determine the PCM size is the distance between the load external surface and the PCM external surface. Such distance can be approximated by  $X_f(t_{melt})$  where  $t_{melt}$  is the desired working time for the PCM. Then the volume of the PCM,  $V$ , can be given by

$$V = \Pi \left( \left( \frac{1}{2} D_{IMD} + X_f(t_{melt}) \right)^2 - \left( \frac{1}{2} D_{IMD} \right)^2 \right) h_{IMD} \quad (5.66)$$

Then the mass of PCM,  $m_{PCM}$ , can be calculated by

$$m_{PCM} = \rho V \quad (5.67)$$

### 5.4.8 Electrical Systems

The component models in the electrical systems were developed by Perullo [141, 142]. The components modeled are:

1. Inverter (Converts DC to AC)
2. Retifier (Converts AC to DC)
3. DC Transformer (Steps up/down DC voltage)
4. Generator (converts torque to current)
5. Motor (converts current to torque)
6. Bus (balances power between connected components)
7. Battery (provides electrical power source)

Since these models were not developed by the author, and for brevity, only overall modeling concepts are introduced here, while more details can be found in the aforementioned references. The overall solver setup and data flow are illustrated in Figure 5.16. Table 5.1 denotes the input and output of each component as well as the computation logic.

Table 5.1: Electrical Element Computation Logic

Element	Input	Calculates	Computation Logic
Motor	Torque, Speed	AC I, V	Vary I to maintain T
Inverter	AC V, I	DC V, I	Vary V out to balance bus
Cable	DC V, I	DC V, I	None
Bus	DC V, I	DC V, I	All V in/out at bus voltage
DC Trans	DC V, I	DC V, I	P out equal to P in
Rectifier	AC V, I	DC V, I	P out equal to P in
Generator	T, N	AC V, I	Vary T to maintain I
Battery	I Demand	I, V	Vary I to maintain P

The major loads that generate heat in the electrical systems are the motor and inverter. The heat generation from these elements are computed by  $P_{heat} = P_{in}\eta$  where  $P_{heat}$  is

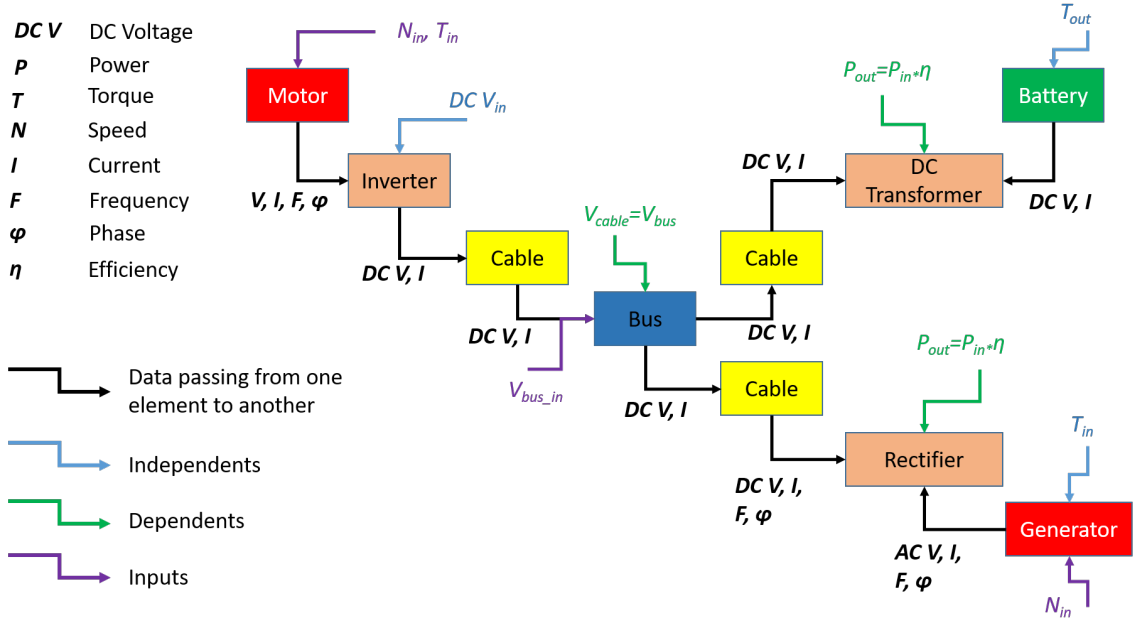


Figure 5.16: Electric element solver setup and data flow [141]

the heat generation, and  $P_{in}$  is the input power. For the inverter, Perullo [142] created a parametric model using a regression equation, which considered two types of losses: conduction losses and switching losses. Regarding the model of the electric motor [142], losses due to windage, copper, and iron are considered, where the iron loss can be further decomposed into losses from eddy currents and hysteresis.

#### 5.4.9 Non-Cryogenic Coolant Weight

The non-cryogenic coolant weight is computed using the coolant volume required for the load and heat exchangers. The volume inside the heat exchangers can be directly obtained using the developed heat exchanger model. The coolant through motor or generator is estimated by 6.5 L per MW, which was provided in the research under the ULI program [32].

#### 5.4.10 Cryogenic Cooling TMS Modeling

##### *Passive Cryogenic Cooling*

There are two options selected for this study in passive cryogenic cooling: 1. use a tank to store the coolant and re-circulate to another tank after cooling, the re-circulated coolant will not be used again through the mission; 2. the fuel is also the cryo-coolant: the coolant can be pumped to the engine or back to the tank (if the required mass flow rate is larger than the fuel flow) in this scenario. The architecture for the first option of the passive cryogenic cooling is shown in Figure 5.17, and the second option is illustrated in Figure 5.18. In this study, the liquid nitrogen is selected for the first case, and liquid hydrogen is selected for the second case.

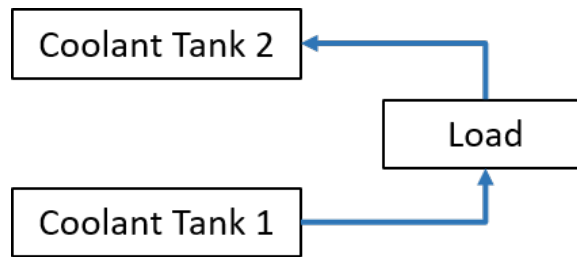


Figure 5.17: Passive cryogenic cooling using stored coolant

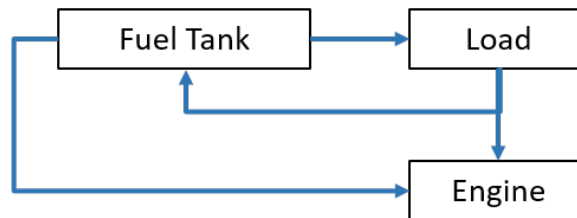


Figure 5.18: Passive cryogenic cooling using fuel (LH2)

##### *Active Cryogenic Cooling*

In an active cryogenic cooling system, the coolant is cooled by other heat sinks after cooling the load, and then is re-circulated to perform the cooling function again. The architecture of the active cryogenic cooling TMS is assumed to use the Claude process, which is illustrated

in Figure 5.19. The flow path direction is  $1 \rightarrow 2a \rightarrow 3a \rightarrow 4a \rightarrow 5a \rightarrow 1 \rightarrow 2 \rightarrow 3 \rightarrow 4 \rightarrow 5 \rightarrow 1$ . However, the actual physics-based model of the active cryogenic cooling is not constructed in this study due to modeling complexity. The corresponding power consumption and weights are estimated using the methods in the following subsection.

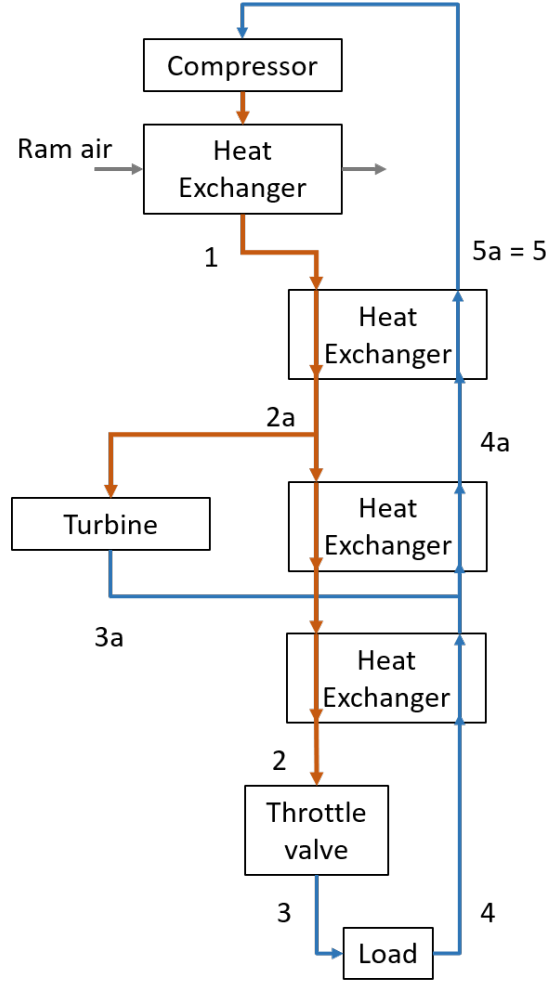


Figure 5.19: Active cryogenic cooling following Claude process)

### *Weight and Power Consumption*

The weight of the tank is calculated in terms of the surface area. Here for simplicity, the total surface area is obtained by using the area of a cubic that has the same volume of the required coolant. The thickness of the wall  $S_w$  is expressed in the following equation [143,

144]:

$$S_w = \frac{p_p d_i}{v(2K/S - p_p)} + c_1 + c_2 \quad (5.68)$$

where  $p_p$  is the proof pressure, which is the burst pressure defined by Brewer [145], safety factor  $S$  and the allowances  $C_1$  and  $C_2$  are taken from [144].  $K$  is the limited stress of the material. The material used in this study is discontinuous reinforced metallic composites (DRXs) suggested by Mital [146]. The insulation material is MAAMF by Brewer [145]. The weight of the insulation layer is  $1.304 \text{ kg/m}^2$  and thickness is  $1.57 \times 10^{-2} \text{ m}$  [143]. The ducts are not modeled in physics, but assumed 50% of the tank weight.

The power consumption of the cryocooler is provided by Plachta [147]:

$$\eta = 10^{-0.92237 + 0.07763 \log_{10} (1 + Q_c)} \quad (5.69)$$

where  $Q_c$  is the power from the load, of which the unit is watt. The power consumption by the cryocooler,  $P_{cooling}$ , is then given by

$$P_{cooling} = Q_c / \eta \quad (5.70)$$

The weight of the cryocooler is estimated using the equation fitted by Palmer [148]:

$$m = 27.5 P_{input} e^{-1.225 (\log_{10} P_{input})} \quad (5.71)$$

where  $m$  is the mass of the cryocooler, in the unit of kg,  $P_{input}$  is the input power for the cooler, in the unit of  $kW$ . A similar relation can be also found in the fitted curve shown by Radebaugh [149].

#### 5.4.11 Ram Drag due to Ram Air Intake

The change of ram drag of the aircraft is mainly caused by intake of more ram air in the electric ECS. The change of ram drag, assuming complete momentum loss [13], can

be expressed as  $\Delta D_{ram} = N_{pack}(\Delta \dot{m}_{air} V_{\infty})$ , where  $D_{ram}$  is the ram drag,  $N_{pack}$  is the number of ECS packs,  $\dot{m}_{air}$  is the ram air mass flow rate entering each pack, and  $V_{\infty}$  is the freestream velocity.

#### 5.4.12 Others

It should be admitted that there are components related to the TMS that are not modeled, such as the coolant reservoir. Only weights are considered for these components. A parametric factor  $K_{other,weight}$  is used here to quantify these weights by multiplying it to the total weight of other components of a local TMS. As suggested by Chakraborty [13],  $K_{other,weight} = 0.25$  is reasonable for subsystems so it is used for this study.

### 5.5 Results

#### 5.5.1 Parameter Values Used in Experiment Set 2

The values used for the thermal management capability analysis in Experiment 2.1 and the low-fidelity KPI evaluation in Experiment 2.2 are summarized in this subsection. The critical condition and the cruise condition are listed in Table 5.2. The properties of the heat sinks used for thermal management capability analysis are summarized in Table 5.3, and the ones for the low-fidelity KPI evaluation are summarized in Table 5.4. The component performances for thermal management capability analysis are summarized in Table 5.5, and the performances for the low-fidelity KPI evaluation are summarized in Table 5.6. The pressure drop through any heat exchanger is assumed to be 5%. It should be noted that these values are only to validate the capability of the proposed methodologies and they can be adjusted in actual applications.

Table 5.2: Operation conditions for E 2.1 and E 2.2

Condition	$\Delta T_s$ ( $^{\circ}F$ )	Altitude (ft)	Mach
Critical	+27	0	0.3
Cruise	0	38000	0.85



Table 5.3: Heat Sink Properties for E 2.1

Heat Sink	T ( $^{\circ}F$ )	P (psi)	Max Mass Flow Rate
Ram air	86	14.7	10% of a single engine air intake
Fan air	140	19.8	5% of a single fan air intake
Fuel	86	20	2 times of engine fuel flow
Bleed	380	43	5% of a single engine air intake
Electrically compressed air	220	30	5% of a single engine air intake
Refrigerant (R134a)	-11	16.7	5% of a single engine air intake
Oil	131	20	5% of a single engine air intake
Water	86	14.7	5% of a single engine air intake

Table 5.4: Heat Sink Properties for E 2.2

Heat Sink	Initial T ( $^{\circ}F$ )	Initial P (psi)
Ram air	-20	4
Fan air	23.7	5.4
Fuel	-10	20
Bleed	380	43
Electrically compressed air	265	20
Refrigerant (R134a)	-11	16.7
Oil	131	20
Water	59	14.7

Table 5.5: Component Performance for E 2.1, under hot-day on-ground condition

Component	$\eta$	$PR$	$\epsilon$
Compressor (air)	0.95	1.6	N/A
Compressor (phase-change gas)	0.9	7	N/A
Turbine	0.9	0.5	N/A
Heat Exchanger (gas/gas)	N/A	N/A	0.95
Heat Exchanger (liquid/gas)	N/A	N/A	0.4
Heat Exchanger (liquid/liquid)	N/A	N/A	0.8

Table 5.6: Component Performance for E 2.2, under cruise condition

Component	$\eta$	$PR$	$\epsilon$
Compressor (air)	0.95	1.6	N/A
Compressor (phase-change gas)	0.8	7	N/A
Heat Exchanger (gas/gas)	N/A	N/A	0.9
Heat Exchanger (liquid/gas)	N/A	N/A	0.9
Heat Exchanger (liquid/liquid)	N/A	N/A	0.8

### 5.5.2 Runtime Analysis of Feasibility-Based Filtering Methodology - E 2.1

The runtime analysis of the feasibility examination methodology is presented in this section. As the algorithm shown in Algorithm 3 and Algorithm 4, for each case, there are a constant number of components to go through at each level, and the number of the levels are also constant. Therefore, the runtime of this program should be  $O(n)$ , where  $n$  is the number of TMS architectures to examine. The experimental results are also shown in Figure 5.20. As shown in this figure, the runtime increases almost linearly as  $n$  increases, proving the  $O(n)$  runtime. In addition, it can be discovered that around 35 seconds are needed to run 300000 cases, that is, 0.0001 second per case, making the filtering process acceptable even when handling millions of TMS architectures. Therefore, the proposed feasibility-based filtering method can fulfill the requirement that the infeasible architectures can be rapidly filtered out.

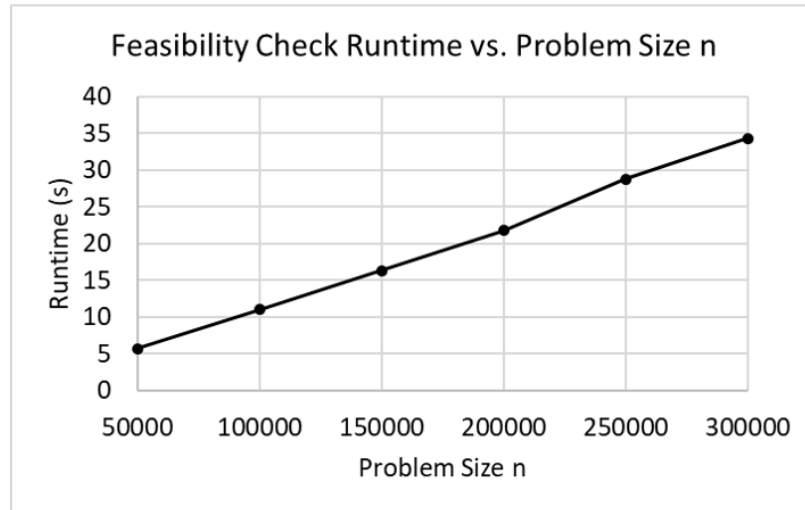


Figure 5.20: Runtime of feasibility check vs. problem size  $n$

### 5.5.3 Feasibility-Based Filtering Results - E 2.1

In this section, loads for the cabin, motor, and battery are varied to show how the results generated from the feasibility-based filtering methodology change with respect to the thermal load requirements.

## Cabin

For the cabin, the gallery load is varied to perform this study. As the functionality and usage of the entertainment systems in gallery expands, the gallery load is a possible increasing source of heat for the cabin. The number of feasible architectures vs. varied gallery load is illustrated in Figure 5.21. As this figure shows, the number of feasible TMS architectures decreases as the cabin gallery load increases, as expected. This figure also demonstrates that the feasibility-based filtering methodology is able to capture the impacts of the increased load. When taking a closer look at what types of architectures are feasible at each load, it is discovered that when the gallery load is not very high, the ram air and fuel can still be effective heat sinks to cool the compressed air. As the gallery load increases, the vapor cycle is needed to cool either the main stream of the supply air or the re-circulated supply air, showing the conventional heat sink is not sufficient. However, it should be noted that such results are obtained with constrained intake of compressed air. If more bleed or electrically compressed air is allowed, then the results should be different, but the corresponding penalty to the propulsion system will also be much larger.

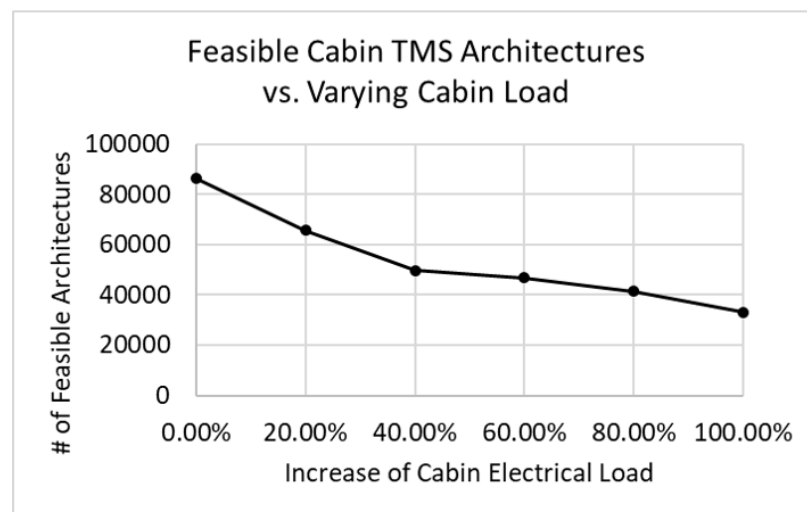


Figure 5.21: Number of feasible architectures vs. varying gallery load

### *Motor*

For the motor, the non-cryogenic cooling option is required here, and oil is used to directly perform the cooling function, with other types of heat sink to cool the oil. The motor efficiency is changed to vary the heat generation. The number of feasible architectures vs. efficiency is shown in Figure 5.22. The number of feasible architectures increases as the efficiency increases, because the heat generation decreases when the efficiency increases. An interesting discovery should be noted here: there is a jump in the number of feasible architectures between efficiency 0.9 and 0.92. When the efficiency is lower than or equal to 0.9, the most feasible architectures require energy storage material such as PCM as part of the cooling system, i.e., the motor needs to be cooled by the oil as well as to reject heat to a PCM shell. As the efficiency increases above 0.9, directly cooling only using oil is possible, and thus, much more feasible architectures begin to appear.

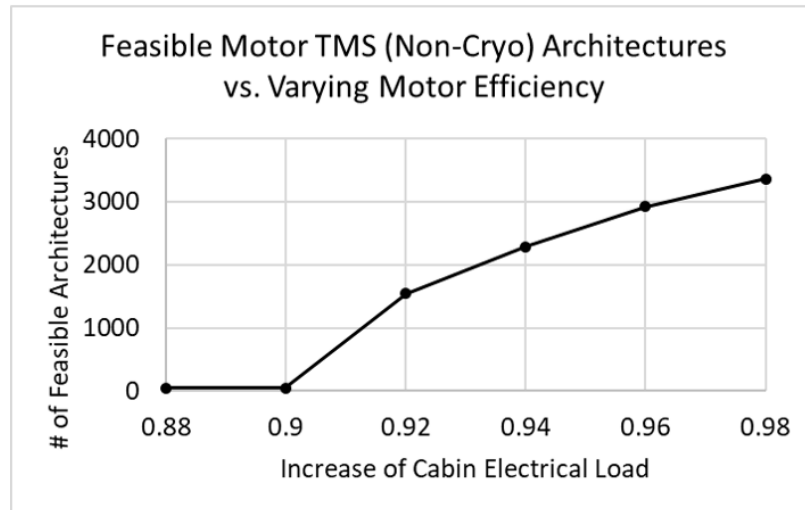


Figure 5.22: Number of feasible architectures vs. varying motor efficiency

### *Battery*

For the battery, the efficiency is also used to create varying cooling load. The corresponding results can be seen in Figure 5.23. Similarly, the number of feasible architectures increases as the efficiency increases, where the cooling load decreases. However, it is noticed that for

the battery, there is a much longer flat section between the efficiency being 0.92 and 0.96, where all feasible architectures are the same. As the actual resulted remaining TMS architectures are traced back to, these 150 architectures require very low temperature cooling or energy storage materials. This is because the battery temperature is relatively low, that is, its temperature starts from the cabin temperature at the beginning, and then is limited by  $45^{\circ}\text{C}$  or  $113^{\circ}\text{F}$ . Due to this working temperature of the battery, the heat transfer through the battery to other media is not very effective, especially when at low altitudes. This discovery also suggests that if the battery can be designed to a higher working temperature, then the thermal management for it would also be much easier.

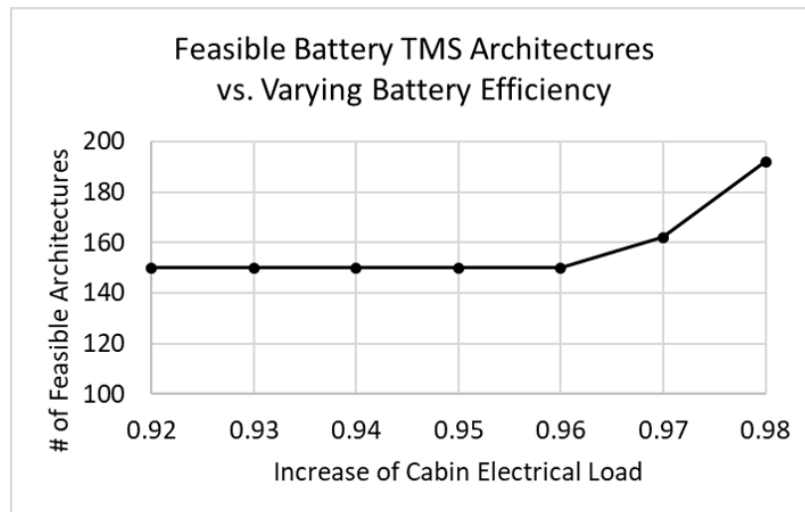


Figure 5.23: Number of feasible architectures vs. varying battery efficiency

### *Eliminated Architectures*

In this subsections, a deeper discussion on why some architectures are eliminated (why they are infeasible) is presented. As diving into the details of the evaluation process for each architecture, the reasons that a certain architecture is determined infeasible can be classified into three categories: 1. the TMS architecture does not match the duty cycle of the load; 2. the heat generated from the load cannot be removed at the top-level TMS architecture; 3. the heat rejected from the top-level architecture cannot be fully removed

by the sub-level architectures. For reason 1, it is obvious that if the duty cycle of a load does not match with the type of TMS architecture, then this architecture will be defined infeasible, due to established duty cycle rules in subsection 5.3.2. In the experiment 2.1, the cabin is a continuous load and its TMS's do not consider energy storage materials due to pre-set regulations, so the duty cycle is not a reason that will rule out cabin TMS architectures. For the battery, its type is "accumulative", allowing for any type of TMS to cool it, so the duty cycle does not influence the feasibility of its TMS architectures either. Therefore, only duty cycle is considered in the feasibility evaluation of motor TMS architectures. Since the type of the load for the motor is "continuous", architectures which only use energy storage materials are not allowed. For reason 2, this situation happens when the selected heat sink cannot fully remove the heat from the load, or the heat sink cannot be fully cooled by sub-architectures. If a selected heat sink cannot remove the heat from the load, it is usually because the allowable temperature difference or the specific heat of the heat sink is so small that the maximum allowed mass flow rate cannot even provide the sufficient cooling capability. When the sub-architectures cannot remove the heat from the heat sink at the top level, it is because the cooling capability of generated sub-architectures are not enough. For reason 3, it happens when the cooling capability of sub-architectures of the top-level ones are sufficient, but the heat accumulated by these sub-architectures cannot be further removed effectively by architectures at the next level. For the three selected loads, the fractions of the architectures that are filtered out based on these three reasons are illustrated in Figure 5.24, Figure 5.25, and Figure 5.26.

It can be seen that most of the infeasible architectures are ruled out due to reason 2: top-level architecture is not able to remove the generated heat. Then the other infeasible architectures are mostly eliminated due to reason 3, besides the reason for inappropriate duty cycle. This discovery shows that the feasibility of a certain architecture mostly depends on the top-level TMS architecture, because the behaviors that the top-level architecture determines the maximum cooling capability of the TMS towards the target load. Comparing

the fraction of feasible architectures for the three loads, it can be found that the remaining fraction of architectures for the cabin is much larger than that for the motor and the battery. This is because the cabin must be cooled by compressed air which already contains a large amount of power that can drive a heat pump. As long as the constructed TMS architecture can appropriately utilize the power embedded inside the heat sink, the constructed architecture is highly likely to be feasible. Considering the motor and the battery, on the one hand, they generate more heat than the cabin in the selected aircraft configurations. On the other hand, there are no specific regulations on the heat sink selections for the motor and battery TMS's, so architectures are populated with the freedoms to use additional power for cooling or not. Many of the generated architectures only rely on the temperature difference between the load and the heat sinks without being compressed, leading to many infeasible architectures. Therefore, the more feasible architectures for the cabin TMS can be found, compared to the other two loads.

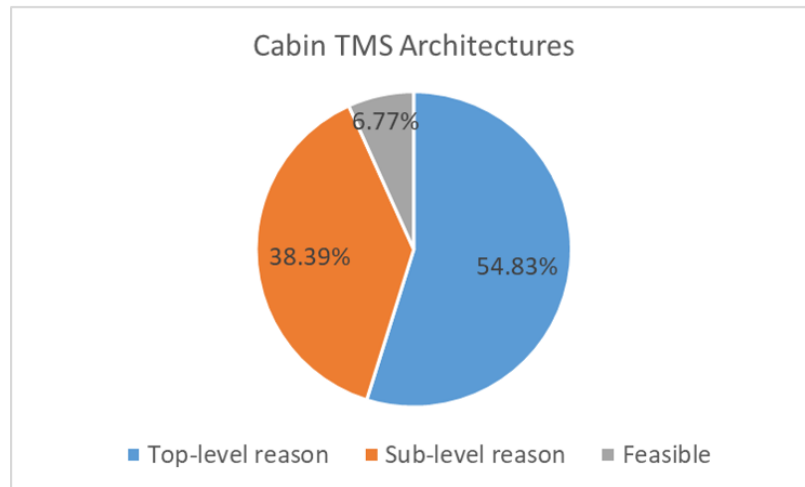


Figure 5.24: Fraction of infeasible architectures for the cabin in terms of different reasons

### *Summary of Feasibility-Based Filtering Methodology*

According to the results presented in previous subsections, the feasibility-based filtering methodology is able to examine the feasibility of a large number of selected TMS architectures in a short period of time. The proposed methodology is also demonstrated to be ca-

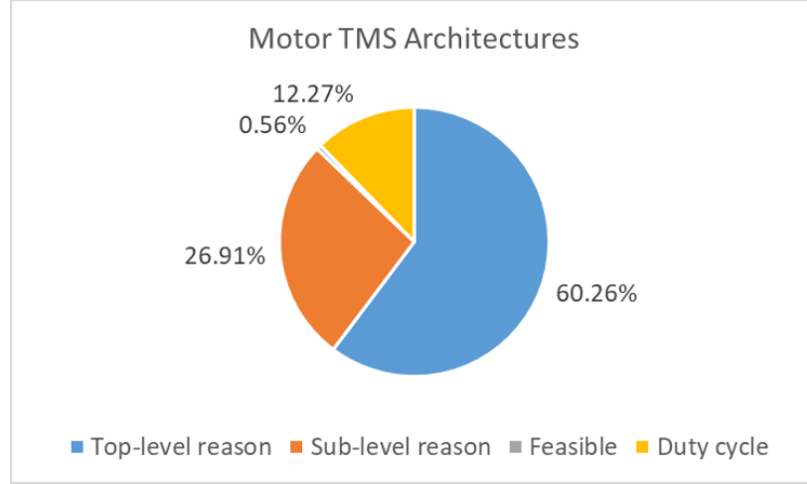


Figure 5.25: Fraction of infeasible architectures for the motor in terms of different reasons

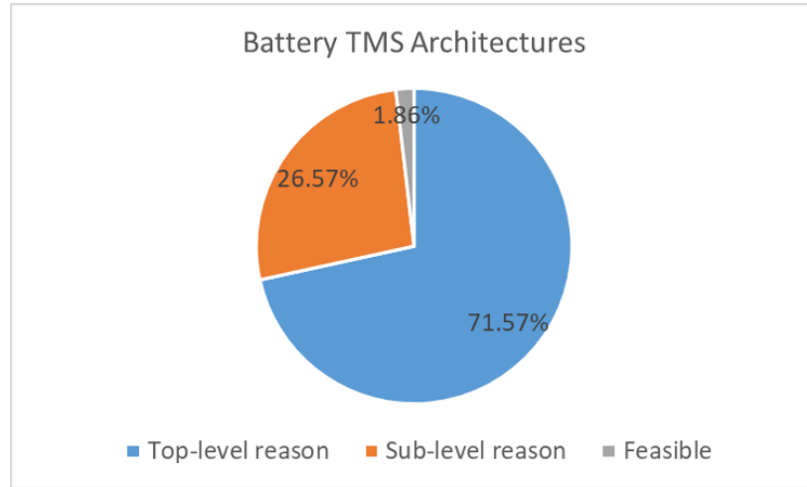


Figure 5.26: Fraction of infeasible architectures for the battery in terms of different reasons

pable of handling varying thermal management load. In summary, the capability to rapidly filter out infeasible TMS architectures is validated.

It has been discussed that a number of architectures might be eliminated by only looking at them without quantitative analysis, which can reduce the computation time of the filtering process, but such approach is not implemented. It is discovered in this subsection that the feasibility of 10000 architectures can be evaluated in around 1 second, and the largest numbers of architecture candidates are one to two million. This means that all the architectures can be evaluated within a few minutes, which is practical to be applied



at early design stages. Therefore, the approach by looking at the visualization of the TMS architectures to determine the feasibility is not necessary in reducing the runtime.

#### 5.5.4 Runtime Analysis of Low-Fidelity KPI Evaluation - E 2.2

The runtime of the KPI evaluation method, as illustrated by Algorithm 5 and Algorithm 6, is shown in this section. As discussed before, the recursive process in this program is the same as applied in the feasibility-based filtering methodology. In addition to the algorithms for the feasibility examination program, only a fixed number of steps of KPI computation processes are added. Therefore, the theoretical computation runtime of the KPI evaluation program is also  $O(n)$ . The experimental results are shown in Figure 5.27, which validates the  $O(n)$  analysis, because the runtime increases linearly as problem size  $n$  increases. The computation time is similar to the one in Figure 5.20, demonstrating the capability of the proposed KPI evaluation method to rapidly estimate metrics of interest for a large number of architectures.

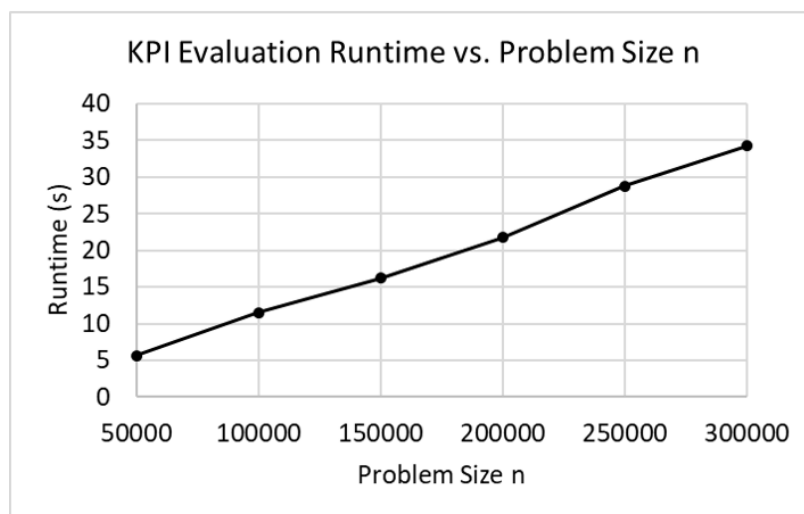


Figure 5.27: Runtime of KPI evaluation vs. problem size  $n$

### 5.5.5 Clustering Results for Local TMS - E 2.2 and E 2.3

As stated in the design of the Experiment Set 2, the cabin, the motor, and the battery are selected as examples to show the capability of the clustering-based methodology for local TMS. With low-fidelity KPI obtained in the previous sections, the clustering results are shown below. It should be also noted that the data points of interest have four metrics (four selected KPI), leading to a four-dimensional space, which is hard to be visualized. Therefore, the clustering presentation are visualized by projecting the results onto 2-dimensional spaces, where 6 2-dimensional spaces are used in total for a 4-dimensional space.

#### *Cabin*

The clustering results for the cabin local TMS for the 160-pax SSA are shown in Figure 5.28. The raw data are scaled, transformed through PCA, and then normalized, to reduce the impacts of dimensionality. Therefore, the values in the presented figures cannot be directly interpreted using the actual four KPI. From the presented results, it can be seen that from certain 2-D spaces, some points of clusters might be seen scattered randomly, but from other 2-D spaces, these points are actually grouped together. In this study, the representative of each cluster is the one that has the minimum components. It should be admitted that such selection might not lead to the optimal solution, and strictly speaking all the candidates in the optimal clusters need to be evaluated to search for the actual optimal solution. However, due to the time limit of the work and computational cost, one representative is selected for each cluster to simplify the problem. The underlying reason to select the TMS with minimum elements as the representative is: a smaller number of components usually leads to lower complexity of the system, lower power and bleed consumption, and lower weight.

From the obtained results, the total number of the clusters is 8, and 4 clusters are identified at the Pareto frontier. In terms of the top level architecture, these 8 clusters can be described as follows in which the first four are at the Pareto frontier:

1. Bleed cooled by ram air.
2. Electrically compressed air cooled by ram air.
3. Bleed cooled by fuel, where fuel driven by a bleed turbine.
4. Electrically compressed air cooled by fuel, where fuel is driven by a electric pump.
5. Bleed cooled by closed-loop heat pumps (driven by bleed); Bleed cooled by fuel with additional bleed-driven heat pumps in the re-circulation path.
6. Electrically compressed air cooled by closed-loop heat pumps (driven by electric power); Electrically compressed air cooled by fuel with additional electric-power-driven heat pumps in the re-circulation path.
7. Bleed cooled by electrical closed-loop heat pumps; Electrically compressed air cooled by bleed-driven closed-loop heat pumps.
8. Architectures with more turbomachines and more re-circulation paths in which many additional cooling cycles are added.

Only visualizations of cabin TMS architectures that are at the Pareto frontier are shown here, as illustrated in Figure 5.29 to Figure 5.32. The non-optimal clusters are not visualized because they are mostly a mixture of different types of architectures. Among the potentially optimal architecture clusters, the first architecture minimizes the power consumption while having a higher bleed extraction. The second architecture minimizes the bleed extraction while having a higher power consumption. The third and fourth ones have low ram air intake but increasing the heat exchanger and ducts weight, The third one has similar characteristics on bleed and power as in the first one, and the fourth one has similar characteristics on bleed and power as in the second one.

For cluster 5 to cluster 8, they are non-optimal because they add more bleed, shaft-power, or weight consumption. For cluster 5, it is non-optimal because its bleed consumption is much higher compared to cluster 1 and cluster 3, while the other metrics are not

improved. Similarly, the cluster 6 adds more electric power consumption compared to cluster 2 and cluster 4, leaving the other objectives almost the same. The cluster 7 is rather a compromise of the cluster 5 and cluster 6, which does not have high bleed or power consumption as does by the cluster 5 or cluster 6. However, it is still non-optimal because it consumes more shaft-power than the optimal architecture that only uses bleed, and it also consumes more bleed than the optimal architecture which only needs shaft-power. The other metrics associated with cluster 6 are not improved either. The last cluster, cluster 8 is penalized by excessive weight associated with the additional turbomachines and recirculation paths. Compared to the added weight, the changes of the other three metrics do not make members of this cluster stand out. It should be noted that the effect of weight in cluster 8 is evaluated after the PCA process and scaling, which is to minimize the impacts of dimensionality. It is still possible to distinguish the members of cluster 8 in terms of other metrics by user-defined similarity (distance) functions. However, such function may bring more influence of the dimensionality. It should also be noted that although the ram drag is one of the metrics, there is not a non-optimal architecture existing due to additional ram air intake. This is because the ram air intake is not greatly penalized by varying or adding the components and heat paths. This can be explained by the fact: if the heat to be removed is constant, and the ram air is the only heat sink that to be discharged, then the required amount of the ram air does not change much with similar heat transfer effectiveness.

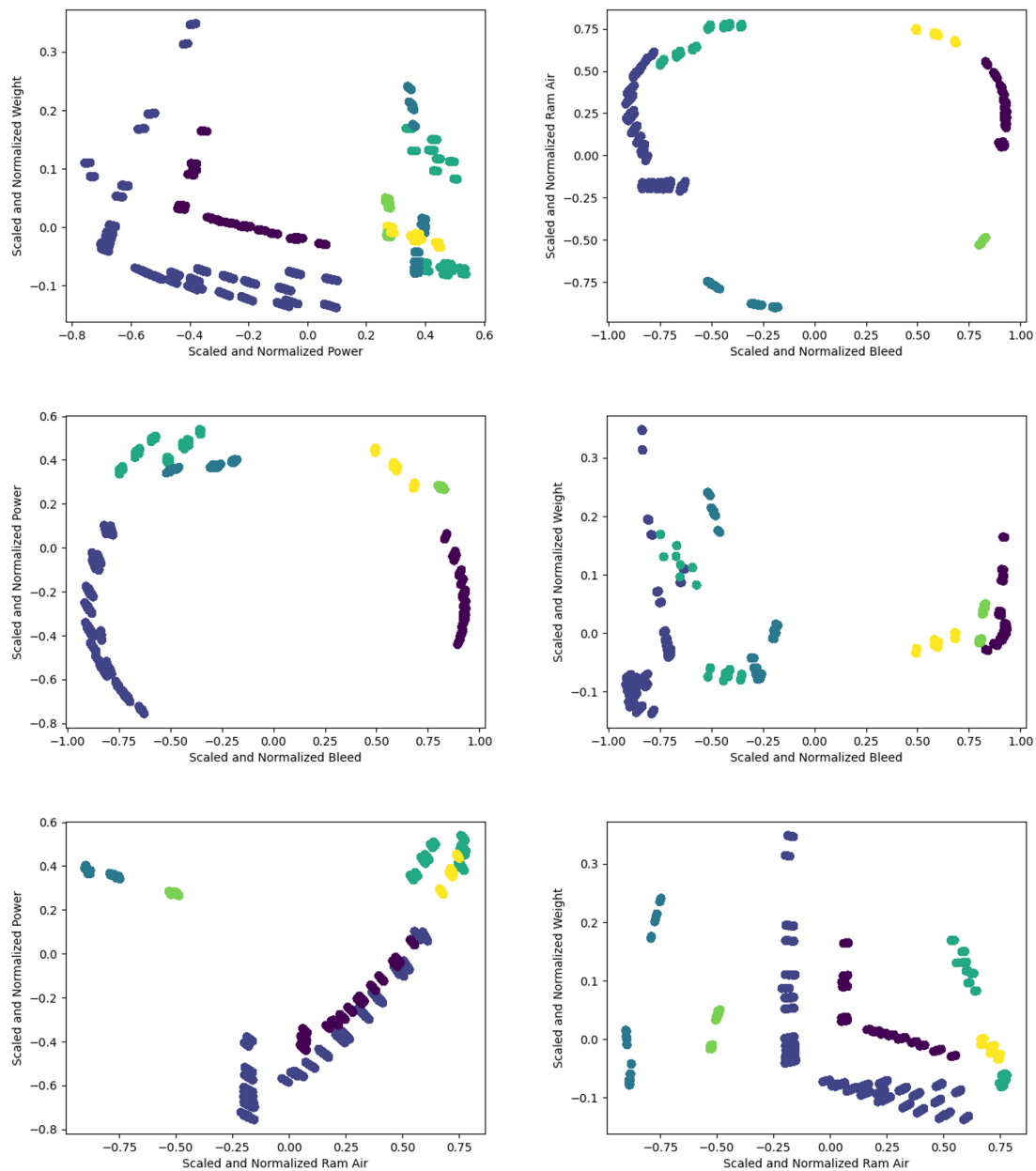


Figure 5.28: Clustering results for cabin KPI

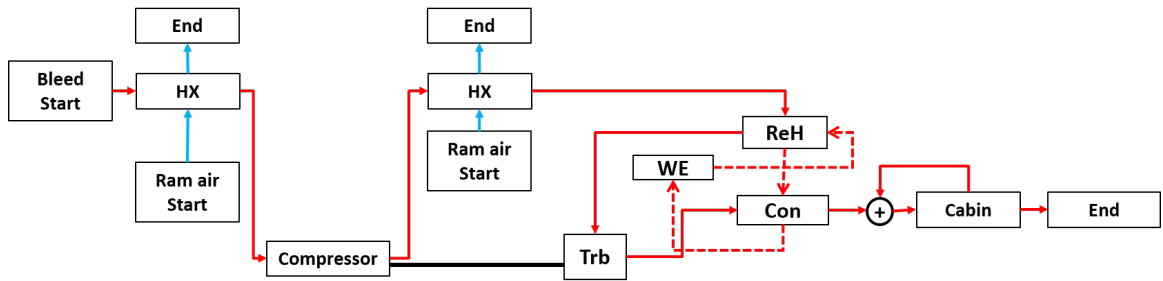


Figure 5.29: Cabin TMS architecture at Pareto frontier: No.1

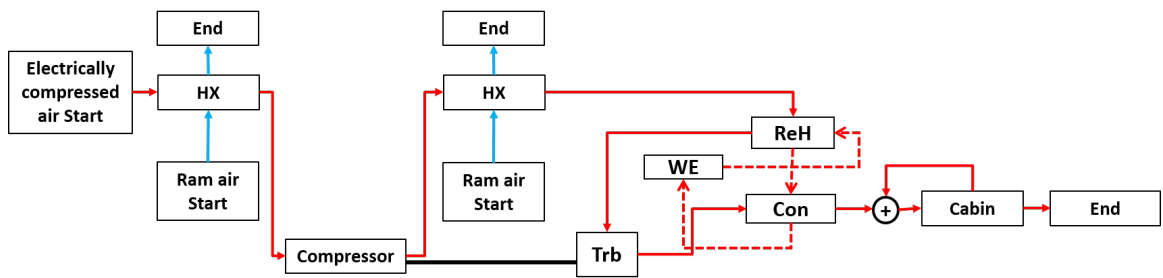


Figure 5.30: Cabin TMS architecture at Pareto frontier: No.2

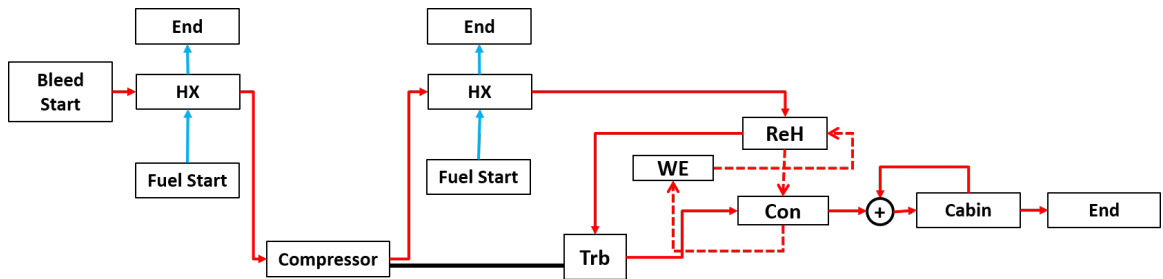


Figure 5.31: Cabin TMS architecture at Pareto frontier: No.3

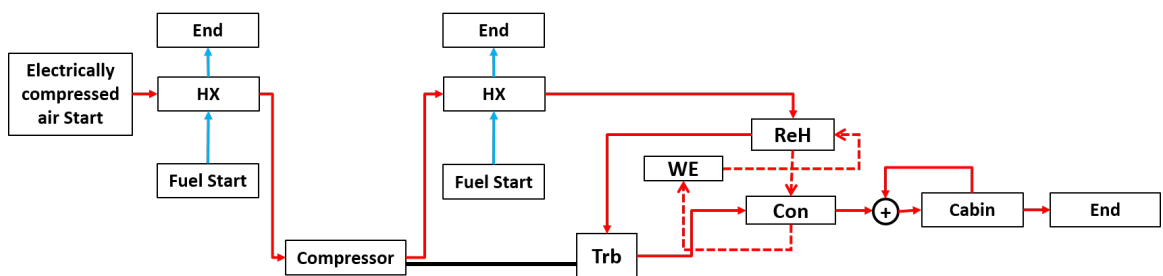


Figure 5.32: Cabin TMS architecture at Pareto frontier: No.4

### *Motor*

The clustering results for the non-cryo motor for the 300-pax TeDP are illustrated in Figure 5.33. Similarly, the clustering effects are not clear in certain 2-D spaces while they are clearly seen in other spaces. Based on the clustering of the motor KPI, 9 clusters are resulted in total, and 5 of them are found to be at the Pareto frontier (the first five as listed below), which are:

1. Top-level architecture cooled by oil and PCM, and oil is further cooled by fan bleed.
2. Top-level architecture cooled by oil and PCM, and oil is further cooled by fuel.
3. Top-level architecture cooled by oil and PCM, and oil is further cooled by ram air.
4. Top-level architecture cooled by oil, and oil is cooled by a vapor cycle.
5. Top-level architecture cooled by oil, and oil is cooled by a closed-loop air cycle.
6. Top-level architecture cooled by oil, and the oil is cooled multiple heat pumps.
7. Top-level architecture cooled by oil and expendable water, and the oil is further cooled by any other type of architecture
8. Top-level architecture cooled by oil and energy storage material, and the oil is further cooled by a vapor cycle
9. Top-level architecture cooled by oil and energy storage material, and oil is cooled by a closed-loop air cycle.

The corresponding architectures of the optimal clusters are visualized in Figure 5.34 to Figure 5.38. It should be noted that three of the architectures require the application of the PCM. The PCM is majorly used for absorption of heat during its critical operation condition, that is, during takeoff and early segments of the climb. In fact, another individual tests on first three architectures without PCM have been also conducted during the cruise

condition. The results turn out that these three architectures without PCM can handle motor heating. The reason that PCM is needed on ground is that the temperature gradient is much smaller than that at high altitude. The architecture 4 and 5 without PCM as shown in Figure 5.37 and Figure 5.38 are feasible during ground while also having good KPI. They are feasible on ground because their cooling temperatures are almost fixed no matter what the ambient conditions are. It should also be noted that the fifth architecture uses a closed-loop air cycle, which is constructed through the Experiment Set 1. This architecture uses a compressor and turbine. However, an additional power source is needed to drive the compressor besides the turbine in the loop. This closed-loop air cycle is lighter compared to the vapor cycle, because the weight of the refrigerant is almost removed. However, the required power consumption is higher. Such architecture of the closed-loop air cycle can also be found in [150].

Cluster 6 to 9 are non-optimal clusters of the architectures. Cluster 6 adds more consumption of shaft-power and bleed, and more weight compared to cluster 4 and 5. In cluster 4 and 5, it can be seen that only one closed-loop heat pump is sufficient to cool the oil loop. Thus, adding more heat pumps will definitely make the architecture feasible, but will also bring more penalties. Although the metrics of the members in cluster 6 differ from each other, the distances within the cluster are shorter than the distances between them and the other optimal clusters. The cluster 7, which unitizes the water as an expendable source to cool the motor, is greatly penalized by the weight of the water. It should be admitted that the high latent heat of the water can provide a large amount of cooling capability, but the weight associated with the expendable water is also substantial. In this cluster, members with differences in other three metrics are alleviated by the weight. However, it is non-optimal because the optimal architecture with PCM adds less weight. For cluster 8 and cluster 9, additional energy storage materials are included, compared to cluster 4 and 5, indicating they are heavier than cluster 4 and 5 which makes the cluster 8 and 9 non-optimal.



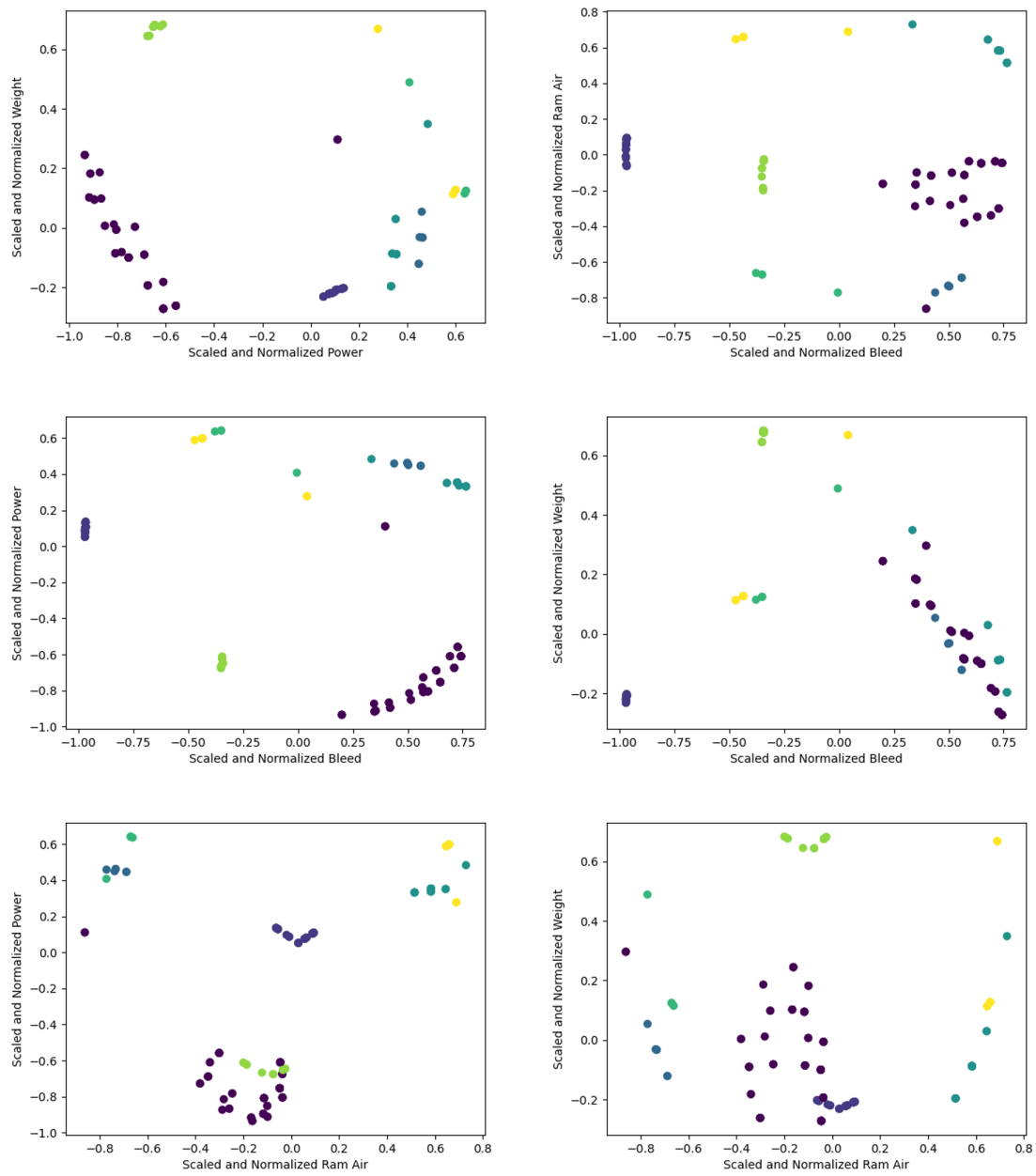


Figure 5.33: Clustering results for motor KPI

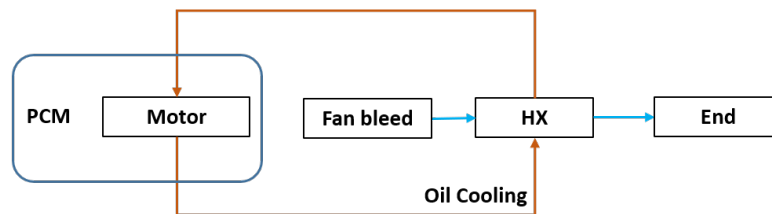


Figure 5.34: Motor TMS architecture at Pareto frontier: No.1

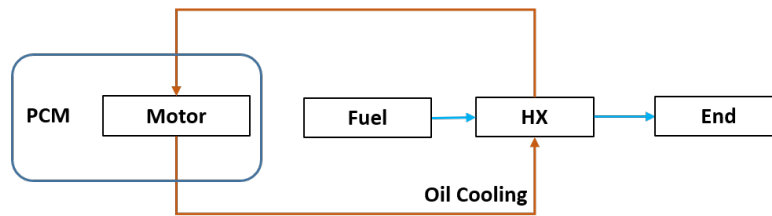


Figure 5.35: Motor TMS architecture at Pareto frontier: No.2

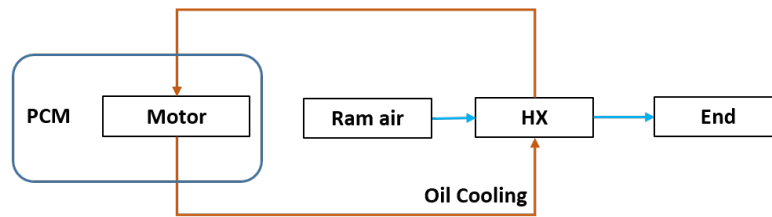


Figure 5.36: Motor TMS architecture at Pareto frontier: No.3

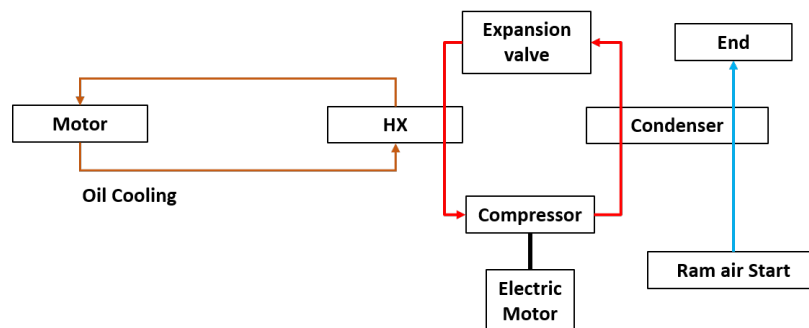


Figure 5.37: Motor TMS architecture at Pareto frontier: No.4

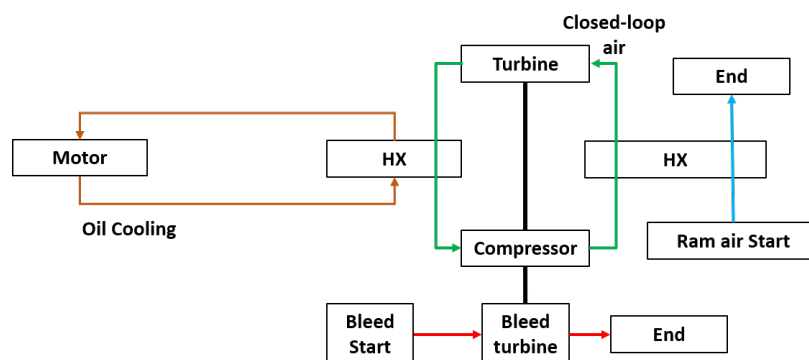


Figure 5.38: Motor TMS architecture at Pareto frontier: No.5

## *Battery*

The clustering results of the battery for the 78-PAX HTeDP are illustrated in Figure 5.39. The characteristics of this figure have already been seen in Figure 5.28 and Figure 5.33, and discussed before. The number of resulted clusters is 5, and 4 of them (first 4 as listed below) are at the Pareto frontier, of which the representatives are listed below:

1. Top-level architecture cooled by air from the air cycle machine (ACS) in ECS.
2. Top-level architecture cooled by PCM only.
3. Top-level architecture cooled by PCM and air from ACS.
4. Top-level architecture cooled by fuel.
5. Top-level architecture cooled by multiple cooling sub-architectures, no matter whether they are heat pumps that require power or not.

The corresponding architectures of the optimal TMS clusters are plotted in Figure 5.40, Figure 5.41, Figure 5.42, and Figure 5.43. The first one uses the air supplied by the air cycle machine (ACS) which is the cooling TMS for ECS. The second one only uses the PCM only. And the third one uses both air from the ACS and the PCM. Considering these three architectures, the air from ACS either comes from the bleed or the electrical compressor, which will either lead to bleed or shaft-power off-take. The PCM in the second representative will add additional weight to the system, but there is no consumption of power or bleed, or additional ram drag. Considering the third cluster, which is a compromise between cluster 1 and cluster 2, the PCM is lighter than that of cluster 2, and the power or bleed consumption is also smaller than that of cluster 1. For the fourth architecture, the fuel is directly used to cool the battery, by which there is no bleed or power consumption due to ACS air. However, such usage of fuel will increase the weight of the ducts as well as the power to pump the fuel. It should be noted that the load type of the battery is "accumulative", that is, the heat generation does not need to be fully removed at any moment of the

mission as long as the highest temperature is controlled below its temperature upper limit. From the actual analysis, any of these architectures cannot fully remove the heat generation from the battery during the on-ground condition. However, as the flight altitude goes higher, the cooling capability of these three architectures can gradually cool the battery to not let its temperature grow over the constraint. For the cluster 5, it is a non-optimal cluster. This cluster is a mixture by different types of the TMS architecture. Additional penalties compared to the other four optimal clusters are caused by adding extra sub-architectures. It can be seen from cluster 1 to cluster 4, the battery can be successfully cooled by using a single cooling cycle. Thus, adding more cooling architectures will only cause more penalties to the TMS. It should be noted that the members within cluster 5 has rather scattered KPI, and a more detailed clustering of them is possible. Nevertheless, these architectures are all non-optimal because of their penalties compared to the other four optimal clusters, so there is no need to perform a further distinguishing of the members within cluster 5.

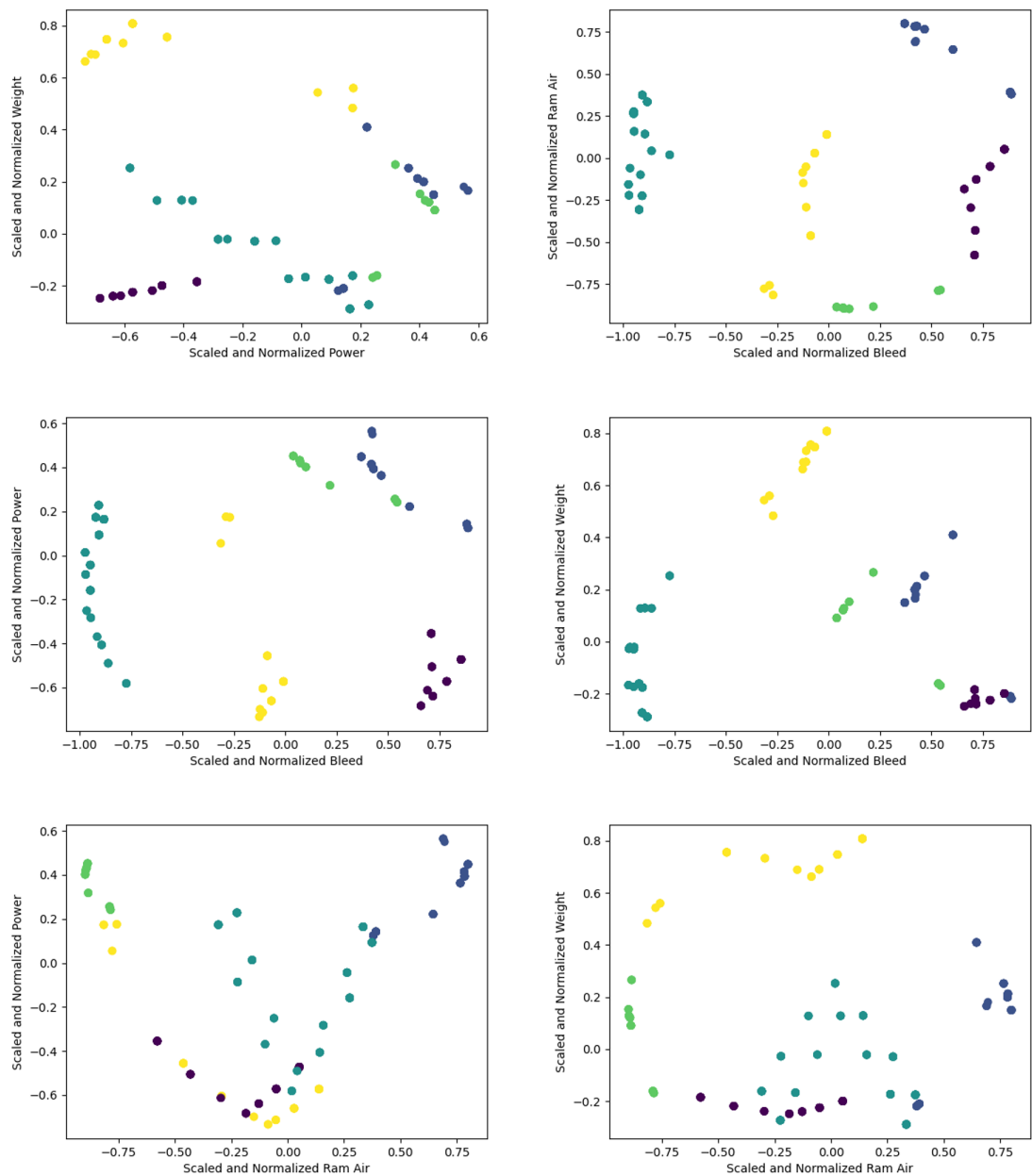


Figure 5.39: Clustering results for battery KPI



Figure 5.40: Battery TMS architecture at Pareto frontier: No.1

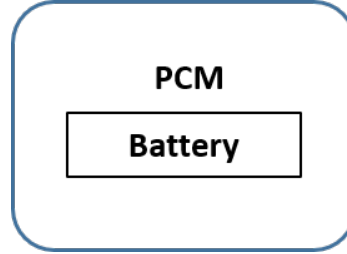


Figure 5.41: Battery TMS architecture at Pareto frontier: No.2

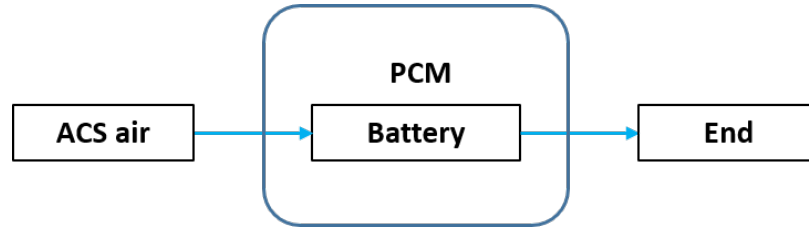


Figure 5.42: Battery TMS architecture at Pareto frontier: No.3

#### 5.5.6 Clustering Results for Global TMS - E2.2 and E 2.3

With obtained optimal local TMS candidates from the local clustering process, the global TMS's are then constructed, using the architecting methodology introduced in the Experiment Set 1 in chapter 4. In this study, the 160-pax SSA, 300-pax non-cryo TeDP configuration, and 78-pax non-cryo HTeDP configuration are selected as examples to illustrate the results of the clustering process for the global TMS's. The same four KPIs are used for the clustering of the global TMS's, and the clustering results are also projected into 2-D spaces.

##### *160-PAX SSA*

As mentioned in the design of experiment, 6 loads are selected for the 160-pax SSA: cabin, generator, fuel tank, engine oil reservoir, hydraulics, and avionics. For the cabin, there



Figure 5.43: Battery TMS architecture at Pareto frontier: No.4

are four candidates as shown above, the generator has three candidates, both fuel tank and engine oil have two candidates, and avionics have one candidate. It should be noted that when the heat generation becomes less, sometimes the number of clusters at the Pareto frontier will be smaller. For example, the avionics in the 160-pax SSA generates a small amount of heat, where only the exhaust from the cabin is enough to cool it. Therefore, only small amount of the ducts weight is added while no penalties on bleed, power, or ram air. In this case, there is one best choice in terms of all four chosen metrics, that is, only one cluster is at the Pareto frontier. For this 160-pax SSA configuration, the clustering results of the global TMS in terms of the KPI are shown in Figure 5.44.

Similar patterns have been found as shown in the local TMS clustering results, where from some of the 2-D dimensions the clustering effects are not clear, while from other domains the clusters are more clear. There are four clusters that are at the Pareto frontier. It would be too much space to visualize all the global TMS with their local TMS's, so only brief descriptions of the four clusters are presented here:

1. Cabin is cooled by a bleed-based TMS which is cooled by ram air. The generator is directly cooled by oil and further cooled by air or fuel. Fuel tank is cooled by ram air, and oil reservoir is cooled by fuel or ram air. Avionics is cooled by cabin exhaust. The options of the other TMS's than the cabin do not create much difference in terms of the KPI.
2. Cabin is cooled by a bleed-based TMS which is cooled by fuel, the other local TMS's are the same as described in the first cluster.
3. Cabin is cooled by a electrically compressed air-based TMS which is cooled by ram air, the other local TMS's are the same as described in the first cluster.

4. Cabin is cooled by a electrically compressed air-based TMS which is cooled by fuel, the other local TMS's are the same as described in the first cluster.



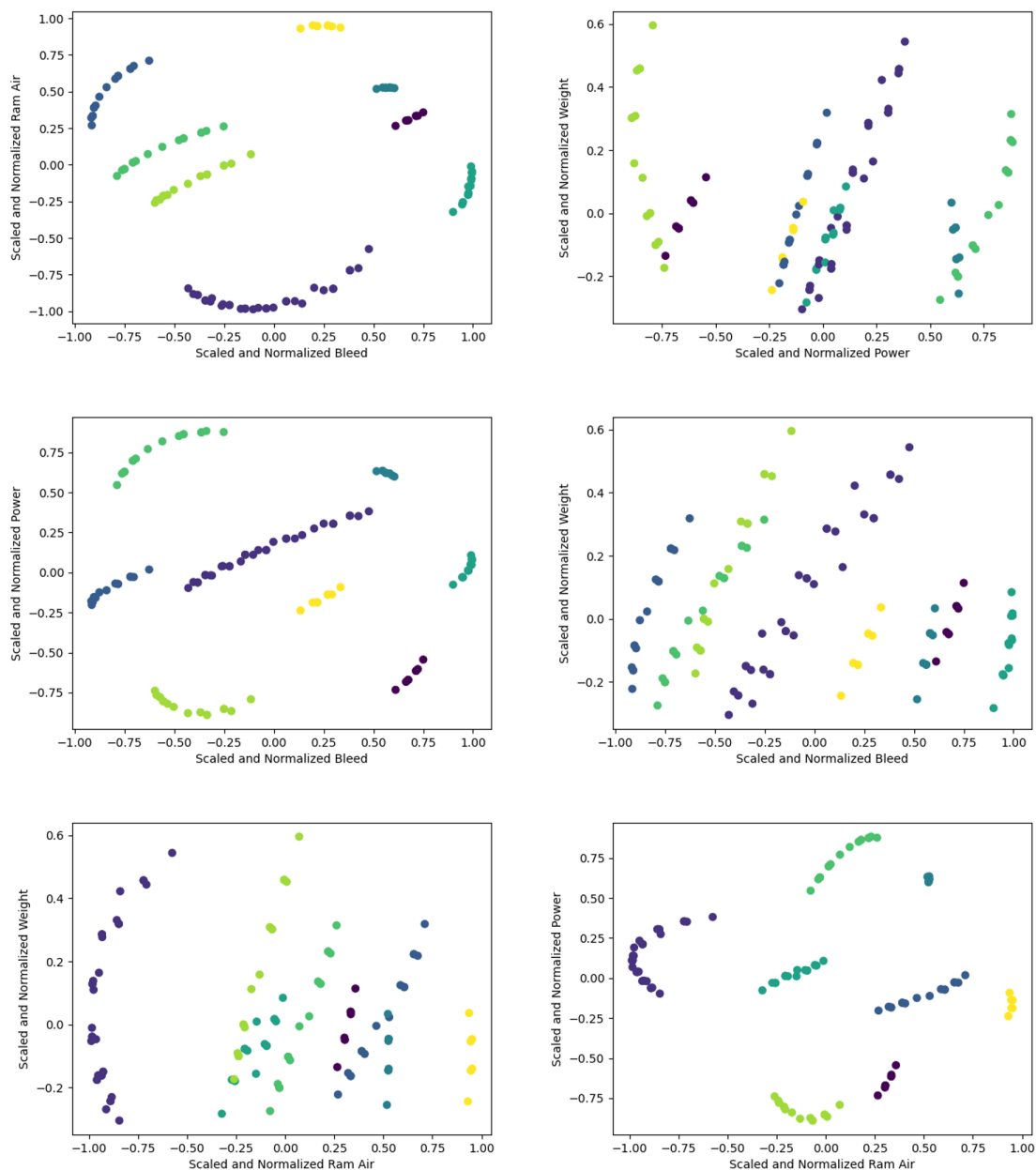


Figure 5.44: Clustering results for 160-pax SSA global TMS

It can be seen that the clusters at the Pareto frontier are dominated by the selection of the cabin TMS. This fact can be explained by the fact that for a conventional commercial aircraft, the largest load to be cooled is the cabin, where the metabolic heat and gallery heat need to be handled. For all the other loads in the commercial aircraft, the heat generation is relatively small compared to the cabin TMS. Therefore, the selection of local TMS's for other loads does not show large influence on the clustering results. It should be also noted that at this architecting stage, the power consumption from the TMS has not been integrated into the generator operation. Thus, the heat generation of the generator does not change for the current study. However, the integrated impacts will be shown in the next chapter.

### *300-PAX Non-Cryo TeDP*

The clustering results for the global TMS of the 300-pax non-cryo TeDP are shown in Figure 5.45. It is noted that the non-cryo TeDP is selected because the local TMS for generator and motor with cryo-option is of limited number, and much fewer global TMS cases will be generated using these options. A small number of architectures might not be able to present the patterns of the clustering results. The loads selected in this experiment are: cabin, electric motor, generator, fuel tank, engine oil reservoir, hydraulics, and avionics.

Compared to the previous clustering results, the pattern of this set of clusters is more scattered. And the needed cluster to distinguish the data points become as many as 37, while the previous clustering only requires around 10 clusters. The clusters at the Pareto frontier are also much more, which is 14 in this experiment. The increasing number of clusters and the clusters at the Pareto frontier can be explained by the fact that as the propulsion system is electrified, the heat generated by the electric motor and generator becomes much larger. Thus, there are three major cooling loads in this configuration, including the cabin. And the different combinations of the candidates for these three loads can create many more clusters than in the commercial aircraft. Due to the large number of clusters at the Pareto frontier, they will not be discussed here in detail.

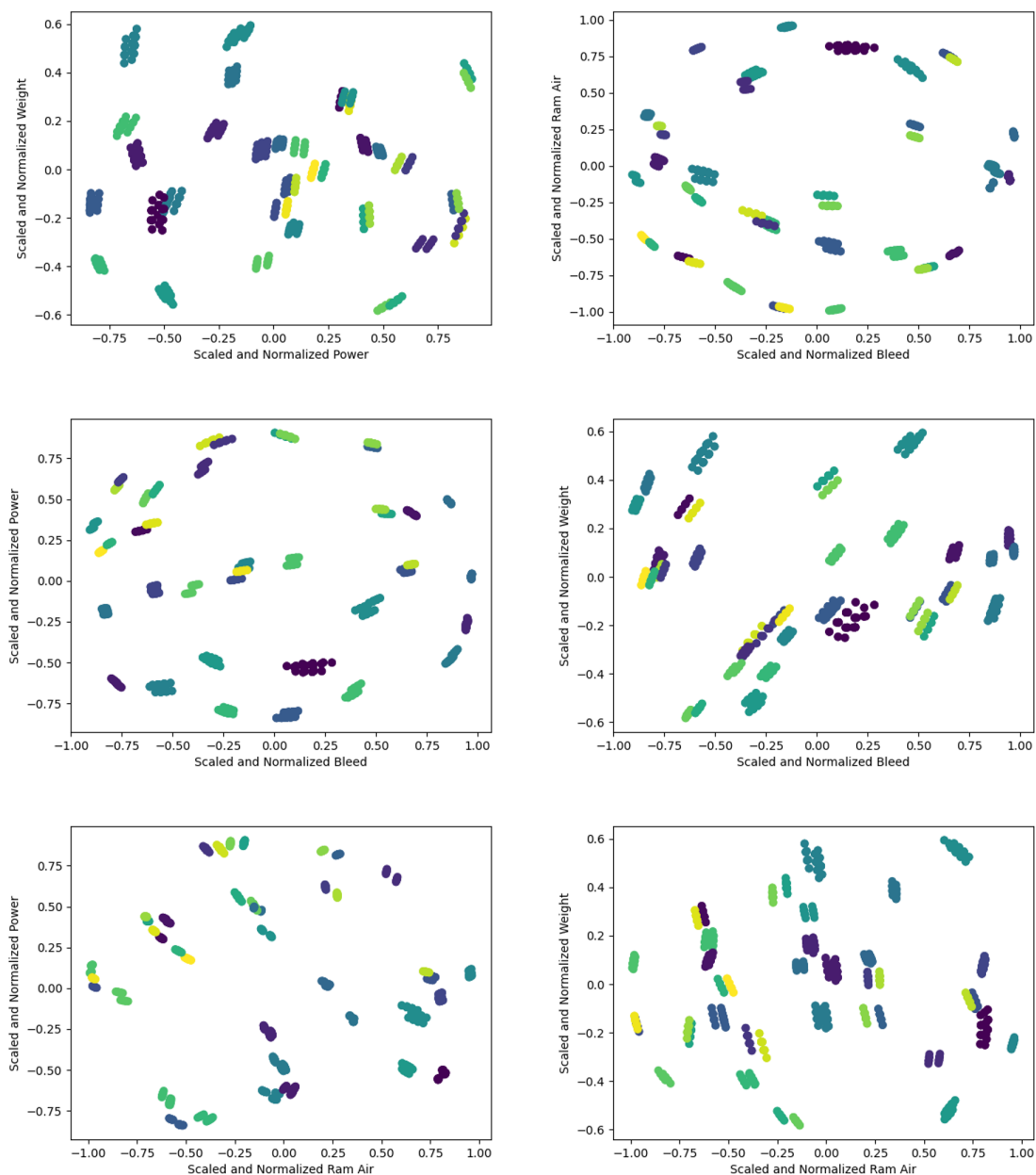


Figure 5.45: Clustering results for 300-pax TeDP non-cryo global TMS

### *78-PAX Non-Cryo HTeDP*

The clustering results for the global TMS of 78-pax non-cryo TeDP are shown in Figure 5.46. A similar scattering pattern of the clusters to the clustering experiment of global TMS of 300-pax TeDP. The loads selected in this experiment are: cabin, electric motor, generator, battery, fuel tank, engine oil reservoir, hydraulics, and avionics, where one more cooling load, the battery, is added compared to the loads in the 300-pax non-cryo TeDP configuration. It should be also noted that even there are many clusters, the visualization may not be very clear. This is because when the number of colors needed is increased to address the increasing number of clusters, some of the colors will look similar to each other.

Compared to the results shown for the 300-pax TeDP concept, the number of data points for global TMS's and the number of clusters both increase. This is due to added one more load, which leads to more combinations of the local TMS's, and such a larger number of combinations of local TMS can also create more clustering patterns.

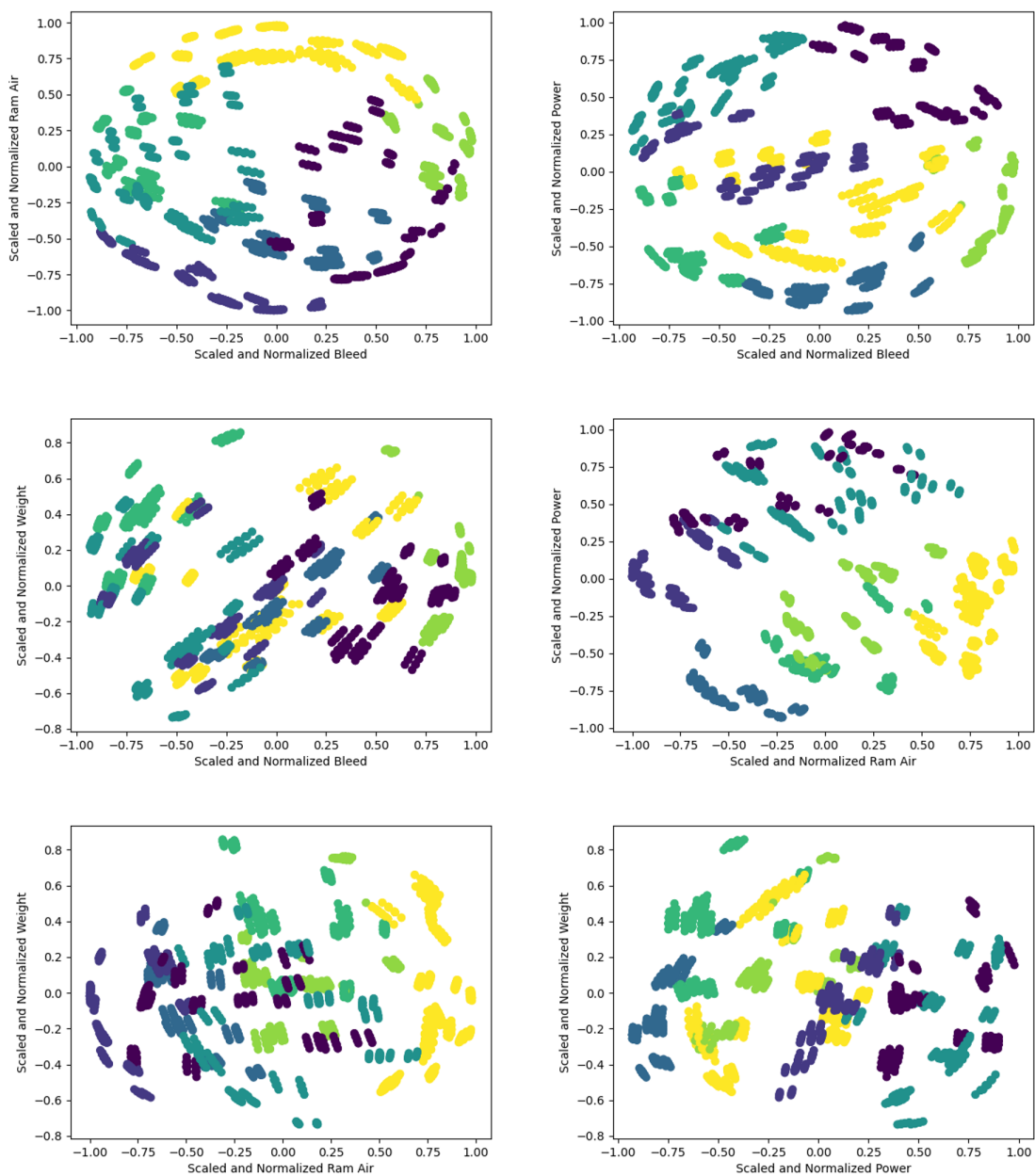


Figure 5.46: Clustering results for 78-pax non-cryo HTeDP global TMS

### 5.5.7 Automatic Creation of Physics-Based Models - E 2.4

In this subsection, the results of the automatic creation of physics-based models will be discussed. It should be noted the Experiment 2.4 is only a convenient approach to automatically construct the TMS models, of which the purpose is to save model construction time. Fundamentally, the method for the Experiment 2.4 is an approach to read strings and write texts to another file, following certain rules, to create models. However, such work can also be completed purely by manual efforts. Therefore, there is not too much to be discussed in terms of academic purpose. In this subsection, an example of this creation process will be presented to help the readers to understand what the input and output look like. The example TMS architecture descriptor as well as the visualization of it are shown in Figure 5.47.

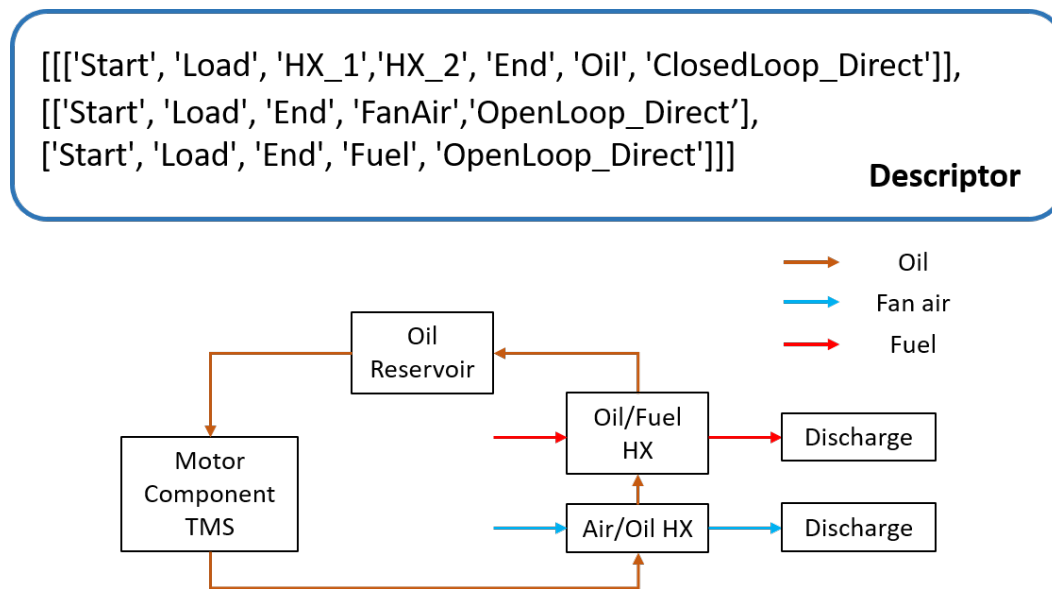


Figure 5.47: Selected TMS architecture descriptor and visualization for the model creation example

The list of lists at the top of this figure are the descriptor. Reading this descriptor and following the model creation process introduced in subsection 5.3.5. The resulted model files are illustrated in Fig . The mdl.mdl file is the major model file describing the components. The setup.list and solver.list are the files automatically created using pre-defined

templates. The solvers added are based on the prescribed constraints or target, such as the minimum mass flow rate, or the target temperature at certain flow station. The execution run file is not shown here, because it is made manually which can execute all created models. In this execution run file, the sizing condition for each type of components are determined, which is to perform the proposed MDP sizing and optimization methodology, as discussed in subsection 5.3.6. It should be also admitted here that all the executions of the models might not work automatically. Inappropriate initial values of the solver setup can lead to converging issues. Therefore, manual efforts are still needed sometimes to tune the model solvers.

The figure displays three screenshots of a code editor, each showing a different file in a project. The top screenshot shows the `mdl.mdl` file, which defines the model structure with elements like `FlowStart`, `ThermLoad`, `ECSHeatExchanger`, and `FlowEnd`, and links their ports. The middle screenshot shows the `setup.list` file, which sets initial conditions and parameters for the model components. The bottom screenshot shows the `solver.list` file, which defines the solver variables, including independent and dependent variables and their equations.

```

mdl.mdl
1 Element FlowStart Start0{}
2 Element ThermLoad{}
3 Element FlowStart Start10{}
4 Element ECSHeatExchanger HX1{}
5 Element FlowStart Start11 {}
6 Element ECSHeatExchanger HX2{}
7 Element FlowEnd End0{}
8 Element FlowEnd End10{}
9 Element FlowEnd End11{}
10 linkPorts( "Start0.Fl_O","Load.Fl_I","FS_1");
11 linkPorts( "Load.Fl_O","HX1.Fl_I1","FS_2");
12 linkPorts( "Start10.Fl_O","HX1.Fl_I2","FS_3");
13 linkPorts( "Start11.Fl_O","HX2.Fl_I2","FS_4");
14 linkPorts( "HX1.Fl_O1","HX2.Fl_I1","FS_5");
15 linkPorts( "HX2.Fl_O1","End0.Fl_I","FS_6");
16 linkPorts( "HX1.Fl_O2","End10.Fl_I","FS_7");
17 linkPorts( "HX2.Fl_O2","End11.Fl_I","FS_8");
18 #include<setup.list>
19 #include<solver.list>
20

setup.list
1 Start0.W = 2;
2 Start0.Tt = 590.67;
3 Start0.Pt = 20;
4 Start10.W = 2;
5 Start10.Tt = 599.67;
6 Start10.Pt = 19.8;
7 Start11.W = 2;
8 Start11.Tt = 545.67;
9 Start11.Pt = 20;
10 ThermLoad.eff = 0.9;
11 ThermLoad.wc = 2000;
12 HX1.dpl = 0.05;
13 HX1.sink_type = "AirAir";
14 HX2.dpl = 0.05;
15 HX2.sink_type = "OilFuel";

solver.list
1 real LoadTout = 612.27;
2 real TargetT1 = 600;
3 real TargetT2 = Start0.Tt;
4 Independent I1{}
5 Independent I2{}
6 Independent I3{}
7 Dependent D1{}
8 Dependent D2{}
9 Dependent D3{}
10 I1.varName = Start0.W;
11 I2.varName = Start10.W;
12 I3.varName = Start11.W;
13 D1.eq_lhs = "Load.Fl_O.Tt";
14 D1.eq_rhs = "LoadTout";
15 D2.eq_lhs = "HX1.Fl_O1.Tt";
16 D2.eq_rhs = "TargetT1";
17 D3.eq_lhs = "HX2.Fl_O1.Tt";
18 D3.eq_rhs = "TargetT2";

```

Figure 5.48: Created model files for the model creation example



#### 5.5.8 Optimization Results - E 2.5

From each selected local loads in the Experiment Set 2, one architecture is selected to perform the optimization using the MDP methodology. The objectives are to minimize the chosen four KPI: bleed off-take, shaft-power extraction, ram air, and weight. Minimizing these four objectives at the same time conflicts with each other. Minimizing bleed would lead to an increase of shaft-power, because bleed and shaft-power are two major power sources for a heat pump in aircraft. If the power consumption of a heat pump is constant, reducing one must lead to the increase of the other. Reducing shaft-power or bleed would also lead to an increase of the ram air. This is because if the power input for a heat pump is reduced, more heat sink is then needed to remove the same amount of heat. Reducing shaft-power, bleed, or ram air, will also lead to an increase of the weight. If the amount of power input is reduced, as well as the amount of the heat sink, the heat exchanger needs to be made more effective, that is, heat exchanging area and the overall volume needs to be larger to remove the same amount of heat. Therefore, the expected optimization results will be a set of designs at a 4-D Pareto frontier, instead of a design minimizing the four selected metrics at the same time.

## Cabin

The selected architecture is illustrated in Figure 5.49, which is selected from the clusters from Experiment 2.3 that are at the Pareto frontier. The design variables are the pressure ratios of the turbomachines and the effectiveness of heat exchangers. The resulted Pareto frontier is shown in Figure 5.50. The data are all normalized by the largest value of each metric. The 4-D Pareto frontier is hard to visualize. From the 2-D domain, only scattered points can be seen. However, such discovery indicates that the four chosen metrics are conflicting. Otherwise, at least the points in one projection will decay.

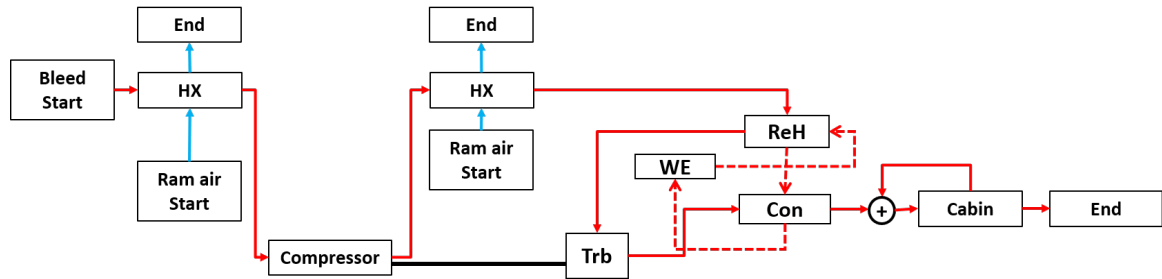


Figure 5.49: Selected cabin TMS for optimization

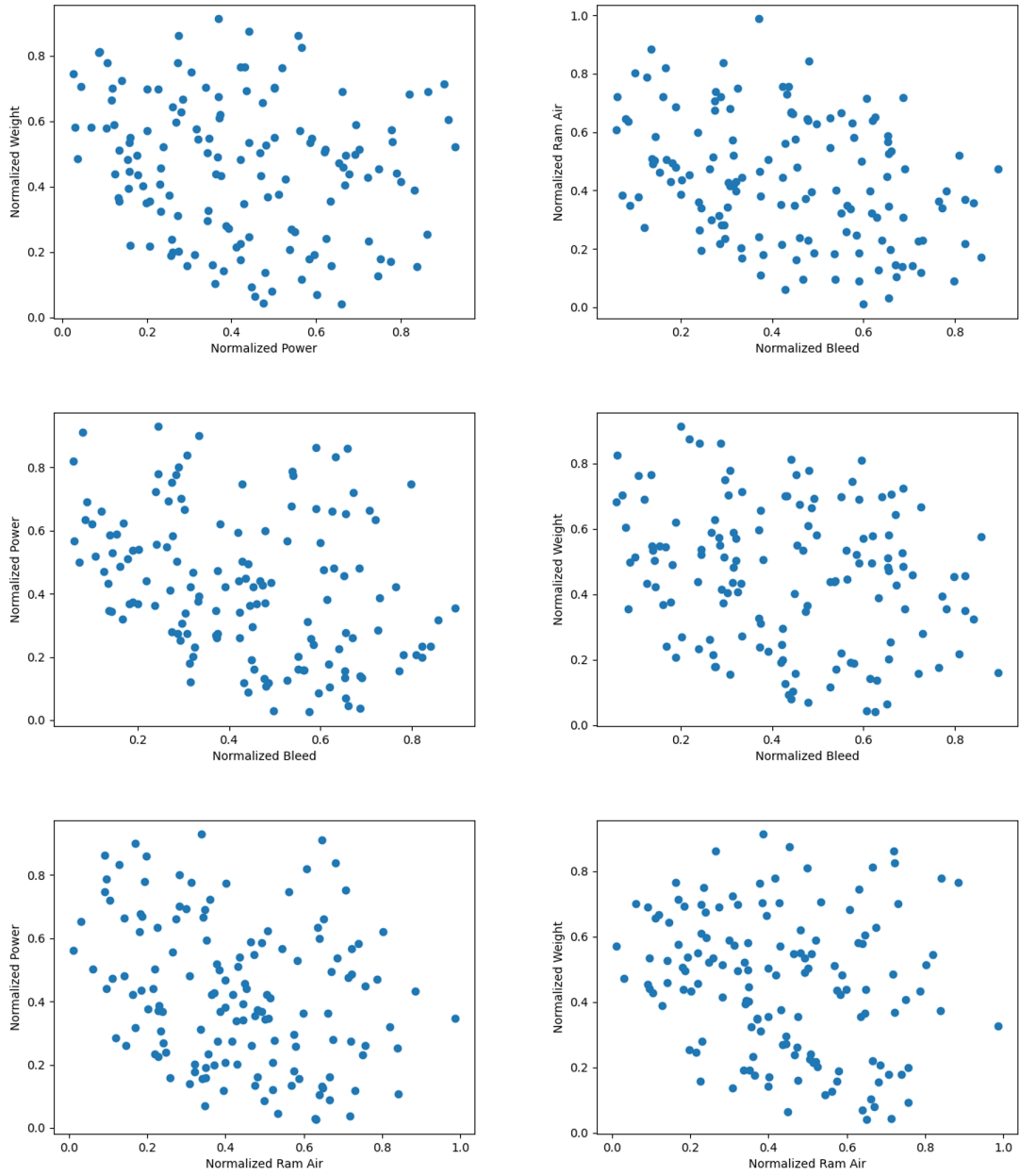


Figure 5.50: Pareto frontier for selected cabin TMS

### *Motor*

The selected TMS for the motor is illustrated in Figure 5.51, in which a vapor cycle is applied to cool the oil loop. The design variables are effectiveness of heat exchangers, pressure ratio of turbomachines, and the mass flow rate of the refrigerant (R134a) in the vapor cycle. The corresponding Pareto frontier can be also found in Figure 5.52. The patterns of this figure is similar to Figure 5.50.

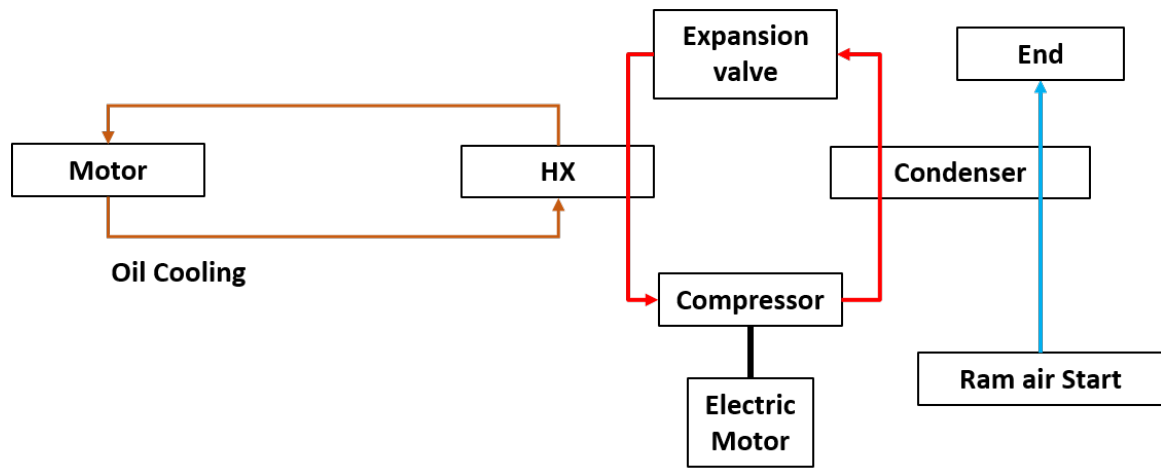


Figure 5.51: Selected motor TMS for optimization

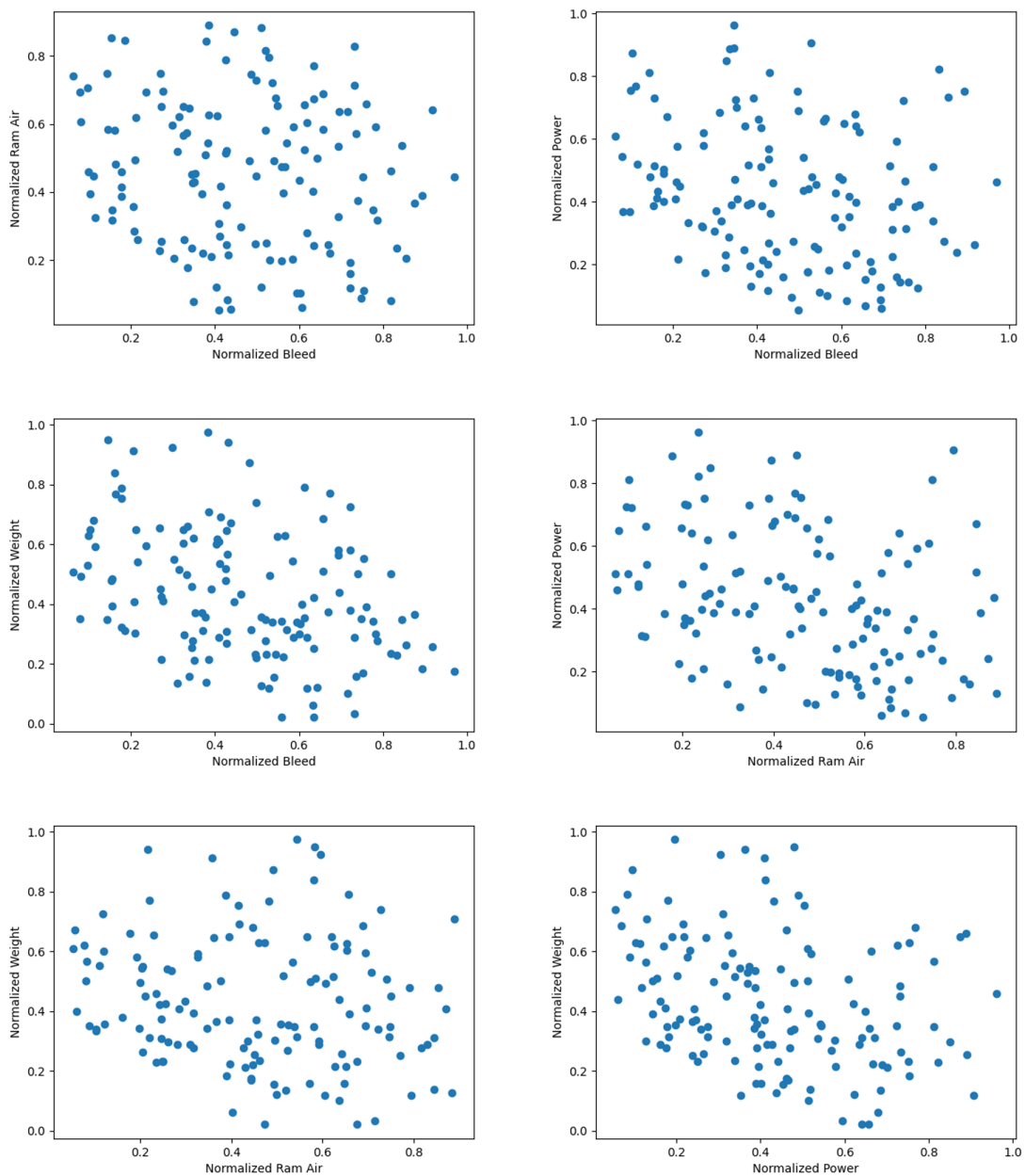


Figure 5.52: Pareto frontier for selected motor TMS

## Battery

The selected TMS for the motor is illustrated in Figure 5.53. The ACS air is the supply to cool the battery while the PCM also absorbs the generated heat at the same time. The design variables are: mass flow rate of supply air (mass flow rate of the engine bleed in addition to the ECS air) and the PCM weight. Assuming the ram air intake and the power consumption to drive the ACS air have fixed relations with the increased engine bleed, there are only two objectives to minimize for this architecture: mass flow rate of engine bleed and weight. Thus, the Pareto frontier is in a 2-D dimension, which is shown in Figure 5.54, where the values of the two objectives are both normalized.

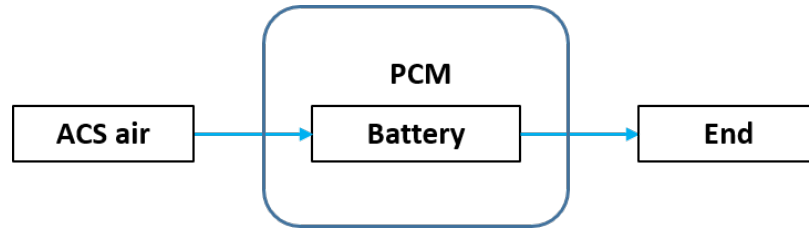


Figure 5.53: Selected battery TMS for optimization

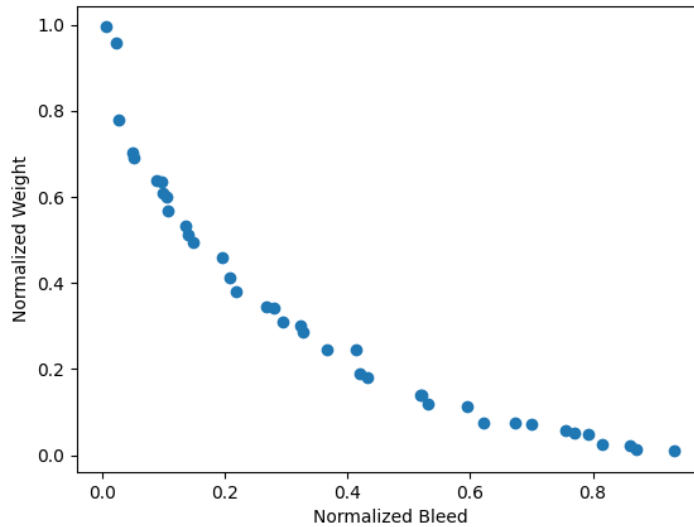


Figure 5.54: Pareto frontier for selected battery TMS

## 5.6 Conclusion for Experiment Set 2

### 5.6.1 Validation of Hypothesis 2

How the results from the Experiment Set 2 can validate the Hypothesis 2 is stated in this section. The Research Question 2, Hypothesis 2, and the proposed criteria to validate Hypothesis 2 are re-stated here as a reminder:

**Research Question 2:** *With a number of thermal management systems architecture candidates, how can the architecture evaluation process rapidly filter out architectures which are not viable, and perform further down-selection of optimal architectures on the left competent architectures based on chosen metrics, where the information required are suitable for conceptual design phase with limited historical data.*

**Hypothesis 2:** Large number of infeasible or non-optimal architectures can be eliminated by filtering process in terms of feasibility and low-fidelity subsystem-level analysis on key performance indicators, and further down-selection of optimal architectures can be done by evaluations using physics-based optimization, sizing, and analysis, where the physics-based models are created automatically from the architecture descriptions.

**Validation Criteria of Hypothesis 2:** If a large number of inviable architecture candidates can be eliminated from the feasibility-based low-fidelity KPI-based filtering process, then the capability of the proposed approach in Hypothesis 2 to narrow down the architecture space is validated. If the model can be automatically constructed from the architecture descriptors generated from Experiment Set 1, on which the optimization and sizing process can be directly performed, then the optimal down selection approach in Hypothesis 2 is validated.

As the results obtained in Experiment 2.1 show, many infeasible TMS architectures can be rapidly filtered out. For example, for the cabin TMS, the number of generated TMS architectures is 1362240, and this number can be reduced to 86189 within 2 minutes. Such results validate the capability of the proposed feasibility-based filtering method that it can

rapidly filter out a large number of architectures in terms of the feasibility.

As the results obtained in Experiment 2.2 and 2.3, still using cabin TMS as an example, the number of architectures is further reduced to 4 in terms of the selected four KPI: bleed off-take, shaft-power extraction, ram air intake, and weight. The performance of the KPI evaluation program is similar to the feasibility-based filtering process. This clustering-based filtering approach can also be applied to the global TMS to narrow down the architecture space. Therefore, the architecture space can be further reduced by the low-fidelity KPI clustering-based filtering methodology. Thus, combining the capability of methods for Experiment 2.1, 2.2 and 2.3, one of the criteria to validate the Hypothesis 2, "a large number of inviable architecture candidates can be eliminated from the feasibility-based low-fidelity KPI-based filtering process", is met, validating the capability of the proposed methodology.

From the results shown by Experiment 2.4, it can be seen that the physics-based models can be automatically constructed in the NPSS environment using the descriptors generated from the Experiment Set 1. And MDP sizing and optimization can be further performed on these constructed models, as shown in Experiment 2.5. Combining both Experiment 2.4 and Experiment 2.5, one of the criteria, "If the model can be automatically constructed from the architecture descriptors generated from Experiment Set 1, on which the optimization and sizing process can be directly performed", is met.

In summary, the two criteria stated to validate the Hypothesis 2 are satisfied by showing results from Experiment 2.1, 2.2, 2.3, 2.4, and 2.5. Therefore, the Hypothesis is validated. Thus, the Research Question 2 is answered and the sub-objective 2 is fulfilled. The sub-objective 2 is listed below:

**Sub-Objective 2:** To develop a capability of the proposed method that rapidly narrows down the architecture space to a reasonable number of candidates to perform further optimal architecture down-selection in terms of chosen metrics, using information and methods suitable for conceptual design.



### 5.6.2 Conclusions

In conclusion, an optimal down selection methodology of the TMS architecture space is proposed in this chapter, which is based on the feasibility of the TMS at the critical operation condition and low-fidelity subsystem-level KPI at the cruise condition. The selected KPI are bleed off-take, shaft-power extraction, ram air intake, and weight penalty. This proposed methodology firstly filters out architectures using the feasibility, then evaluates the KPI of each architecture using a low-fidelity approach. The obtained KPI are grouped using clustering method to further reduce the number of architecture candidates. Then physics-based models are constructed automatically using the architecture descriptor that is generated from Experiment Set 1. Finally, the constructed models are sized and optimized through a proposed MDP sizing and optimization methodology.

This proposed methodology addresses the Research Question 2 and Hypothesis 2 by conducting the Experiment Set 2. And it further fulfills the sub-objective 2 of the whole thesis. In this experiment set, the cabin from a 160-pax SSA, the motor from a 300-pax non-cryo TeDP concept, and the battery from a 78-pax non-cryo HTeDP concept are used for the experiments on local TMS architectures. These three aircraft configurations are also used to conduct experiments on the global TMS architectures. It is demonstrated that the proposed methodology is able to rapidly filter out infeasible and non-optimal TMS architectures in terms of low-fidelity KPI, and can further perform a higher-fidelity sizing and optimization on the automatically constructed models. The demonstrated capability also validates the Hypothesis 2.

## **CHAPTER 6**

### **EXPERIMENT SET 3 - INTEGRATION OF TMS ARCHITECTING WITH AIRCRAFT DESIGN**

In the Experiment Set 1, the TMS architectures space are populated at both local and global level. In the Experiment Set 2, architecture space is narrowed down by filtering out infeasible and non-optimal architectures, following which a higher-fidelity sizing and optimization is performed. However, such architecting process is conducted with fixed thermal management requirements. In such a manner, the impacts of the TMS are not fed back to the aircraft sizing process, and the thermal management requirement for each load is not updated in terms of the newly sized vehicle either. Therefore, the interactions between the aircraft sizing and the TMS architecting are still unknown. To address this problem, the Research Question 3, Hypothesis 3, and Experiment Set 3 are proposed. The experimental methodology is proposed in this Chapter to conduct the Experiment Set 3, which integrates the TMS architecting process with the aircraft sizing process. The aircraft concepts, integration environment, and modeling methodologies have been presented in the author's previous work [46, 22, 23, 29, 32, 94].

This chapter is organized as follows: the design of the Experiment Set 3 is shown in section 6.1; the integration process is introduced in section 6.2; then the method to model the aircraft and the mission, as well as the approach to sizing the vehicle, are introduced in section 6.3; the explanations and processes for other modules in the integrated process are presented in section 6.4; the obtained results from the integration process are then stated in section 6.6; and finally the conclusions from the Experiment Set 3 are drawn in section 6.7.

## 6.1 Design of Experiment Set 3

### 6.1.1 Overview of Research Questions 3, Hypothesis 3, and Design of Experiment Set 3

The overview of Research Question 3, Hypothesis 3, and the Experiment Set 3 are re-stated here as a guidance of more detailed design of the Experiment Set 3 and the corresponding experimental methodology:

**Research Question 3:** *How can the interactions of thermal management systems architecting process and aircraft sizing process be identified, what are the differences between the initial solutions before resizing and the final converged solutions of both the aircraft and the TMS, and how to explain such differences?*

**Hypothesis 3:** The interactions of thermal management systems architecting process and design of aircraft can be identified by integration of the thermal management systems architecting process into the aircraft design loop, and differences between the converged design solutions and the initial solutions from the design loop can be discovered and explained through the proposed integrated process.

The Initial statement of the Experiment Set 3 is:

**Experiment 3:** Integrate the TMS architecting process into the design loop of the aircraft, and observe the differences of design solutions through the design loop. The concepts of interest are: a 160-pax conventional aircraft with possibility to electrify the subsystems (such as MEA), a 300-pax N3-X-like TeDP, and a 78-pax HTeDP. The integration environment and the vehicle models are constructed first without the TMS's, then the TMS's are integrated into them.

#### *How Experiment Set 3 Is Used for Validation of Hypothesis 3*

The capability to feed back the influence of the TMS architecting on vehicle level can be validated if the proposed integration methodology can update the design requirements for both the aircraft and the TMS. The capability to compare the converged design solutions

with the ones generated using initial design requirements can be validated if the differences and corresponding explanations for such differences can be identified through the integrated analysis.

### 6.1.2 Cases of Interest in Experiment Set 3

#### *160-PAX Conventional Aircraft*

The design specifications of the 160-pax conventional SSA concept has been shown in Table 4.1, and it is shown below again as a reminder in Table 6.1. The selected loads for thermal management are: cabin, avionics, hydraulics, fuel tank, engine oil reservoir, and generator. The design mission profile is also plotted in Figure 6.1, in which the reserved mission is also considered.

Table 6.1: Design specifications of the 160-pax conventional aircraft [46]

Parameters	Value
Passenger capacity	160
Design payload weight, lbm	33 600
Design range, nmi	3020
Cruise Mach number	0.78
Maximum cruise altitude, ft	41 000
Maximum payload weight, lbm	47 000

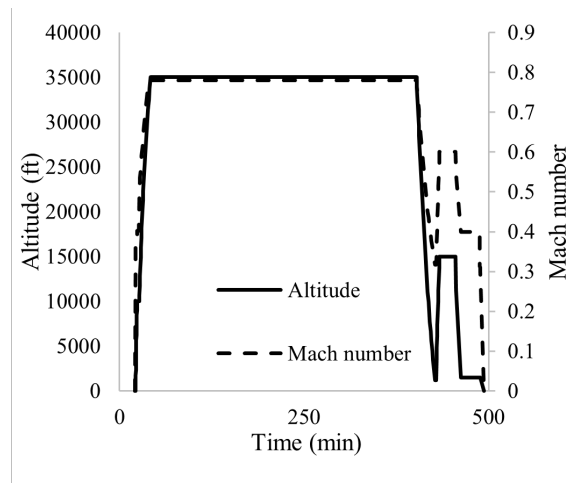


Figure 6.1: Design mission profile for 160-pax SSA concept

### 300-PAX TeDP Concept

The design specifications of the 300-pax TeDP aircraft has been shown in Table 4.2, and it is shown below again as a reminder in Table 6.2. The selected loads for thermal management are: cabin, avionics, hydraulics, fuel tank, oil reservoir, generator and motor. Moreover, a non-cryo TMS option and a cryogenic TMS option will be studied in this study. The configuration of this concept is illustrated in Figure 6.2, and the design mission profile is shown in Figure 6.3.

Table 6.2: Design specifications of the N3-X-like TeDP concept [23, 77]

Parameters	Value
Passenger capacity	305
Design payload weight, lbm	64 000
Design range, nmi	7530
Cruise Mach number	0.84
Maximum cruise altitude, ft	43 000

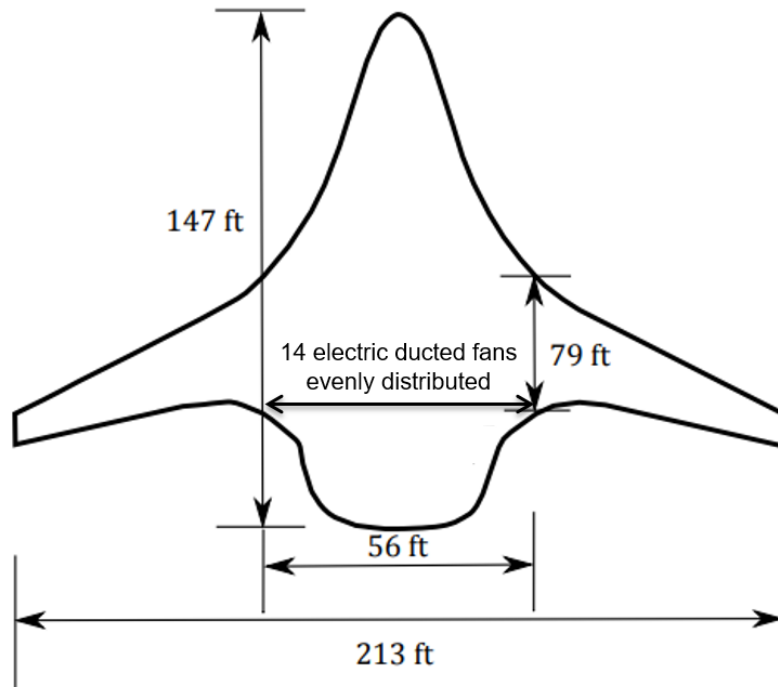


Figure 6.2: 305-PAX TeDP concept configuration [23, 77]

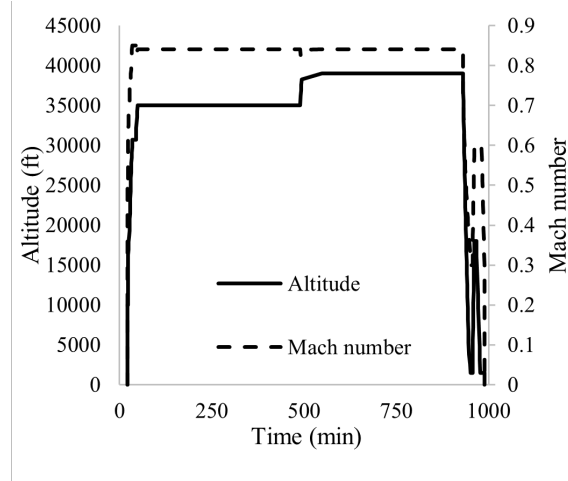


Figure 6.3: Design mission profile for 300-pax TeDP aircraft

### *78-PAX HTeDP Concept*

The design specifications of the 78-pax HTeDP concept has been shown in Table 4.3, and it is shown below again as a reminder in Table 6.3. The selected loads for thermal management are: cabin, avionics, hydraulics, fuel tank, oil reservoir, generator, motor, and battery. Only non-cryo TMS options are considered in this concept. The configuration of this concept is illustrated in Figure 6.4, and the design mission profile is shown in Figure 6.5.

Table 6.3: Design specifications of the HTeDP concept [28, 29]

<b>Parameters</b>	<b>Value</b>
Passenger capacity	78
Design payload weight, lbm	18 060
Design range, nmi	1980
Cruise Mach number	0.80
Maximum cruise altitude, ft	41 000
Maximum payload weight, lbm	23 350

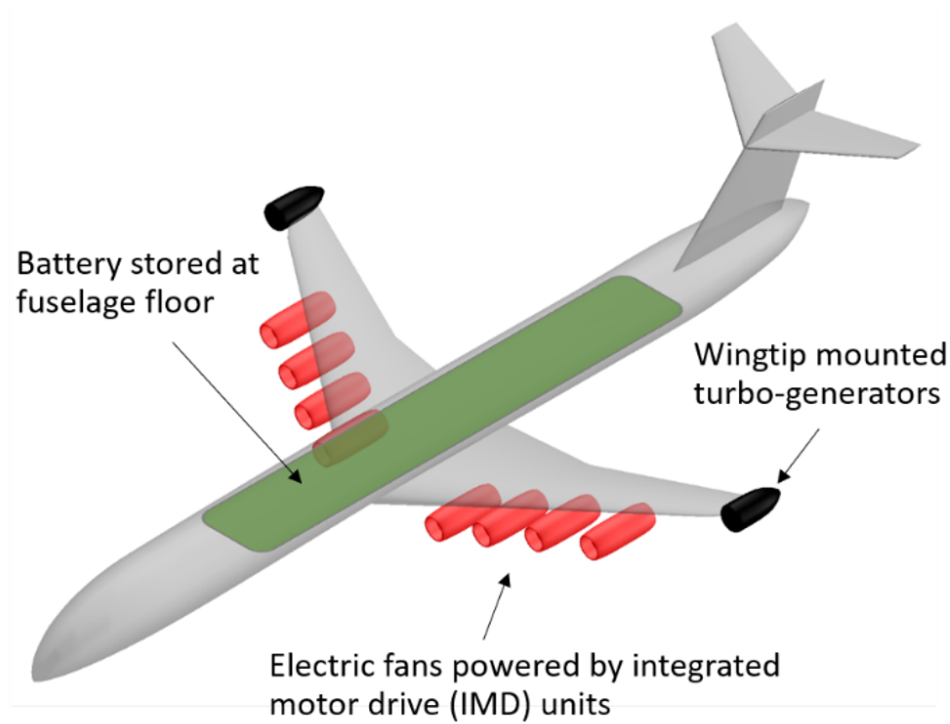


Figure 6.4: HTeDP configuration for the ULI aircraft [28, 29]

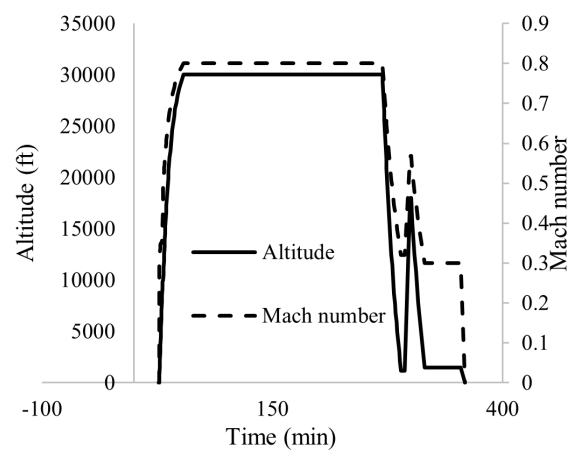


Figure 6.5: Design mission profile for 78-pax HTeDP aircraft

### 6.1.3 Design of Experiment 3

The design and execution process of the Experiment 3 is discussed here: with the concept of interest selected, the aircraft is sized firstly without integration of the TMS. The initial TMS solutions are then constructed using the load requirements from the sized aircraft, in which the optimal architectures are identified by conducting the Experiment Set 1 and Experiment Set 2. It should be noted that due to the selection of the KPI, ram air, weight, shaft-power and bleed extraction, four objectives are used to determine the optimality. Therefore, there is no best one in terms of these four objectives. Instead, several different global TMS solutions that are at the Pareto frontier will be selected. Then the influences of the TMS are fed back to the aircraft sizing process, which will update the thermal load requirements. Such process will repeat until the solutions of TMS and aircraft converge. After the design loop is converged, the design solutions then can be identified and compared to the initially architected solutions. This integrated process will be conducted in a 160-pax conventional aircraft, a 300-pax TeDP concept, and a 78-pax HTeDP concept.

## **6.2 Integration Methodology**

To conduct the Experiment 3, a methodology to integrate the TMS architecting process to the aircraft design loop is needed. The overview of this proposed method is discussed in this section. The integrated design process starts from an initial sizing of the aircraft layout with its performance requirements such as payload, range, number of passengers, and etc. The initial descriptions of the heating and cooling loads are obtained from the initially sized aircraft, such as the heat generation from electric propulsion system by using power requirements with a nominal efficiency, or cabin cooling load by using the number of passengers and corresponding electronics. From this description of the heating and cooling loads, the TMS architecture space then can be populated (Experiment Set 1) and the optimal design of the TMS can be conducted based on chosen metrics (Experiment Set



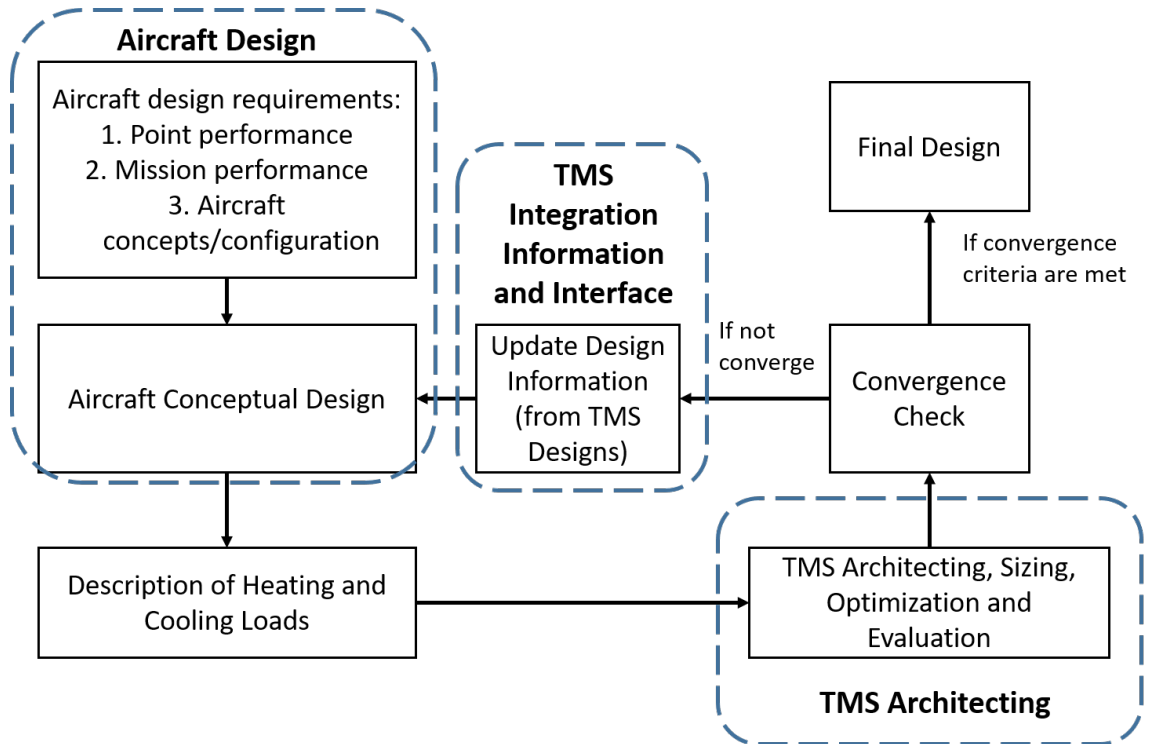


Figure 6.6: Overview of integrated design loop of aircraft and TMS

2). The characteristics of the architected TMS are then fed back to the aircraft design phase to update the weight, aerodynamics, and propulsion characteristics to resize the aircraft, following which the thermal requirements are also updated which might lead to new design of TMS. Thus, the interactions of the designs of TMS and the aircraft are linked in a design loop. When the design solutions of both the aircraft and the TMS are converged, the design loop is terminated and the final design decisions are reached. This process can be illustrated in Figure 6.6. The aircraft design module and TMS integration information and information will be discussed in detail in subsequent sections. The methodologies for TMS architecting module have been introduced in previous two chapters, but an overall architecting process will also be shown later.

## **6.3 Methodologies for Aircraft Modeling, Sizing, and Analysis**

### **6.3.1 Aircraft Conceptual Design Requirements**

The design of an aircraft is driven by its requirements. The design requirements can be usually categorized into three types: 1. Point performance; 2. Mission performance; 3. Aircraft concepts/configurations.

The point performance requirements dictate the performance requirements has to be met at certain flight conditions. For example, the specified climb rate after takeoff, the flight altitude and Mach number during cruise, and service ceiling are all point performance requirements. The takeoff and landing performance such as takeoff field length and landing approaching speed are also specified by point performance requirements.

The mission requirements usually specify the payload and the range of a mission. For commercial aircraft, the payload requirement is often about the number of passengers to carry and the cargo weight. The range requirements usually specified the maximum distance that the aircraft is capable to transport with certain payload.

The aircraft concepts or configurations requirements determine the overall geometry layout of the aircraft, and its propulsion types. For example, the geometry layout requirements can specify the placement of lifting surfaces (for example, canard or conventional configurations) and the geometry of the fuselage (for example, shapes). The propulsion requirements can determine the types of propulsion systems to be applied. For example, the types of propulsion systems can be turbofan, electric propulsion, hybrid propulsion, and etc. In reality, the selection of aircraft concepts/configurations is part of the design process. However, the focus of this research proposal is to address the thermal management problem of increasing cooling load caused by novel concepts. Therefore, the integrated design process will not change the concept within the loop.

### 6.3.2 Aircraft Design and Sizing Methodology

The general aircraft design methodologies [36, 37, 38] have been introduced in literature review, of which the general design processes are illustrated in Figure 6.7 and Figure 6.8. As stated by Nam [36] three activities are performed to size the aircraft: 1. Power matching; 2. Energy matching; 3. Volume balance. The power matching is performed through constraint analysis, where Master Equation developed by Mattingly [37] is used. The energy matching is performed by a mission performance analysis, where the mission fuel fraction of each mission segment is used. This method was provided by Raymer [38]. The volume balancing is assumed satisfied all systems. The actual check of the volume is out of the scope of this study and requires much higher fidelity in physics modeling. The details of these approaches are not discussed here because they have been already mature and applied for a long time, and the corresponded references also provide a lot of information regarding them.

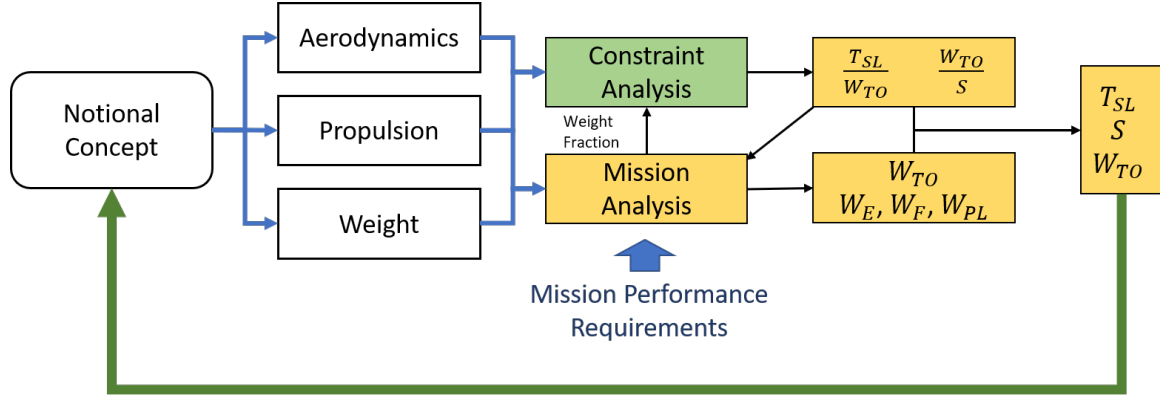


Figure 6.7: Mattingly's Aircraft Design Process [37]

### 6.3.3 Modeling, Integration, and Mission Analysis Environment

The modeling, integration, and analysis are implemented through the GT-HEAT environment [151]. Only the fundamental ideas and execution process of GT-HEAT are introduced here, and more detailed descriptions, methodologies, and use cases of GT-HEAT can be found in a set of papers by Gladin and Perullo [151, 152, 153]. The GT-HEAT

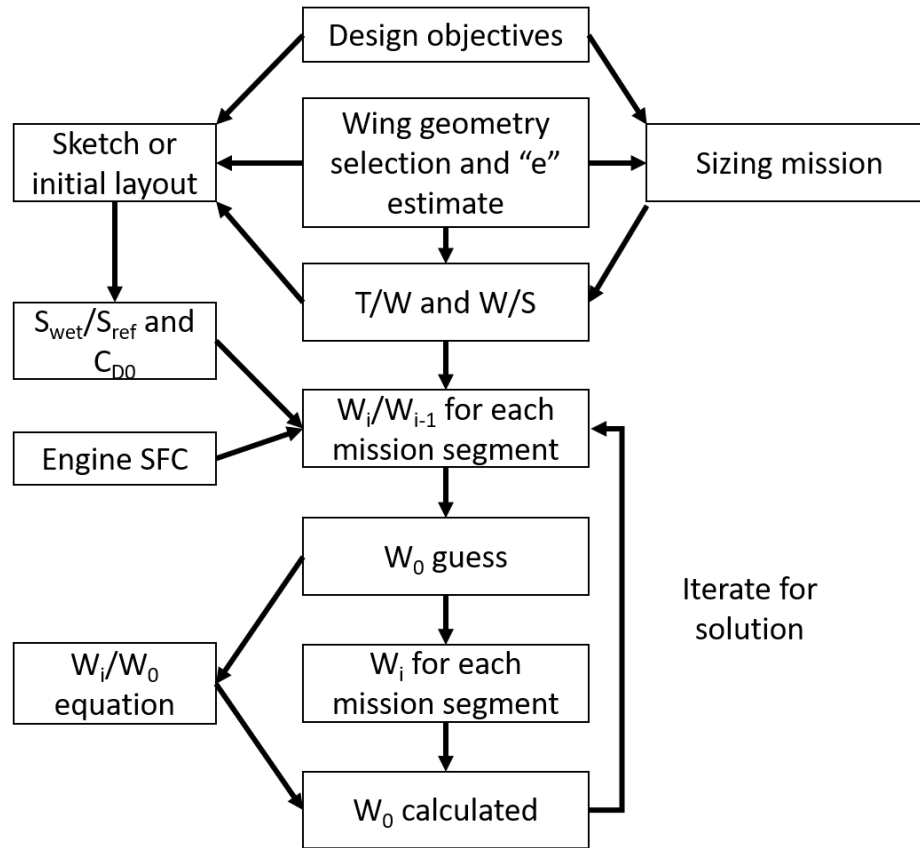


Figure 6.8: Raymer's Aircraft Design Process [38]

environment integrates the propulsion system, the vehicle, and the mission, allowing the exchange of information among these three modules simultaneously at every time step of the mission (or every mission point). The GT-HEAT functional architecture is illustrated in Figure 6.9. The overall integrated mission analysis can be represented by three modules: 1. mission assembly module; 2. vehicle analysis module; and 3. engine assembly module. The Numerical Propulsion System Simulation (NPSS) [124] is used as the basic modeling environment of the propulsion system, and the Flight Optimization System (FLOPS) [154, 155] is used to model the airframe properties, and the mission analysis module is realized by functions developed by Aerospace Systems Design Laboratory (ASDL) in Georgia Tech. It should be also noted that the NPSS in GT-HEAT does not only model the propulsion system, but also models power distribution systems, TMS, energy storage system, and etc.

The process of the mission analysis of GT-HEAT works clockwise as shown in Figure 6.9. The execution process starts from the mission assembly. A user defined mission profile is read in the mission assembly, and the corresponding flight conditions, such as altitude and Mach number for each mission point, are sent to the vehicle analysis module. The vehicle analysis module then computes the required states, such as the required thrust, to perform the flight in the received operating conditions from mission module. Then the required states are provided to the engine assembly to evaluate the engine performance. Then the fuel flow are fed back to the vehicle module and the mission module to update the fuel weight. During the sizing mission, the mission starts with the an initial guessed vehicle airframe weight and total fuel weight, and the mission will be executed for several iterations until the weight is converged. During the off-design missions, the airframe weight comes from the sizing mission, while the fuel weight is still determined by several iterations of executions of the mission analysis until the value is converged.

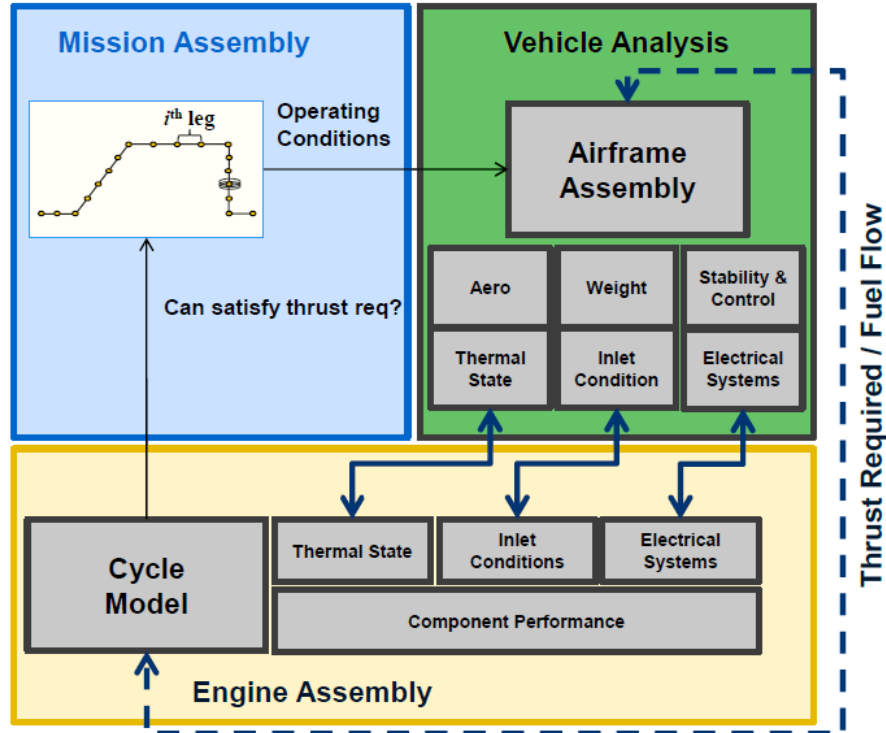


Figure 6.9: GT-HEAT functional architecture [151, 152, 153]

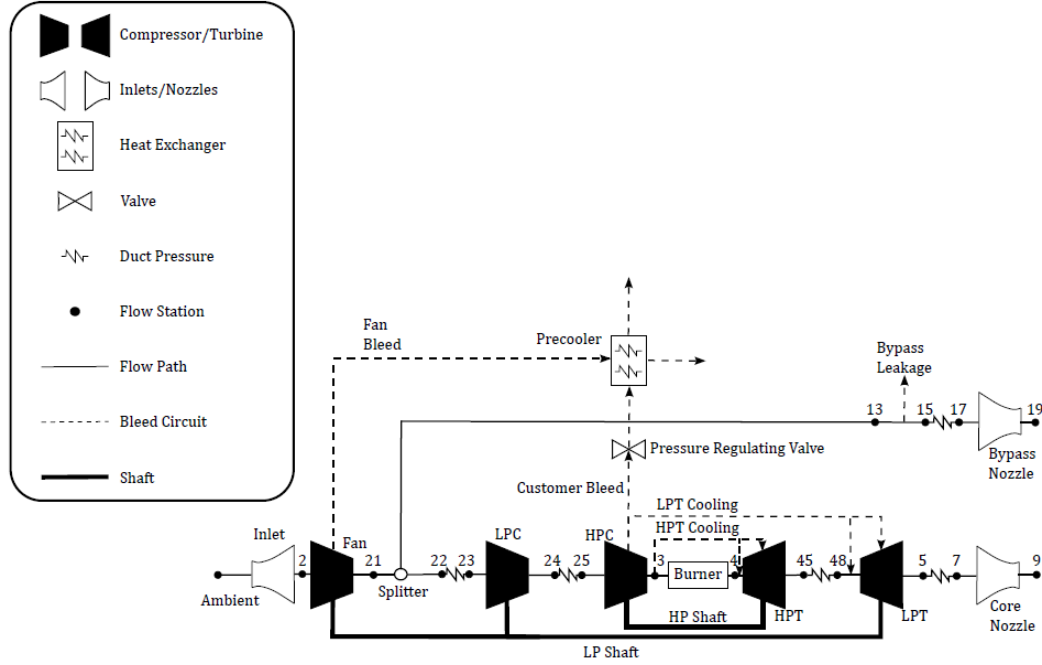


Figure 6.10: Gas turbine model architecture for 160-pax SSA [156]

#### 6.3.4 Propulsion System Models

##### *160-PAX SSA Concept*

The propulsion system model for the 160-pax SSA concept has been discussed in the author's previous work [46]. This model was based Ozcan's gas turbine model [156] which is sized through a Multiple Design Point (MDP) sizing approach [98], in which the modeling details can be found. The architecture of the gas turbine is shown in Figure Figure 6.10 [156]. The sizing points are selected as: (i) Aerodynamic Design Point (ADP); (ii) Top of climb; (iii) Takeoff; (iv) Sea-level static, installed, ISA + 27 °F (hot day). In the MDP approach, the necessary thrust as well as secondary power off-takes (shaft-power and/or bleed) corresponding to each sizing point are used to size the gas turbine components.

### 300-PAX TeDP Aircraft

The 300-pax model has been discussed in the author's previous paper [22, 23]. The overall propulsion system is shown in Figure 6.11, which is divided into three components - gas generator, electrical system, and distributed fan system. The electrical systems models are already discussed in Chapter .chapter 5, so they will not be discussed here. The models of generator, inlet, fan, and nozzle will be briefly introduced, where the models of inlet, fan, and nozzle were constructed to capture the boundary layer ingestion (BLI) effects.

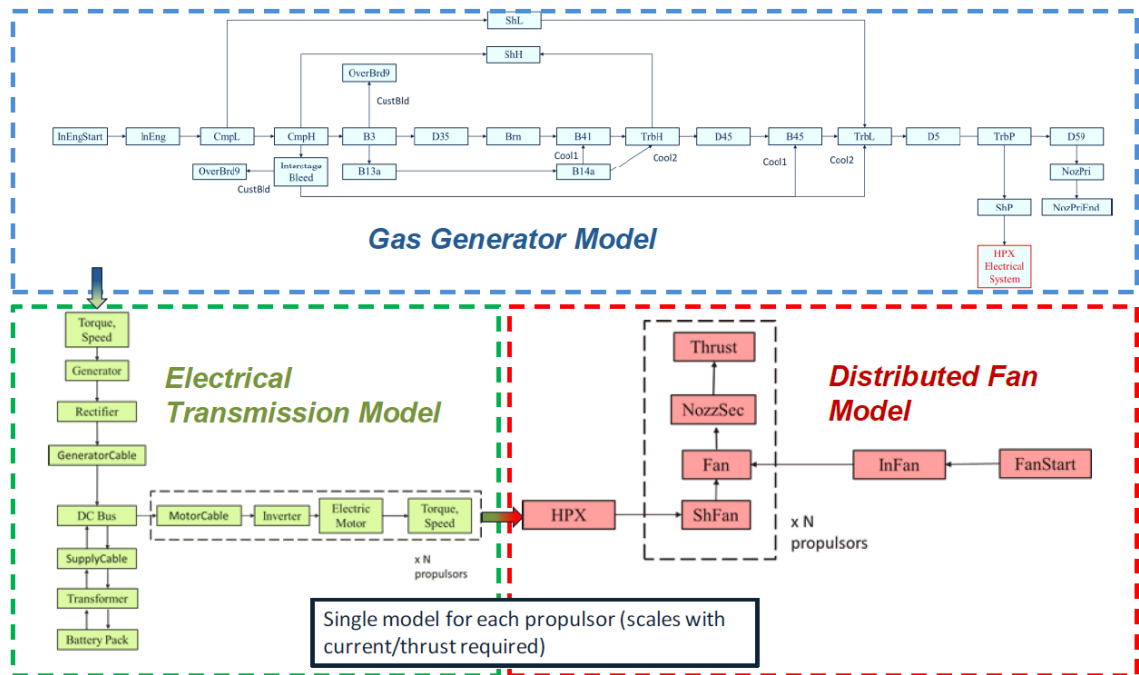


Figure 6.11: 300-pax TeDP propulsion system model schematic [153]

The gas generator model came from the previous research for a partially electric distributed aircraft [153]. The gas generator is of a two spool turboshaft architecture, and it uses parametric performance maps generated by "CMPGEN" [157] to analyze the on-design and off-design performance.

The inlet model for this study is from Gladin's previous work [77], where a detailed description of the modeling approach can be found. This model takes the boundary layer properties generated in the section of BLI modeling to compute the inlet recovery. This

method models the boundary layer using the integral boundary layer used by Plas [158], and the pre-entry zone is also taken into account.

The fan is modeled by a new parallel compressor approach by Pokhrel [159]. The conventional PC model is constructed based on the assumption that the static pressure is always constant at the exit of fan, but Pokhrel proposed and verified that the static pressure at the exit of the fan is also a function of the intensity of distortion. In this section, only the summarized concepts and results of this model will be shown here, and other details can be found in Pokhrel's paper [159]. The new PC model has the same architecture as that of the conventional one, as presented in Figure 6.12. One compressor is decomposed into two parallel compressors, or two sectors, one ingests clean flow while the other one takes in the distorted flow. However, the new PC model modifies the assumption of the original one which states the static pressure at the fan exit is constant for both of these two parallel compressors. The new model computes the static pressure of the clean sector in terms of the distortion intensity at critical angle. When the distorted sector is greater or equal to the critical angle, the static pressure of the clean sector can be expressed in the following equation, where  $P_{s_{clean}}$  is the static pressure of the clean sector, the  $P_{s_{dist}}$  is the static pressure of the distorted sector.

$$P_{s_{clean}} = \left(1 + \frac{dP_c/P_{crit}}{2}\right) * P_{s_{dist}} \quad (6.1)$$

When the distorted sector is smaller than the critical angle, the static pressure of a sector of certain angular position is expressed in the following equation, where  $P_{s_i}$  is the static pressure of the sector in certain angular position represented by  $i$ ,  $A_{dist}$  is the area of the distorted sector,  $A_{crit}$  is the area of the sector equal to critical angle, and  $P_{s_{clean,i}}$  is the static pressure of a clean sector in the same position.

$$P_{s_i} = P_{s_{dist}} * \frac{A_{dist}}{A_{crit}} + P_{s_{clean,i}} * \left(1 - \frac{A_{dist}}{A_{crit}}\right) \quad (6.2)$$



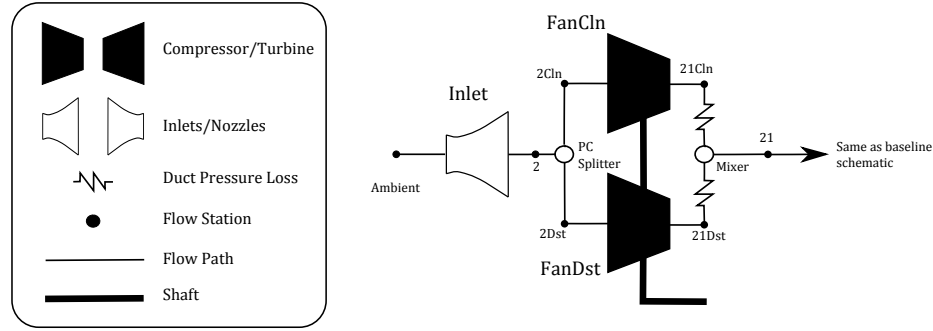


Figure 6.12: Parallel compressor model architecture [77]

The nozzle model used in this study was developed and verified by Shi [160]. This nozzle model comprises of a analytic turbulent pipe flow solution, and a mixing model which uses the generated entropy through the nozzle to predict the pressure drop in terms of different BLI distortion levels. An  $m$  parameter, between 0 and 1, is applied to approximate the nozzle geometry, where 0 indicates a sudden expansion while 1 indicates an infinitely long duct, and this concept of using  $m$  to estimate geometry influence comes from the work of Moore [161]. This  $m$  and two other parameters with physical meaning, which cannot be quantified before analysis due to model simplification, serve as calibration parameters. With these parameters, the pressure drop in the nozzle is calculated and then the discharge coefficient and gross thrust coefficient are computed. This model is able to run in both on-design mode as well as off off-design mode, and it can also predict nozzle performance when the nozzle is choked. Its algorithm is illustrated in Figure 6.13 [160], and the pressure drop calculation process is illustrated in Figure 6.14 [160].

### 78-PAX HTeDP Aircraft

The propulsion system model for the 78-PAX HTeDP was developed for the ULI program, and it has been introduced in the author's previous paper [29, 32]. The architecture of the propulsion system is shown in Figure 6.15 [28, 29]. The electric propulsors, in which fans are driven by motors to provide the thrust, are powered from two sources: the turbo-generators and the battery. As mentioned before, there are eight motors, and two turboshaft engines. Four motors are distributed on each side of the wing, and are powered by the

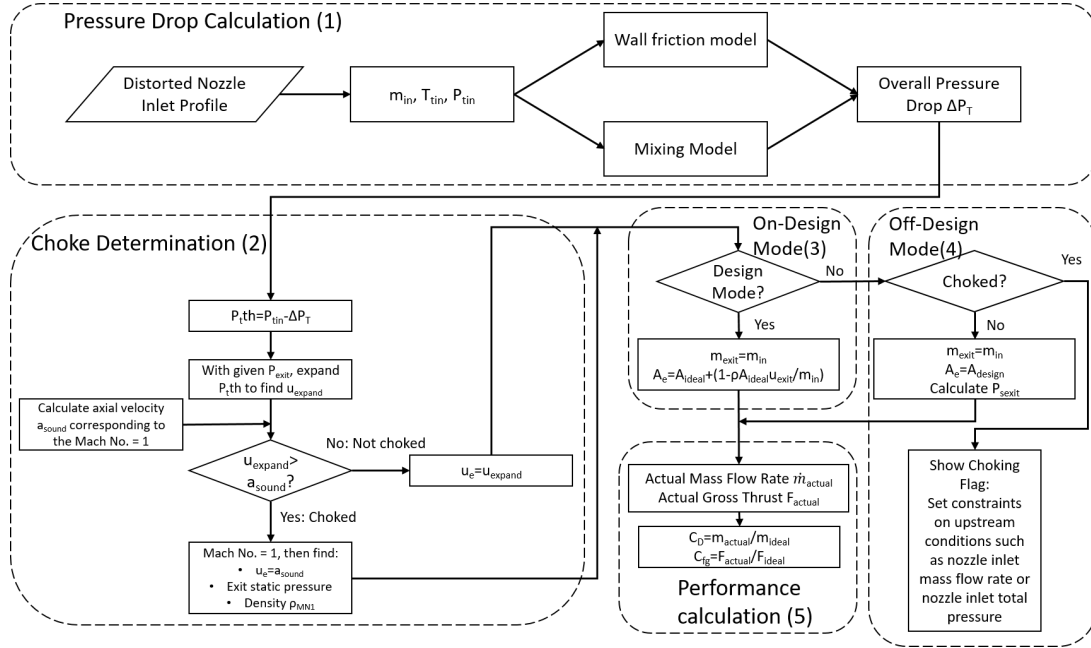


Figure 6.13: Nozzle algorithm overview [160]

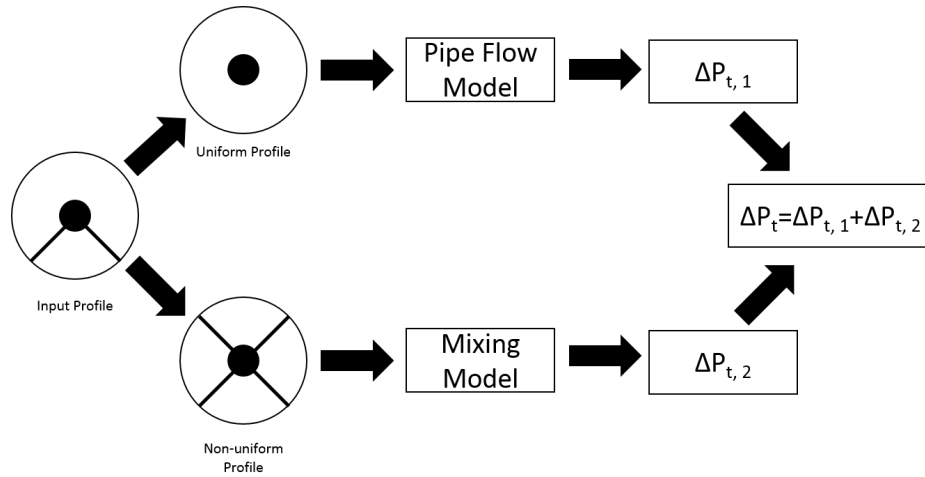


Figure 6.14: Nozzle pressure drop calculation process [160]

turboshaft engine that is mounted at the wing tip at the same side of the wing. There is only one battery stack installed, thus it supplies electricity to all eight propulsors. It should be also noted that the number of cells in the battery stack is adjusted during off-design missions, to supply sufficient electrical energy that comes the battery due to hybridization while minimizing the weight of installed battery. More details can be found in the mentioned references.

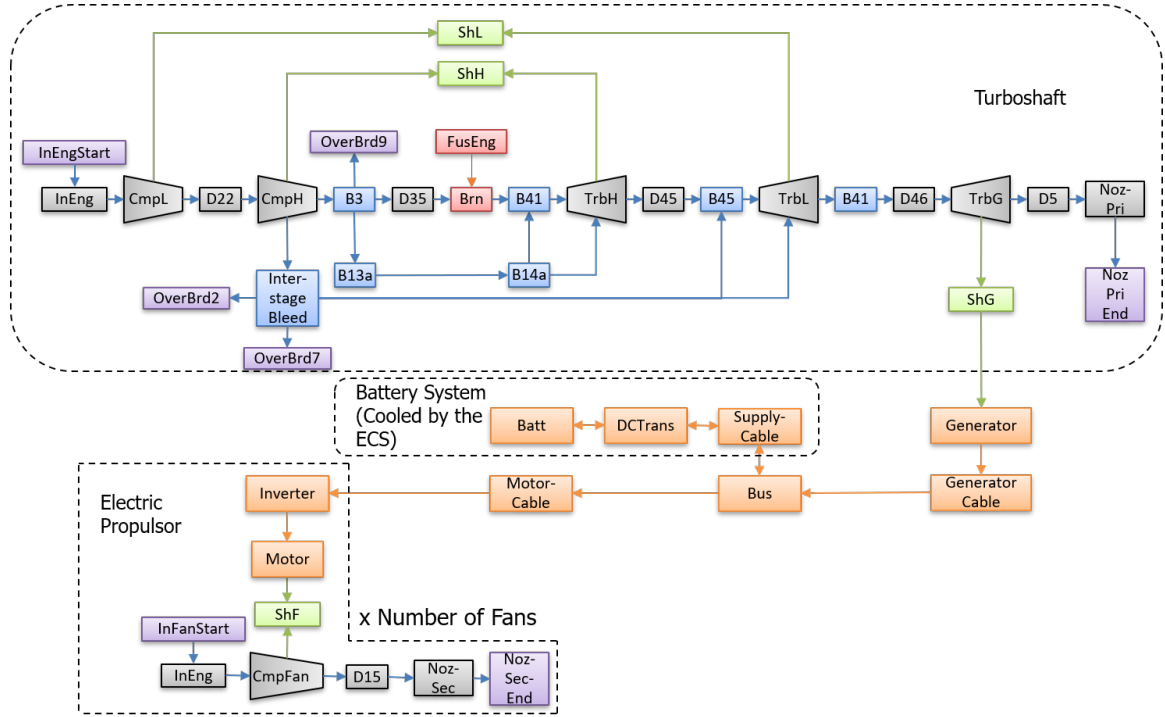


Figure 6.15: Architecture of the propulsion system [28, 29]

## 6.4 Other Modules in Integration Process

### 6.4.1 Obtaining Descriptions of Heating and Cooling Loads

The required power generation and consumption of major component such as generators, motors, batteries, electric propulsion system, and etc. can be obtained from the sized aircraft. The power to be transmitted in a electrical transmission system can also be computed from the required power generation and consumption. The efficiency of each electrical devices can be computed from their models developed in Experiment Set 2. Then the cooling load can be calculated from the power generation or consumption and the efficiency:  $P_{heat} = \eta P$  where  $P_{heat}$  is the generated heat,  $P$  is the power consumption or generation of the device, and  $\eta$  is the efficiency. The heat generated from hydraulics can also be predicted by the models developed in Experiment Set 2, which use the information of aircraft design. The heating or cooling loads for the cabin is specified by the mission requirements which determine the number of passengers and the required galley electronics. It should be noted

that the convection, conduction, and radiation to the ambient is also considered during the calculation of these loads.

#### 6.4.2 TMS Architecting Module in the Design Loop

The detailed methodologies for TMS architecting have been discussed in chapter 4 and chapter 5. Only the overall process integrated into the aircraft design loop is introduced here. With the obtained thermal management requirements, the method in Experiment 1.1 populates the local TMS architecture space for each load. Then the method in Experiment 2.1 filters infeasible architecture. Low-fidelity KPI of the remaining local TMS architectures are evaluated and clustered to further reduce the local TMS architecture candidates, as in Experiment 2.2 and 2.3. The representatives of the local TMS clusters are selected to construct the global TMS, using the method in Experiment 1.2. And the global TMS architectures are clustered, as in Experiment 2.3. Furthermore, the remaining TMS are optimized and sized, through the methods in Experiment 2.4 and 2.5. Finally the impacts of the global TMS can be evaluated and feed back to the aircraft sizing module. This integrated architecting process is shown in Figure 6.16.

#### 6.4.3 Convergence Criteria for the Design Loop

After the TMS is architected and selected for a set of requirements and description of loads at certain iteration, the designs of the TMS and the aircraft are compared with the designs from the last iteration. If the designs from two iterations are similar to each other within a tolerance then the solutions are determined to be converged and the design loop is terminated, otherwise the characteristics of the current design of TMS are fed back and perform further resizing. To determine the similarity of the aircraft designs, the sizing wing loading and thrust-to-weight ratio are used as the parameters to be compared, because these two parameters are the most important parameters to be determined during the conceptual design. The similarity of the TMS is determined by the selected architecture. If the architectures

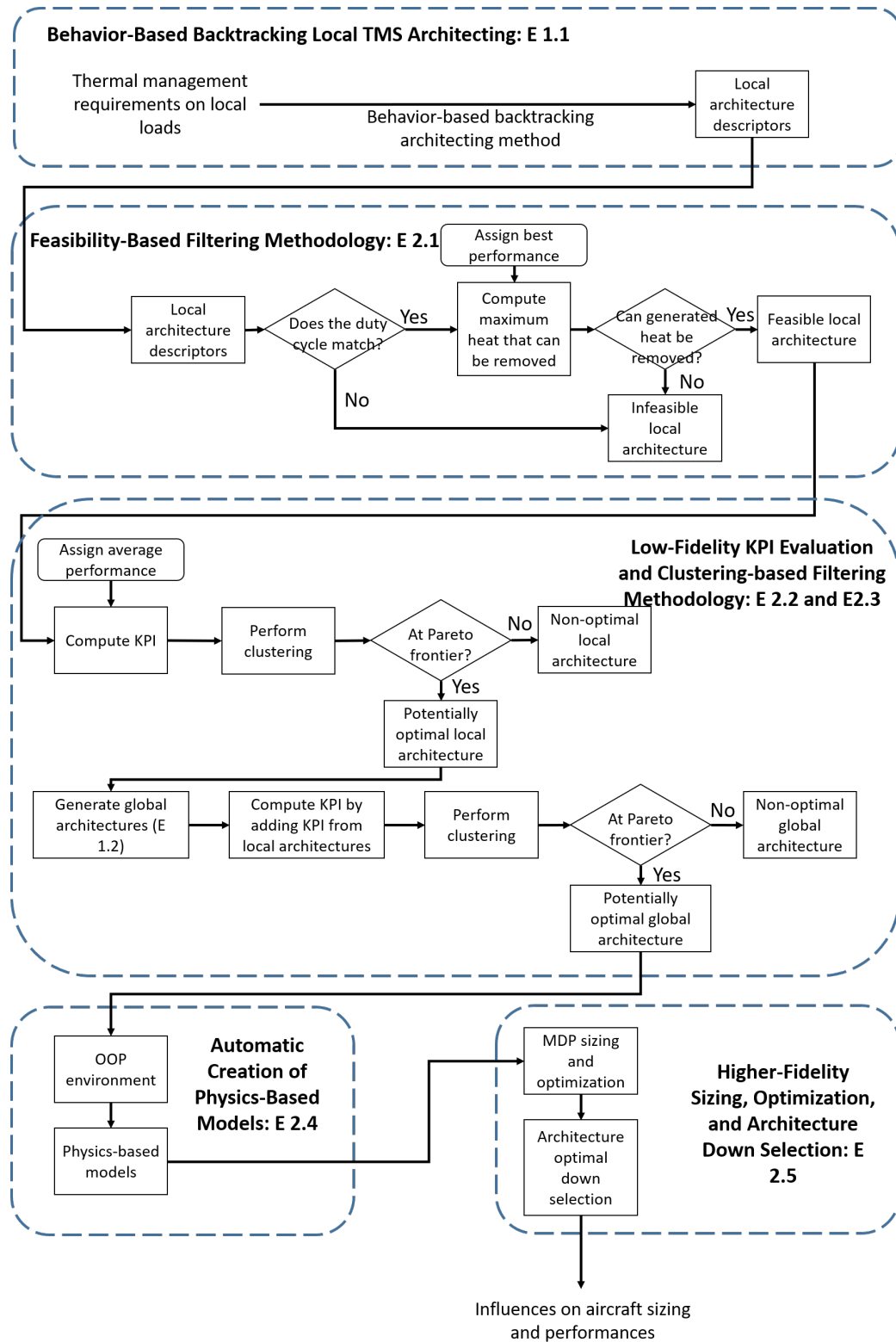


Figure 6.16: TMS architecting process in the integrated design loop

are the same then the TMS design solutions are determined to be converged.

## 6.5 TMS Information Feedback and Interface

If the designs are not converged, the characteristics of the current design of the TMS are fed back to the aircraft design module to resize the aircraft, which will influence the heating and cooling load requirements and the TMS architecting. As discussed in section 2.2, the aerodynamics, weight, and propulsion aspects of the aircraft will be affected by TMS. The aerodynamics is influenced by the added ram drag caused by ram air cooling, which is calculated using the following equation, where  $\dot{m}_{ram}$  is the mass flow rate of the ram air taken in,  $V_\infty$  is the free stream speed, and  $\Delta D_{ram}$  is the additional ram drag. This relation is obtained by assuming complete momentum loss of the ram air.

$$\Delta D_{ram} = \Delta \dot{m}_{ram} V_\infty \quad (6.3)$$

The weight of the aircraft is influenced by the weight added by the additional components in TMS, and upsize of the generators, motors, and electrical systems due to higher power consumption caused by TMS. The propulsion aspect of the aircraft is influenced by the bleed and power extraction caused by the TMS, which usually leads to a larger size of the engine and higher fuel consumption. These variations of the aircraft characteristics will further influence the heating and loading requirements. Moreover, the design of the TMS itself will influence the heating and cooling loads. Since the TMS requires power to perform the cooling and heating function, the corresponded power generation, transmission, and consumption process will generate more heat, leading to a higher cooling load requirement, which may need a higher power consumption for cooling. Some of such interactions among the design of TMS and the cooling loads through parameters at different levels can be shown in Figure 6.17. The interfaces of bleed and power extraction are at the propulsion system module. The interfaces of ram drag and weight are at the airframe module. Such

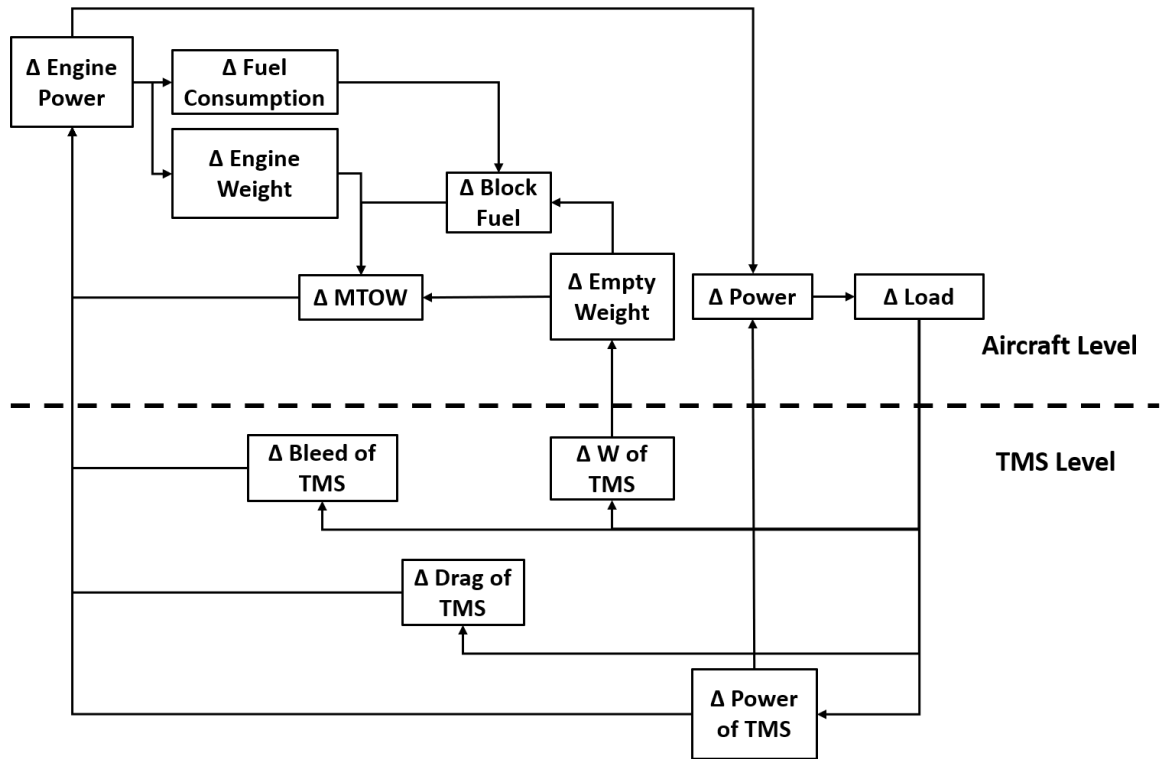


Figure 6.17: Interactions of TMS design and loads

propulsion or airframe modules mean the modules in the GT-HEAT environment.

## 6.6 Results

In this section, the results from the integrated design and analysis of the chosen configurations and their TMS are presented. Due to the space limitation of this thesis, as well as the time limitation for the research, it is not possible to investigate all potential global TMS where all the local TMS candidates that are at the Pareto frontier (see chapter 5, local TMS at the Pareto frontier simply means that are Pareto-optimal) are enumerated. Therefore, in this integrated design process, only selected optimal local TMS candidates for loads that have significant thermal management requirements, such as cabin for commercial aircraft or motor for electrified propulsion system, are considered to perform the Experiment 3. In addition, before the convergence of the design loop, if the a local TMS has been chosen in the previous iteration for a load, and it is still Pareto-optimal in this iteration, then it will be

chosen by default. Only when this local TMS becomes infeasible or non-optimal, the local TMS for the same load will be re-selected, based on the Experiment Set 2. In this section, the 160-pax SSA, 300-pax TeDP with both cryo and non-cryo cooling options, and 78-pax non-cryo HTeDP are chosen to generate the results for the experiment on the integrated design process.

#### 6.6.1 Integrated Design and Analysis on 160-PAX SSA

##### *Discoveries from Integrated Design Process*

In this subsection, the 160-pax SSA is selected for study. The chosen loads are: cabin, generator, fuel tank, engine oil reservoir, hydraulics, avionics. Firstly, the aircraft is initially sized without TMS. As discussed in subsection 5.5.6, the selection of the TMS for the cabin determines the overall global TMS architecture. Therefore, it is interesting to show the heat that needs to be removed by the TMS from the cabin through the whole mission, considering the heat transfer through the cabin wall. The heat that needs to be removed is illustrated in Figure 6.18, where the heat is normalized in terms of the value for the cruise condition. It can be seen that during takeoff, climb, and decent, the heat that needs to be removed is larger than that during cruise. This is because the ambient temperature is higher, and less heat can be rejected to the ambient through the cabin wall.

As mentioned before, the selection of the TMS for the cabin determines the overall global TMS architecture. Therefore, for the first design iteration, two local TMS candidates are selected for the cabin, while only one architecture is selected for other loads. However, if updated thermal management requirements in the following design iteration change the optimal candidates for other loads, then the local TMS for other loads will be re-selected. The chosen two TMS candidates are illustrated in Figure 6.19 and Figure 6.20, where the first one utilizes the extracted bleed from the engine as the supply air and the second uses the electrically compressed air (E-Charged-Air). Thus, there are two global TMS chosen at the first iteration corresponding these two cabin TMS. The local TMS for other loads are



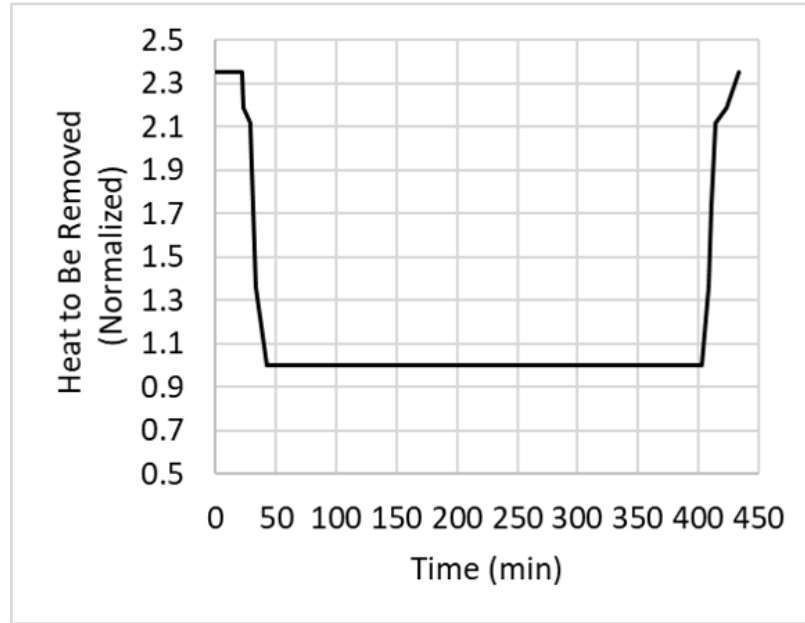


Figure 6.18: Cabin heat that needs to be removed by TMS

the same for these two global TMS. The corresponding local TMS architectures are shown in Figure 6.21 to Figure 6.25. The global TMS architecture with the bleed cabin TMS is shown in Figure 6.26, and the global TMS with the E-Charged-Air is shown in Figure 6.27.

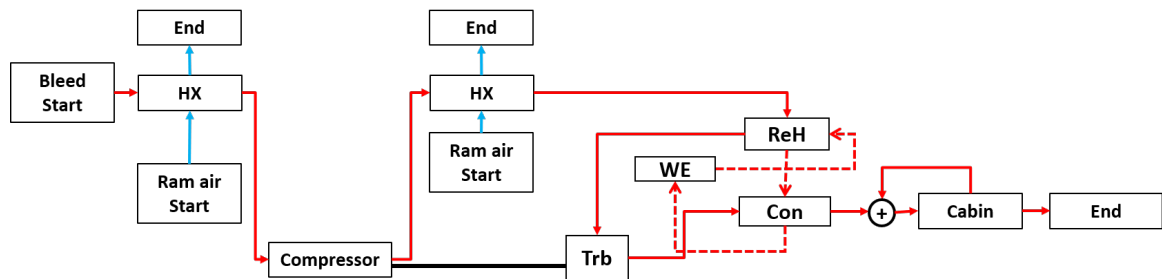


Figure 6.19: Cabin TMS using bleed for 160-pax SSA

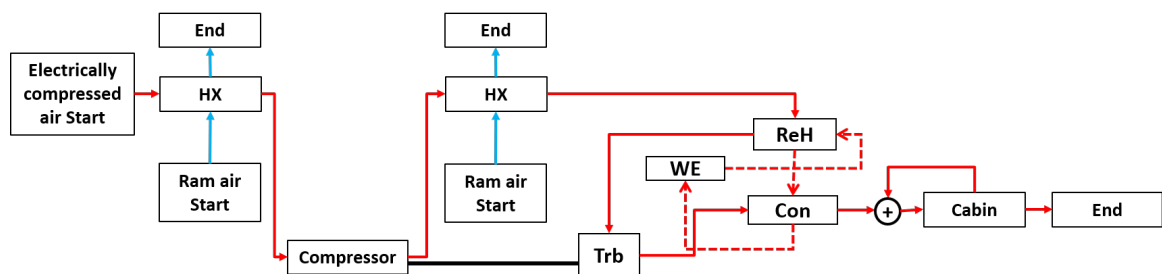


Figure 6.20: Cabin TMS using E-Charged-Air for 160-pax SSA

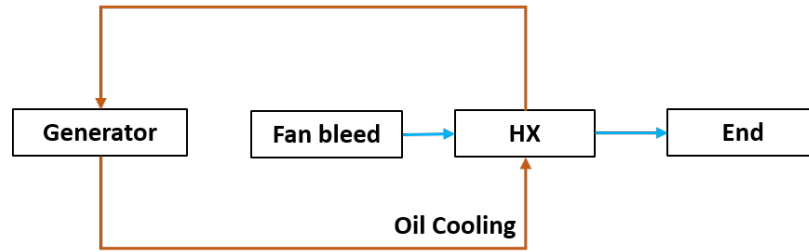


Figure 6.21: Generator TMS for 160-pax SSA

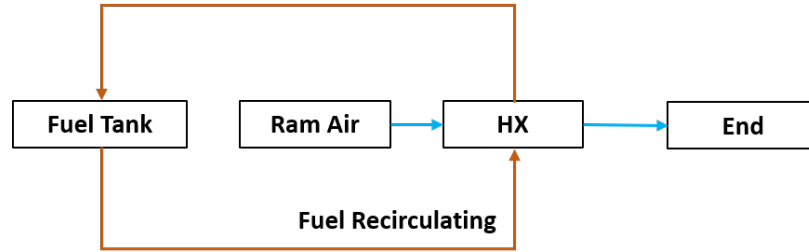


Figure 6.22: Fuel tank TMS for 160-pax SSA

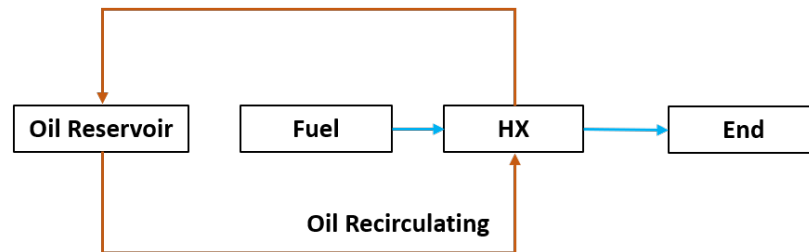


Figure 6.23: Oil reservoir TMS for 160-pax SSA

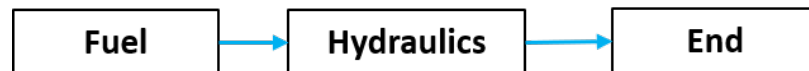


Figure 6.24: Hydraulics TMS for 160-pax SSA



Figure 6.25: Avionics TMS for 160-pax SSA

Then the impacts of the TMS solutions generated in the first iteration are fed back to the aircraft sizing phase through the integrated design process. The cabin heat that needs to be removed is the same as for the initial sized aircraft, because the TMS does not influence the cabin heat generation or heat transfer. However, the heat generation from the generator is affected in the global TMS that uses E-Charged-Air for cabin cooling, which is shown

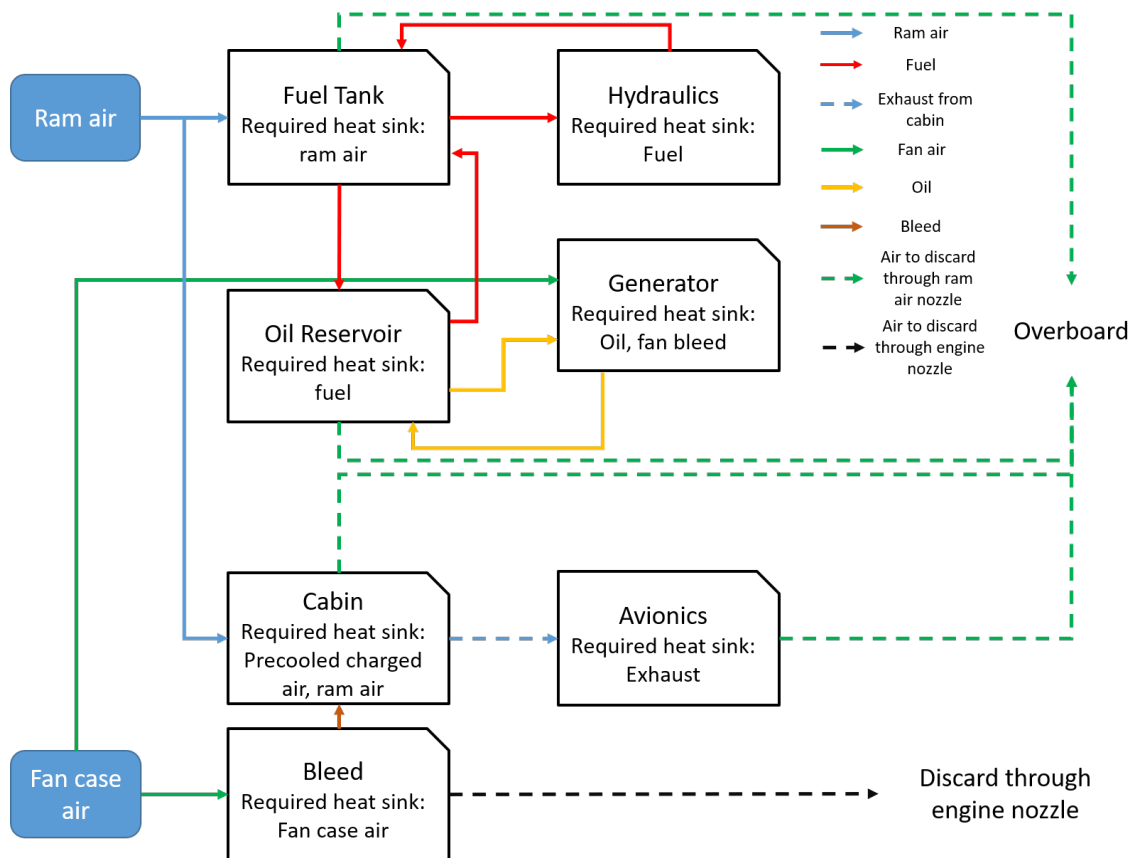


Figure 6.26: Global TMS for 160-pax SSA using Bleed for Cabin

in Figure 6.28, where the heat generation is normalized by the value used in the initially sized aircraft. At the on-ground condition, the heat generation can be increased as much as more than 30%. The increased heat generation comes from the additional power that is required to drive the electrical compressor to compress the air. The additional required power corresponds to the required intake compressed air, which is shown in Figure 6.29, normalized by the value at the cruise condition. It should be also noted that the generator performance in the aircraft with bleed as the heat sink for the cabin is not influenced by the TMS, because the power required from the generator is mostly used to provide the power for the cabin and the flight deck in this global TMS, as illustrated in Figure 6.30 where the heat generation is a constant through the whole mission.

However, the increase of the heat generation in the generator is not large enough to change the local TMS solution for the generator, even 30% is increased. This is because

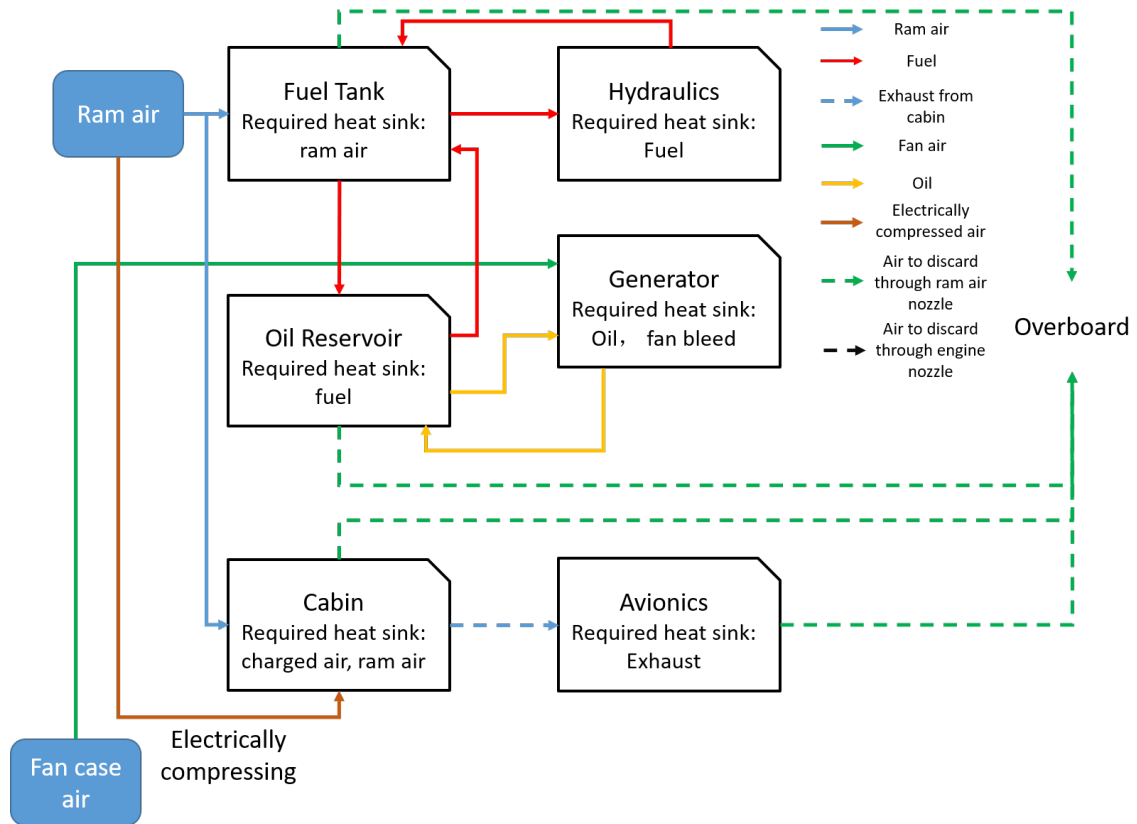


Figure 6.27: Global TMS for 160-pax SSA using E-Charged-Air for Cabin

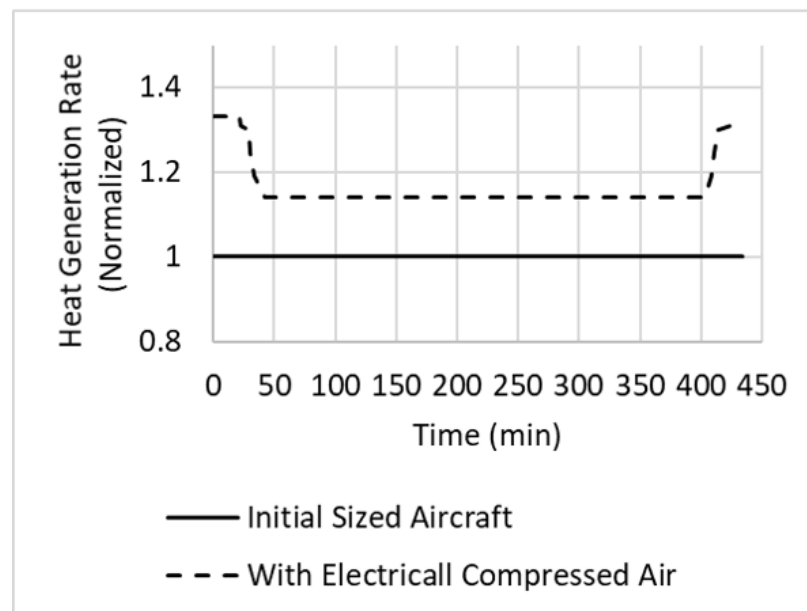


Figure 6.28: Generator heat generation comparison for 160-pax SSA between initially sized aircraft and the aircraft with E-Charged-Air for cabin cooling

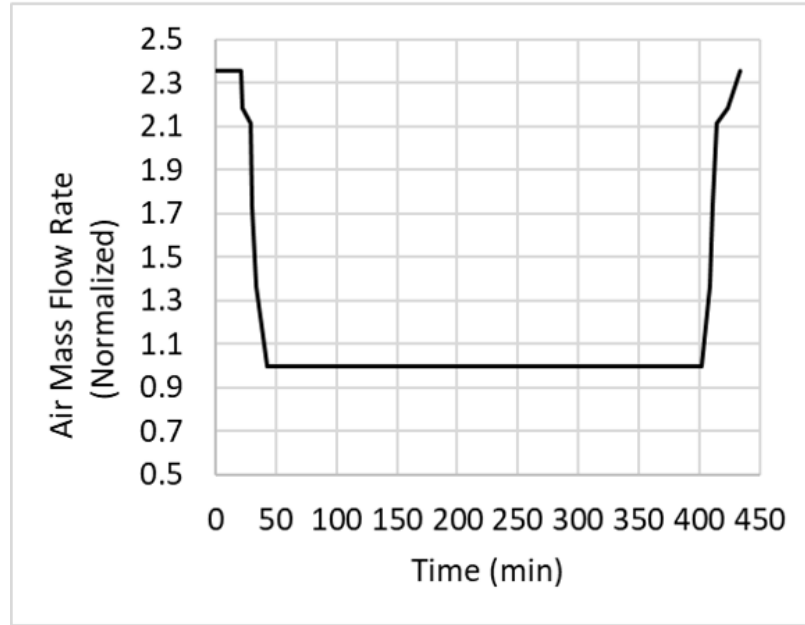


Figure 6.29: Required cabin supply air mass flow rate for 160-pax SSA

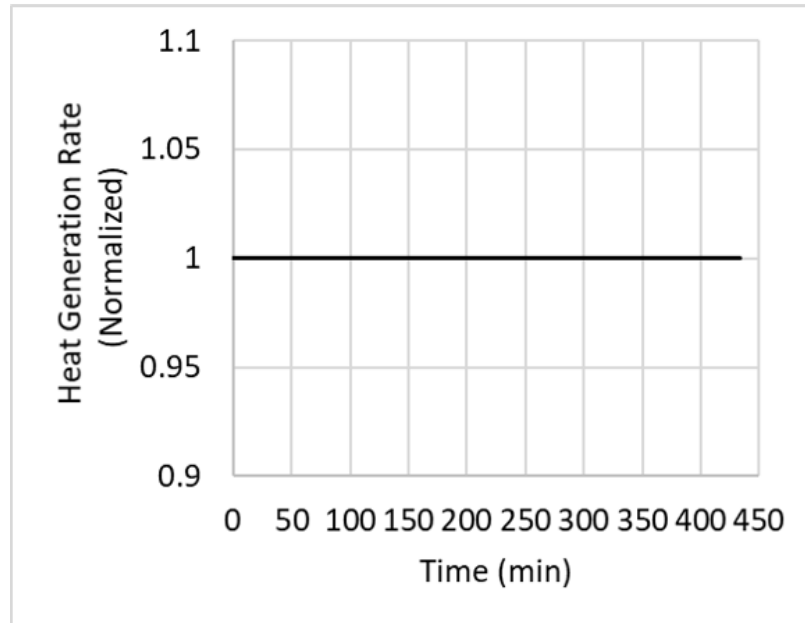


Figure 6.30: Generator heat generation through the mission for 160-pax SSA with bleed for cabin cooling

the total electrical power consumption in such a configuration is not very large. Considering the large amount of available engine air intake, there is enough fan case air to cool the generator. Finally, the converged TMS solutions are the same as shown before in Figure 6.19 to Figure 6.27.

### *Performances of Converged Aircraft Designs*

The performances of the converged aircraft designs are discussed in this subsection. The TMS adds bleed off-take, shaft-power extraction, ram drag, and weight to the vehicle. The TMS weight itself directly contributes to the operating empty weight (OEW). And due to the increase OEW, more fuel is needed to balance the induced drag caused by the increased weight, and the engine also needs to be upsized to provide more thrust. The bleed and shaft-power extraction also requires more fuel to be burned as well as more air intake, which all contribute the vehicle weight. The added ram drag also increases the required thrust, leading to a larger size of the engine. In addition, for the aircraft with E-Charged-Air to cooling the cabin, the size of generators needs to be increase to provide sufficient electrical power, besides weight added by the electrical motor and compressor to charge the air. Therefore, the aircraft with either TMS will have a higher OEW and MTOW, which can be seen from Figure 6.31, in which the OEW, fuel weight ( $W_f$ ) for the design mission, and MTOW are compared for the initially sized aircraft and vehicles with two types of the global TMS as shown before. The values for each item are normalized by the value for the aircraft sized without TMS.

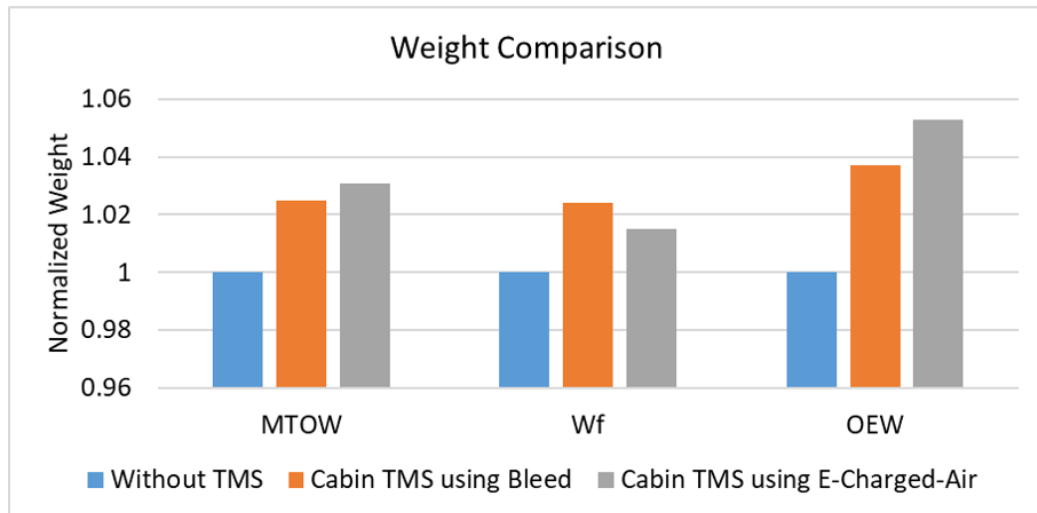


Figure 6.31: Weight comparison among aircraft without TMS and aircraft with two types of global TMS

As expected, both MTOW and OEW of aircraft with TMS increase. And the MTOW and OEW of the aircraft with E-Charged-Air to cool the cabin increase the most. This is because the electrical compressors and the motors to drive them, as well as the increased size of the generators, contribute a large amount of weight to the OEW. However, it should be noted that even though the aircraft that uses E-Charged-Air is heavier than the one using bleed, the mission total fuel burn for the design mission of the aircraft that uses E-Charged-Air is smaller. This result demonstrates the point that using bleed will degrade the engine performance much more than using the shaft-power extraction. And this fact leads to the More-Electric Initiative, which is to electrify the aircraft subsystems.

To further understand the impacts of the two TMS on the mission block fuel, multiple missions with different payloads and ranges are analyzed. The mission block fuel burn of the aircraft using bleed for selected missions is plotted in Figure 6.32, and the mission block fuel of the aircraft using E-Charged-Air is shown in Figure 6.33. Mission ranges and payloads are normalized by the design range and payload. It should be noted that these mission fuel burn is presented in a  $\Delta$  sense, where the  $\Delta$  mission block fuel is the block fuel of each aircraft compared to the aircraft sized without TMS. A positive  $\Delta$  block fuel means a fuel penalty, while a negative  $\Delta$  block fuel indicates a block fuel reduction.

It can be seen from these two figures that the aircraft with TMS that uses bleed for cabin cooling has larger penalty on block fuel burn, ranging from 1.1% to 2.3%. And the corresponding block fuel burn penalty for the aircraft with the other type of TMS is 0.9% to 1.5%. A more clear comparison between these aircraft with two types of TMS can be seen in Figure 6.34. A fuel burn reduction from 0.5% to 1.3% can be found in all chosen missions. Thus, in terms of the block mission fuel burn, the TMS using E-Charged-Air has a better performance than the one using bleed. However, in terms of OEW and MTOW, the TMS with bleed is better.

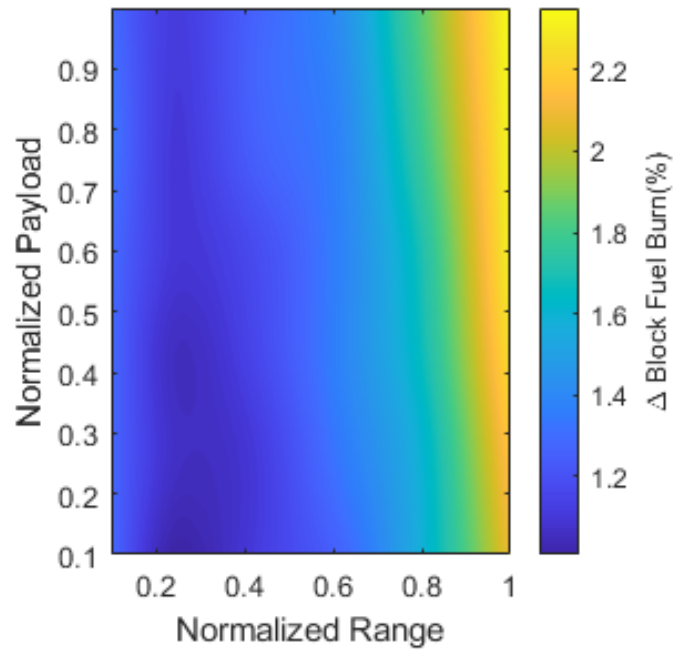


Figure 6.32:  $\Delta$  mission block fuel burn of aircraft with bleed for cabin cooling relative to aircraft sized without TMS

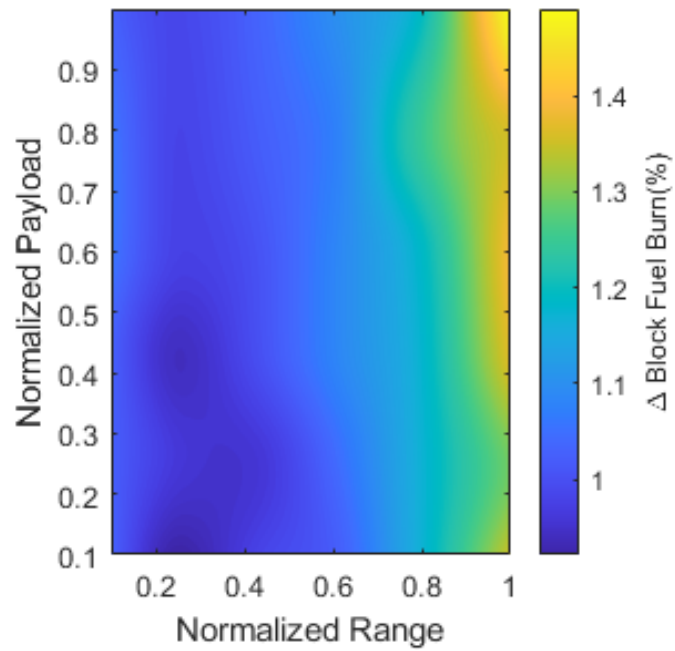


Figure 6.33:  $\Delta$  mission block fuel burn of aircraft with E-Charged-Air for cabin cooling relative to aircraft sized without TMS



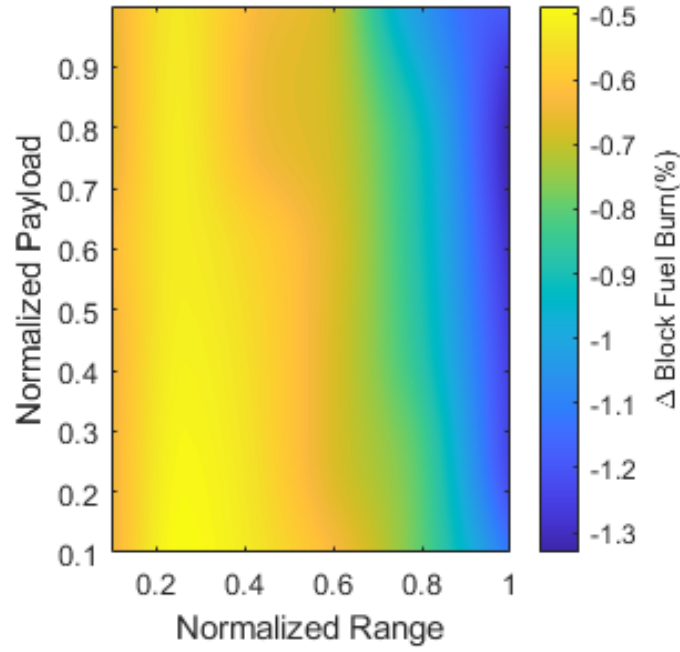


Figure 6.34:  $\Delta$  mission block fuel burn of aircraft with E-Charged-Air for cabin cooling relative to aircraft with bleed to cool the cabin

#### 6.6.2 Integrated Design and Analysis on 300-PAX TeDP

For the 300-pax TeDP configuration, both cryogenic cooling approaches as non-cryogenic cooling methods are selected for study. When the cryogenic options are chosen, the motor and generator are assumed superconducting, and the efficiency is 99.7%, as taken from Felder's work [17]. If the non-cryogenic cooling methods are used, then the efficiencies of motor and generator are scaled from the work done by the ULI program, from the author's previous paper [29]. Similarly, it is impossible to investigate all the optimal options of each local TMS due to time and computational cost, only limited candidates are researched to study the integrated design process for the 300-pax TeDP concept. For this experiment, multiple candidates are selected for the electric motor (assuming inverter is integrated with it), while only one optimal architecture is selected for each other local loads. However, if the thermal management requirements for these loads make the previously selected TMS infeasible during the iteration, new local TMS architecture will be re-selected.

### *Discoveries from Integrated Design Process*

Following the integrated design process, the aircraft is firstly sized without the TMS impacts. The initially sized aircraft have two types of propulsion systems: 1. propulsion system with superconducting motor and generator; 2. electrical propulsion systems working at common temperature conditions. The required shaft-power of the motor and generator is illustrated in Figure 6.35, where the values are normalized by the motor power during cruise. The power difference is because one generator is used to drive seven motors. It can be also seen that the power production at takeoff and climb is much higher than that during cruise, indicating the major heat generation are at these mission segments as well. The corresponding heat generation for motor and generator is shown in Figure 6.36 and Figure 6.37, for non-superconducting and superconducting motor and generator, where the values are also normalized by the value for non-superconducting motor at cruise. It is found that the difference in heat generation between takeoff and cruise is larger than the difference in shaft-power requirement. This is because the generator and motor are less efficient during takeoff and climb. Therefore, additional power consumption added to the generator may cause severe heating problems during these early mission segments.

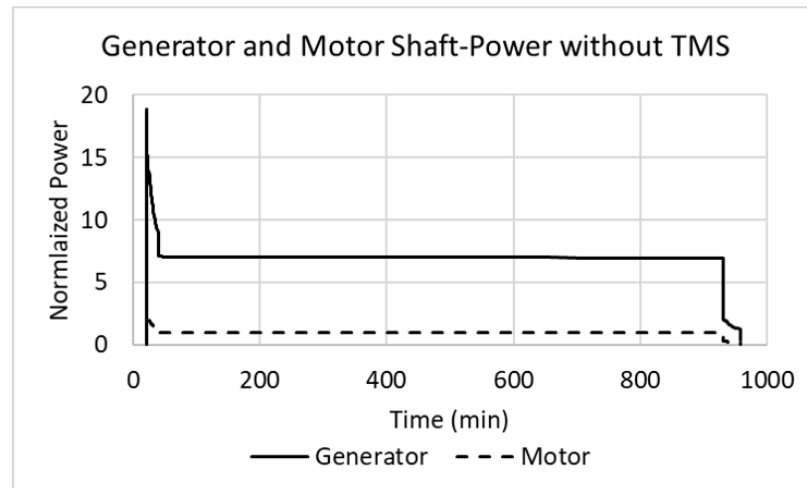


Figure 6.35: Shaft-power of motor and generator through the mission

After initially sizing the aircraft, the obtained thermal load requirements are used to

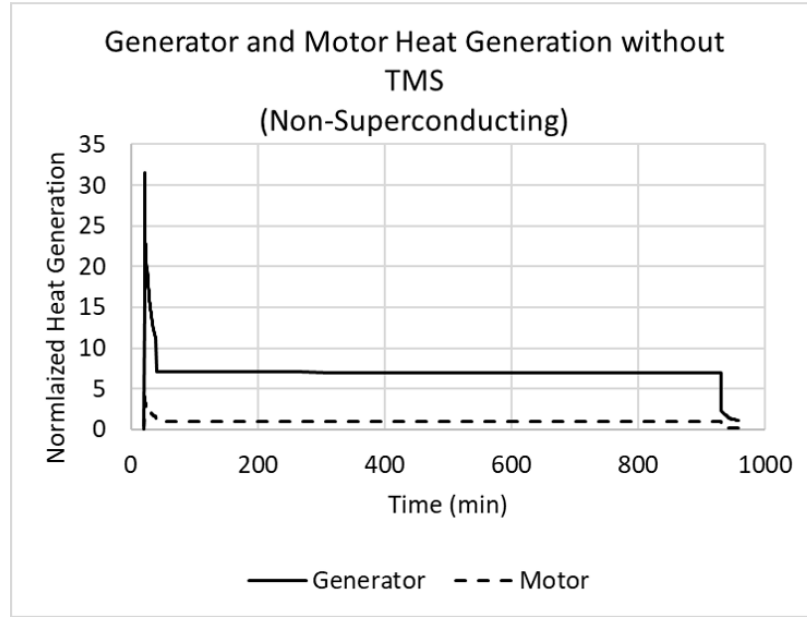


Figure 6.36: Heat generation of non-superconducting motor and generator through the mission

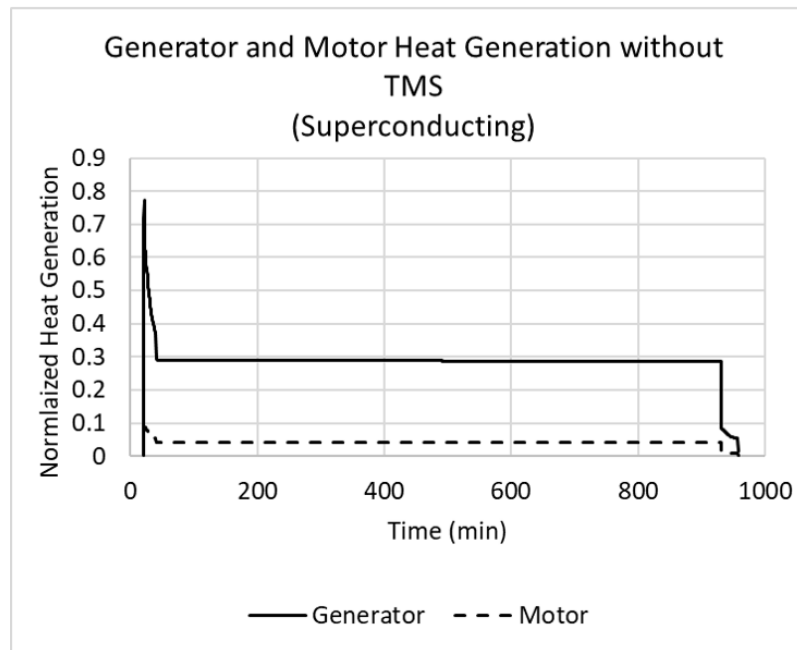


Figure 6.37: Heat generation of conducting motor and generator through the mission

generate and optimal down select architecture for each local TMS. As planned before, only multiple optimal candidates are selected for the electric motor. The candidates including both cryogenic and non-cryogenic approach. It should be noted here that the electrical

systems with cryogenic cooling option is considered superconducting. For the superconducting systems, the efficiencies of motors and generators are set to 99.7%, as discussed before. For the active cryogenic cooling, the same jet fuel is used, so there is no need to update the fuel properties or turboshaft engine characteristics. For the passive cryogenic cooling option in this study, the LH2 is used as both fuel and the cryogenic coolant. The turboshaft is assumed to have the same thermal efficiency as the one that burns jet fuel as in configurations with non-superconducting devices or active cryogenic cooling TMS. However, the fuel properties are replaced with the values for LH2. It should be noted that the volume of the fuel is not considered in this study for simplicity. The purpose of this experiment is to demonstrate the capability of the integrated design approach. Higher fidelity sizing methods are needed if the volume of fuel needs to be considered.

For the first TMS design iteration, one passive and one active cryogenic cooling approach is considered for the motor and generator, three other non-cryogenic TMS are also studied for the motor, while there is only one non-cryogenic TMS for the generator. The five local TMS are illustrated in Figure 6.38 to Figure 6.42. The passive cryogenic TMS (PCryo) uses the LH2 from the fuel tank to cool both the motor and the generator. The active cryogenic TMS (ACryo) uses the Claude process to cool the motor and the generator, which is introduced before in section 5.4. The three non-cryogenic TMS all use oil (Polyalphaolefin) as the direct coolant for motor cooling. One uses an additional PCM to absorb excessive heat and uses fan bleed to cool the oil (PCM). One uses a vapor cycle to cool the oil (Vapor), and another one uses a closed-loop air cycle to cool the oil (Closed-air).

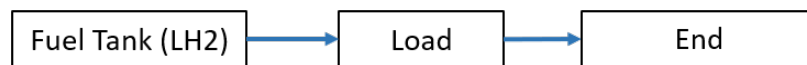
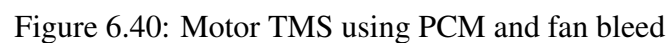


Figure 6.38: Passive cryogenic cooling TMS for motor and generator

The non-cryogenic TMS for the generator is shown in Figure 6.43, where the oil is used to directly cool it, and both fan bleed and fuel is used to cool the oil. For the other loads, the cabin TMS is the one that uses the bleed as the heat sink, and the ram air is also used



229

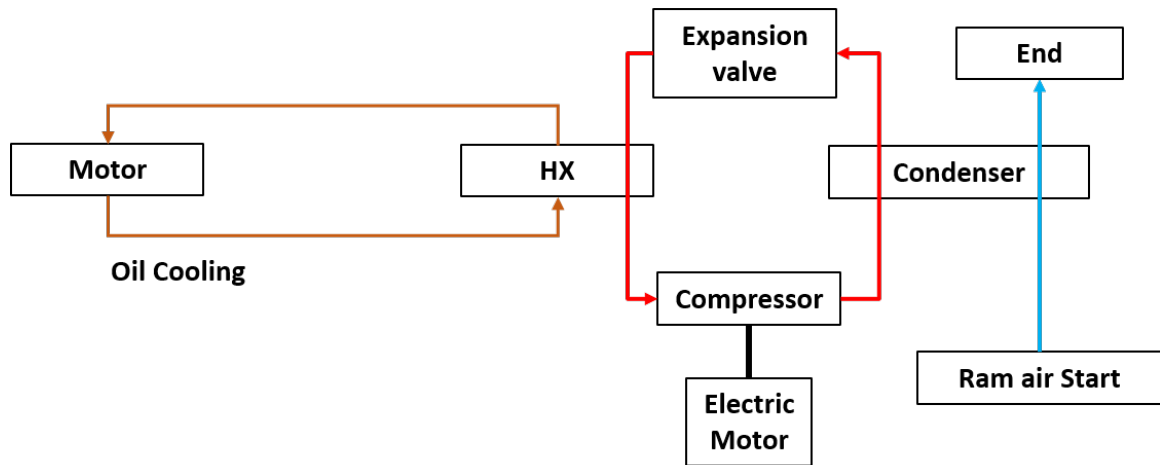


Figure 6.41: Motor TMS using vapor cycle

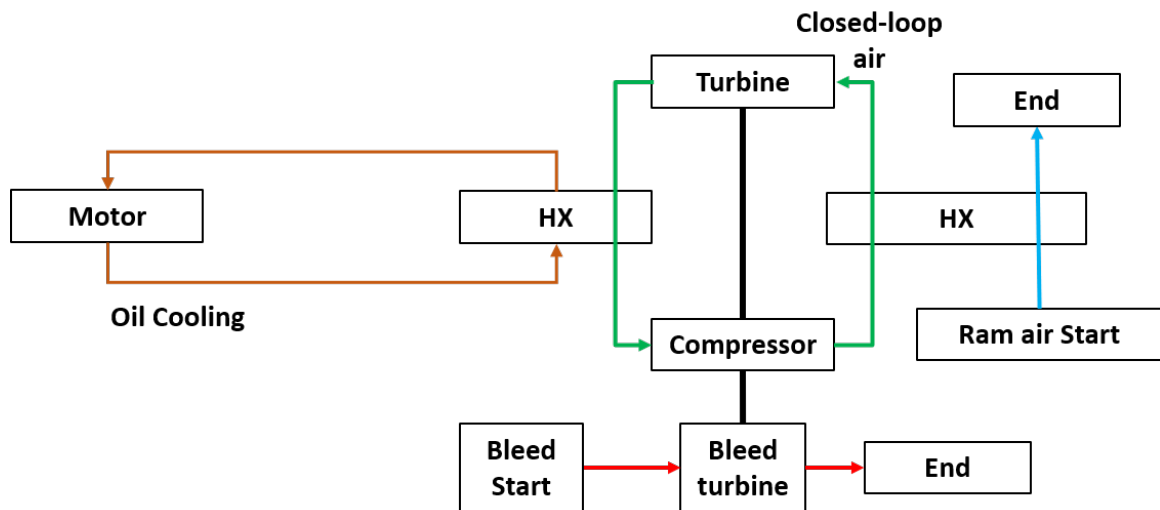


Figure 6.42: Motor TMS using closed-loop air cycle

or non-superconducting systems. The other loads with non-superconducting systems or active cryogenic cooling systems, they are the same as in the 160-pax aircraft, as illustrated in Figure 6.22 to Figure 6.25, which are all re-sized in terms of the 300-pax aircraft. For these loads in superconducting systems with passive cryogenic systems, they are all cooled by exhaust, either the LH2 after cooling the motor or generator, or from the cabin. This architecture is illustrated in Figure 6.44.

Then the corresponding global TMS are shown in Figure 6.45 to Figure 6.49. The Figure 6.45 and Figure 6.46 are the global TMS architectures with motors and generators

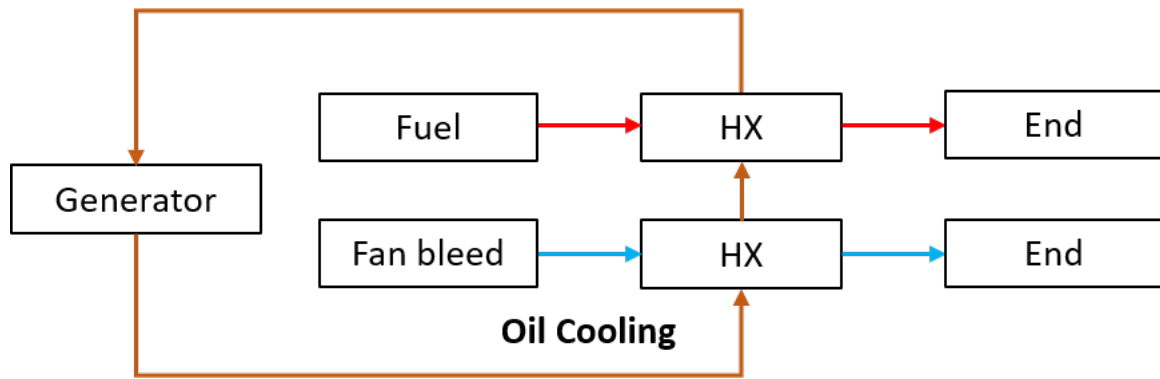


Figure 6.43: Non-cryogenic TMS for generator, using fuel and fan air to cool the oil

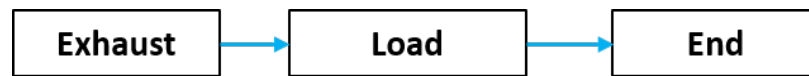


Figure 6.44: Loads cooling using exhaust with superconducting systems cooled by passive cryogenic cooling approach

cooled by passive and active cryogenic method respectively. Figure 6.47 illustrates the global TMS with motor with PCM and its oil cooled by fan bleed, Figure 6.48 presents the global TMS with motor oil cooled by vapor cycle, and Figure 6.49 shows the global TMS with motor oil cooled by closed-loop air cycle.

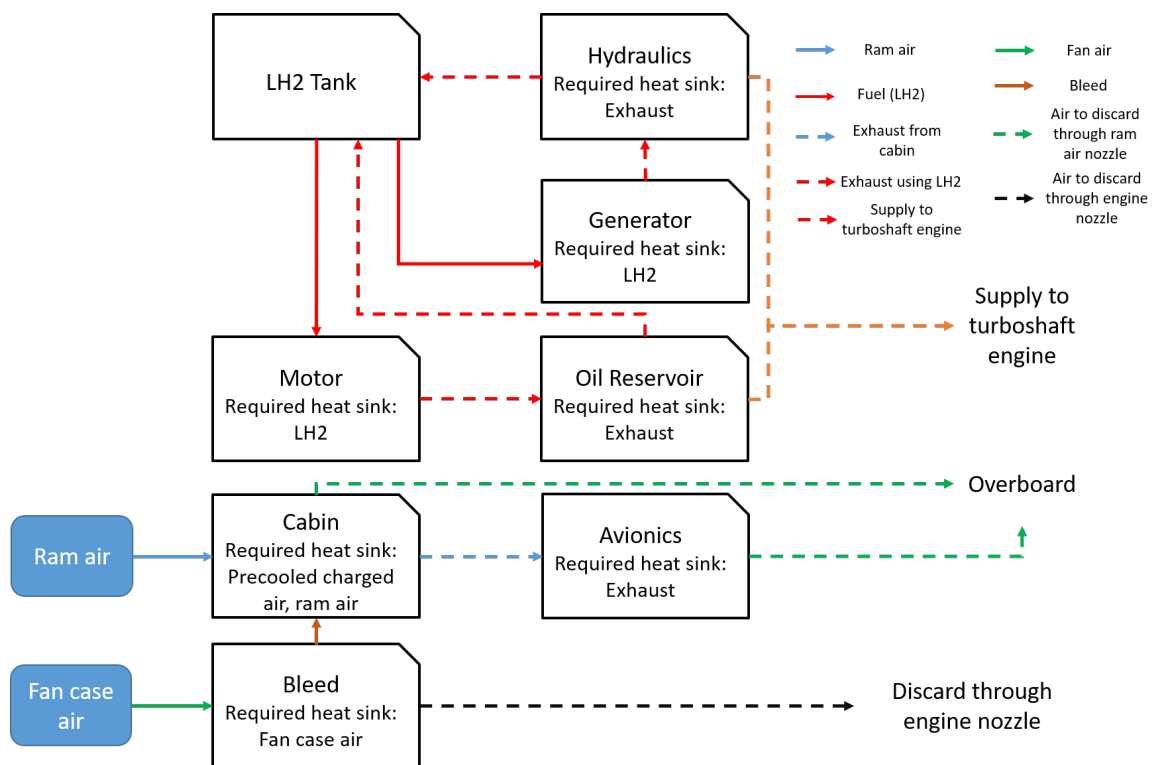


Figure 6.45: Global TMS for 300-pax TeDP with passive cryogenic cooling



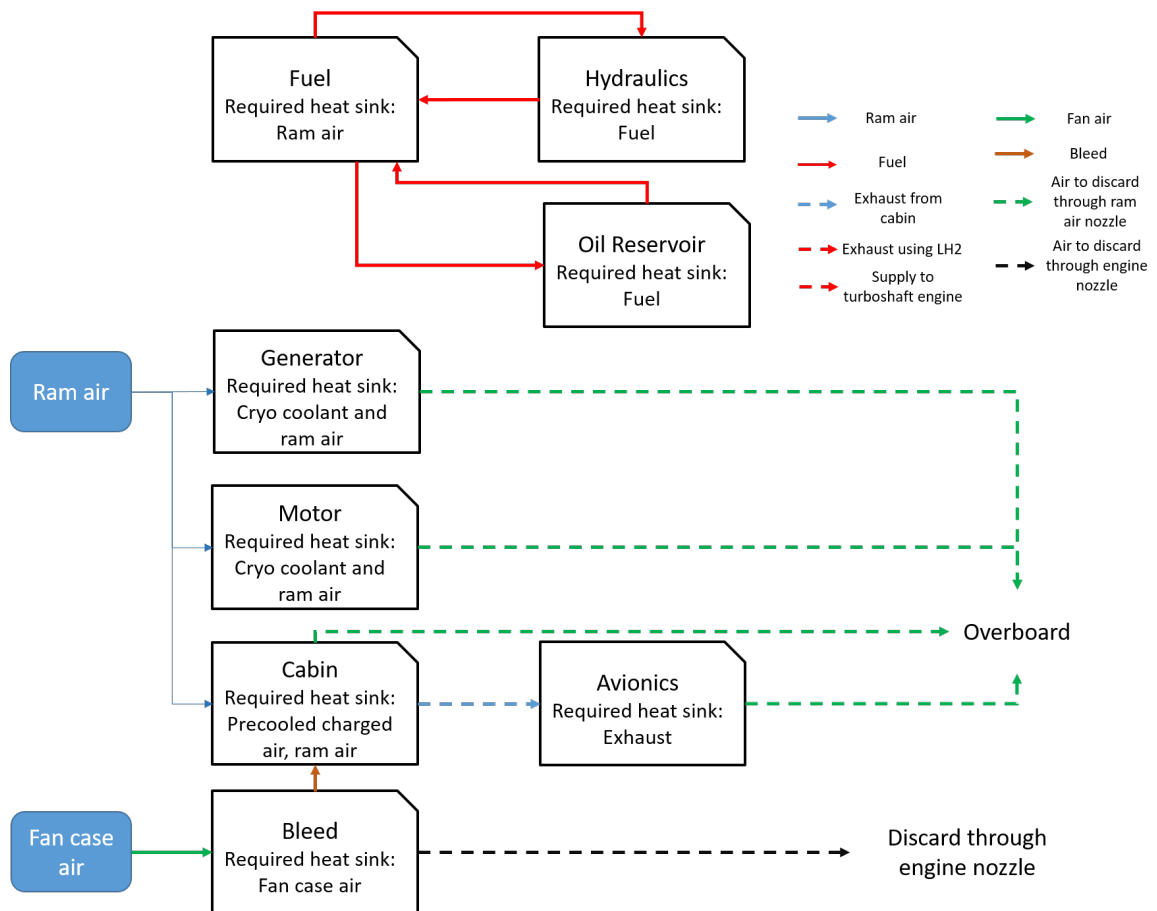


Figure 6.46: Global TMS for 300-pax TeDP with active cryogenic cooling

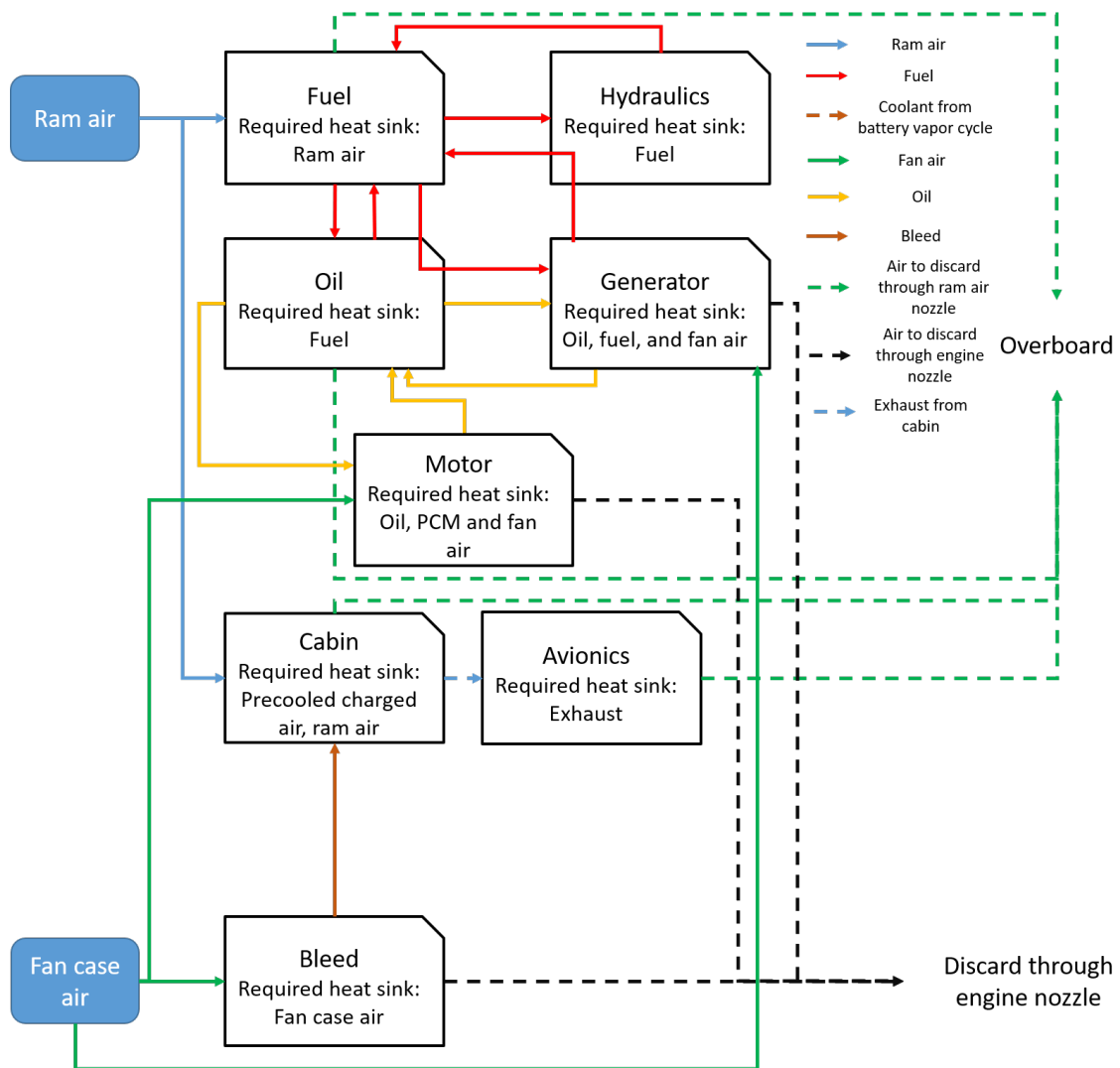


Figure 6.47: Global TMS for 300-pax TeDP with motor cooled by PCM and fan bleed

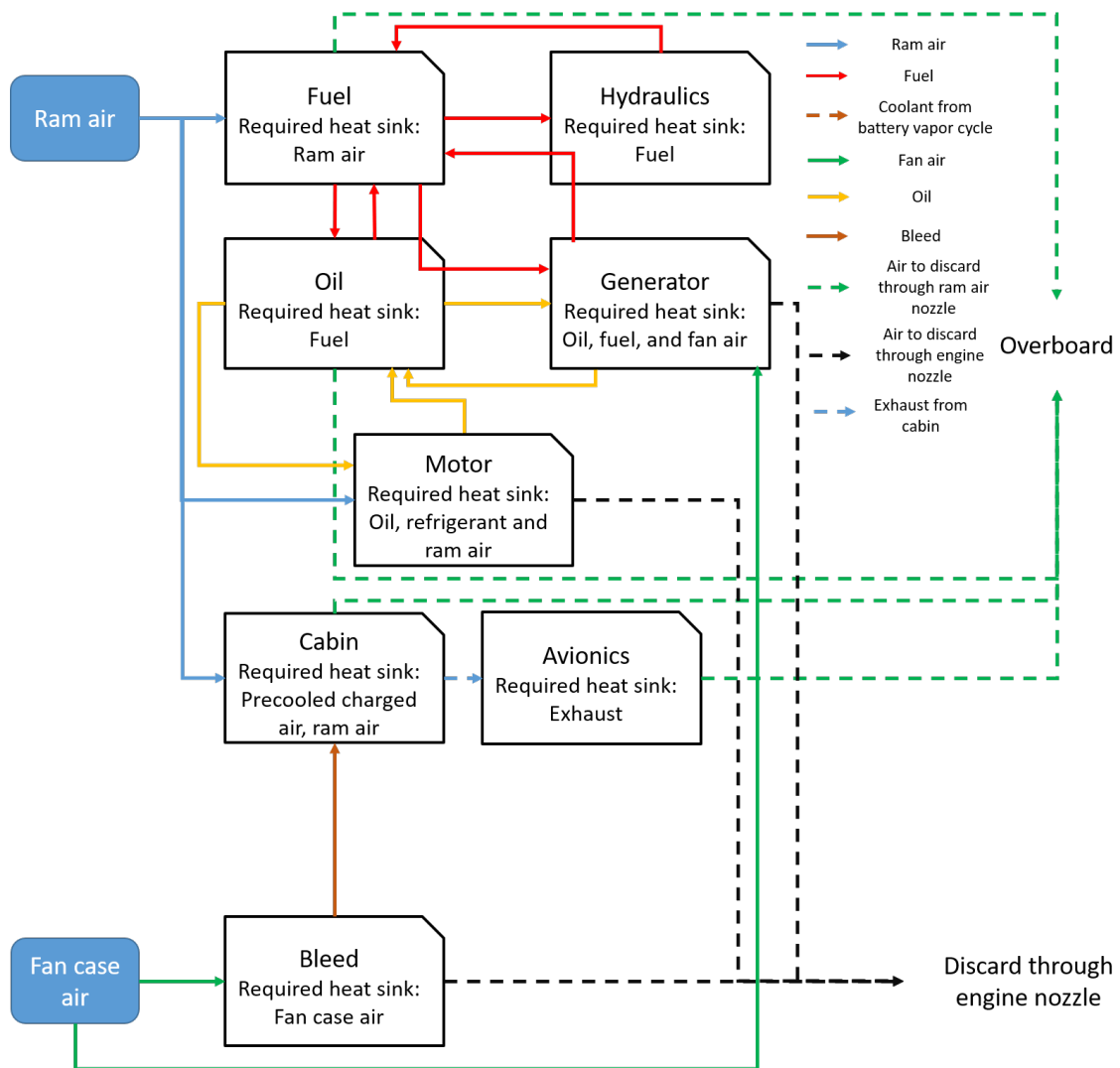


Figure 6.48: Global TMS for 300-pax TeDP with motor oil cooled by vapor cycle

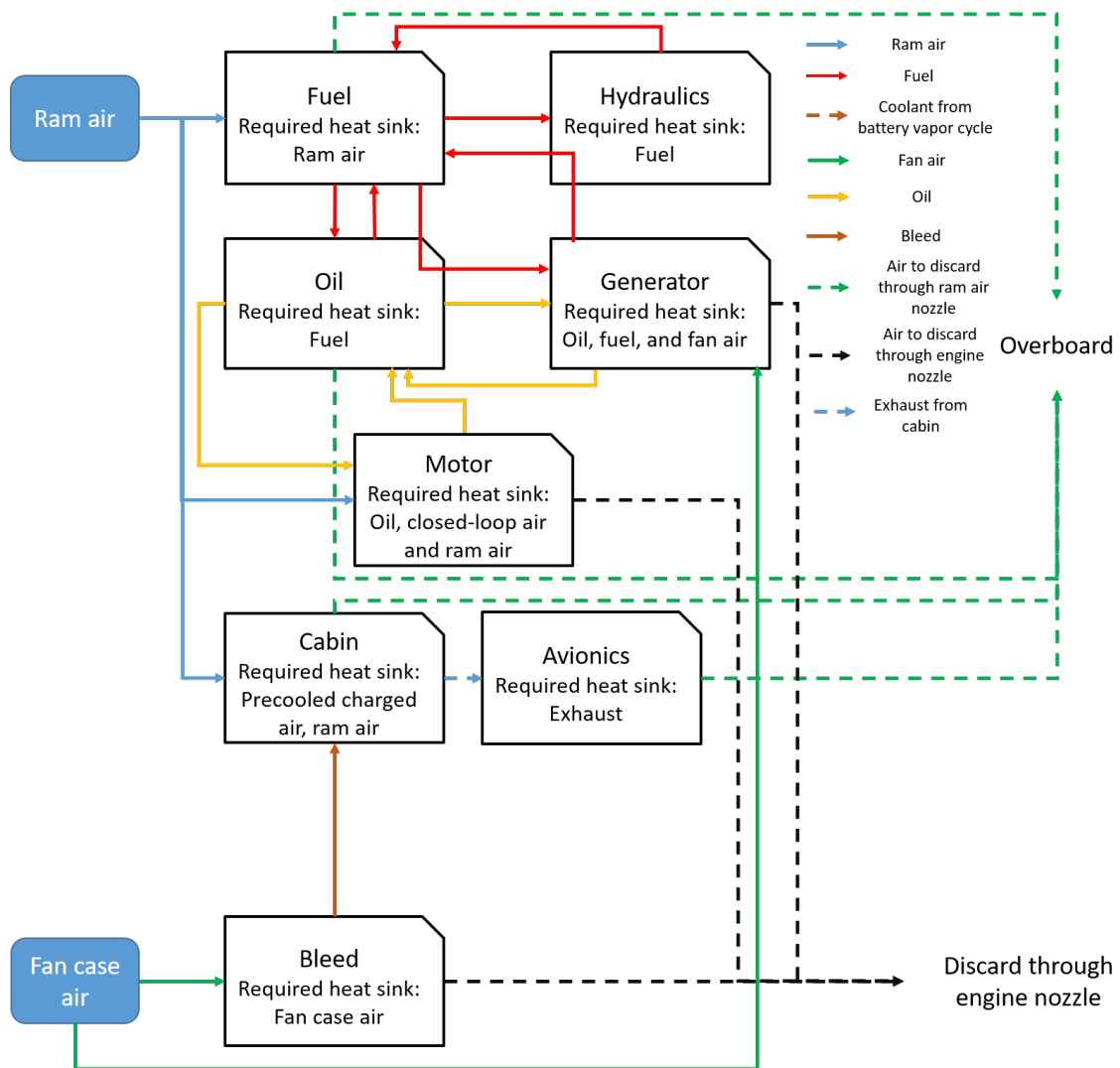


Figure 6.49: Global TMS for 300-pax TeDP with motor oil cooled by closed-loop air cycle

With the impacts of these generated TMS fed back to the integrated design process, the aircraft is resized. Figure 6.50 to Figure 6.55 show the shaft-power requirement and heat generation from the motors and generators for these five global TMS, along with the initially sized aircraft as a baseline. Each of the figure is normalized with the value of the initially sized aircraft at the cruise condition.

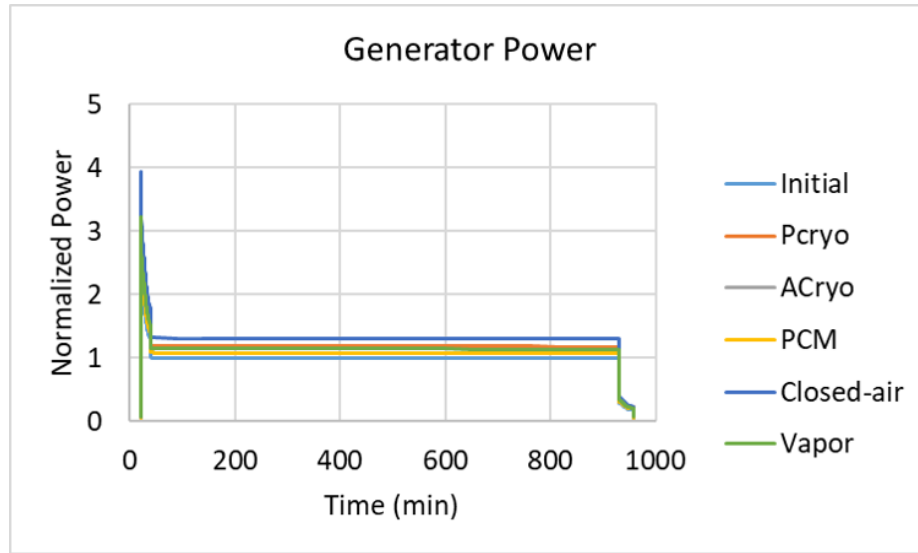


Figure 6.50: Shaft-power requirement of the generator

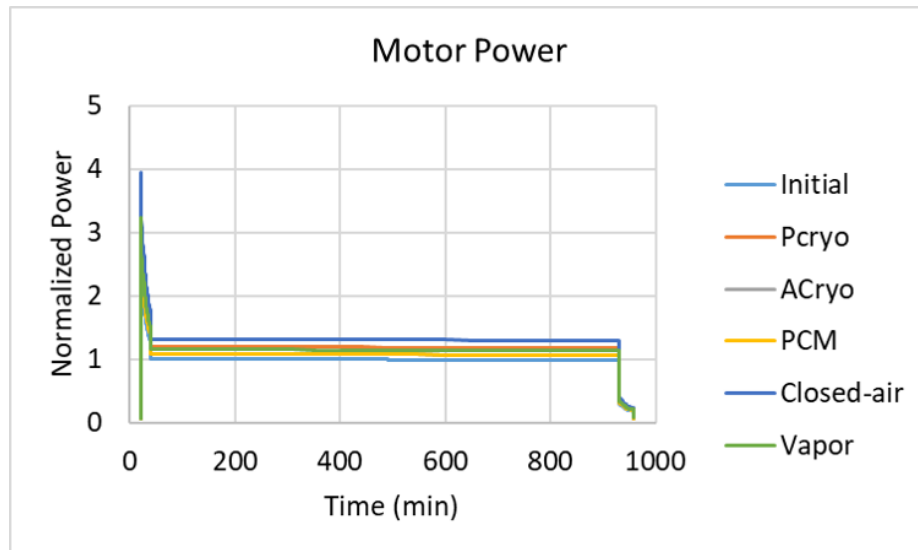


Figure 6.51: Shaft-power requirement of the motor

From Figure 6.50 and Figure 6.51, it can be seen that the shaft-power required for

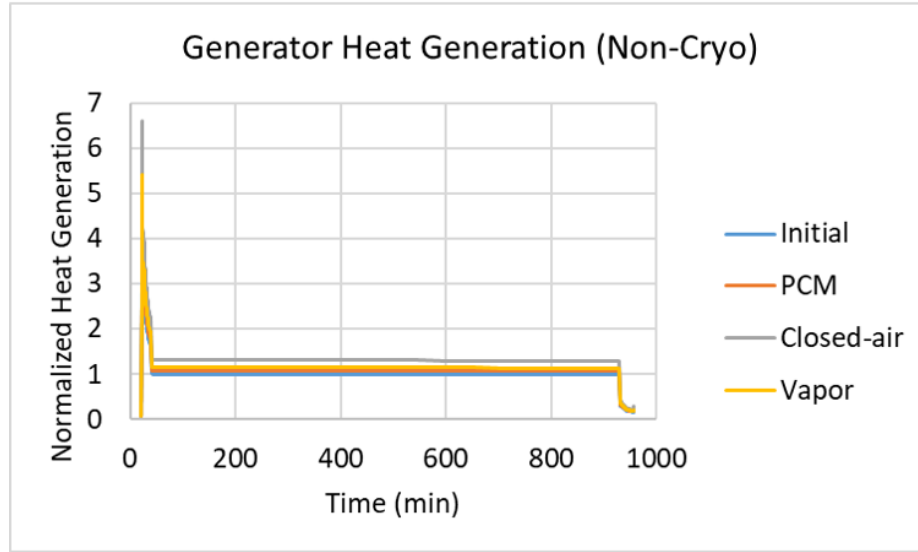


Figure 6.52: Heat generation from the generator without cryogenic cooling

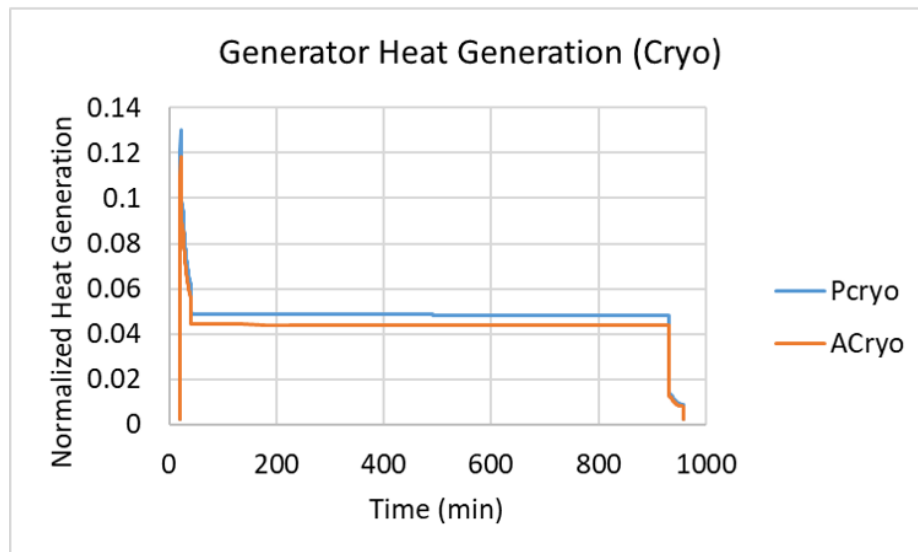


Figure 6.53: Heat generation from the generator with cryogenic cooling

each architecture following the sequence: Closed-air>PCryo>Vapor>ACryo>PCM. The closed-air has the largest impact not mainly because of the added weight due to the turbomachines, considering the vapor cycle has a larger weight than it. It is because the closed-loop air cycle has the lowest coefficient of performance (COP) in all these five architectures, i.e., the closed-loop air cycle has a COP less than half of the vapor cycle, leading to the largest added power consumption to the generator. The power consumption

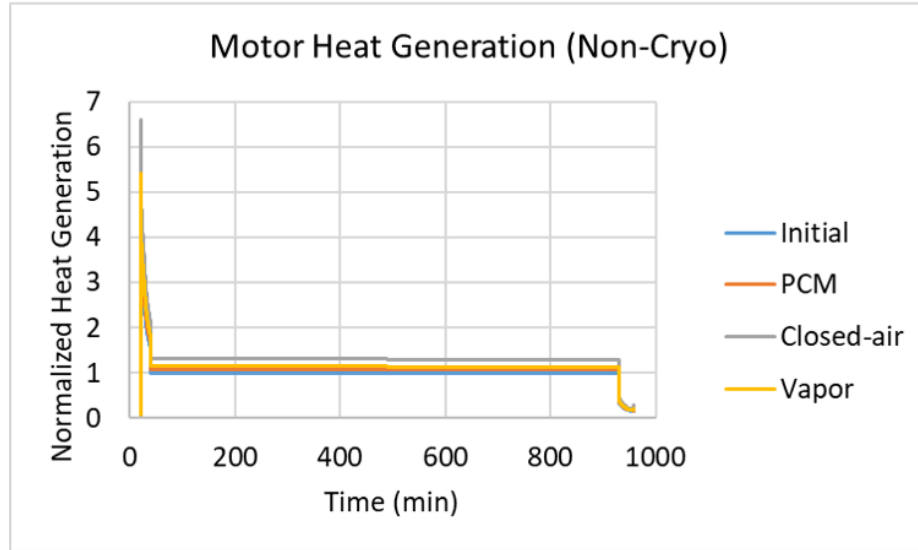


Figure 6.54: Heat generation from the motor without cryogenic cooling

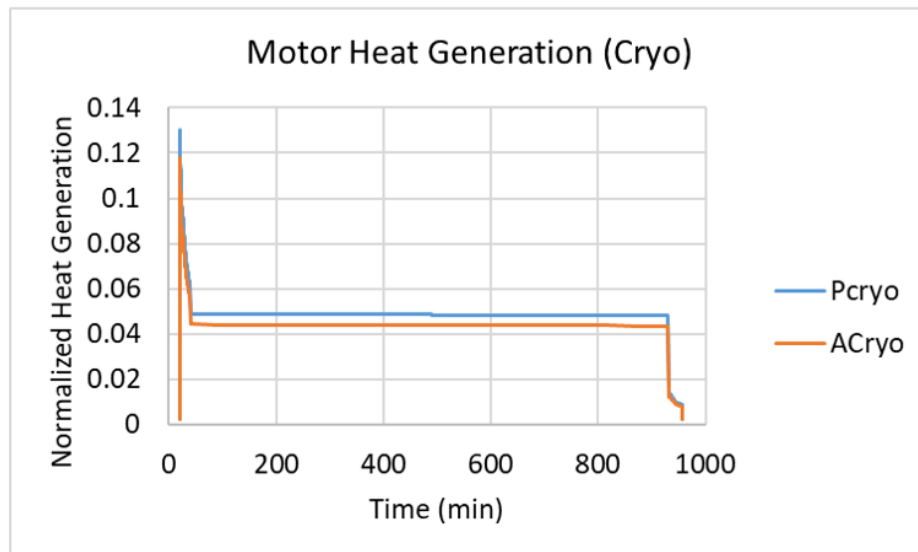


Figure 6.55: Heat generation from the motor with cryogenic cooling

of the PCryo architecture is the second largest, although the only power consumption due to the TMS is the power to pump the flow. Such increase of the required shaft-power is because the PCryo architecture needs a very heavy fuel tank, which is a pressure vessel and should be covered by sufficient insulation. This fuel tank significantly increase the OEW of the aircraft, further making the required shaft-power increase. Corresponding to such results on shaft-power, the heat generation from these architectures follow a similar

trend. For superconducting systems, because of the very high efficiency (99.7%), the heat generation is very small, compared to the other non-superconducting systems. It should be also noted that the heat generated by the generator with the closed-loop air cycle is significantly larger than other systems, which are illustrated in Figure 6.56 more clearly, where the value is normalized by the value at the same moment from the initial design mission. The increased amount of the heat from the generator is also larger than that from the motor, because the TMS only directly adds electrical load to the generator. Any increase of the required propulsive power produced by the motor will also increase the required power from the generator. Therefore, the heat penalty by the added TMS on the generator is more severe than on the motor. And such influence is reflected in the next design iteration.

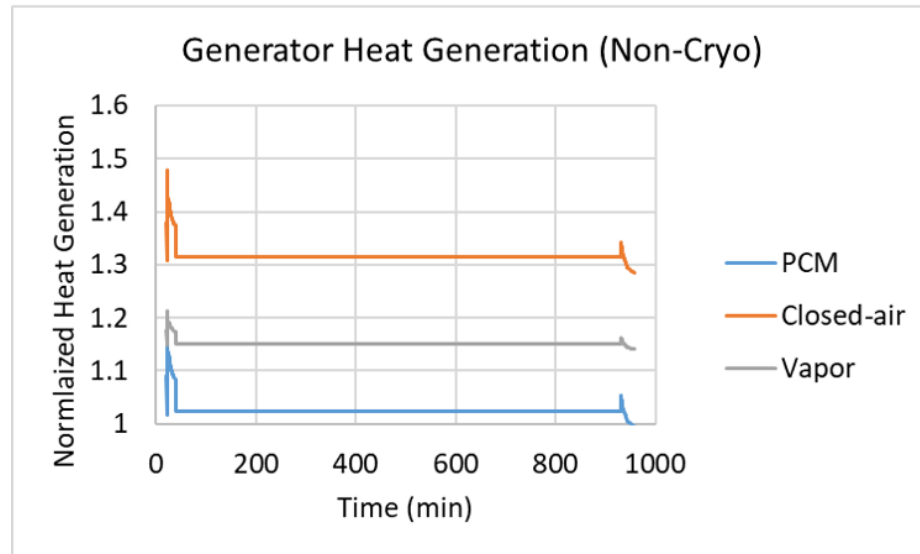


Figure 6.56: Heat generation from the motor with non-cryogenic cooling

With the newly sized aircraft and the corresponding thermal requirements of each load, TMS architectures are populated and optimally down selected again. In this design iteration, the feasible architectures for the generator with the closed-loop air cycle change. The previously selected architecture in which oil is applied to direct cooling and then be cooled by both fan bleed and fuel, is not feasible any more. This is because the previously discussed heating issue of the generator due to low COP of the closed-loop air cycle. The gap between the heat generation and the cooling capability can be shown in Figure 6.57, where



the "Heat\_Gen\_Initial" denotes the heat generation from generator in the initially sized aircraft, "Heat\_Gen\_Closed-Air" denotes the heat generation from the generator in the aircraft that is sized with closed-air cycle to cool the motor, and "Heat\_Remove\_Initial" is the heat removal by the initially selected TMS architecture which is illustrated by Figure 6.43. It should be noted that the figure is zoomed in to the early mission segments for a more clear view of the heating problem during when the heat generation is the largest. The power shown in this figure is also normalized by the heat generation for the initially sized aircraft during cruise. When the cooling capability can fully satisfy the thermal management requirements, the heat removal and heat generation are equal to each other. However, when the generated heat cannot be fully removed, a gap appears, as shown in this figure during early mission segments. It is observed that the heat generated from the generator in the initially sized aircraft can be fully removed. When the power consumption in the generator increases due to the motor TMS (closed-air loop), the maximum cooling capability becomes lower than the peak heat generation. Therefore, the initially selected generator TMS architecture becomes infeasible. In this new design iteration, to compensate such increased heat generation in the generator, a new local TMS architecture is selected, which is illustrated in Figure 6.58, where a PCM is also used to absorb the excessive heat during early mission segments. And the corresponding global TMS is shown in Figure 6.59. After this iteration, the TMS solutions for all the selected architectures are fixed, while only values of sizing parameters change through the integrated design process until the convergence is met. The aircraft performance with the converged designs will be discussed in the next subsection.

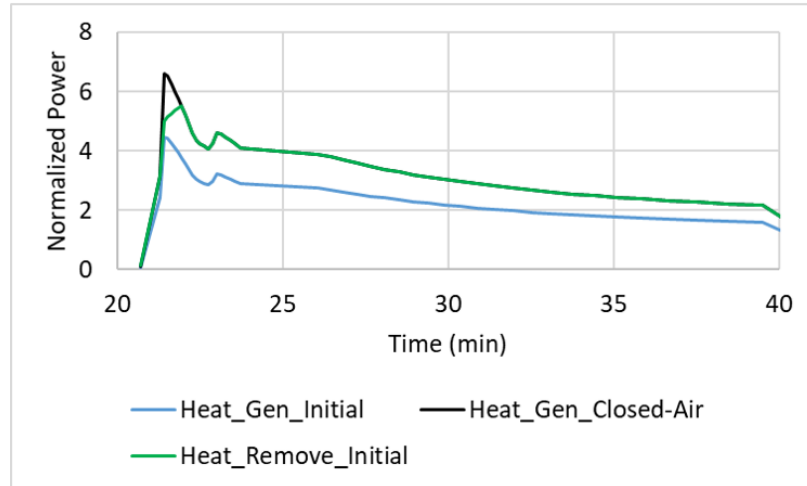


Figure 6.57: Gap between cooling capability and heat generation of the generator using the initially selected TMS architecture (aircraft sized with closed-air cycle as TMS for the motor)

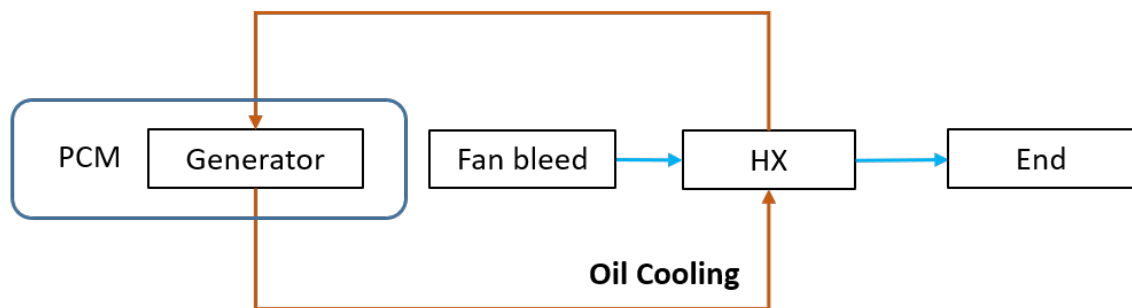


Figure 6.58: New local TMS for generator with closed-loop air cycle

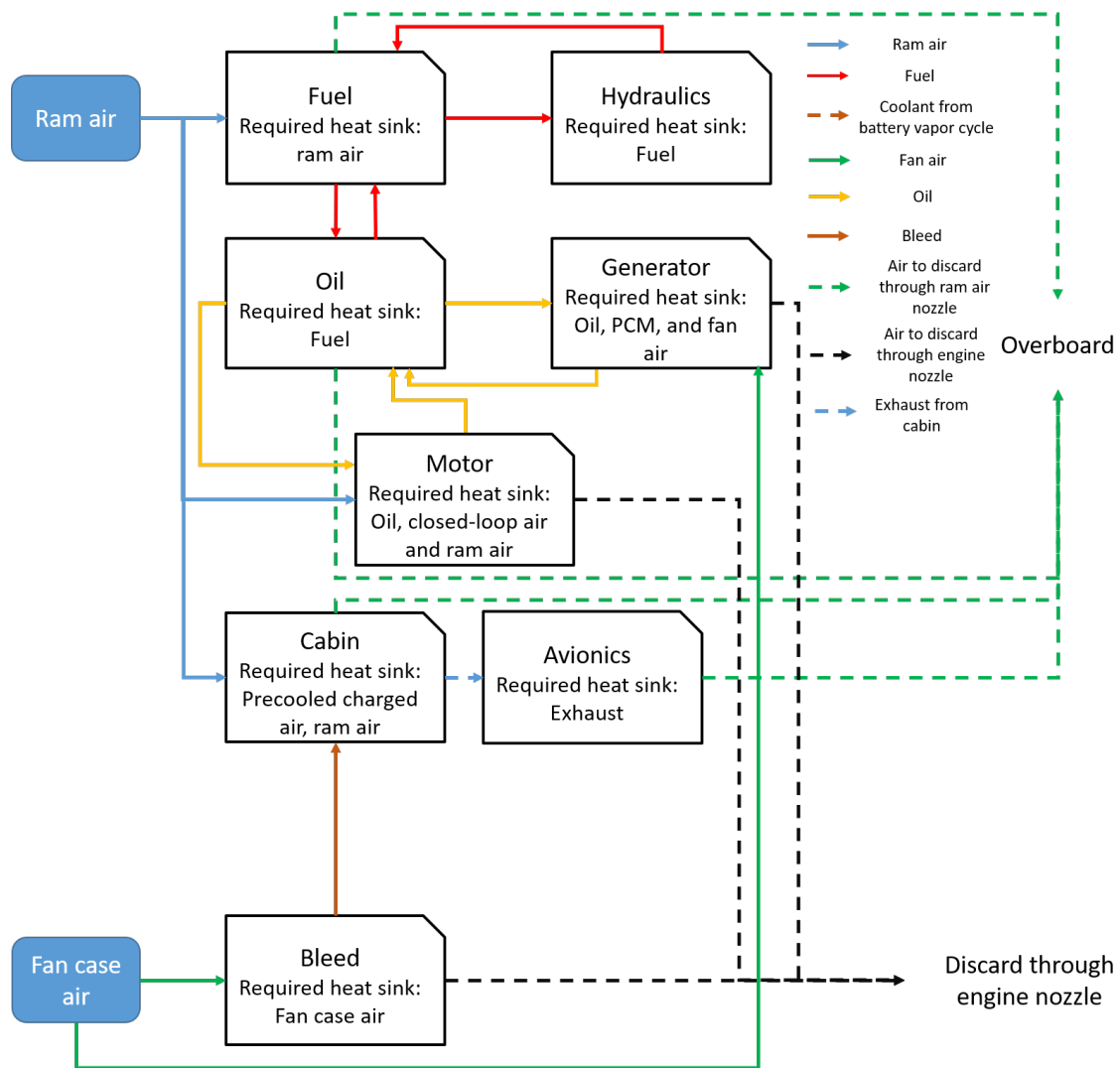


Figure 6.59: Global TMS for 300-pax TeDP with motor oil cooled by closed-loop air cycle, with new generator TMS

### *Performances of Converged Aircraft Designs*

With the selected TMS architectures presented before, the MTOW,  $W_f$ , and OEW of the converged aircraft design are presented in Figure 6.60. The values are presented by the corresponding item weight of the initially sized aircraft.

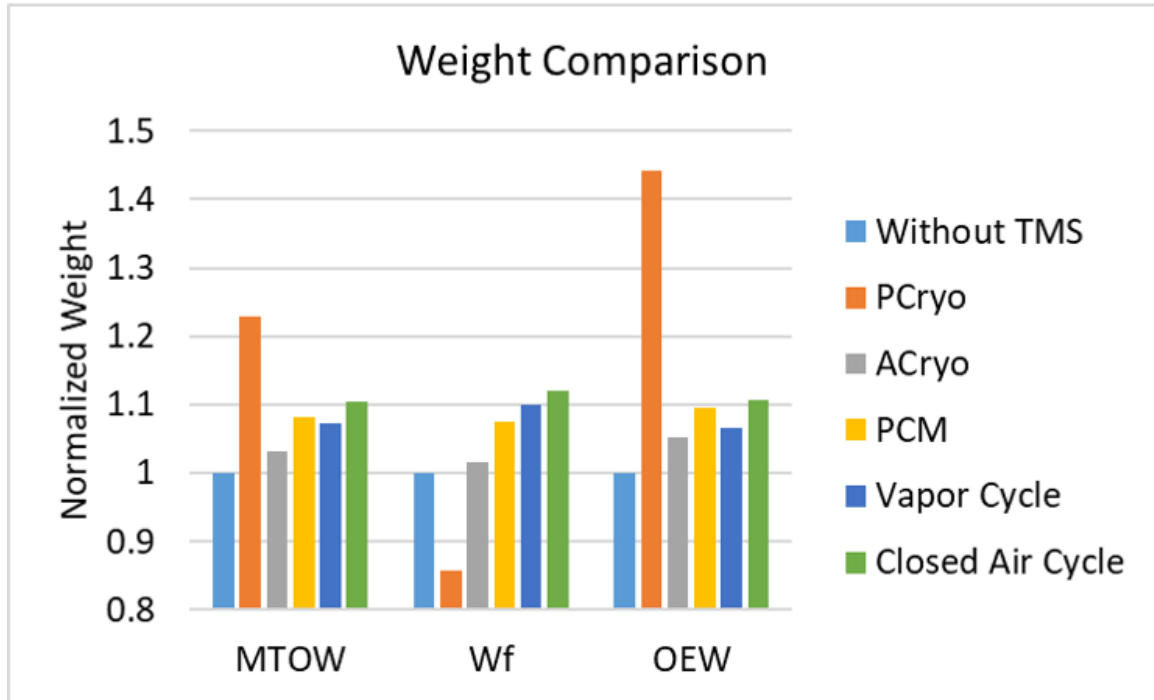


Figure 6.60: Weight comparison for aircraft with selected TMS

As this figure shows, all designs with TMS has a higher weight in MTOW and OEW. The architecture with PCM and the passive cryocooling mostly contribute to the aircraft OEW by the weights of their own. As seen from the results, the aircraft with LH2 for passive cooling has the highest OEW and MTOW. This is contributed by the tank to hold LH2. However, the fuel weight by this architecture is reduced. The total mission energy consumption is indeed increased, but due to high energy density of LH2, the fuel weight is still reduced, although with a higher MTOW. It should be also noted that the gravimetric index (GI) for this LH2 aircraft is 29.8%, which is slightly beyond today's technology level (GI=15-20%) but is more realistic than the target set by Clean Sky 2 [162] (GI = 38%). Then the aircraft with closed-loop air cycle has the second largest weight. On the one

hand, the closed-loop air cycle itself contributes to the weight by the TMS weight itself. On the other hand, due to the increased power load by this TMS, the generator needs to be resized larger to accommodate such change. In addition, the converged solution also uses PCM for generator cooling. Therefore, this architecture also contributes a significant amount of weight to the aircraft. The third largest weight increase in MTOW and OEW is brought by the TMS with PCM for the motor, because the weight of the PCM is directly used to absorb the excessive heat generated from the motor during early segment. And the TMS with vapor cycle is even lighter than the one using PCM, despite it has a larger power consumption. However, due to rather high COP, the corresponding penalty is not large. Surprisingly, the TMS with active cryo-cooling approach has the smallest impact on the weight penalty. However, such small influences are estimated from the optimistic assumption that the efficiency of the motor and generator can be as high as 99.7%. Such small heat generation leads to low power consumption as well as a small weight of the cryocooler. Such small heat generation also requires a small amount of the coolant, which also leads to a small tank. It should be noted that the reason that the passive cryogenic cooling architecture needs a large tank is not because of the amount of the required coolant, it is because the needed amount of fuel that is sufficient for the mission.

The influences of the chosen TMS on the mission block fuel are investigated by evaluating multiple missions with different payloads and ranges. The mission block fuel burn for the five selected TMS architectures are illustrated in Figure 6.61 to Figure 6.65.

From these figures, it can be seen that the superconducting system with LH2 as the fuel has a fuel weight reduction relative to the original TeDP without superconducting system, despite large weight penalty due to fuel tank system. This is mainly because the high specific energy of LH2 relative to the jet fuel. However, such analysis relies on the optimistic expectation on the performances of the superconducting systems. In addition, the weight of the total tank system only considers the tank and the ducts. However, as [163] showed, the LH2 is only 6% percent of the total fuel tank system, where the weights of other parts

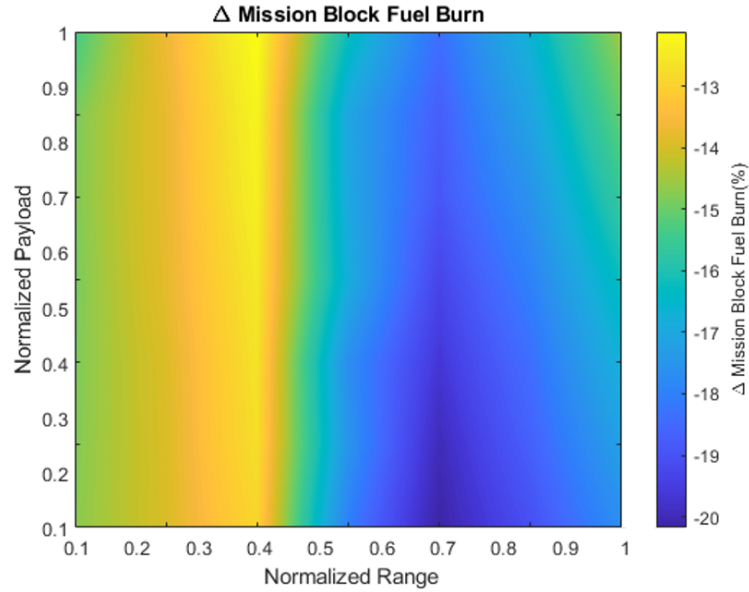


Figure 6.61:  $\Delta$  mission block fuel burn of aircraft with passive cryo-cooling relative to aircraft sized without TMS

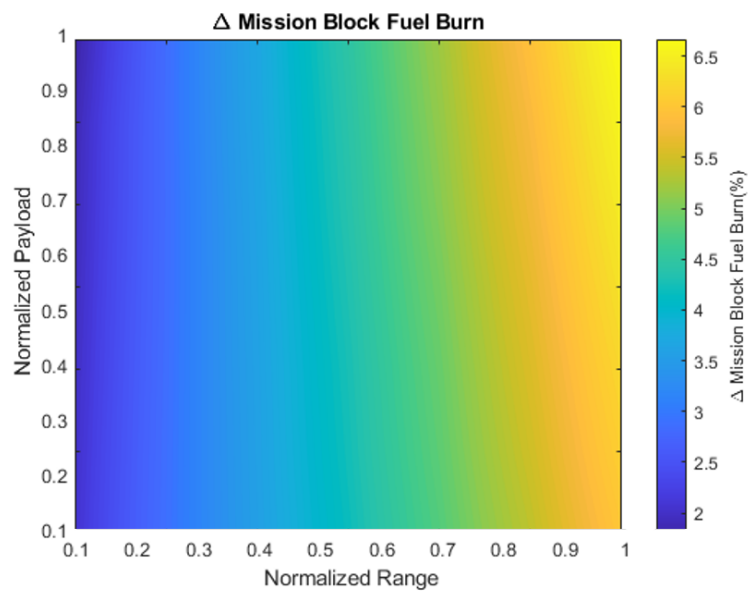


Figure 6.62:  $\Delta$  mission block fuel burn of aircraft with active cryo-cooling relative to aircraft sized without TMS

that are not considered in this study are expected to contribute much more weight to the OEW and MTOW if included. Regarding aircraft with other four TMS architectures, the aircraft with active cryogenic cooling has the best fuel burn performance, due to low heat

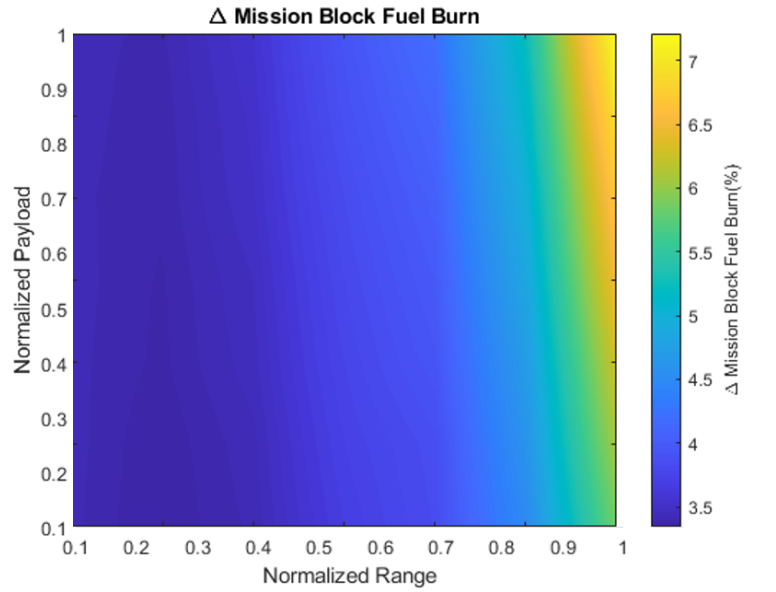


Figure 6.63:  $\Delta$  mission block fuel burn of aircraft with PCM for motor cooling relative to aircraft sized without TMS

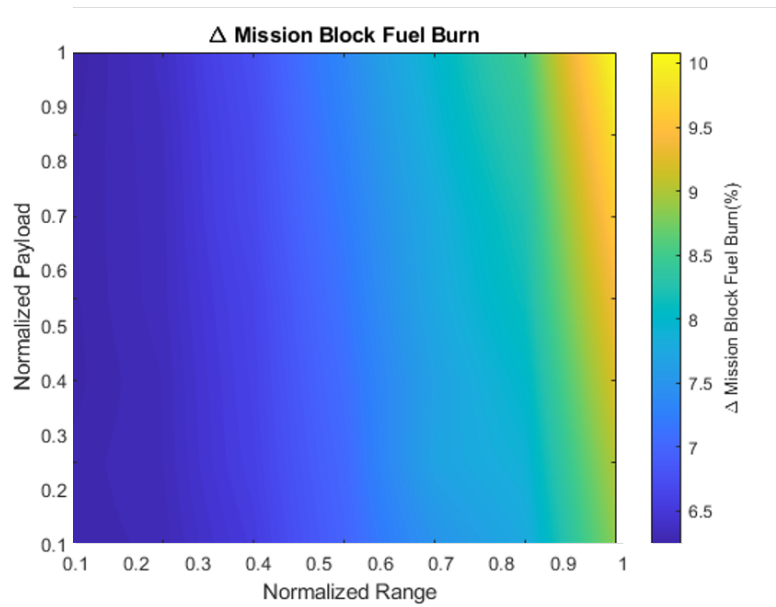


Figure 6.64:  $\Delta$  mission block fuel burn of aircraft with vapor cycle for motor cooling relative to aircraft sized without TMS

generation through the superconducting systems. If only the non-superconducting systems are allowed to be implemented, the TMS with PCM to absorb the motor excessive heat has the best fuel performance. This is because the PCM is only needed during early mission segments, which does not require a large weight to handle the thermal management re-

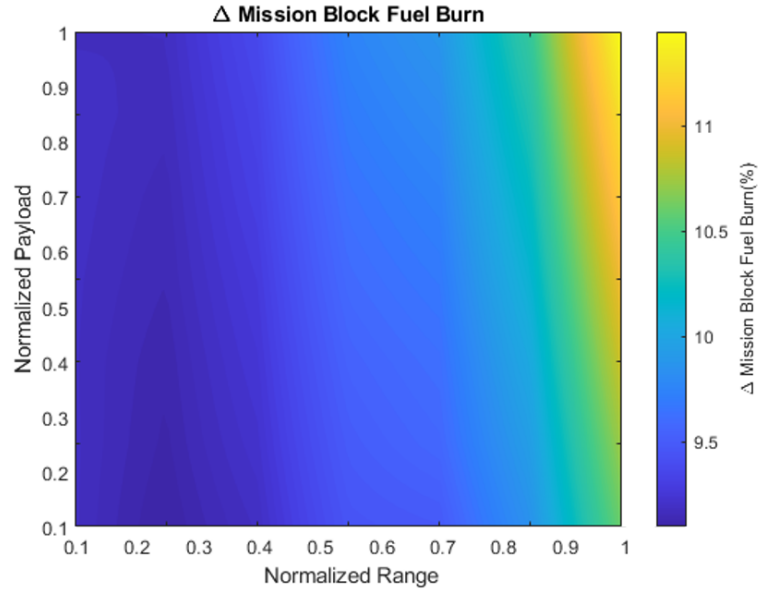


Figure 6.65:  $\Delta$  mission block fuel burn of aircraft with closed-loop air cycle for motor cooling relative to aircraft sized without TMS

quirement. Then the next best one is TMS using vapor cycle, and the worst one is the TMS with closed-loop air cycle, in terms of the block fuel burn. Although the closed-loop air cycle is lighter than the vapor cycle, the COP is much smaller, which leads to a larger size of the generator as well as a heavier generator TMS. In summary, if the superconducting technologies are promising, then the aircraft with active cryogenic cooling has the optimal fuel economy. If the cooling options are limited to non-cryogenic approaches, then using PCM to assist motor cooling has the best fuel performance.

### 6.6.3 Integrated Design and Analysis on 78-PAX Non-Cryo HTeDP

For an HTeDP aircraft, the newly load is the battery, which can provide the electric power in addition to the turboshaft generators during hybridization operation. Therefore, in the experiment for integrated design of HTeDP, only multiple candidates are chosen for the battery TMS, while only one is selected for each other load. In this experiment, the ULI aircraft [28, 29] is used as the vehicle platform for the study, where the electrical system, including the electrified propulsion systems, are required to be non-superconducting and to



be cooled by non-cryogenic cooling methods. Similar to the 300-pax TeDP configuration, the efficiencies of electrical systems are looked up through efficiency maps, which were constructed in the ULI program [29].

However, the sizing process of the aircraft regarding the newly added load, the battery, is different from the process for other loads such as motors or generators. The other loads are usually sized with the whole aircraft at its design mission, but for the battery, it is usually not sized during the design mission, that is, the aircraft is still sized without the battery at its design mission. Then for missions with shorter ranges or lower payloads, the battery is installed to the aircraft to provide the hybridization energy source. The size of the battery is adjustable in terms of the mission to perform. Such sizing strategy is chosen for the battery because the energy density of the battery is still low at the current technology level. If the battery is sized along with the aircraft sizing process, then MTOW of the aircraft would be too large. Therefore, to provide hybridization as well as to avoid high takeoff weight, the battery is only added in missions with shorter ranges and lower payloads.

This sizing strategy leads to a new question: is the TMS of the battery sized during the aircraft mission or not? One approach is to use the existing TMS for other loads to provide additional cooling power for the battery without resizing the TMS for other loads. If the maximum cooling capability of these TMS is reached, and it cannot further cool the battery to keep it under the temperature limit, then this selected mission with the corresponding power-splits is determined infeasible. Here the power-splits (PS) as the fraction of power required from the battery over the total required power, as shown by the following equation:

$$PS = \frac{\text{Power from Battery}}{\text{Total Required Power}} \quad (6.4)$$

The second battery TMS sizing strategy is to resize the existing TMS with the anticipated heat generation from the battery. And another strategy is to individually design a TMS with the anticipated load. These strategies along with the corresponding TMS are incorporated into the integrated design process, which will be discussed in the following subsection.

In this experiment, missions with shorter ranges and lower payloads are selected for the study, instead of the design mission, because only short-range and low-payload missions can be operated on with battery. For this study, a typical mission with range = 600 nmi, and payload = 8127 lbm, or normalized range = 0.3, and normalized payload = 0.45 (normalized by the design values) is selected. The power-splits selected are: 0.17 for climb and 0.235 for cruise. It should be noted that there exists an optimal power-split for each selected mission. However, to determine the optimal power-splits is out of the scope of this study, so the power-splits for all missions to be presented in this experiment are fixed.

### *Discoveries from Integrated Design Process*

As presented before, the loads for the 78-pax HTeDP concept are: cabin, motor, generator, battery, fuel tank, oil reservoir, hydraulics, and avionics. Following the integrated design process, the aircraft is sized without these loads. And then the TMS need to be generated for all the loads and integrated. However, the situations would be different if the battery TMS strategy is different. Now let us consider the three strategy for battery TMS as presented before: 1. using existing TMS for other loads without resizing; 2. using existing TMS resized for the battery; 3. designing an individual TMS for the battery.

If the battery is cooled by existing TMS without resizing. Then the battery TMS is not sized in the aircraft sizing phase, and the battery is not considered as a load in the integrated design process. For this case, only cabin, motor, generator, fuel tank, oil reservoir, hydraulics, and avionics are considered. The selected local TMS are the same as presented before for the 160-pax SSA and 300-pax TeDP, because they are always at the Pareto frontier after the feasibility-based and KPI-based filtering process, with the current given heat generation. The cabin is the air cycle machine using bleed and ram air, which is the same as in Figure 6.19. The motor TMS is selected as the oil-cooling TMS with PCM which is shown in Figure 6.40. Generator is cooled by fan bleed and fuel-cooled oil, as shown in Figure 6.43. The fuel tank is cooled by ram air as shown in Figure 6.22. The oil

reservoir and hydraulics are both cooled by fuel as shown in Figure 6.23 and Figure 6.24. The avionics are still cooled by exhaust as in Figure 6.25. And the global TMS is illustrated in Figure 6.66 for the design mission (without battery). The TMS solutions do not change through the integrated design process, and the corresponding power consumption from the generator and the motor are shown in Figure 6.67 to help the readers to get a better understanding that how this aircraft operates through the design mission. The values are normalized by the power of motor during cruise, and it should also be noted that one generator is driving four electric motors.

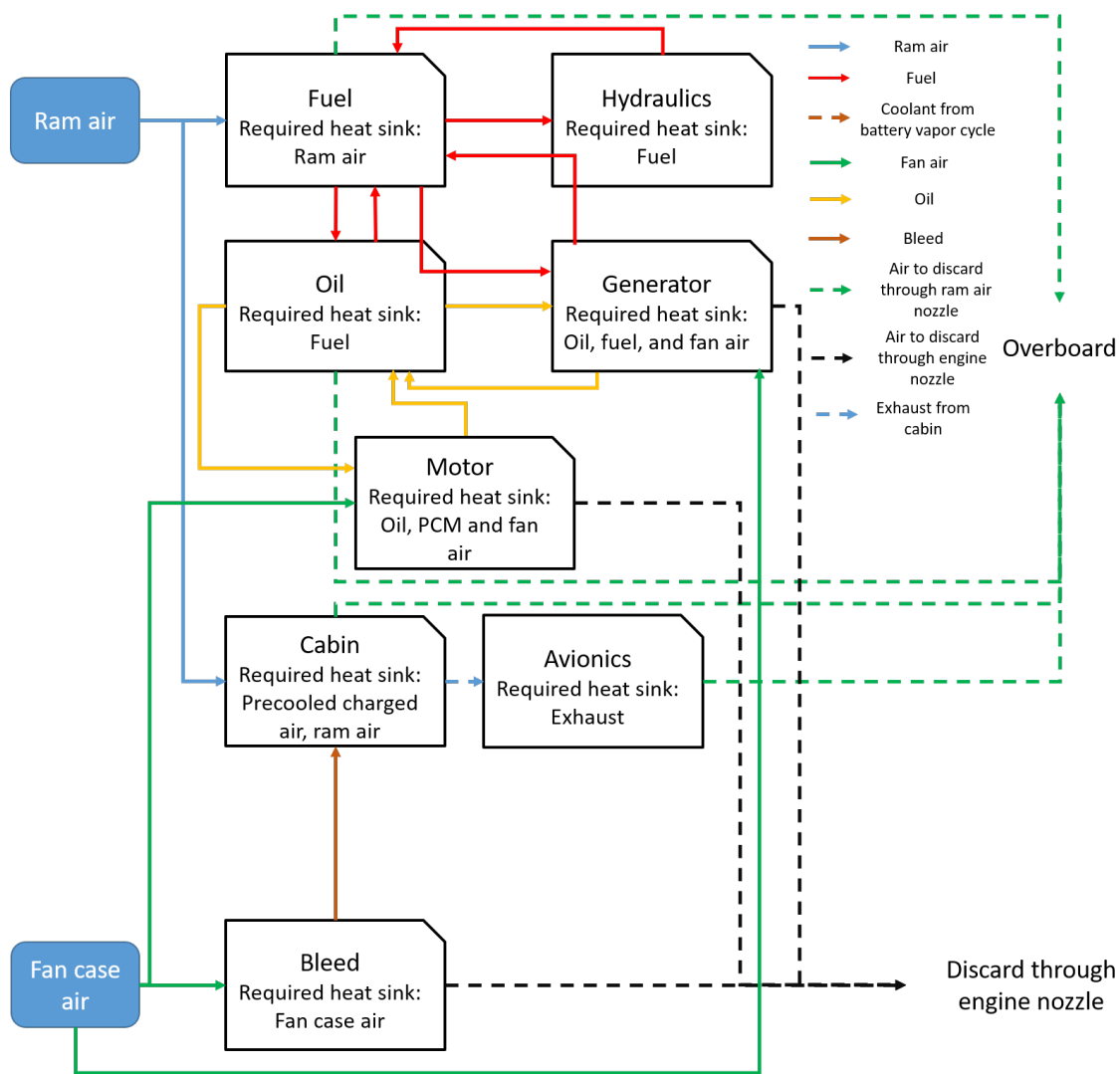


Figure 6.66: Global TMS for 78-pax HTeDP with without battery installed: battery TMS strategy 1

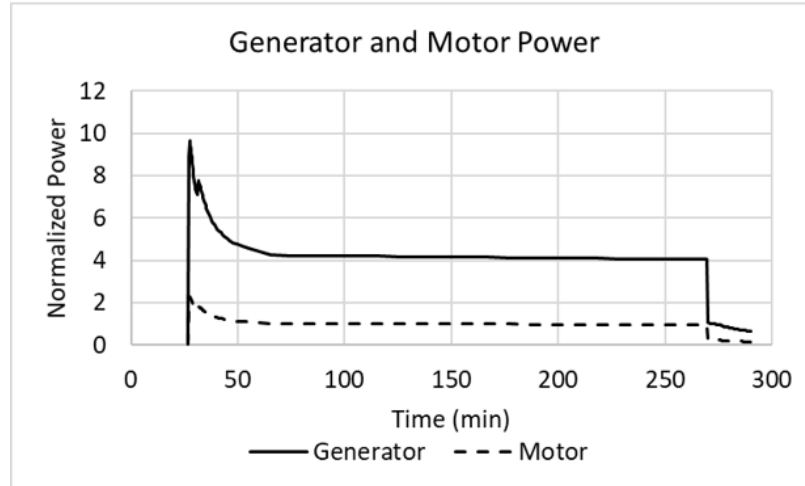


Figure 6.67: Generator and motor power for design mission without battery

With this converged design, now the battery TMS architecture constructing begins. Using the methods shown in Experiment Set 1 and Experiment Set 2, the selected TMS architecture for the battery is the one uses the air supplied from ACS, which is in the cabin TMS. However, with battery TMS design strategy 1, where the cabin TMS is not resized, the maximum air that can be supplied to the battery is constrained by the maximum allowed corrected shaft speed of the ACS in the cabin TMS. The air supplied to the battery is simply the total amount of air through the ACS minus the air supplied to the cabin. The total amount of air reaches to its maximum value when the corrected shaft speed reaches the maximum allowed value. In this study, the maximum corrected speed is 0.98. Thus, the battery TMS architecture is simply using the air from ACS to cool the load, which is illustrated in Figure 6.68. And the overall schematic of the ACS and the battery TMS together are shown in Figure 6.69, where ACS supplies air to both cabin and the battery.



Figure 6.68: Battery TMS architecture using ACS air

Before showing the results with the integrated battery TMS, it is important to understand how the ACS shaft speed schedule is determined to cool the battery. The method to determine the ACS shaft speed schedule is shown in Figure 6.70. An initial execution of

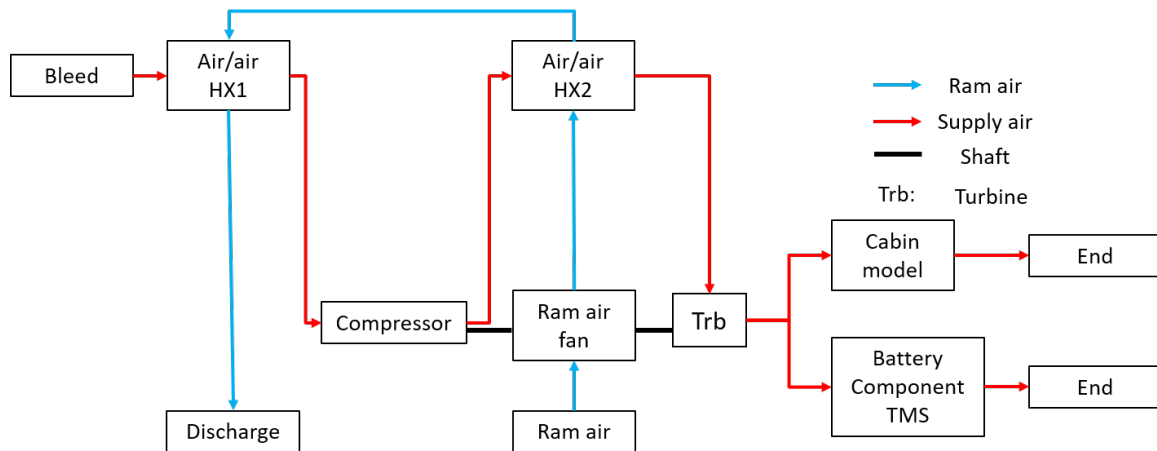


Figure 6.69: Integrated illustration of battery TMS and ACS

the selected hybrid mission will be run first, with initial set schedule which can merely cool the cabin. Then the maximum battery temperature along the mission is checked against its maximum allowed value. If it is lower than the temperature limit, then the mission is feasible in terms of the battery temperature. Otherwise, shaft speed of the ACS is increased. Then the mission is re-run again, and the temperature is also checked again. This process repeats until the temperature satisfies the constraint or the shaft speed reaches its maximum allowed value which will return a flag that this mission is infeasible in terms of the selected power-splits.

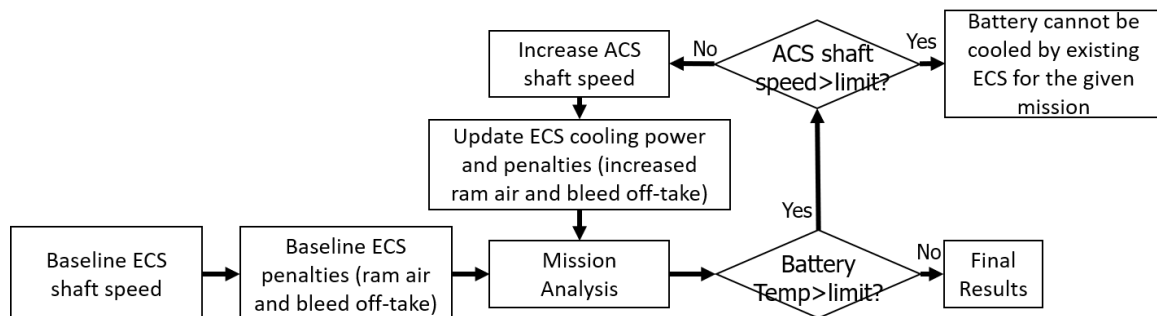


Figure 6.70: Method to determine ACS shaft speed schedule

With this battery TMS architecture integrated to the aircraft, the power by generator, motor, and the battery for the selected mission is shown in Figure 6.71, which are normal-

ized by the power value of the motor during cruise. The battery only supplies the power at takeoff, climb, cruise. When the aircraft is at its descent condition, the battery stops working. It should be noted that the power in this figure is by one generator, one motor, and the whole battery stack which is to supply power to all eight motors. Since the aircraft is already a converged solution using the battery TMS strategy 1, there is no need to feed back the influences of the battery TMS to the aircraft sizing process. Then the overall global TMS with battery is shown in Figure 6.72. The corresponding battery temperature profile is also shown in Figure 6.73, along with the flight altitude as a reminder of mission operation conditions, and  $45^{\circ}C$  is used as the upper limit of the battery temperature. It can be seen that the battery temperature is gradually increased as the mission progresses, indicating not all generated heat from the battery is removed by the TMS. Because the load type of the battery is defined as "accumulative" in this context, of which the TMS does not need to remove all generated heat at any moment as long as the temperature limit is not violated. The increase of the ACS shaft speed schedule is also minimized, to use the minimal supply air from the ACS to cool the battery. This can be seen from the fact that the maximum battery temperature in this selected mission is very close to its upper limit. In addition, it is also discovered that once the aircraft begins to descend, the battery temperature gradually decreases. This is because the battery is not used during the descent segment, meaning there is no heat generated. Meanwhile, the cabin can also absorb small amount of the heat from the battery, because the battery is installed right under the cabin floor, which can be seen in Figure 6.4.

Now let us consider the other two battery TMS strategies. The second strategy is still using the existing TMS while resizing it, and the third one is using an individual TMS to cool the battery. For these two strategies, a critical sizing mission is needed. As shown in the author's previous work, the most critical missions are the missions with short ranges, assuming the power-splits are fixed. This is because when the range is shorter, the total energy provided by the battery becomes less, and a lighter battery stack is installed. How-

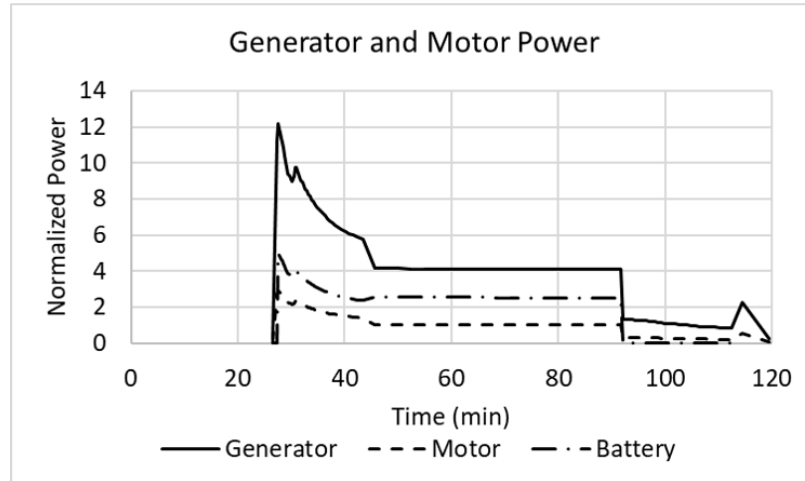


Figure 6.71: Generator, motor, and battery power for selected hybrid mission

ever, when power-splits are fixed while only varying the range, the required power from the battery is the almost the same, which also makes the heat generation from the battery the same through different mission ranges. Therefore, a lighter battery is easier to be heated by the same amount of heat generation, leading to the fact that the battery temperature is more likely to be limited during short-range missions. For this study, a mission with shorter range is selected: range = 396 nmi, and payload = 5418 lbm, which is 0.2 range and 0.3 payload after normalization.

For strategy 2 and 3, the battery TMS needs to be sized or resized, and their characteristics need to be fed back to aircraft size process. Therefore, the heat load for the battery needs to be identified before constructing the battery TMS. Following the integrated design process, the aircraft without TMS is still initially sized using the design mission. However, the next process changes. Originally the TMS will be generated and down selected in this stage. However, the thermal requirements of the battery is unknown yet, so there is a need to run the selected hybrid mission before defining the thermal requirements of the TMS. Therefore, the integrated design process for hybrid aircraft is updated to Figure 6.74, where a hybrid mission analysis is needed after sizing the aircraft. In each iteration of the integrated design loop, the hybrid mission will be analyzed to update the thermal management requirements for the TMS.

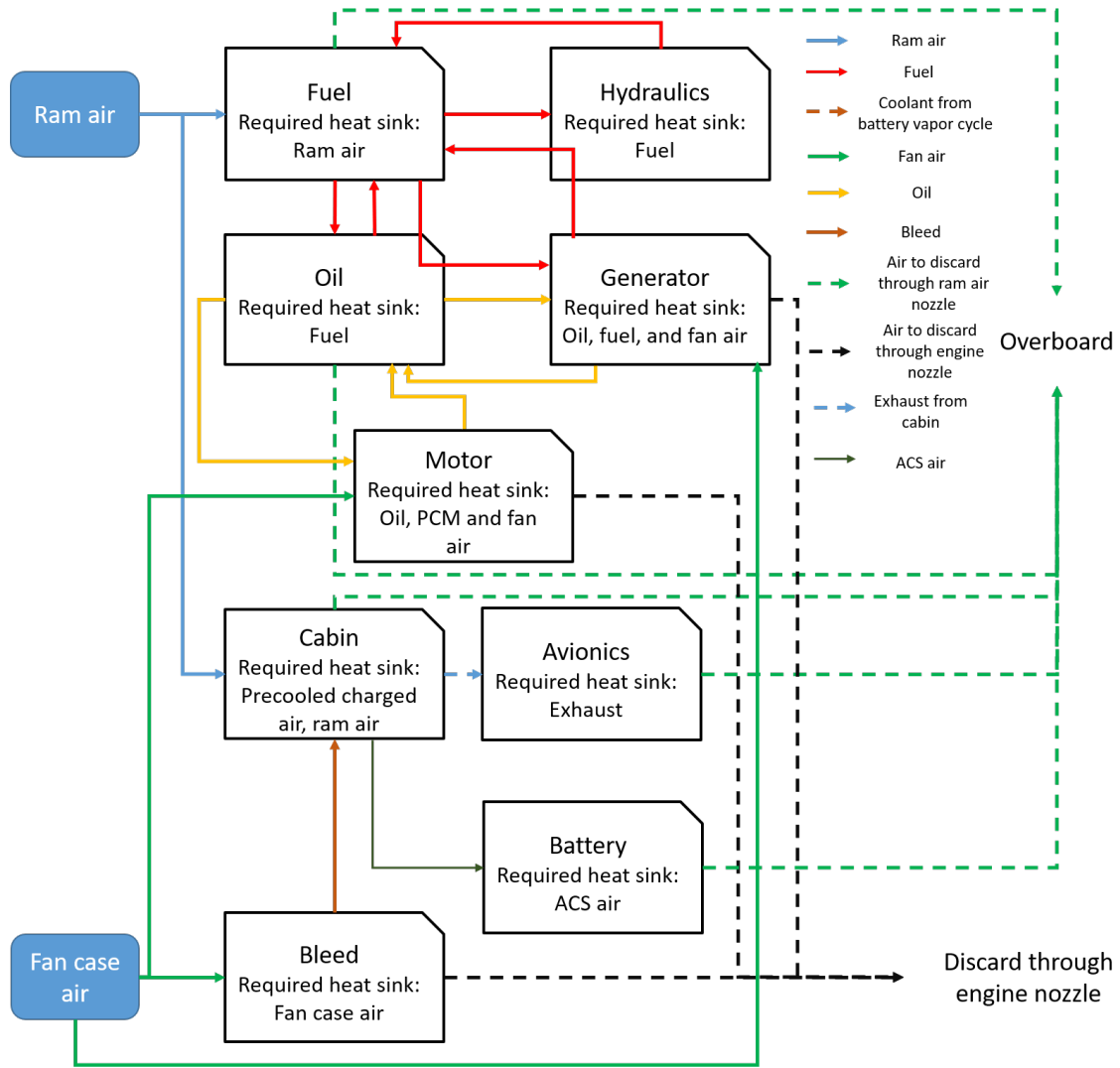


Figure 6.72: Global TMS with battery TMS design strategy 1 for hybrid missions

The local architectures selected using strategy 2 is the same as strategy 1, for all the loads. Thus, the global TMS architecture is also the same. The only difference is the ACS (cabin TMS or ECS) is resized to provide more air for the battery cooling. The local architectures selected using strategy 3 are also chosen the same as by using strategy 1, except the battery TMS. For this experiment on strategy 3, the requirement to construct an individual TMS is that the generated TMS architecture does not take heat sink from other local TMS, that is, the TMS using "Exhaust" or "ECS air", is not an option anymore. Due to this constraint, the optimal architecture candidates identified by the methods presented in chapter 5 can be distinguished in two types: 1. open-loop cooling with PCM, such ram



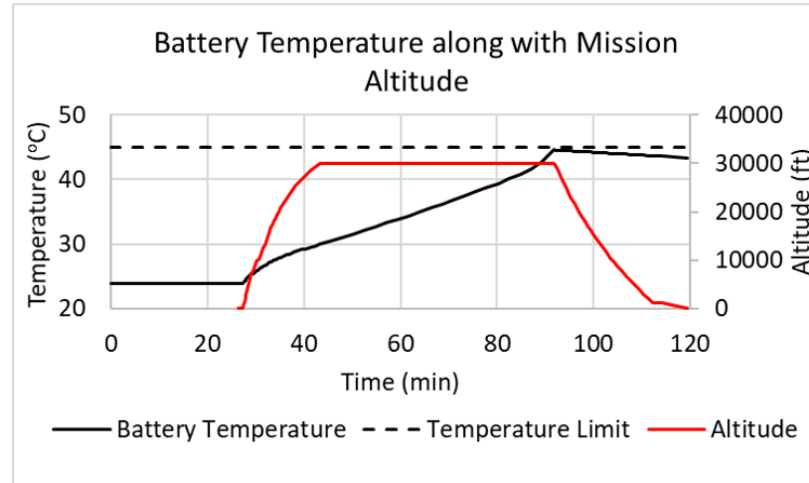


Figure 6.73: Battery temperature profile for selected typical mission with battery TMS strategy 1

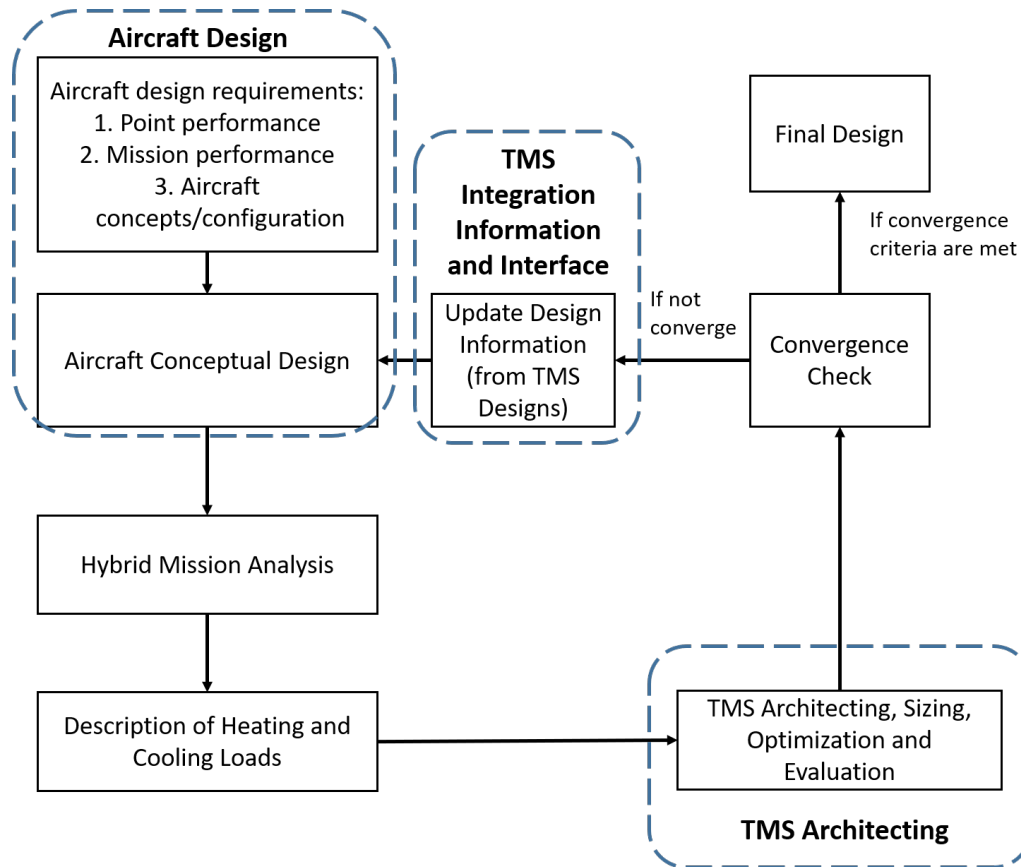


Figure 6.74: Updated integrated design loop of aircraft and TMS for hybrid aircraft

air cooling or fuel cooling plus PCM; 2. closed-loop heat pumps, such as vapor cycle and closed-loop air cycle. It should be noted that the open-loop air cycle, such as the ACS, is

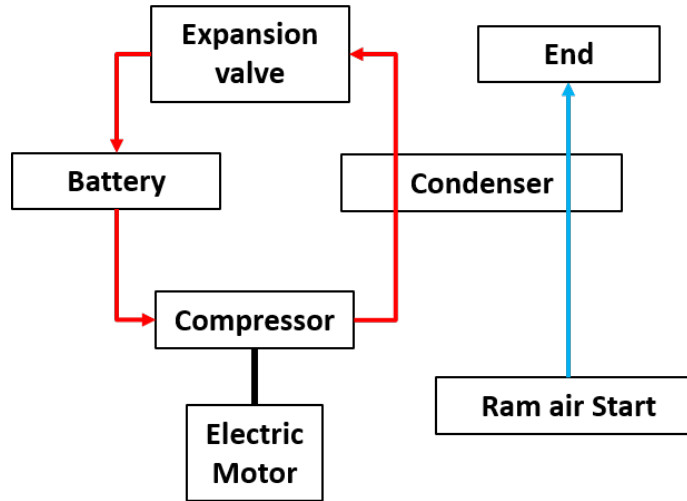


Figure 6.75: Battery TMS architecture using vapor cycle

not generated for the battery because such type of TMS is excluded by the requirements that only cabin uses a open-loop air cycle, which has been introduced in chapter 4. The option with PCM is not used, because usually the PCM is designed with battery, which should not be considered in the aircraft sizing phase. Therefore, for this experiment, the vapor cycle is selected for the strategy 3. In summary, strategy 2 still uses the ACS for cabin while resizing it, and strategy 3 uses an individually built vapor cycle. The architecture for strategy 2 is the same as shown in Figure 6.68 and Figure 6.69. The battery TMS architecture chosen for strategy 3 is illustrated in Figure 6.75.

With such chosen local TMS architectures, the final converged aircraft and TMS designs can be obtained. There are no changes in the architectures through the integrated design loop, because the chosen TMS architectures do not generate large weight penalty or power consumption to the overall system. Thus, there is no much power consumption in the electrical systems, including the electrical propulsion system. The obtained global TMS architecture of strategy 2 is still the same as the strategy 1 as shown in Figure 6.66. The global TMS architecture of strategy 3 is illustrated in Figure 6.76.

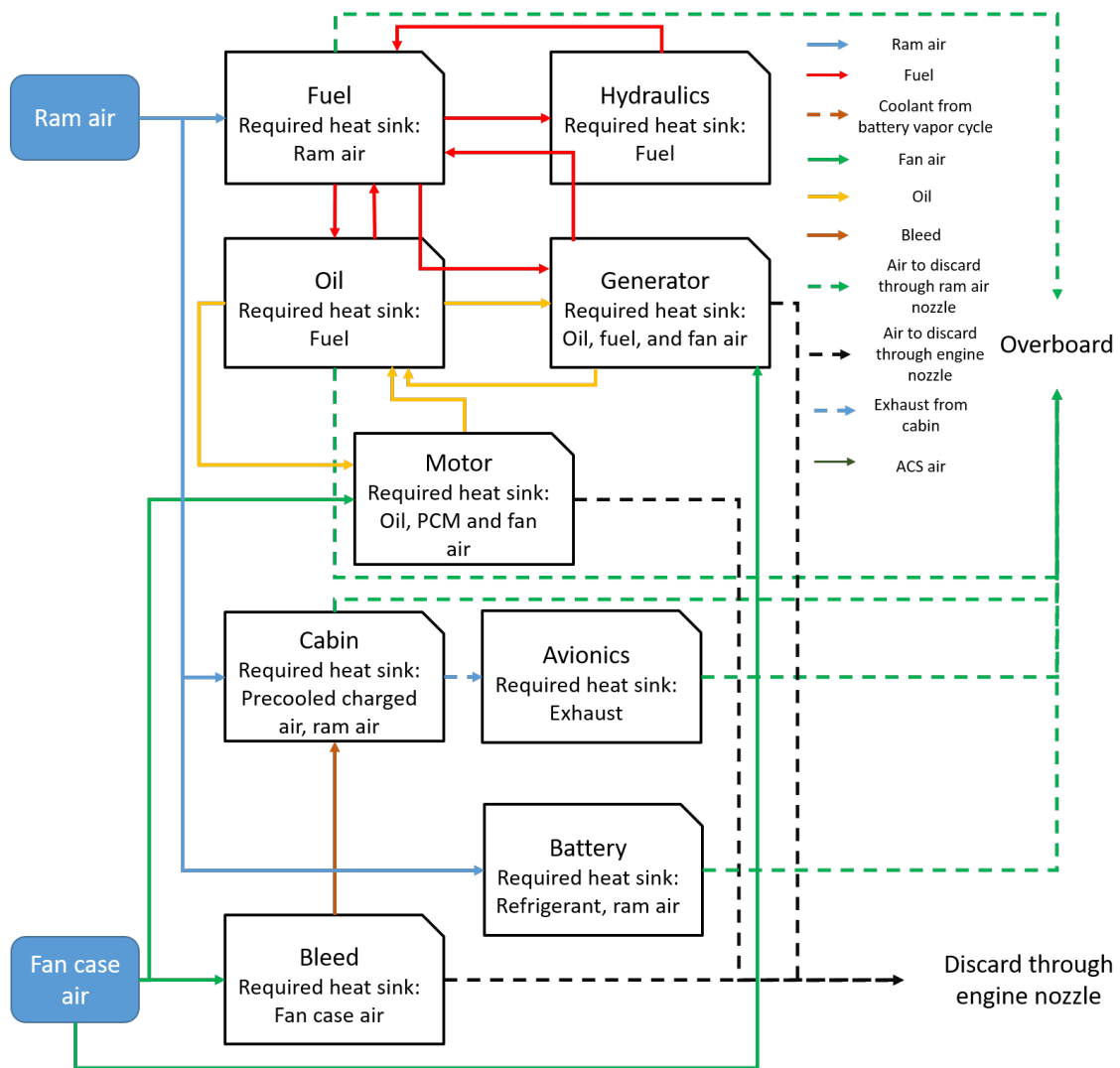


Figure 6.76: Global TMS for 78-pax HTeDP with battery installed: battery TMS strategy  
3

Comparing the aircraft with the TMS design solutions for three battery TMS strategies, the generator power, motor power, and battery power for the typical mission (normalized payload = 0.45, normalized range = 0.3) are shown in Figure 6.77, Figure 6.78, and Figure 6.79. The values in these figures are normalized by the values of the aircraft generated from strategy 1 of the same moment. From these results, it can be seen that the strategy 3 has the biggest increase in power consumption both generator and motor. This is because individually size a TMS is larger than resizing an existing TMS. In addition, it can be found that the strategy 3 has a larger impact on the generator than on the motor. This is because the motor power consumption is only influenced by the added weight due to adding the TMS, while the battery TMS for strategy 3 not only increase the weight, but also directly consumes more power for cooling. In Figure 6.79, the battery power becomes 0 when the aircraft starts to descend. The battery power is almost proportional to the motor power, because the power splits is determined by the propulsive power requirement. The corresponding battery temperature profiles are also presented in Figure 6.80. It is found that the three temperature curves are almost overlapped with each other, because all three strategies can cool the battery, and the cooling schedules are all optimized to minimize the required cooling power.

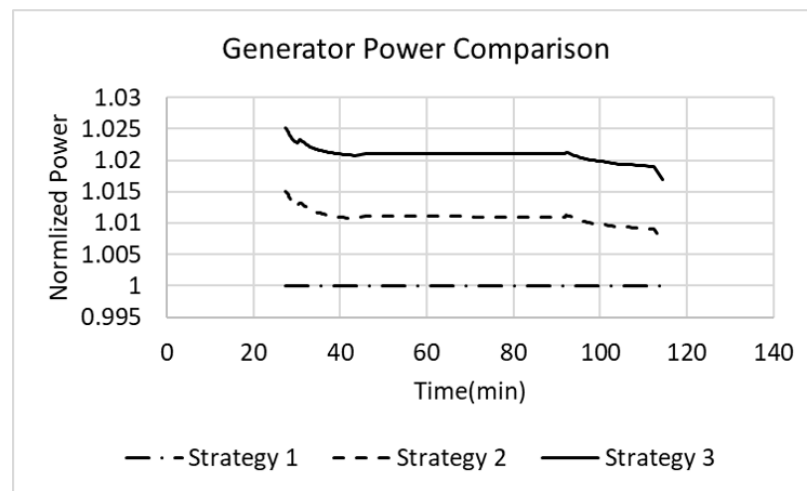


Figure 6.77: Generator power comparison for selected hybrid mission

However, the situation is different for the selected mission with shorter range (nor-

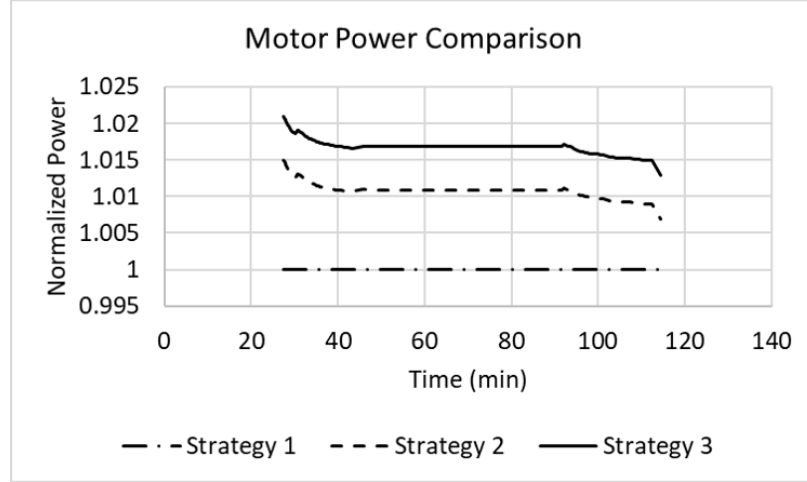


Figure 6.78: Motor power comparison for selected hybrid mission

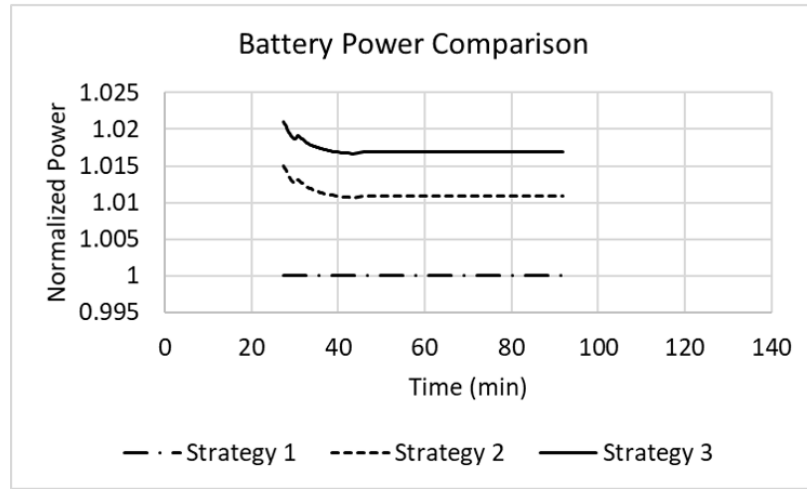


Figure 6.79: Battery power comparison for selected hybrid mission

malized range = 0.2, normalized payload = 0.3). The corresponding battery temperature profiles are shown in Figure 6.81. The battery temperature from TMS designed using strategy 2 and strategy 3 are below the temperature limit, since they are sized in terms of this mission. However, the battery TMS using strategy 1 cannot provide sufficient cooling capability to keep the battery under its maximum allowed temperature. This fact shows that although the TMS designed by strategy 1 has a smaller impact on the vehicle itself, such strategy can limit the feasible missions using hybrid power. Such effects are also shown in the next subsection.

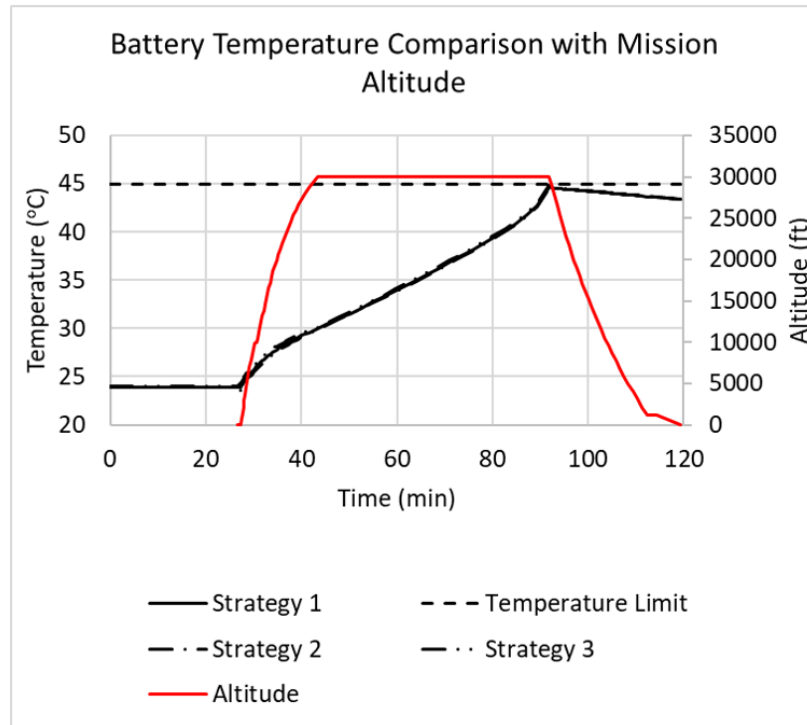


Figure 6.80: Battery temperature comparison for selected hybrid mission

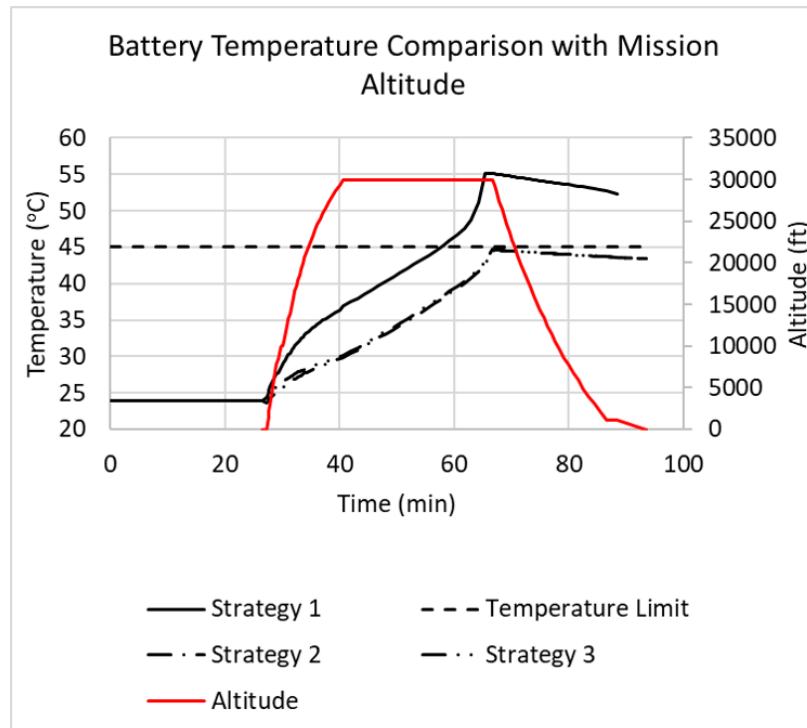


Figure 6.81: Battery temperature comparison for hybrid mission with shorter range

### *Performances of Converged Aircraft Designs*

Firstly the MTOW, OEW (battery is not included in OEW), and fuel weight for the selected typical mission are compared, which is shown in Figure 6.82. Obviously aircraft with all types of TMS solutions have penalties on weight and fuel burn. The TMS with existing ACS as the battery TMS has the lowest penalty, because the battery itself does not have any impacts on the MTOW or OEW, and it does not influence the already existed TMS. The TMS with resized ACS has the second largest impact on weight, since the turboshaft engine needs to be sized larger to provide more bleed. In addition, the size of the ACS itself also increases. The TMS with vapor cycle has the largest impacts on weight, because of the additional weight of the added components from the vapor cycle, as well as the need for a larger generator to provide the additional power for cooling. However, there is an interesting finding that the fuel weight of the selected typical mission for aircraft with resized ACS and vapor cycle are almost the same, although the weight penalty of aircraft with vapor cycle is larger. This is because resized ACS uses more bleed to cool the battery, and such bleed extraction is more detrimental to the engine than the shaft-power extraction which is used by the vapor cycle.

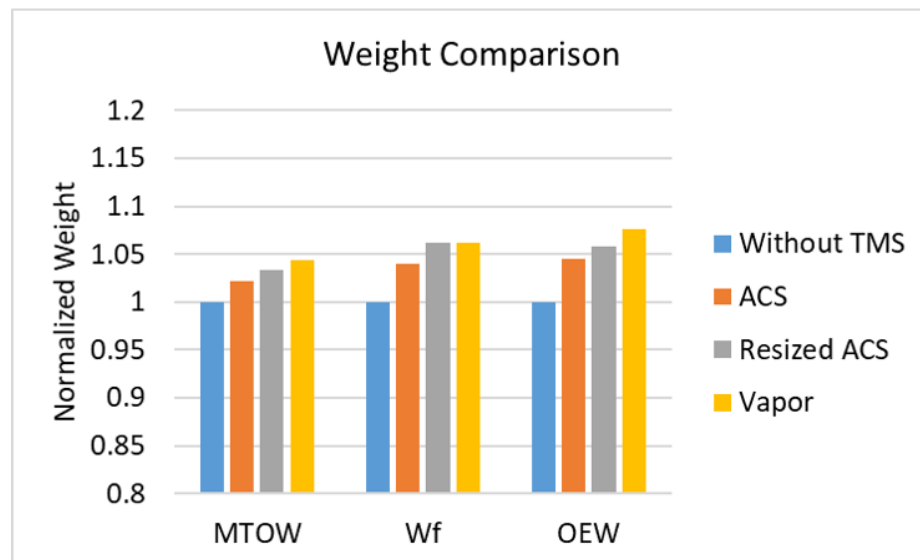


Figure 6.82: Weight comparison for aircraft with selected TMS

The corresponding  $\Delta$  block fuel burn for missions with different payloads and ranges for these three design solutions are shown in Figure 6.83, Figure 6.84, and Figure 6.85. These values are compared to the aircraft without TMS performing the same missions. Only missions with low payloads and short ranges are selected for the hybridization purpose. In addition to the  $\Delta$  block fuel burn, the battery temperature constraint is also plotted. The missions that are covered by the brown area are infeasible missions in terms of the battery temperature. It is seen that the fuel burn penalty by the strategy 1 is the smallest, due to non small impact of the battery TMS. The fuel burn penalty of strategy 3 is slightly higher than strategy 2, due to higher penalty weight. However, there are more infeasible missions for strategy 1 in terms of the battery temperature, because the cooling capability for the battery is limited by the originally sized ACS. In contrast, the TMS with strategy 2 and strategy 3 have a more larger feasible mission space. Therefore, it can be concluded here that although TMS design using strategy 1, which is to use existing TMS without resizing, can have minimal impacts on the aircraft fuel burn. However, the battery cooling capability is constrained by the originally sized TMS for other loads. Using strategy 2 and 3 will have larger influences on the block fuel burn and weight, but the operational missions are less limited.



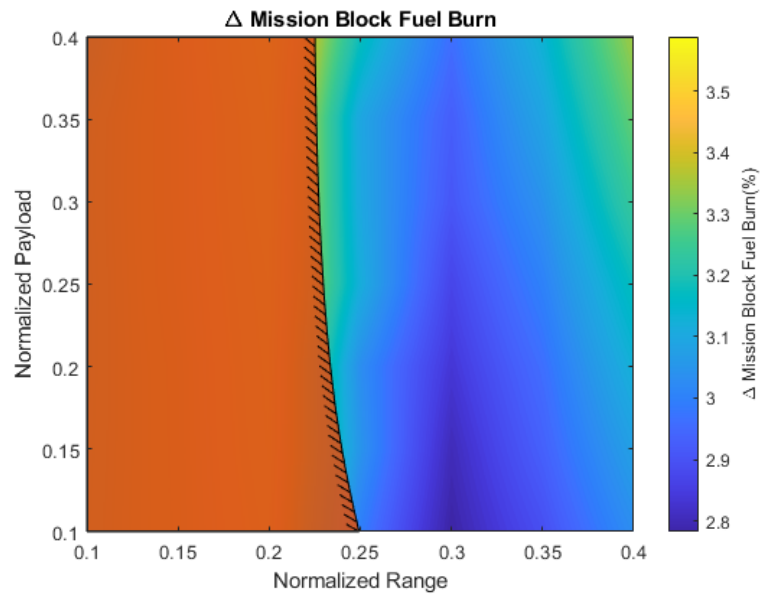


Figure 6.83:  $\Delta$  mission block fuel burn of aircraft with strategy 1

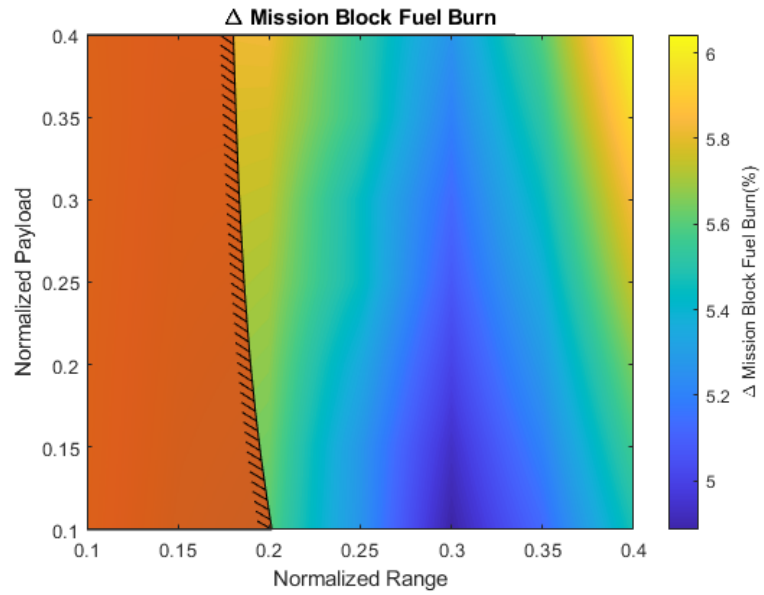


Figure 6.84:  $\Delta$  mission block fuel burn of aircraft with strategy 2

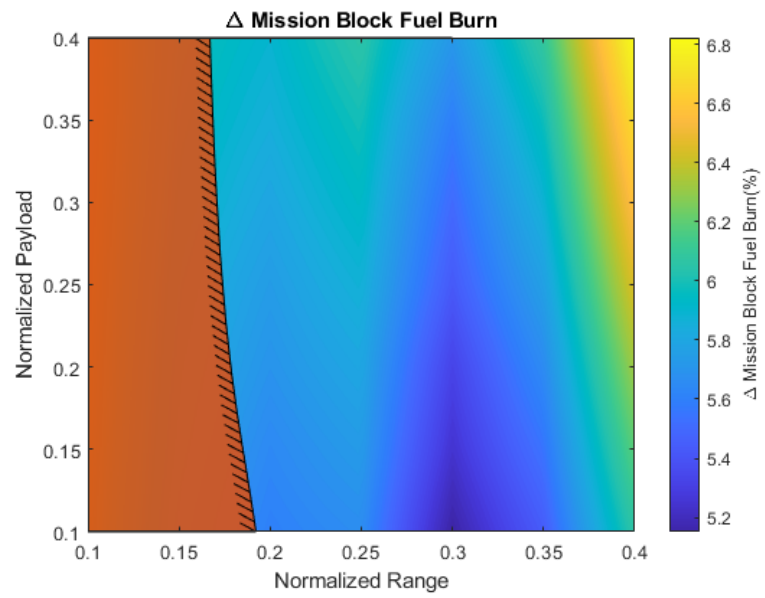


Figure 6.85:  $\Delta$  mission block fuel burn of aircraft with strategy 3

## 6.7 Conclusion for Experiment Set 3

### 6.7.1 Validation of Hypothesis 3

How the results from the Experiment Set 3 can validate the Hypothesis 3 are discussed in this section. The Research Question 3, Hypothesis 3, and the proposed criteria to validate the Hypothesis 3 are re-stated here as a reminder:

**Research Question 3:** *How can the interactions of thermal management systems architecting process and aircraft sizing process be identified, what are the differences between the initial solutions before resizing and the final converged solutions of both aircraft and TMS, and how to explain such differences?*

**Hypothesis 3:** The interactions of thermal management systems architecting process and design of aircraft can be identified by integration of the thermal management systems architecting process into the aircraft design loop, and differences between the converged design solutions and the initial solutions from the design loop can be discovered and explained through the proposed integrated process.

**Validation Criteria of Hypothesis 3:** The capability to feedback the influence of TMS architecting to vehicle level can be validated if the proposed integration methodology can update the design requirements for aircraft, TMS, and other subsystems, in terms of the initially designed TMS, thus leading to a design loop. The capability to compare the converged design solutions from the design loop with the ones generated using initial design requirements can be validated if the differences and corresponding explanations for such differences can be identified through the integrated analysis.

As the results obtained from the Experiment Set 3 show, the aircraft sizing requirements are updated using the fed back TMS information, and the TMS architecture requirements are also from the aircraft sizing process. For example, in the 160-pax SSA, the cabin thermal management load determines the feasible and optimal cabin TMS architectures. Then the selected cabin TMS architecture brings additional weight, ram drag, bleed off-

take, and shaft-power extraction of the aircraft sizing. Such impacts are fed back to the aircraft sizing process, leading to a larger size of the vehicle as well as its propulsion system. Using the 300-pax TeDP configuration as another example, both cryogenic and non-cryogenic TMS are investigated. Considering the cryogenic cooling option, the system becomes superconducting with this option, and the efficiencies of the electrical devices are also influenced significantly. Such changes in the efficiencies further affect the heat generation from the electrical components. Such interactions between the TMS and the aircraft systems leads to dramatically different aircraft in terms of if the cooling option is cryogenic or not. For the 78-pax HTeDP, different battery TMS strategies have been studied. The different strategies can lead to different optimal TMS architectures. And these TMS architectures can further determine the feasible missions for hybrid operations, in terms of the battery temperature. The interactions above which are identified from the integrated design loop demonstrate that the proposed integrated design methodology can update the design requirements among the vehicle, TMS, and other subsystems. And once the design loop is converged, then the final design solutions are obtained. Therefore, one of the criteria is validated.

Moreover, considering the integrated design process for the 300-pax TeDP configuration with closed-loop air cycle as the motor TMS, the initially architected generator TMS is different from the final design solution. The initial design uses fuel and fan air-cooled oil as the heat sink. However, due to increased power consumption from the motor TMS, the closed-loop air cycle, more heat is generated from the generator. And the initial generator TMS architecture cannot fulfill its thermal management functionality. Therefore, a PCM is added to absorb the excessive heat generated from the generator during early mission segments. Such difference between the initial and final TMS solutions, as well as the identified reasoning, satisfying the criteria to validate the capability to compare converged design solutions and solutions within the the design loop.

In summary, the Hypothesis 3 is validated by the Experiment Set 3, by using a 160-pax

SSA, a 300-pax TeDP, and a 78-pax HTeDP, by which the Research Question 3 is answered. Therefore, the sub-objective 3 is fulfilled, which is stated below:

**Sub-Objective 3:** To investigate the interactions between the TMS architecting process and the aircraft sizing process.

#### 6.7.2 Conclusions

In conclusion, an integrated design methodology of the aircraft and the TMS is proposed in this chapter, in which the thermal management requirements are derived from the aircraft sizing process, and the information of the TMS is also fed back to the aircraft sizing. When this design loop converges, the final design of the aircraft as well as the corresponding TMS are obtained.

This proposed integrated design methodology addresses the Research Question 3 and Hypothesis 3 by conducting the Experiment Set 3. And it further fulfills the sub-objective 3 of the whole thesis. In this experiment set, a 160-pax SSA, a 300-pax TeDP configuration with either cryogenic or non-cryogenic cooling, and a non-cryogenic HTeDP configuration are designed using the proposed integrated design process with selected thermal loads. It is demonstrated that the proposed methodology is able to identify the interactions among the aircraft and TMS design. This integrated design methodology can also provide explanations on how the optimal TMS architectures change through iterations.

## **CHAPTER 7**

### **CONCLUSIONS, CONTRIBUTIONS, AND RECOMMENDATIONS FOR FUTURE WORK**

This chapter concludes the dissertation by reviewing the overall thesis, and then presenting the conclusions and a summary of contributions. Finally, recommendations for future research avenues are also discussed.

#### **7.1 Overview of the Thesis**

Thermal management systems (TMS's) are to ensure correct functioning of devices as well as safety and comfort of passengers and crews. In addition to the functionality of the TMS, it also has a large impact on the aircraft performance. Therefore, the design and architecting of the TMS are important. Moreover, heating problems are becoming more severe in commercial applications due to trends of electrification of subsystems and propulsion systems. These changes correspond to new aircraft concepts such as More-Electric Aircraft, Turbo-electric Distributed Propulsion Systems, and hybrid aircraft. However, due to the lack of data of these novel configurations, empirical methods are not applicable any more. Motivated by such challenges, the overarching research objective of this thesis is proposed: To develop a thermal management systems architecting methodology suitable for conceptual design phase of commercial aircraft, which is capable of handling increasing cooling loads and emerging aircraft concepts with limited historical data and information available during early design stage.

Observing that there is no methodology that can systematically generates intuitive and non-intuitive thermal management system architectures, the first sub-objective is formulated: to develop a capability of the proposed method that sufficiently explores the thermal management systems architecture space by systematically identifying both intuitive

and non-intuitive architectures. Realizing the number of generated TMS architectures is too large, the second sub-objective is proposed: to develop a capability of the proposed method that rapidly narrows down the architecture space to a suitable number of candidates to perform further optimal architecture down-selection in terms of chosen metrics, using information and methods suitable for conceptual design. Driven by the fact that the thermal management solution may influence the vehicle design greatly by adding additional weight or ram drag, or extracting more bleed and power, the third sub-objective is composed: to investigate the impacts of thermal management systems architecting process on the final converged design solutions of the aircraft and subsystems.

Three research questions are then asked to address these three sub-objectives, one for each. They are summarized below:

**Research Question 1 - Sub-Objective 1:** *With given potential heating and cooling load descriptions and aircraft concepts, how can the thermal management systems architecture space be populated, without over-conservatism that eliminates unconventionally but potentially optimal architectures?*

**Research Question 2 - Sub-Objective 2:** *With a number of thermal management systems architecture candidates, how can the architecture evaluation process rapidly filter out inviable architectures, and perform further down-selection of optimal architectures on the remaining competent architectures based on chosen metrics, where the information required are suitable for conceptual design phase with limited historical data?*

**Research Question 3 - Sub-Objective 3:** *How can the interactions of thermal management systems architecting process and aircraft sizing process be identified, and what are the differences between the initial solutions before resizing and the final converged solutions of both aircraft and TMS, and how to explain such differences?*

Three Hypotheses are also made to address the research questions, one for each:

**Hypothesis 1:** The architecture space of thermal management system architectures can be populated without over-conservatism by using a behavior-based backtracking thermal

management system architecting methodology.

**Hypothesis 2:** Large number of infeasible or non-optimal architectures can be eliminated by filtering process in terms of feasibility and low-fidelity subsystem-level analysis on key performance indicators, and further down-selection of optimal architectures can be done by evaluations using physics-based optimization, sizing, and analysis, where the physics-based models are created automatically from the architecture descriptions.

**Hypothesis 3:** The interactions of thermal management systems architecting process and design of aircraft can be identified by integration of the thermal management systems architecting process into the aircraft design loop, and differences between the converged design solutions and the initial solutions from the design loop can be discovered and explained through the proposed integrated process.

Three sets of experiments are designed to validate the hypotheses. A 160-pax single-isle small aircraft, a 300-pax turbo-electric distributed propulsion system configuration, and a 78-pax hybrid turbo-electric distributed propulsion system configuration, along with the thermal loads on them, are used in these experiments. These experiments using proposed experimental methodologies successfully validate the proposed hypotheses, further fulfilling the three sub-objectives, leading to the fulfillment of the overarching objective.

## 7.2 Conclusions

To conduct the designed experiments, three experimental methodologies are proposed. For the Experiment Set 1, a methodology to systematically populate both intuitive and non-intuitive TMS architectures at both global and local levels is formulated. This proposed method constructs the TMS architectures following the fundamental physics thermal cycles. It firstly create the behavioral architectures, and then converts them to structural architectures. This conversion is archived by enumerating components that are compatible for each behavior. The backtracking algorithm is used to systematically enumerate TMS solutions while ensuring the compatibility of each behavior and components.



From the results obtained in the Experiment Set 1, it is discovered that some of the generated local TMS architectures match the existing ones in the literature, and others are less commonly discussed in previous works. In addition, the number of generated TMS architectures at either the global level or the local level is very large - at the order that is larger than one hundred thousand architectures. This proposed methodology addresses the Research Question 1 and Hypothesis 1 by conducting the Experiment Set 1. And it further fulfills the sub-objective 1 of the whole thesis. Through the Experiment Set 1, a 160-pax conventional concept, a 300-pax TeDP concept, and a 78-pax HTeDP concept are used to validate the capability of the proposed method, which further validate the Hypothesis 1. It is demonstrated that the proposed behavior-based backtracking TMS architecting methodology is able to populate the intuitive architectures, which match existing ones in the literature, and it is also able to populate the non-intuitive architectures that have not been seen.

For the Experiment Set 2, an optimal down-selection methodology of the TMS architecture space is proposed, which is based on the feasibility of the TMS at the critical operation condition and low-fidelity subsystem-level key performance indicators (KPIs) at the cruise condition. The selected KPIs are bleed off-take, shaft-power extraction, ram air intake, and weight penalty. This proposed methodology firstly filters out architectures using the feasibility, then evaluates the KPIs of each architecture using a low-fidelity approach. The obtained KPIs are grouped using clustering method to further reduce the number of architecture candidates. Then physics-based models are constructed automatically using the architecture descriptor that is generated from Experiment Set 1. Finally, the constructed models are sized and optimized through a proposed multi-design point (MDP) sizing and optimization methodology.

As the results from Experiment 2.1 show, many infeasible TMS architectures can be rapidly filtered out. For example, for the cabin TMS, the number of generated TMS architectures is 1362240, and this number can be reduced to 86189 within 2 minutes. These

results validate the capability of the proposed feasibility-based filtering method and it can rapidly filter out a large number of architectures in terms of the feasibility. As the results obtained in Experiment 2.2 and 2.3, still using cabin TMS as an example, the number of architectures is further reduced to 4 in terms of the selected four KPI: bleed off-take, shaft-power extraction, ram air intake, and weight. The performance of the KPI evaluation program is similar to the feasibility-based filtering process. This clustering-based filtering approach can also be applied to the global TMS to narrow down the architecture space. Therefore, the architecture space can be further reduced by the low-fidelity KPI clustering-based filtering methodology. Thus, combining the capability of methods for Experiment 2.1, 2.2 and 2.3, one of the criteria to validate the Hypothesis 2, "large number of inviable architecture candidates can be eliminated from the feasibility-based low-fidelity KPI-based filtering process", is met, validating the capability of the proposed methodology. From the results shown by Experiment 2.4, it can be seen that the physics-based models can be automatically constructed in the NPSS environment using the descriptors generated from the Experiment Set 1. MDP sizing and optimization can be further performed on these constructed models, as shown in Experiment 2.5. Combining both Experiment 2.4 and Experiment 2.5, one of the criteria, "If the model can be automatically constructed from the architecture descriptors generated from Experiment Set 1, which the optimization and sizing process can be directly performed on", is met. In summary, the two criteria stated to validate the Hypothesis 2 are satisfied by showing results from Experiment 2.1, 2.2, 2.3, 2.4, and 2.5. Therefore, the Hypothesis is validated. Thus, the Research Question 2 is answered and the sub-objective 2 is fulfilled.

In conclusion, this proposed methodology addresses the Research Question 2 and Hypothesis 2 by conducting the Experiment Set 2. And it further fulfills the sub-objective 2 of the whole thesis. In this experiment set, the cabin from a 160-pax SSA, the motor from a 300-pax non-cryo TeDP concept, and the battery from a 78-pax non-cryo HTeDP concept, are used for the experiments on local TMS architectures. These three aircraft configurations

are also used to conduct experiments on the global TMS architectures. It is demonstrated that the proposed methodology is able to rapidly filter out infeasible and non-optimal TMS architectures in terms of low-fidelity KPI, and can further perform a higher-fidelity sizing and optimization on the automatically constructed models. The demonstrated capability also validates the Hypothesis 2.

For the Experiment Set 3, an integrated design methodology of the aircraft and the TMS is proposed, in which the thermal management requirements are derived from the aircraft sizing process, and the information of the TMS is also fed back to the aircraft sizing. When this design loop converges, the final design of the aircraft as well as the corresponding TMS are obtained.

As the results obtained from the Experiment Set 3 show, the aircraft sizing requirements are updated using the TMS information that is fed back, and the TMS architecture requirements are also revised from the aircraft sizing process. For example, in the 160-pax SSA, the cabin thermal management load determines the feasible and optimal cabin TMS architectures. Then the selected cabin TMS architecture brings additional weight, ram drag, bleed off-take, and shaft-power extraction of the aircraft sizing. Corresponding impacts are looped back to the aircraft sizing process, leading to a larger size of the vehicle as well as its propulsion system. Using the 300-pax TeDP configuration as another example, both cryogenic and non-cryogenic TMS are investigated. Considering the cryogenic cooling option, the system becomes superconducting with this option, and the efficiencies of the electrical devices are also influenced significantly. The changes in the efficiencies further affect the heat generation from the electrical components. The interactions between the TMS and the aircraft systems lead to dramatically different aircraft designs depending on if the cooling option is cryogenic or not. For the 78-pax HTeDP, different battery TMS strategies have been studied. The different strategies can result in different optimal TMS architectures. And these TMS architectures can further determine the feasibility for hybrid missions, in terms of the battery temperature. The interactions that are identified from the

integrated design loop demonstrate that the proposed integrated design methodology can update the design requirements among the vehicle, TMS, and other subsystems. And once the design loop is converged, then the final design solutions are obtained. Therefore, one of the criteria to validate Hypothesis 3 is met. Moreover, considering the integrated design process for the 300-pax TeDP configuration with closed-loop air cycle as the motor TMS, the initially architected generator TMS is different from the final design solution. The initial design uses fuel and fan air-cooled oil as the heat sink. However, due to increased power consumption from the motor TMS, the closed-loop air cycle, more heat is generated from the generator. The initial generator TMS architecture cannot fulfill its updated thermal management functionality. Therefore, a PCM is added to absorb the excessive heat generated from the generator during early mission segments. These differences between the initial and final TMS solutions, as well as the identified reasoning, satisfy the criteria to validate the capability to compare converged design solutions and solutions within the the design loop.

This proposed integrated design methodology addresses the Research Question 3 and Hypothesis 3 by conducting the Experiment Set 3. And it further fulfills the sub-objective 3 of the whole thesis. In this experiment set, a 160-pax SSA, a 300-pax TeDP configuration with either cryogenic or non-cryogenic cooling, and a non-cryogenic HTeDP configuration are designed using the proposed integrated design process with selected thermal loads. It is demonstrated that the proposed methodology is able to identify the interactions among the aircraft and TMS design. This integrated design methodology can also provide explanations on how the optimal TMS architectures change through iterations.

With these three sub-objectives fulfilled, the overarching research objective, "to develop a thermal management systems architecting methodology suitable for conceptual design phase of commercial aircraft, which is capable of handling increasing cooling loads and emerging aircraft concepts with limited historical data and only information available during early design stage", can then be met.

### 7.3 Contributions

The primary contributions of this thesis are the three experimental methods, of which the description and capabilities are summarized below. Some of other findings are also included.

1. The behavior-based backtracking TMS architecting methodology in Experiment Set 1: This methodology uses the behaviors following the fundamental physics to avoid using empirical relations or historical data. The systematic architecture generation capability is realized by the backtracking process. With this behavior-based backtracking TMS architecting, a large number of TMS can be systematically populated without over-conservatism, to expand the TMS architecture space.
2. The feasibility-based and low-fidelity KPI clustering-based filtering methodology in Experiment Set 2: As commonly required in the conceptual design phase, the computational cost should be rather small to conduct parametric analysis. This proposed methodology following a recursive manner can rapidly filter out infeasible TMS architectures by using the best performances of the components. Similarly, the KPI of each TMS are computed using a low-fidelity approach, enabling rapid evaluation of a large number of cases. Then a clustering-based filtering approach is proposed to further narrow down the architecture space.
3. In addition to the filtering process, a multi-design point (MDP) sizing and optimization methodology is also a very important contribution: This MDP method optimizes the performances of the TMS as well as ensuring all the constraints at different operation conditions are satisfied.
4. Automatic creation of the physics-based model: this model creation process automatically reads in TMS architecture descriptor and re-write them as NPSS model

files. Although it is fundamentally a read-write process, it greatly reduces the manual effort to construct the models for further analysis.

5. The integrated design methodology for Experiment Set 3: this methodology presents a design framework, which incorporates the proposed methodologies in Experiment Set 1 and Experiment Set 2 into the aircraft and TMS sizing loop. Through this integrated design loop, the interactions between the aircraft sizing and TMS design can be identified. It should be also noted that the purpose of this integrated design process is not to identify the best TMS architectures. Instead, it is to help the designers to identify a set of potential optimal candidates. With such insights, the designers can perform further higher-fidelity analysis and more detailed design.
6. In addition to the integrated design process, the proposed way to update the battery TMS requirement is also a contribution. This proposed approach determines what should be done if a certain load is not sized along with the aircraft. This approach is simply described as to perform the aircraft sizing first, and then perform the sizing condition of this load.

#### **7.4 Recommendations for Future Work**

Although the presented methodologies as well as the designs of experiments are sufficient to demonstrate the hypotheses and to fulfill the sub and overarching research objectives, there are still other research avenues that can improve the current methodologies:

1. The first one is to improve the visualization of the TMS architectures. Currently, the generated TMS architectures are store in the form of lists, which can be easily used in computer. However, it is difficult to be visualized. All the illustrations in this dissertation are made by manual efforts. To give the users a more intuitive understanding of the generated TMS architecture, an automatic program is needed to visualize the TMS architectures.

2. The second research avenue is the uncertainty quantification of the generated TMS. In this study, it should be noted that all the values are deterministic. However, in reality, such models are all created with certain uncertainties. Therefore, to truly determine an optimal TMS design, uncertainties need to be considered. Therefore, this architecting methodology can be greatly improved if uncertainties can be captured in the future work.
3. The third one is to improve the optimization speed. It should be noted that even with simpler TMS architectures, a multi-objective optimization is computationally expensive. Therefore, an approach to speed up the optimization process is needed. A current thought on this issue is to use parallel computation to accelerate the optimization process. The parallel computation would work because the current selected optimization methodology is based on Genetic Algorithm.
4. The fourth one is also related to the optimization process, but it is not on the optimization computation itself. To speed up the optimization, surrogate models may be of interest. However, the effort to construct the surrogate models should also be considered. Therefore, an efficient design of experiments is needed to populate the training data.
5. Another limitation of this dissertation is that the modeling and analysis of the TMS architectures only use steady-state approach without incorporating transient controller models. Therefore, one of the future research avenue is to convert the constructed steady-state models to transient models. The corresponding controller architecture and control logic should also be studied.
6. The last thought on future work is the modeling improvement on the superconducting electrical systems. For the current application, the efficiencies are fixed constant based on literature. And the corresponding power consumption and weight are dependent on regression equations. Therefore, a higher-fidelity modeling of the su-

perconducting system as well as the cryogenic cooling architectures are needed. In addition, the fidelity of the turboshaft engine that burns the liquid Hydrogen also needs to be improved.



# **Appendices**

## APPENDIX A

### PHASE CHANGE MODELING EQUATIONS AND PARAMETERS

#### A. Relative Humidity Calculation Equations

The equations to compute RH are presented below [133]:

$$v = 1 - \frac{T_k}{T_{crit}} \quad (\text{A.1})$$

$$P_{vp} = \frac{1000P_{hpa}WAR}{B + 1000WAR} \quad (\text{A.2})$$

$$\xi = C_0v + C_1v^{1.5} + C_2v^{3.5} + C_4v^4 + C_5v^7 \quad (\text{A.3})$$

$$P_{ws} = P_{crit}e^{\xi \frac{T_{crit}}{T_k}} \quad (\text{A.4})$$

$$\alpha = A_0 + A_1(T_k - 273) + A_2(T_k - 273)^2 + A_3(T_k - 273)^3 \quad (\text{A.5})$$

$$\lambda = B_0 + B_1(T_k - 273) + B_2(T_k - 273)^2 + B_3(T_k - 273)^3 \quad (\text{A.6})$$

$$\beta = e^{\lambda} \quad (\text{A.7})$$

$$f = e^{\alpha(1 - \frac{P_{ws}}{P_{vp}}) + \beta(1 - \frac{P_{ws}}{P_{vp}})} \quad (\text{A.8})$$

$$RH = 100 \frac{P_{vp}}{P_{ws}f} \quad (A.9)$$

where  $T_k$  is the temperature of the air sample (in kelvin),  $P_{hpa}$  is the pressure of the air sample (in hecto-pascals),  $T_{crit}=647.096 \text{ K}$  is the critical temperature,  $P_{crit}=220,640 \text{ hPa}$  is the critical pressure,  $B=621.9907 \text{ g/kg}$  is the ratio of molecular weight of water to molecular weight of air,  $P_{vp}$  is the pressure of water vapor (in hecto-pascals),  $P_{ws}$  is the saturation vapor pressure (in hecto-pascals), and  $f$  is an enhancement factor accounting for change in saturation vapor pressure in air versus in vacuum. The coefficients in the above equation system are summarized in Table Table A.1.

Table A.1: List of coefficients for calculating RH

$A_0 = 3.536e^{-4}$	$A_1 = 2.932e^{-5}$	$A_2 = 2.932e^{-5}$	$A_3 = 8.575e^{-9}$
$B_0 = -10.7588$	$B_1 = 6.325e^{-2}$	$B_2 = 2.536e^{-4}$	$B_3 = 6.338e^{-7}$
$C_0 = -7.8595$	$C_1 = -1.8441$	$C_2 = -11.7866$	$C_3 = 22.6807$
$C_4 = -15.9619$	$C_5 = 1.8012$		

## B. Enthalpy Calculation Equations

The following ASHRAE relationships [134] are used to compute the specific enthalpies of dry air  $h_{da}$ , saturated water vapor  $h_{wv}$ , and saturated liquid water  $h_{lw}$  as a function of temperature  $t_c$  (in degrees Celsius):

$$h_{da}(t_c) = 1.006t = At_c \left[ \frac{kJ}{kg(dryair)} \right] \quad (A.10)$$

$$h_{wv}(t_c) = 2501 + 1.805t = B + Ct_c \left[ \frac{kJ}{kg(water)} \right] \quad (A.11)$$

$$h_{lw}(t_c) = 4.186t = Dt_c \left[ \frac{kJ}{kg(water)} \right] \quad (A.12)$$

Using the temperature and pressure of the moist air and a  $RH = 100\%$ , the saturation WAR is first computed using WAR calculation function introduced before:  $WAR_{sat} = WAR_{Cales}(P, T, 100)$ . This allows the WAR corresponding to water vapor and liquid water to be computed as

$$WAR_{vap} = \min(WAR_{sat}, WAR) \quad (A.13)$$

$$WAR_{liq} = WAR - WAR_{vap} \quad (A.14)$$

Using the definitions of  $WAR_{vap}$  and  $WAR_{liq}$ , the mass of dry air  $M_{da}$ , water vapor  $M_{wv}$  and liquid water  $M_{lw}$  present in a total mass  $M_{ma}$  of moist air is computed as

$$M_{da} = M_{ma} \left( \frac{1}{1 + WAR} \right) \quad (A.15)$$

$$M_{wv} = M_{da} WAR_{vap} \quad (A.16)$$

$$M_{lw} = M_{da} WAR_{liq} \quad (A.17)$$

The enthalpy of the moist air stream  $H_{ma}$  is then built up as the sum of the enthalpy of dry air, water vapor, and liquid water (if present):

$$H_{da}(t_c) = M_{da} h_{da}(t_c) \quad (A.18)$$

$$H_{wv}(t_c) = M_{wv} h_{wv}(t_c) \quad (A.19)$$

$$H_{lw}(t_c) = M_{lw} h_{lw}(t_c) \quad (A.20)$$

$$H_{ma}(t_c) = H_{da}(t_c) + H_{wv}(t_c) + H_{lw}(t_c) \quad (\text{A.21})$$

## REFERENCES

- [1] I. Moir and A. Seabridge, *Aircraft Systems: Mechanical, electrical, and avionics subsystems integration*. John Wiley & Sons, 2011, vol. 52.
- [2] ———, *Design and development of aircraft systems*. John Wiley & Sons, 2012, vol. 67.
- [3] D. Schlabe and J. Lienig, “Model-based thermal management functions for aircraft systems,” in *SAE 2014 Aerospace Systems and Technology Conference*, 2014.
- [4] J. V. Vargas and A. Bejan, “Thermodynamic optimization of finned crossflow heat exchangers for aircraft environmental control systems,” *International Journal of Heat and Fluid Flow*, vol. 22, no. 6, pp. 657–665, 2001.
- [5] J. Roskam, *Airplane Design: Part 5-Component Weight Estimation*. DARcorporation, 1985.
- [6] E. Walters, M. Amrhein, T. O’Connell, S. Iden, P. Lamm, K. Yerkes, M. Wolff, K. McCarthy, B. Raczkowski, J. Wells, *et al.*, “Invent modeling, simulation, analysis and optimization,” in *48th AIAA Aerospace Sciences Meeting Including the New Horizons Forum and Aerospace Exposition*, 2010, p. 287.
- [7] R. Roberts and S. Eastbourn, “Vehicle level tip-to-tail modeling of an aircraft,” *International Journal of Thermodynamics*, vol. 17, no. 2, pp. 107–115, 2014.
- [8] R. A. Roberts and D. D. Decker, “Energy optimization of an aircraft focused on component sizing and control architecture interactions,” in *11th International Energy Conversion Engineering Conference*, 2013, p. 3805.
- [9] R. Roberts, S. Eastbourn, and A. Maser, “Generic aircraft thermal tip-to-tail modeling and simulation,” in *47th AIAA/ASME/SAE/ASEE Joint Propulsion Conference & Exhibit*, 2011, p. 5971.
- [10] J. S. Cloyd, “A status of the united states air force’s more electric aircraft initiative,” in *IECEC-97 Proceedings of the Thirty-Second Intersociety Energy Conversion Engineering Conference (Cat. No. 97CH6203)*, IEEE, vol. 1, 1997, pp. 681–686.
- [11] J. Engelland, “The evolving revolutionary all-electric airplane,” *IEEE Transactions on Aerospace and Electronic Systems*, no. 3, pp. 217–220, 1984.
- [12] D. P. Rubertus, L. D. Hunter, *et al.*, “Electromechanical actuation technology for the all-electric aircraft,” *IEEE Transactions on Aerospace and Electronic Systems*, no. 3, pp. 243–249, 1984.

- [13] I. Chakraborty, "Subsystem architecture sizing and analysis for aircraft conceptual design," Ph.D. dissertation, Georgia Institute of Technology, 2015.
- [14] J. J. Treacy, "Flight safety issues of an all-electric aircraft," *IEEE Transactions on Aerospace and Electronic Systems*, no. 3, pp. 227–233, 1984.
- [15] I. Staack, H. Ellström, M. Bergman, P. Sarwe, and P. Krus, "More electrical environmental control system simulation," in *28th Congress of the International Council of the Aeronautical Sciences (ICAS 2012), 23-28 September 2012, Brisbane, Australia*, ICAS, 2012.
- [16] N. Seki, N. Morioka, H. Saito, and H. Oyori, "A study of air/fuel integrated thermal management system," SAE Technical Paper, Tech. Rep., 2015.
- [17] J. Felder, H. Kim, and G. Brown, "Turboelectric distributed propulsion engine cycle analysis for hybrid-wing-body aircraft," in *47th AIAA aerospace sciences meeting including the new horizons forum and aerospace exposition*, 2009, p. 1132.
- [18] C. Ross, M. Armstrong, M. Blackwelder, C. Jones, P. Norman, and S. Fletcher, "Turboelectric distributed propulsion protection system design trades," *SAE ASTC*, 2014.
- [19] J. Welstead and J. L. Felder, "Conceptual design of a single-aisle turboelectric commercial transport with fuselage boundary layer ingestion," in *54th AIAA Aerospace Sciences Meeting*, 2016, p. 1027.
- [20] J. Felder, H. Kim, G. Brown, and J. Kummer, "An examination of the effect of boundary layer ingestion on turboelectric distributed propulsion systems," in *49th AIAA aerospace sciences meeting including the new horizons forum and aerospace exposition*, 2011, p. 300.
- [21] C. Liu, G. Doulgeris, P. Laskaridis, and R. Singh, "Thermal cycle analysis of turboelectric distributed propulsion system with boundary layer ingestion," *Aerospace Science and Technology*, vol. 27, no. 1, pp. 163–170, 2013.
- [22] M. Shi, M. Pokhrel, J. Gladin, E. Garcia, and D. N. Mavris, "Model fidelity requirements in boundary layer ingestion propulsion system conceptual design," *18th AIAA Aviation Technology, Integration, and Operations Conference, AIAA AVIATION Forum*, AIAA 2018-3835, 2018.
- [23] M. Shi, M. Pokhrel, J. C. Gladin, E. Garcia, and D. N. Mavris, "Modeling fidelity requirements of mission-level analysis on boundary layer ingestion propulsion system," *AIAA Scitech 2019 Forum*, AIAA 2019-1590, 2019.

- [24] M. Pokhrel, M. Shi, J. Ahuja, J. Gladin, and D. N. Mavris, “Conceptual design of a bli propulsor capturing aero-propulsive coupling and distortion impacts,” *AIAA Scitech 2019 Forum*, AIAA 2019-1588, 2019.
- [25] NASA, “Hybrid wing body goes hybrid,” *NASA Official Website*, 2013, online: <https://www.nasa.gov/content/hybrid-wing-body-goes-hybrid>, accessed March. 9, 2021.
- [26] C. Müller, D. Scholz, and T. Giese, “Dynamic simulation of innovative aircraft air conditioning,” *DGLR: Deutscher Luft-und Raumfahrtkongress. Bonn: Deutsche Gesellschaft für Luft-und Raumfahrt*, 2007.
- [27] J. W. Pratt, L. E. Klebanoff, K. Munoz-Ramos, A. A. Akhil, D. B. Curgus, and B. L. Schenkman, “Proton exchange membrane fuel cells for electrical power generation on-board commercial airplanes,” *Applied energy*, vol. 101, pp. 776–796, 2013.
- [28] C. Perullo, A. Alahmad, J. T. Wen, M. D’Arpino, M. Canova, D. N. Mavris, and M. Benzakein, “Sizing and performance analysis of a turbo-hybrid-electric regional jet for the nasa uli program,” *2019 AIAA/IEEE Electric Aircraft Technologies Symposium (EATS)*, AIAA 2019-4490, 2019.
- [29] C. Perullo, M. Shi, G. Cinar, A. Alahmad, M. Sanders, D. N. Mavris, and M. J. Benzakein, “An update on sizing and performance analysis of a hybrid turboelectric regional jet for the nasa uli program,” *2020 AIAA/IEEE Electric Aircraft Technologies Symposium (EATS)*, AIAA 2020-3590, 2020.
- [30] Y. Sun and H. Smith, “Review and prospect of supersonic business jet design,” *Progress in Aerospace Sciences*, vol. 90, pp. 12–38, 2017.
- [31] H. Welge, C. Nelson, and J. Bonet, “Supersonic vehicle systems for the 2020 to 2035 timeframe,” in *28th AIAA Applied Aerodynamics Conference*, 2010, p. 4930.
- [32] M. Shi, J. Gladin, and D. N. Mavris, “A systematic methodology for populating the aircraft thermal management system architecture space,” *AIAA Scitech 2021 Forum*, (AIAA 2021-1295), 2021.
- [33] M. Shi, I. Chakraborty, J. C. Tai, and D. N. Mavris, “Integrated gas turbine and environmental control system pack sizing and analysis,” in *2018 AIAA Aerospace Sciences Meeting*, 2018, p. 1748.
- [34] D. H. Petley and S. C. Jones, “Thermal management for a mach 5 cruise aircraft using endothermic fuel,” *Journal of Aircraft*, vol. 29, no. 3, pp. 384–389, 1992.
- [35] A. Donovan, “Vehicle level transient aircraft thermal management modeling and simulation,” Ph.D. dissertation, Wright State University, 2016.



- [36] T. Nam, "A generalized sizing method for revolutionary concepts under probabilistic design constraints," Ph.D. dissertation, Georgia Institute of Technology, 2007.
- [37] J. D. Mattingly, W. H. Heiser, and D. T. Pratt, *Aircraft engine design*. American Institute of Aeronautics and Astronautics, 2002.
- [38] D. Raymer, *Aircraft Design: A Conceptual Approach 5e and RDSWin STUDENT*. American Institute of Aeronautics and Astronautics, Inc., 2012.
- [39] M. Shi, M. Sanders, A. Alahmad, C. Perullo, G. Cina, and D. N. Mavris, "Design and analysis of the thermal management system of a hybrid turboelectric regional jet for the nasa uli program," *2020 AIAA/IEEE Electric Aircraft Technologies Symposium (EATS)*, AIAA 2020-3572, 2020.
- [40] R. M. Traci, R. Acebal, and T. Mohler, "Integrated thermal management of a hybrid electric vehicle," *IEEE Transactions on Magnetics*, vol. 35, no. 1, pp. 479–483, 1999.
- [41] S. R. Nuzum, A. Donovan, R. A. Roberts, and M. Wolff, "Dynamic modeling at a vehicle level of a cryogenic based thermal system for a high powered system," in *AIAA Science and Technology Forum and Exposition 2016*, vol. 672, 2016.
- [42] K. McCarthy, E. Walters, A. Heltzel, R. Elangovan, G. Roe, W. Vannice, C. Schemm, J. Dalton, S. Iden, P. Lamm, *et al.*, "Dynamic thermal management system modeling of a more electric aircraft," SAE Technical Paper, Tech. Rep., 2008.
- [43] A. Maser, E. Garcia, and D. Mavris, "Characterization of thermodynamic irreversibility for integrated propulsion and thermal management systems design," in *50th AIAA Aerospace Sciences Meeting including the New Horizons Forum and Aerospace Exposition*, 2012.
- [44] M. Dooley, N. Lui, R. Newman, and C. Lui, "Aircraft thermal management - heat sink challenge," in *SAE Technical Paper*, 2014, pp. 01–2193.
- [45] E. Vredenburg and F. Thielecke, "Thermal management investigations for fuel cell systems on-board commercial aircraft," SAE Technical Paper, Tech. Rep., 2013.
- [46] M. Shi, I. Chakraborty, Y. Cai, J. C. Tai, and D. N. Mavris, "Mission-level study of integrated gas turbine and environmental control system architectures," in *2018 AIAA Aerospace Sciences Meeting*, 2018, p. 1751.
- [47] I. Chakraborty and D. N. Mavris, "Integrated assessment of aircraft and novel subsystem architectures in early design," *Journal of Aircraft*, vol. 54, no. 4, pp. 1268–1282, 2017.

- [48] ———, “Assessing impact of epistemic and technological uncertainty on aircraft subsystem architectures,” *Journal of Aircraft*, vol. 54, no. 4, pp. 1388–1406, 2017.
- [49] W. Chen, D. W. Fogg, M. Izenzon, and C. Kurwitz, “A highly stable two-phase thermal management system for aircraft,” SAE Technical Paper, Tech. Rep., 2012.
- [50] J. Rheaume and C. E. Lents, “Design and simulation of a commercial hybrid electric aircraft thermal management system,” in *2018 AIAA/IEEE Electric Aircraft Technologies Symposium*, 2018, p. 4994.
- [51] E. J. Alyanak and D. L. Allison, “Fuel thermal management system consideration in conceptual design sizing,” in *57th AIAA/ASCE/AHS/ASC Structures, Structural Dynamics, and Materials Conference*, 2016, p. 0670.
- [52] S. Park, “A comprehensive thermal management system model for hybrid electric vehicles,” 2011.
- [53] A. J. Fleming, Q. H. Leland, K. L. Yerkes, L. J. Elston, and S. K. Thomas, “Aircraft thermal management using loop heat pipes: Experimental simulation of high acceleration environments using the centrifuge table test bed (postprint),” AIR FORCE RESEARCH LAB WRIGHT-PATTERSON AFB OH PROPULSION DIRECTORATE, Tech. Rep., 2006.
- [54] P. McCluskey, Y. Saadon, Z. Yao, J. Shah, and J. Kizito, “Thermal management challenges in turbo-electric and hybrid electric propulsion,” in *2018 International Energy Conversion Engineering Conference*, 2018, p. 4695.
- [55] E. Rechtin and M. W. Maier, *The art of systems architecting*. CRC Press, 2010.
- [56] J. Lang, “Creating architectural theory,” *The role of the behavioral sciences in environmental. design.*, 1987.
- [57] P. G. Rowe, *Design thinking*. MIT press, 1987.
- [58] E. Rechtin, *Systems architecting: Creating and building complex systems*, 1. Prentice Hall Englewood Cliffs, NJ, 1991, vol. 199.
- [59] M. Strauss, B. St. Rock, L. Zeidner, N. Desai, and H. Reeve, “Application of a technology screening methodology for rotorcraft alternative power systems,” in *48th AIAA Aerospace Sciences Meeting Including the New Horizons Forum and Aerospace Exposition*, 2010, p. 1505.
- [60] L. Zeidner, H. Reeve, R. Khire, and S. Becz, “Architectural enumeration and evaluation for identification of low-complexity systems,” in *10th AIAA Aviation Technology, Integration, and Operations (ATIO) Conference*, 2010, p. 9264.

- [61] S. Becz, A. Pinto, L. Zeidner, R. Khire, H. Reeve, and A. Banaszuk, "Design system for managing complexity in aerospace systems," in *10th AIAA Aviation Technology, Integration, and Operations (ATIO) Conference*, 2010, p. 9223.
- [62] J. Homitz, R. P. Scaringe, G. S. Cole, A. Fleming, and T. Michalak, "Comparative analysis of thermal management architectures to address evolving thermal requirements of aircraft systems," SAE Technical Paper, Tech. Rep., 2008.
- [63] L. F. Pellegrini, R. Gandolfi, G. Silva, and S. Oliveira Jr, "Exergy analysis as a tool for decision making in aircraft systems design," in *45th AIAA Aerospace Sciences Meeting and Exhibit*, vol. 23, 2007, pp. 16 485–16 496.
- [64] R. A. Roberts and D. D. Decker, "Control architecture study focused on energy savings of an aircraft thermal management system," *Journal of Dynamic Systems, Measurement, and Control*, vol. 136, no. 4, p. 041 003, 2014.
- [65] M. Bodie, G. Russell, K. McCarthy, E. Lucas, J. Zumberge, and M. Wolff, "Thermal analysis of an integrated aircraft model," in *48th AIAA Aerospace Sciences Meeting Including the New Horizons Forum and Aerospace Exposition*, 2010, p. 288.
- [66] J. A. Parrilla, "Hybrid environmental control system integrated modeling trade study analysis for commercial aviation," Ph.D. dissertation, University of Cincinnati, 2014.
- [67] D. F. Rancruel, "A decomposition strategy based on thermoeconomic isolation applied to the optimal synthesis/design and operation of an advanced fighter aircraft system," Ph.D. dissertation, Virginia Tech, 2003.
- [68] R. Figliola, R. Tipton, and H. Li, "Exergy approach to decision-based design of integrated aircraft thermal systems," *Journal of aircraft*, vol. 40, no. 1, pp. 49–55, 2003.
- [69] D. Bender, "Integration of exergy analysis into model-based design and evaluation of aircraft environmental control systems," *Energy*, vol. 137, pp. 739–751, 2017.
- [70] I. Pérez-Grande and T. J. Leo, "Optimization of a commercial aircraft environmental control system," *Applied thermal engineering*, vol. 22, no. 17, pp. 1885–1904, 2002.
- [71] T. J. Leo and I. Pérez-Grande, "A thermoeconomic analysis of a commercial aircraft environmental control system," *Applied Thermal Engineering*, vol. 25, no. 2, pp. 309–325, 2005.

- [72] A. Garcia Garriga, S. S. Ponnusamy, and L. Mainini, “A multi-fidelity framework to support the design of more-electric actuation,” in *2018 Multidisciplinary Analysis and Optimization Conference*, 2018, p. 3741.
- [73] B. Peherstorfer, K. Willcox, and M. Gunzburger, “Survey of multifidelity methods in uncertainty propagation, inference, and optimization,” *SIAM Review*, vol. 60, no. 3, pp. 550–591, 2018.
- [74] D. Bryson, M. Rumpfkeil, and R. Durscher, “Framework for multifidelity aeroelastic vehicle design optimization,” in *18th AIAA/ISSMO Multidisciplinary Analysis and Optimization Conference*, 2017, p. 4322.
- [75] D. Böhnke, B. Nagel, and V. Gollnick, “An approach to multi-fidelity in conceptual aircraft design in distributed design environments,” in *2011 Aerospace Conference*, IEEE, 2011, pp. 1–10.
- [76] Y. Cai, Z. Gao, I. Chakraborty, S. I. Briceno, and D. N. Mavris, “Integrated assessment of active flow control architectures for commercial aircraft,” in *55th AIAA Aerospace Sciences Meeting*, 2017.
- [77] J. C. Gladin, “A sizing and vehicle matching methodology for boundary layer ingesting propulsion systems,” Ph.D. dissertation, Georgia Institute of Technology, 2015.
- [78] A. FAA, *AC 25-20-Pressurization, Ventilation and Oxygen Systems Assessment for Subsonic Flight Including High Altitude Operation*. Federal Aviation Administration, 1996.
- [79] J. H. Redmond and F. W. Bott, “Development of cryogenic electric motors,” *SAE Transactions*, pp. 257–268, 1964.
- [80] *Sysml diagram taxonomy*, <https://sysml.org/>, Accessed: 2019-07-03.
- [81] L. E. Hart, “Introduction to model-based system engineering (mbse) and sysml,” in *Delaware Valley INCOSE Chapter Meeting, Ramblewood Country Club, Mount Laurel, New Jersey*, 2015.
- [82] D. E. Knuth, *Art of computer programming, volume 2: Seminumerical algorithms*. Addison-Wesley Professional, 2014.
- [83] S. Dasgupta, C. Papadimitriou, and U. Vazirani, *Algorithms*. The McGraw-Hill Companies, Inc, 2008, vol. 9.
- [84] J. Kleinberg and E. Tardos, *Algorithms Design*. Pearson Education, Inc, 2005, vol. 2.

- [85] R. L. Graham, D. E. Knuth, O. Patashnik, and S. Liu, “Concrete mathematics: A foundation for computer science,” *Computers in Physics*, vol. 3, no. 5, pp. 106–107, 1989.
- [86] H. Hausen and H. Linde, *Tieftemperaturtechnik: Erzeugung sehr tiefer Temperaturen, Gasverflüssigung und Zerlegung von Gasgemischen*. Springer-Verlag, 2013.
- [87] F. Reif, *Fundamentals of statistical and thermal physics*. Waveland Press, 2009.
- [88] L. C. Lichty, *Combustion engine processes*. McGraw-Hill, 1967.
- [89] N. R. Council *et al.*, *The airliner cabin environment: air quality and safety*. National Academies Press, 1986.
- [90] ———, *The airliner cabin environment and the health of passengers and crew*. National Academies Press, 2002.
- [91] R.-F.-R. Gagliu and K. P. Abin, *Modeling and simulation of novel environmental control system for a combat aircraft*, Masters Dissertation, Linköping University, 2018.
- [92] G. Van Rossum and F. L. Drake Jr, *Python reference manual*. Centrum voor Wiskunde en Informatica Amsterdam, 1995.
- [93] R. Hettinger, “Python 3.8.8 documentation,” *Python.org*, 2021, online: <https://docs.python.org/3.8/>, accessed March. 21, 2021.
- [94] M. Shi, Y. Cai, J. C. Gladin, and D. N. Mavris, “A multi-design point sizing methodology for environmental control systems,” in *AIAA Scitech 2020 Forum*, 2020-0013, 2020.
- [95] E. Kindler and I. Krivy, “Object-oriented simulation of systems with sophisticated control,” *International Journal of General Systems*, vol. 40, no. 3, pp. 313–343, 2011.
- [96] J. Lewis and W. Loftus, *Java software solutions foundations of programming design (vol, 2008*.
- [97] J. S. Schutte, “Simultaneous multi-design point approach to gas turbine on-design cycle analysis for aircraft engines,” Ph.D. dissertation, Georgia Institute of Technology, 2009.
- [98] J. Schutte, J. Tai, and D. Mavris, “Multi design point cycle design incorporation into the environmental design space,” in *48th AIAA/ASME/SAE/ASEE Joint Propulsion Conference & Exhibit*, 2012, p. 3812.

- [99] J. Schutte, J. Tai, J. Sands, and D. Mavris, "Cycle design exploration using multi-design point approach," in *ASME Turbo Expo 2012: Turbine Technical Conference and Exposition*, American Society of Mechanical Engineers, 2012, pp. 271–281.
- [100] B. K. Kestner, J. S. Schutte, J. C. Gladin, and D. N. Mavris, "Ultra high bypass ratio engine sizing and cycle selection study for a subsonic commercial aircraft in the n+ 2 timeframe," in *ASME 2011 Turbo Expo: Turbine Technical Conference and Exposition*, American Society of Mechanical Engineers, 2011, pp. 127–137.
- [101] T. L. Bergman, F. P. Incropera, D. P. DeWitt, and A. S. Lavine, *Fundamentals of heat and mass transfer*. John Wiley & Sons, 2011.
- [102] J. D. Mattingly, *Elements of propulsion: gas turbines and rockets*. American Institute of Aeronautics and Astronautics, 2006.
- [103] J. E. Hesselgreaves, R. Law, and D. Reay, *Compact heat exchangers: selection, design and operation*. Butterworth-Heinemann, 2016.
- [104] J. Han, J. Pei, and M. Kamber, *Data mining: concepts and techniques*. Elsevier, 2011.
- [105] R. Xu and D. C. Wunsch, "Survey of clustering algorithms," 2005.
- [106] M. Steinbach, G. Karypis, V. Kumar, *et al.*, "A comparison of document clustering techniques," in *KDD workshop on text mining*, Boston, vol. 400, 2000, pp. 525–526.
- [107] T. Hastie, R. Tibshirani, J. Friedman, and J. Franklin, "The elements of statistical learning: Data mining, inference and prediction," *The Mathematical Intelligencer*, vol. 27, no. 2, pp. 83–85, 2005.
- [108] B. Everitt, S. Landau, and M. Leese, "Cluster analysis. 1993," *Edward Arnold and Halsted Press*, 1993.
- [109] E. Forgey, "Cluster analysis of multivariate data: Efficiency vs. interpretability of classification," *Biometrics*, vol. 21, no. 3, pp. 768–769, 1965.
- [110] J. MacQueen *et al.*, "Some methods for classification and analysis of multivariate observations," in *Proceedings of the fifth Berkeley symposium on mathematical statistics and probability*, Oakland, CA, USA, vol. 1, 1967, pp. 281–297.
- [111] X. Zhuang, Y. Huang, K. Palaniappan, and Y. Zhao, "Gaussian mixture density modeling, decomposition, and applications," *IEEE Transactions on Image Processing*, vol. 5, no. 9, pp. 1293–1302, 1996.

- [112] W. S. Sarle, *Algorithms for clustering data*, 1990.
- [113] G. Karypis, E.-H. Han, and V. Kumar, “Chameleon: Hierarchical clustering using dynamic modeling,” *Computer*, vol. 32, no. 8, pp. 68–75, 1999.
- [114] L. O. Hall, I. B. Ozyurt, and J. C. Bezdek, “Clustering with a genetically optimized approach,” *IEEE Transactions on Evolutionary computation*, vol. 3, no. 2, pp. 103–112, 1999.
- [115] G. P. Babu and M. N. Murty, “Clustering with evolution strategies,” *Pattern recognition*, vol. 27, no. 2, pp. 321–329, 1994.
- [116] A. Ghozeil and D. B. Fogel, “Discovering patterns in spatial data using evolutionary programming,” in *Proceedings of the 1st annual conference on genetic programming*, 1996, pp. 521–527.
- [117] L. A. Zadeh, “Fuzzy sets,” in *Fuzzy sets, fuzzy logic, and fuzzy systems: selected papers by Lotfi A Zadeh*, World Scientific, 1996, pp. 394–432.
- [118] N. R. Pal, J. C. Bezdek, and E.-K. Tsao, “Generalized clustering networks and kohonen’s self-organizing scheme,” *IEEE transactions on Neural Networks*, vol. 4, no. 4, pp. 549–557, 1993.
- [119] B. Schölkopf, A. Smola, and K.-R. Müller, “Nonlinear component analysis as a kernel eigenvalue problem,” *Neural computation*, vol. 10, no. 5, pp. 1299–1319, 1998.
- [120] D. Arthur and S. Vassilvitskii, “K-means++: The advantages of careful seeding,” in *Proceedings of the eighteenth annual ACM-SIAM symposium on Discrete algorithms*, Society for Industrial and Applied Mathematics, 2007, pp. 1027–1035.
- [121] F. Pedregosa, G. Varoquaux, A. Gramfort, V. Michel, B. Thirion, O. Grisel, M. Blondel, P. Prettenhofer, R. Weiss, V. Dubourg, J. Vanderplas, A. Passos, D. Cournapeau, M. Brucher, M. Perrot, and E. Duchesnay, “Scikit-learn: Machine learning in Python,” *Journal of Machine Learning Research*, vol. 12, pp. 2825–2830, 2011.
- [122] K. Pearson, “Liii. on lines and planes of closest fit to systems of points in space,” *The London, Edinburgh, and Dublin Philosophical Magazine and Journal of Science*, vol. 2, no. 11, pp. 559–572, 1901.
- [123] H. Hotelling, “Analysis of a complex of statistical variables into principal components,” *Journal of educational psychology*, vol. 24, no. 6, p. 417, 1933.
- [124] R. W. Claus, A. L. Evans, and G. J. Follen, “Multidisciplinary propulsion simulation using npss,” *AIAA Paper*, no. 92-4709, 1992.

- [125] T. J. Ypma, “Historical development of the newton–raphson method,” *SIAM review*, vol. 37, no. 4, pp. 531–551, 1995.
- [126] K. Deb, *Multi-objective optimization using evolutionary algorithms*. John Wiley & Sons, 2001, vol. 16, NA.
- [127] K. Deb, A. Pratap, S. Agarwal, and T. Meyarivan, “A fast and elitist multiobjective genetic algorithm: Nsga-ii,” *IEEE transactions on evolutionary computation*, vol. 6, no. 2, pp. 182–197, 2002.
- [128] P. P. Walsh and P. Fletcher, *Gas turbine performance*. John Wiley & Sons, 2004.
- [129] M. Shi, K. Milios, J. C. Gladin, and D. N. Mavris, “System-level study of different super/turbocharger architectures for rotorcraft diesel engine,” in *2018 AIAA Aerospace Sciences Meeting*, 2018–2027, 2018.
- [130] W. M. Kays and A. L. London, *Compact heat exchangers*. McGraw-Hill, New York, NY, 1984.
- [131] H. Navarro and L. Cabezas-Gómez, “Effectiveness-ntu computation with a mathematical model for cross-flow heat exchangers,” *Brazilian Journal of Chemical Engineering*, vol. 24, no. 4, pp. 509–521, 2007.
- [132] J.-Y. San and C.-L. Jan, “Second-law analysis of a wet crossflow heat exchanger,” *Energy*, vol. 25, no. 10, pp. 939–955, 2000.
- [133] V. Oyj, “Calculation formulas for humidity—humidity conversion formulas,” *Vaisala: Helsinki, Finland*, 2013.
- [134] A. Handbook, “Refrigeration, american society of heating, refrigerating and air conditioning engineers,” *Atlanta*, 2002.
- [135] C. Müller and D. Scholz, “The vapor compression cycle in aircraft air-conditioning systems,” 2017, Technical Note.
- [136] H. D. Baehr and S. Kabelac, *Thermodynamik*. Springer-Verlag Berlin Heidelberg, 2006.
- [137] S. Kakac, H. Liu, and A. Pramuanjaroenkij, *Heat exchangers: selection, rating, and thermal design*. CRC press, 2012.
- [138] N. Majumdar, B. Mathur, and S. Kaushik, “Prediction of direct solar radiation for low atmospheric turbidity,” *Solar Energy*, vol. 13, no. 4, pp. 383–394, 1972.



- [139] J. Lienhard IV and V. Lienhard, “Jh (2011) a heat transfer textbook,” *Cambridge Massachusetts*,
- [140] L. Mansouri, M. Balistrrou, and B. Baudoin, “One-dimensional time-dependent modeling of conductive heat transfer during the melting of an initially subcooled semi-infinite pcm,” in *Congrès français de mécanique*, AFM, Association Française de Mécanique, 2017.
- [141] C. A. Perullo, D. Trawick, W. Clifton, J. C. Tai, and D. N. Mavris, “Development of a suite of hybrid electric propulsion modeling elements using npss,” in *Turbo Expo: Power for Land, Sea, and Air*, American Society of Mechanical Engineers, vol. 45578, 2014, V01AT01A042.
- [142] C. Perullo and D. N. Mavris, “Assessment of vehicle performance using integrated npss hybrid electric propulsion models,” in *50th AIAA/ASME/SAE/ASEE Joint Propulsion Conference*, 2014, p. 3489.
- [143] C. Winnefeld, T. Kadyk, B. Bensmann, U. Krewer, and R. Hanke-Rauschenbach, “Modelling and designing cryogenic hydrogen tanks for future aircraft applications,” *Energies*, vol. 11, no. 1, p. 105, 2018.
- [144] D. Dampfkesselausschuss and T. Essen, “Technische regeln für dampfkessel,” *Verband der TÜV eV: Berlin, Germany*, 2010.
- [145] G. D. Brewer, *Hydrogen aircraft technology*. Routledge, 2017.
- [146] S. K. Mital, J. Z. Gyekenyesi, S. M. Arnold, R. M. Sullivan, J. M. Manderscheid, and P. L. Murthy, “Review of current state of the art and key design issues with potential solutions for liquid hydrogen cryogenic storage tank structures for aircraft applications,” *Aerospace Engineering Papers*, NASA, 2006.
- [147] D. W. Plachta, R. Christie, E. Carlberg, and J. Feller, “Cryogenic propellant boil-off reduction system,” in *AIP Conference Proceedings*, American Institute of Physics, vol. 985, 2008, pp. 1457–1466.
- [148] J. Palmer and E. Shehab, “Modelling of cryogenic cooling system design concepts for superconducting aircraft propulsion,” *IET Electrical Systems in Transportation*, vol. 6, no. 3, pp. 170–178, 2016.
- [149] R. Radebaugh, “Cryocoolers for aircraft superconducting generators and motors,” in *AIP Conference Proceedings*, American Institute of Physics, vol. 1434, 2012, pp. 171–182.
- [150] H. C. Holly, “The closed-loop air-cycle option for equipment cooling on aircraft,” SAE Technical Paper, Tech. Rep., 1984.

- [151] C. A. Perullo, J. Tai, and D. Mavris, “A new sizing and synthesis environment for the design and assessment of advanced hybrid and electric aircraft propulsion systems,” *International Association of Airbreathing Engines (ISABE)*, ISABE-2015-20286, 2015.
- [152] J. C. Gladin, C. Perullo, J. C. Tai, and D. N. Mavris, “A parametric study of hybrid electric gas turbine propulsion as a function of aircraft size class and technology level,” *55th AIAA Aerospace Sciences Meeting*, AIAA 2017-0338, 2017.
- [153] J. C. Gladin, D. Trawick, C. Perullo, J. C. Tai, and D. N. Mavris, “Modeling and design of a partially electric distributed aircraft propulsion system with gt-heat,” *55th AIAA Aerospace Sciences Meeting*, AIAA 2017-1924, 2017.
- [154] L. McCullers, *Flight optimization system, release 8.11, user’s guide*, NASA Langley Research Center, Hampton, VA 23681-0001, Oct. 2009.
- [155] —, “Aircraft configuration optimization including optimized flight profiles,” in *Proceedings of a Symposium on Recent Experiences in Multidisciplinary Analysis and Optimization*, NASA CP-2327, 1984, pp. 395–412.
- [156] M. F. Ozcan, I. Chakraborty, and D. N. Mavris, “Impact of subsystem secondary power requirements on gas turbine sizing and performance,” in *16th AIAA Aviation Technology, Integration, and Operations Conference*, 2016.
- [157] G. E. Company, “Extended parametric representation of compressor fans and turbines. volume 1: Cmpgen user’s manual,” *NASA CR174645*, 1984.
- [158] A. Plas, “Performance of a boundary layer ingesting propulsion system,” Ph.D. dissertation, Massachusetts Institute of Technology, 2006.
- [159] M. Pokhrel, J. C. Gladin, E. Garcia, and D. N. Mavris, “A methodology for quantifying distortion impacts using a modified parallel compressor theory,” in *To be published in the ASME Turbo Expo 2018, Lillestrom(Oslo), Norway*, 2018.
- [160] M. Shi, M. Pokhrel, J. C. Gladin, E. Garcia, and D. N. Mavris, “Convergent nozzle gross thrust coefficient and discharge coefficient calculation with boundary layer ingestion (bli) effects,” in *53rd AIAA/SAE/ASEE Joint Propulsion Conference*, 2017, p. 5057.
- [161] F. Moore, “A theory of rotating stall of multistage axial compressors: Part i—small disturbances,” *ASME J. Eng. Gas Turbines Power*, vol. 106, no. 2, pp. 313–320, 1984.
- [162] “Hydrogen powered aviation: A fact-based study of hydrogen technology, economics, and climate impact by 2050,” Tech. Rep., 2020.

- [163] R. Ahluwalia, T. Hua, J.-K. Peng, S. Lasher, K. McKenney, J. Sinha, and M. Gardiner, “Technical assessment of cryo-compressed hydrogen storage tank systems for automotive applications,” *International journal of hydrogen energy*, vol. 35, no. 9, pp. 4171–4184, 2010.